



Dissertation

zur Erlangung des Grades
doctor rerum naturalium (Dr.rer.nat.)
in der Wissenschaftsdisziplin
Molekulare Biotechnologie

Development of a fiber-based sensor for the molecular detection of pathogens using *Legionella* as an example

eingereicht an der
Mathematisch-Naturwissenschaftlichen Fakultät
der Universität Potsdam

von

Natascha Heinsohn

Disputation 08.11.2022

Supervisor:
Prof. Carsten Beta

Reviewer:
Prof. Carsten Beta
Prof. Frank Bier
Prof. Dieter Jahn

Published online on the
Publication Server of the University of Potsdam:
<https://doi.org/10.25932/publishup-56683>
<https://nbn-resolving.org/urn:nbn:de:kobv:517-opus4-566833>

Abstract

Fiber-based microfluidics has undergone many innovative developments in recent years, with exciting examples of portable, cost-effective and easy-to-use detection systems already being used in diagnostic and analytical applications. In water samples, *Legionella* are a serious risk as human pathogens. Infection occurs through inhalation of aerosols containing *Legionella* cells and can cause severe pneumonia and may even be fatal. In case of *Legionella* contamination of water-bearing systems or *Legionella* infection, it is essential to find the source of the contamination as quickly as possible to prevent further infections. In drinking, industrial and wastewater monitoring, the culture-based method is still the most commonly used technique to detect *Legionella* contamination. In order to improve the laboratory-dependent determination, the long analysis times of 10-14 days as well as the inaccuracy of the measured values in colony forming units (CFU), new innovative ideas are needed. In all areas of application, for example in public, commercial or private facilities, rapid and precise analysis is required, ideally on site.

In this PhD thesis, all necessary single steps for a rapid DNA-based detection of *Legionella* were developed and characterized on a fiber-based miniaturized platform. In the first step, a fast, simple and device-independent chemical lysis of the bacteria and extraction of genomic DNA was established. Subsequently, different materials were investigated with respect to their non-specific DNA retention. Glass fiber filters proved to be particularly suitable, as they allow recovery of the DNA sample from the fiber material in combination with dedicated buffers and exhibit low autofluorescence, which was important for fluorescence-based readout.

A fiber-based electrophoresis unit was developed to migrate different oligonucleotides within a fiber matrix by application of an electric field. A particular advantage over lateral flow assays is the targeted movement, even after the fiber is saturated with liquid. For this purpose, the entire process of fiber selection, fiber chip patterning, combination with printed electrodes, and testing of retention and migration of different DNA samples (single-stranded, double-stranded and genomic DNA) was performed. DNA could be pulled across the fiber chip in an electric field of 24 V/cm within 5 minutes, remained intact and could be used for subsequent detection assays e.g., polymerase chain reaction (PCR) or fluorescence *in situ* hybridization (FISH). Fiber electrophoresis could also be used to separate DNA from other components e.g., proteins or cell lysates or to pull DNA through multiple layers of the glass microfiber. In this way, different fragments experienced a moderate, size-dependent separation. Furthermore, this arrangement offers the possibility that different detection reactions could take place in different layers at a later time. Electric current and potential measurements were collected to investigate the local distribution of the sample during migration. While an increase in current signal at

high concentrations indicated the presence of DNA samples, initial experiments with methylene blue stained DNA showed a temporal sequence of signals, indicating sample migration along the chip.

For the specific detection of a *Legionella* DNA, a FISH-based detection with a molecular beacon probe was tested on the glass microfiber. A specific region within the 16S rRNA gene of *Legionella* spp. served as a target. For this detection, suitable reaction conditions and a readout unit had to be set up first. Subsequently, the sensitivity of the probe was tested with the reverse complementary target sequence and the specificity with several DNA fragments that differed from the target sequence. Compared to other DNA sequences of similar length also found in *Legionella pneumophila*, only the target DNA was specifically detected on the glass microfiber. If a single base exchange is present or if two bases are changed, the probe can no longer distinguish between the DNA targets and non-targets. An analysis with this specificity can be achieved with other methods such as melting point determination, as was also briefly indicated here. The molecular beacon probe could be dried on the glass microfiber and stored at room temperature for more than three months, after which it was still capable of detecting the target sequence. Finally, the feasibility of fiber-based FISH detection for genomic *Legionella* DNA was tested. Without further processing, the probe was unable to detect its target sequence in the complex genomic DNA. However, after selecting and application of appropriate restriction enzymes, specific detection of *Legionella* DNA against other aquatic pathogens with similar fragment patterns as *Acinetobacter haemolyticus* was possible.

Zusammenfassung

Die faserbasierte Mikrofluidik hat in den letzten Jahren viele innovative Entwicklungen erfahren, mit spannenden Beispielen für portable, kostengünstige und einfach zu bedienende Nachweissysteme die bereits in diagnostischen und analytischen Fragestellungen Anwendung finden. In Wasserproben sind Legionellen als Humanpathogene ein ernstzunehmendes Risiko. Eine Infektion erfolgt über das Einatmen legionellenhaltiger Aerosole und kann schwerwiegende Pneumonien hervorrufen oder sogar tödlich verlaufen. Im Falle einer Legionellenkontamination von Wasserführenden Systemen beziehungsweise einer Legionellen-assoziierten Infektion ist es maßgeblich die Quelle der Kontamination möglichst schnell zu finden, um weitere Infektionen zu vermeiden. In der Überwachung von Trink- Prozess- und Abwasser ist die kulturbasierte Methode immer noch die am häufigsten verwendete Technik, um einen Legionellenbefall nachzuweisen. Um Alternativen zu einer laborabhängigen Bestimmung mit ihren langen Analysezeiten von 10-14 Tagen und der ungenauen Messwertausgabe in koloniebildenden Einheiten (KBE) zu finden, bedarf es neuer innovativer Ideen. In allen Anwendungsbereichen, zum Beispiel in öffentlichen, gewerblichen oder privaten Einrichtungen, ist eine schnelle und präzise Analyse erforderlich, idealerweise vor Ort.

Im Rahmen dieser Doktorarbeit wurden alle notwendigen Einzelschritte für einen schnellen DNA-basierten Nachweis von Legionellen auf einer faserbasierten, miniaturisierten Plattform entwickelt und charakterisiert. Im ersten Schritt wurde eine schnelle, einfache und geräteunabhängige chemische Lyse der Bakterien und Extraktion der genomischen DNA etabliert. Daraufhin wurden verschiedene Materialien hinsichtlich ihres unspezifischen DNA-Rückhalts untersucht. Glasfaserfilter erwiesen sich als besonders geeignet, da sie in Kombination mit den geeigneten Puffern eine Rückgewinnung der DNA-Probe aus dem Fasermaterial ermöglichen und für eine fluoreszenzbasierte Auslese eine geringe Autofluoreszenz aufweisen.

Eine faserbasierte Elektrophoreseeinheit wurde entwickelt, um durch Anlegen eines elektrischen Feldes verschiedene Oligonukleotide innerhalb einer Fasermatrix zu bewegen. Ein besonderer Vorteil gegenüber Lateral-Flow-Tests ist die Möglichkeit der gezielten Bewegung, auch nachdem die Faser mit Flüssigkeit gesättigt ist. Hierfür wurde der gesamte Prozess der Faserauswahl, der Strukturierung der Faserchips, der Kombination mit gedruckten Elektroden und der Prüfung der Retention und Migration verschiedener DNA-Proben (einzelsträngige, doppelsträngige und genomische DNA) bearbeitet. Die DNA konnte in einem elektrischen Feld von 24 V/cm innerhalb von 5 Minuten über den Faserchip gezogen werden, blieb dabei intakt und konnte für nachfolgende Detektionsnachweise z.B. Polymerase-Ketten-Reaktion (PCR) oder Fluoreszenz *in situ* Hybridisierung (FISH) genutzt werden. Die Faserelektrophorese konnte außerdem zur Separation der DNA von anderen Komponenten z.B.

Proteinen oder Zelllysaten verwendet werden oder um DNA durch mehrere Lagen der Glasfaser zu steuern. Dabei erfuhren verschiedene Fragmente einen moderaten, größenabhängigen Trenneffekt. Außerdem bietet diese Anordnung die Möglichkeit, dass unterschiedliche Nachweisreaktionen zu einem späteren Zeitpunkt in verschiedenen Schichten stattfinden könnten. Strom- und Potentialmessungen wurden erhoben, um die lokale Verteilung der Probe während der Migration zu untersuchen. Während ein Anstieg des Stromsignals bei hohen Konzentrationen die Anwesenheit von DNA-Proben anzeigte, konnten nach ersten Experimenten mit Methylenblau-gefärbter DNA zeitlich aufeinanderfolgende Signale detektiert werden und somit prinzipiell eine Probenmigration nachgewiesen werden.

Für den spezifischen Nachweis der Legionellen-DNA wurde ein FISH-basierter Nachweis mit einer molekularen Sonde auf der Glasmikrofaser getestet. Als Ziel für die Sonde diente eine bestimmte Region innerhalb des 16S rRNA-Gens von Legionellen. Für diesen Nachweis mussten zunächst geeignete Reaktionsbedingungen und eine Ausleseeinheit bestimmt werden. Anschließend wurde die Sensitivität der Sonde mit der umgekehrt komplementären Zielsequenz und die Spezifität mit verschiedenen DNA-Fragmenten, die sich von der Zielsequenz unterschieden, getestet. Im Vergleich zu abweichenden DNA-Sequenzen ähnlicher Länge, die auch in *Legionella pneumophila* vorkommen, wurde nur die Ziel-DNA spezifisch auf der Glasmikrofaser erkannt. Liegt ein einzelner Basenaustausch vor oder werden zwei Basen geändert, so kann die Sonde nicht mehr zwischen der Ziel-DNA und den abweichenden DNA-Fragmenten unterscheiden. Eine Detektion mit dieser Genauigkeit ist mit anderen Methoden wie z.B. der Schmelzpunktbestimmung möglich, wie hier prinzipiell demonstriert wurde. Es wurde ferner gezeigt, dass die Sonde auf der Glasmikrofaser eingetrocknet und über drei Monate bei Raumtemperatur gelagert werden kann und danach immer noch in der Lage ist, die Zielsequenz nachzuweisen. Schließlich wurde die Anwendbarkeit des faserbasierten FISH-Nachweises auch für genomische Legionellen-DNA getestet. Ohne weitere Prozessierung war die Sonde nicht in der Lage ihre Zielsequenz in der komplexen genomischen DNA zu erkennen. Nach der Auswahl und Anwendung geeigneter Restriktionsenzyme war eine spezifische Detektion der *Legionellen*-DNA gegenüber anderen Wasserkeimen mit ähnlichem Fragmentmuster wie *Acinetobacter haemolyticus* möglich.

Table of contents

1. Introduction.....	1
1.1. Water as a valuable resource	1
1.2. Microbes in water.....	1
1.3. German Drinking Water Ordinance.....	2
1.4. Morphology and epidemiology of <i>Legionella</i>	3
1.5. Detection methods for <i>Legionella</i>	6
1.5.1. Culture method.....	7
1.5.2. Immunological methods	8
1.5.3. Polymerase chain reaction.....	9
1.5.4. Flow cytometry	9
1.5.5. Fluorescence <i>in situ</i> hybridization.....	10
1.6. Fiber-based microfluidic devices	12
1.6.1. Fabrication techniques.....	13
1.6.2. Detection principles and applications.....	14
1.7. Electrophoresis.....	17
2. Material and methods.....	19
2.1. Instruments	19
2.2. Materials.....	20
2.3. Microbiological methods.....	24
2.3.1. Bacterial cultivation and storage	24
2.3.2. Cell number determination.....	25
2.3.3. Growth curve and correlation of optical density to cell number	27
2.3.4. Bacterial viability test.....	27
2.4. Molecular biological methods.....	28
2.4.1. Absorbance measurement.....	28
2.4.2. Bacterial lysis and DNA Extraction	28
2.4.3. PCR and real-time PCR	29
2.4.4. Agarose gel electrophoresis.....	30
2.4.5. DNA ladders	31
2.4.6. Fluorescence <i>in situ</i> hybridization.....	31
2.4.6.1. Rapid hybridization detection protocol.....	31
2.4.6.2. Hybridization prediction and calculation of Gibbs free energy changes.....	32
2.4.6.3. Cooling curve of hybridization.....	32
2.4.6.4. Significance test.....	33

2.4.7. Fragmentation of gDNA by restriction enzymes.....	33
2.4.8. Interaction of DNA molecules with different fiber substrates.....	34
2.4.9. Methylene blue labeling of DNA.....	36
2.5. Fabrication and characterization methods for paper-based materials.....	36
2.5.1. Long-term storage of detection reagents on glass microfiber	36
2.5.2. Patterning of fiber materials.....	36
2.5.3. Application methods for conductive materials on fiber	38
2.5.4. Characterization of the fiber-electrophoresis chip fabrication	40
2.5.5. Experimental implementation of the fiber-based electrophoresis	40
2.5.6. Measurement board	41
2.5.7. Heating element.....	42
2.6. Protein biochemical methods	43
2.6.1. DNA-protein-mixture preparation	43
2.6.2. Paper-based ELISA.....	43
2.6.3. Flow cytometry	43
3. Results and Discussion	45
3.1. Growth curve and correlation of optical density to cell number.....	45
3.2. Bacterial lysis and DNA extraction	46
3.2.1. Lysis efficiency.....	47
3.2.2. Extraction efficiency.....	49
3.3. Characterization of the fiber chip fabrication	52
3.3.1. Patterning.....	52
3.3.2. Characterization of imprinted electrodes.....	53
3.3.3. Erosion of contact electrodes	55
3.4. Interaction of DNA with fiber materials under heat treatment.....	56
3.4.1. Influence of substrate and 3D structure of cellulose on DNA retention	58
3.4.2. Alternative filter materials for DNA recovery after heat application	60
3.4.3. Options for reducing the evaporation of liquids in glass microfibers.....	61
3.4.4. Test of different pore sizes and suitable elution buffers for DNA recovery from glass microfibers	62
3.5. Fiber electrophoresis.....	64
3.5.1. Migration of DNA samples in cellulose with imprinted PEDOT:PSS electrodes	64
3.5.2. Migration of DNA samples in glass microfiber with imprinted PEDOT:PSS electrodes	66
3.5.2.1. Single channel fiber electrophoresis chip	66
3.5.2.2. Dual channel fiber electrophoresis chip.....	70
3.5.3. Migration of DNA samples in glass microfiber with carbon paste imprinted electrodes..	72

3.5.3.1. Velocity of migration of DNA samples in glass microfibers.....	75
3.5.3.2. Reduction of pore size and voltage	77
3.5.3.3. Alternative detection of migrated DNA by staining via GelRed	78
3.5.3.4. Test of DNA integrity	80
3.5.3.5. Cross-layer chip arrangement for targeted DNA separation	83
3.5.3.6. Separation of DNA from HRP as an exemplary protein.....	85
3.5.3.7. Separation of DNA from a bacterial cell lysate	86
3.5.3.8. Current and potential based read-out of DNA sample migration.....	89
3.6. Fluorescence <i>in situ</i> hybridization (FISH)	94
3.6.1. Basic characterization of operating conditions and read out.....	95
3.6.2. Buffer selection and fluorescence detection	95
3.6.3. Sensitivity	101
3.6.4. Specificity	104
3.6.4.1. Test of non-target sequences.....	104
3.6.4.2. Influences of single- and double nucleotide variations.....	105
3.6.5. Combination of glass microfiber electrophoresis and detection with FISH	111
3.6.6. Long-term storage of detection reagents on glass microfiber	112
3.6.7. Test of bacterial DNA	115
3.6.7.1. Fragmented gDNA from <i>L. pneumophila</i> Philadelphia.....	116
3.6.7.2. Fragmented gDNA from other bacterial strains.....	120
4. Summary and outlook	127
5. References.....	133
6. Appendix.....	150
6.1. Abbreviation	150
6.2. Circuit diagram HVADC.....	152
6.3. Microscopic determination of the layer thickness of a carbon paste electrode	152
6.4. Electrophoretic migration of DNA samples in cellulose filters with imprinted electrodes consisting of PEDOT:PSS.....	153
6.4.1. Alternative cellulose material and reduced chip geometry.....	155
6.4.2. Influence of cellulose patterning on DNA detection.....	158
6.5. Test of a new channel pattern via fiber electrophoresis with textile dyes	159
6.6. Current based read-out of DNA sample migration on glass microfiber with imprinted electrodes consisting of PEDOT:PSS.....	160
6.7. Repetitions of the current-based readout of DNA.....	162
6.8. Restriction digestion of genomic <i>L. pneumophila</i> Philadelphia DNA by restriction enzymes SmlI and BseI	162

6.9. Restriction digestion of gDNA from <i>L. pneumophila</i> Philadelphia, <i>E. coli</i> and <i>P. aeruginosa</i> by restriction enzymes HaeIII and HhaI	164
6.10. Paper-based ELISA	166
6.11. Bacterial viability test by staining with ChemChrome V6	167
6.12. Octave script.....	168
7. Acknowledgement.....	174

1. Introduction

1.1. Water as a valuable resource

Access to clean water is not only a basic human right but also the basis of various human activities every day. Besides drinking water, people also need it for food preparation, personal hygiene and laundry. In industry water is also used as a solvent or for cleaning and cooling of processes and products. The daily per capita consumption of drinking water in Germany was 125 liters of water in 2019 (Bundesverband der Energie- und Wasserwirtschaft e.V., 2019). Accordingly, the quality of water is particularly important and is subject to special monitoring and requirements. Foreign substances can spread quickly through the often widely branched pipe systems and can thus reach and infect many people (Jankowski, 2013). The Drinking Water Ordinance regulates the microbiological and chemical parameters to be tested and the frequency of drinking and tap water to be monitored. Furthermore, the obligations of the supply companies and the monitoring authorities are regulated and requirements and critical values are specified.

1.2. Microbes in water

Pathogens can enter human bodies, for example, by oral ingestion (e.g. *Escherichia coli*), skin absorption (e.g. *Pseudomonas aeruginosa*) or aspiration (e.g. *Legionella pneumophila*) for example. The relevant pathogens for monitoring microbial water quality are listed in Table 1. Besides *Enterococci* and *E. coli* occurring from fecal contamination, soil bacteria like *Clostridium perfringens* or *P. aeruginosa* and ubiquitous in natural water reservoirs occurring *Legionella* species (spp.) are investigated as indicator parameters. According to the WHO among all pathogens that can be transmitted through water, *Legionella* is the most severe health burden in Europe (Amtsblatt der Europäischen Union, 2020).

Table 1: Indicator organisms and intervention values for German drinking water testing (Bundesamt der Justiz, 2001).

Pathogen	Threshold value	Comment
<i>Escherichia coli</i>	0/100 ml	General requirements for drinking water
<i>Enterococci</i>	0/100 ml	General requirements for drinking water
<i>Clostridium perfringens</i>	0/100 ml	If the water is surface water or has been contaminated by surface water.
<i>Pseudomonas aeruginosa</i>	0/250 ml	If intended for delivery in sealed containers.
<i>Legionella</i> spp.	100/100 ml	Special indicator parameter for drinking water installation plants.

1.3. German Drinking Water Ordinance

In general, a continuous increase in the absolute number of legionellosis cases has been observed. In only four years the case numbers of patients suffered or died from Legionnaire's disease in Germany have almost doubled from 880 cases in 2015 to 1548 cases in 2019 (Robert Koch Institut, 2020, 2016). Table 2 provides an overview of the submitted case numbers from 2015 to August 2020. The overall cases in 2020 decreased probably due to the corona pandemic but was still high with 1281 cases (Robert Koch Institut, 2021). In the list of notifiable diseases in Germany, legionellosis was ranked 21st in 2017 to 2019, ahead of deaths caused by hepatitis A and D, malaria or measles (Robert Koch Institut, 2018, 2019a, 2020). In 2020, despite the enormous number of infections with the coronavirus, legionellosis was listed in 20th place and continues to be a dangerous threat (Robert Koch Institut, 2021).

Table 2: Case numbers of Legionnaires' disease reported to the German Robert Koch Institute by year (Robert Koch Institut, 2016, 2017, 2018, 2019a, 2020, 2021).

	Year					
	2015	2016	2017	2018	2019	2020
Total cases in Germany	880	992	1281	1443	1548	1281

Trends in Legionnaires' disease case numbers in the context of the COVID-19 pandemic have recently been studied (Brodhun and Buchholz, 2020). They noted that the number of cases classified as community associated, for example illnesses acquired in the private or job-related environment showed a slightly increase in 2020, with 593 cases compared to the same period in 2019 with 517 cases, accounting for 83 % of all cases compared to 70 % in 2019. In contrast, the travel-associated cases decreased 2.5-fold from 164 cases in 2019 compared to 66 cases in 2020 in the first half of the year. Usually, the number of travel-associated cases rises from April onwards with the start of the vacation pre-season and shows the first peaks in June. In comparison in April and Mai of 2020 the number of cases initially remained almost zero due to the corona pandemic and only rose slowly again after the first easing and less travel warning in mid-June. Meanwhile, the diseases in hospitals or nursing homes remained the same in both years, with generally low numbers of about 24 cases. Because the Legionnaires' disease is likely underdiagnosed, since not all pneumonias are tested for legionellosis the true number of cases may be 1.8-2.7 times higher than reported (Collier et al., 2021). Despite this underreporting, it should be taken into account that the number of cases are also increasing due to increased awareness and testing.

1.4. Morphology and epidemiology of *Legionella*

Legionella is a genus of Gram-negative, obligate aerobic and rod-shaped bacteria with a diameter of 0.3 to 0.9 μm and a length of 2 to 20 μm whose morphology may vary depending on culture conditions (Bartram et al., 2007). *Legionella* grown on surfaces or in liquid media shows coccoid, bacillary and filamentous forms, in which several bacterial cells are attached to chains or arrange in branches (Katz et al., 1984). Microscopic images showing the bacterial morphologies can be seen in Figure 1 a) and b). *Legionella* can be found ubiquitous in natural water reservoirs or soil and biofilms but also in anthropogenic water systems such as fountains, swimming pools, showers, or cooling towers (Molmeret et al., 2005; Steinert et al., 2002).

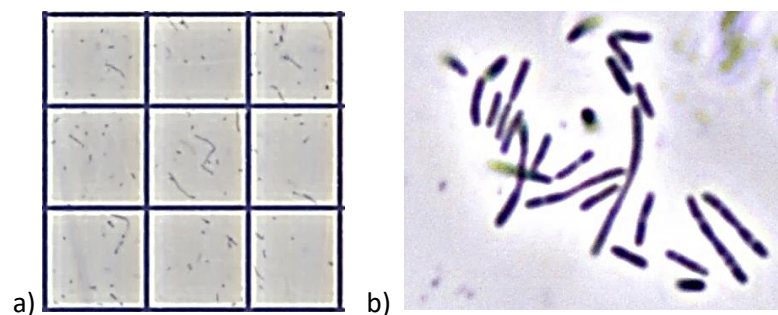


Figure 1: Bright field microscopic images a) x 10 and b) x 100 of *Legionella pneumophila* Philadelphia in a counting chamber Neubauer-improved showing coccoid, bacillary and filamentous forms of bacterial cells.

Currently 57 *Legionella* species and at least 79 different serogroups are known (Robert Koch Institut, 2019b). The genome size varies from 2.37 Mb (*Legionella adelaidensis*) to 4.88 Mb (*Legionella santacrucis*). For *L. pneumophila* Philadelphia, a genome size of 3.4 Mb was determined (Gomez-Valero et al., 2019). Optimal growth temperatures for *Legionella* ranges from 20°C to 45°C, but the genus demonstrates a high temperature tolerance and grows even at temperatures of 0°C to 63°C (Söderberg and Cianciotto, 2008). The bacteria were first reported in Philadelphia, USA, in 1976 at the 58th annual American Legion convention at the Bellevue Stratford Hotel, where 221 veterans suffered from pneumonia. After a detailed analysis by the Center for Disease Control, *L. pneumophila* was identified as the causative agent of this pneumonia. Therefore, the bacterium was named in memory of the diseased and 34 deceased members of the American Legion and after the pneumonia-like disease process (Fraser et al., 1977; McDade et al., 1977). The source of the infection during the Legionnaires' convention was later found to be the contaminated air-conditioning system in the hotel (Abu Kwaik et al., 1998).

Legionella use amino acids as primary source of energy and iron plays an important role in the survival and intracellular proliferation of *Legionella* in their host cells (Cianciotto, 2007; Tesh et al., 1983). The bacterial locomotion is achieved through a mostly unipolar flagellum (Bosshardt et al., 1997). They colonize as a facultative intracellular parasite a number of protozoa, in particular amoebae and ciliates (Harb et al., 2000). Parasitism in protozoa thereby protects the bacteria from excessive pH and temperature fluctuations, osmotic stress, as well as UV radiation and other hostile environmental influences. In addition, intracellular proliferation in host cells offers the advantage of developing resistance to antibiotics and biocides or enhancing existing resistance (Abu Kwaik et al., 1998; Declerck, 2010). *Legionella* are also capable of forming biofilms. On the one hand, this attracts potential host organisms for intracellular replication, which use the biofilm as a nutrient source. On the other hand, the formation of a biofilm reduces external factors such as fluctuating temperature or pH, pollutant input, radiation and other inactivating factors (Alleron et al., 2008; Declerck, 2010). In addition, the protective biofilm favors the colonization of primarily anthropogenically created aquatic systems. *Legionella* can also enter a viable but not culturable (VBNC) state in which the bacteria exhibit a low level of metabolic activity, but they can recover their culturability when environmental conditions improve (Alleron et al., 2008; Hwang et al., 2006; Xu et al., 1982). This status can be caused by conditions such as abiotic stress, extreme temperatures or low-nutrient environment, but the bacteria remain still infectious (Alleron et al., 2008; Dietersdorfer et al., 2018). Cultivation of VBNCs on standard culture media is not possible (England et al., 1982; Hussong et al., 1987). The resuscitation of the bacteria to a culturable form could be achieved for example by the uptake of amoebae such as *Acanthamoeba castellanii* (Steinert et al., 1997).

It is difficult to specify an infectious dose because it depends on the susceptibility of people, virulence status of the bacteria, water source and dissemination of the *Legionella*-containing aerosols but people became ill after only short exposure or even from sources localized up to 3 kilometers away. In the United States, the number of cases of Legionnaires' disease reported to Center of Disease Control and Prevention increased 10-fold in the years 2000-2018 (National Center for Immunization and Respiratory Diseases, 2021).

Infection of the human organism occurs through inhalation of *Legionella* as contaminated aerosols distributed from, for example, air conditioning systems, whirlpools, showers, irrigation systems or dental equipment. Furthermore, stagnating water piping systems, e.g. in hospitals or hotels, in combination with low water temperatures turned out to be high technical risk factors for infections with *Legionella* (Steinert et al., 2002). After inhalation and colonization of the human lung, the bacteria proliferate in alveolar macrophages and epithelial cells (DebRoy et al. 2006).

L. pneumophila can cause two respiratory diseases called Pontiac fever and Legionnaires' disease. Pontiac fever, named for the location of the first outbreak, is an influenza-like, not life-threatening disease. It is characterized by a short incubation time of mostly 8-24 hours and symptoms like fever, chills, cough, impaired sensory perception, and chest, head, and muscle pain. Patients recover within a few days even without antibiotic therapy and no deaths are reported so far (Edelstein, 2007; Robert Koch Institut, 2019b). Legionnaires' disease, on the other hand, causes serious pneumonia, which can lead to death. After an incubation period of 2-10 days, symptoms such as fever, cough, dyspnea, chest pain, diarrhea, vomiting and impairment of the central nervous system can occur (Edelstein, 2007). Mainly elderly people, smokers, people with immunosuppression or cardiovascular problems are considered to be in a risk group for being affected by an infection with the Legionnaires' disease. There is no vaccine available at this time and although treatment with antibiotics is possible, the lethality rate is still between 5-13 % (Buchholz et al., 2010). Human-to-human transmission may be left out because it has only been described in one case (Correia et al., 2016).

All *Legionella* are potential human pathogens. In total, however, about 90 % of all of all Legionnaires' disease are due to *L. pneumophila* (Viasus et al., 2022). As a pathogenic bacterium, *L. pneumophila* requires numerous virulence factors for colonization and manipulation of the host cell. In particular, secretion systems and surface structures serve intracellular survival, replication and transport of effector proteins within the host cell. The intracellular life cycle of *L. pneumophila* is depicted in Figure 2. The uptake of the *Legionella* cell into the host cell occurs mainly via phagocytosis or opsonin-mediated uptake and begins with the binding of the type IV pilus of the *Legionella* cell to the surface receptors of amoebae or macrophages (Bellinger-Kawahara and Horwitz, 1990; Bozue and Johnson, 1996; Stone and Abu Kwaik, 1998). In addition, the Dot/Icm (defect in organelle trafficking and intracellular multiplication) type IV secretion system also plays an important role in the efficiency of phagocytosis. Through the use of effector proteins, the fusion of phagosome and lysosome is prevented, allowing *Legionella* to escape degradation by the host cell (Hilbi et al., 2008). In order to establish a replicative niche, mitochondria, ribosomes, and rough endoplasmic reticulum (ER) vesicles are recruited, associated and fused with the so called Legionella containing vacuole (LCV) (Wieland et al., 2004). Nutrients are extracted from the host cell in order to replicate intracellularly and form flagella. The final step in the intracellular infection cycle is the exit of the host cell mediated by membrane lysis and pore formation to allow transmission to new cells to begin a new infection cycle (Alli et al., 2000; Molmeret et al., 2004; Molofsky and Swanson, 2004).

Also parts of the outer membrane, the Lipopolysaccharide (LPS), is a characteristic component of gram-negative bacteria and its composition vary between bacterial strains which makes it suitable for differentiation (Lüneberg et al., 1998). In the case of *Legionella*, lipid A is composed of long-chain

branched fatty acids and the O-specific side chain contains a repeat unit, the so called legionaminic acid (Knirel et al., 1994; Palusińska-Szys and Russa, 2009; Zähringer et al., 1995). Other important virulence factors at the membrane surface of *L. pneumophila* are the major outer membrane protein (MOMP), the macrophage infectivity potentiator (Mip), the heat shock protein (Hsp60) and the flagellum (Bellinger-Kawahara and Horwitz, 1990; Garduño et al., 1998; Heuner and Steinert, 2003; Hoffman and Garduno, 1999; Horwitz, 1988; Riboldi-Tunnicliffe et al., 2001; Wagner et al., 2007). In addition to Mip, another Peptidyl-Prolyl-*cis/trans*-Isomerase called PpiB has been shown to play a role in growth at extreme temperatures, sliding motility and intracellular replication (Rasch et al., 2019).

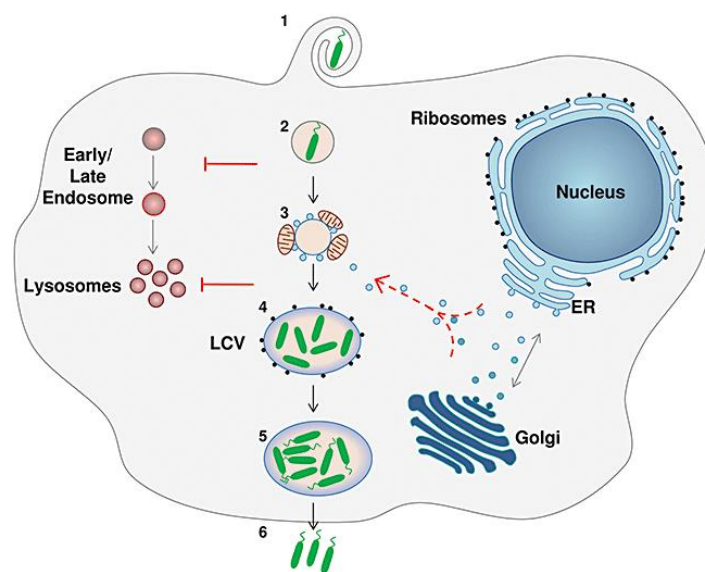


Figure 2: Schematic representation of the intracellular life cycle of *L. pneumophila* in a host cell reprinted from Franco et al. (1) Internalization of the bacteria by the host cell. (2) Prevention of the endocytic pathway by avoiding fusion with endosomes and delivery to lysosomes. (3) Mitochondria and vesicles of the rough ER are recruited to fuse with the phagosome. (4) Formation of an ER-like *Legionella* containing vacuole (LCV) surrounded by ribosomes. (5) *Legionella* begin to replicate intracellularly and become flagellated. (6) Lysis of the host cell results in the release of the bacteria (Franco et al., 2009).

1.5. Detection methods for *Legionella*

Various methods exist for the detection of *Legionella*, which are briefly described below. *Legionella* infections in humans must be reported to the competent state authority and the Robert-Koch-Institute, with detailed information on the source of exposure or the location and facility to enable an infection tracking (Bundesamt für Justiz, 2000; Robert Koch Institut, 2019b). If infection with *Legionella* has been confirmed, disinfection measures must be initiated or the facilities must be closed and renovated (Deutscher Verein des Gas- und Wasserfaches e.V., 2015). In the clinical context, the culture

method, immunological methods or polymerase chain reaction (PCR) are mainly used to detect the pathogens from secretions of the respiratory tract, lung tissue or pleural fluid (Robert Koch Institut, 2019c). For the detection of *Legionella* in water samples, the culture-based method is still most extensively discussed in the regulations. In addition, methods such as flow cytometry or PCR are becoming slowly more relevant for monitoring of water samples. Occasionally, fluorescence *in situ* hybridization is also used to detect *Legionella* contaminated samples.

1.5.1. Culture method

Bacterial infection or water contamination with *Legionella* can be verified by cultivation on a selective nutrient agar. This medium contains besides L-cysteine as an essential amino acid, charcoal, iron pyrophosphate and antibiotics such as Cefazolin or Polymyxin B for the selective growth of *Legionella* (Xebios Diagnostics GmbH, 2022). Nevertheless, it could be seen that also other strains are able to grow on this medium. Human samples, such as sputum, bronchioalveolar lavage, tracheal secretion, lung tissue or pleural fluid can serve as the basis for cultivation (Robert Koch Institut, 2019b).

For water samples, a distinction is made between drinking water and waste water or cooling water. In drinking water installations the highest allowed tolerable value is 100 colony forming units (CFU)/100 ml (Bundesamt der Justiz, 2001). In case of a detection of more than 100 CFU/100 ml, the water-bearing systems must be kept under observation and further sample should be tested (Deutscher Verein des Gas- und Wasserfaches e.V., 2015, 2009). From 1000 CFU/100 ml disinfection measures, such as heat inactivation, are needed and at values of 100,000 CFU/100 ml the plant must be immediately closed and remediation measures must be initiated. For process water the crucial values for evaporative cooling systems and wet separators are 10,000 CFU/100 ml and for cooling towers 50,000 CFU/100 ml (Bundesministeriums der Justiz und für Verbraucherschutz, 2017).

According to the international standard ISO 111731:2017, the latter water samples can be used for direct plating on an agar plate because *Legionella* is expected to exceed 10^4 CFU/l but it cannot be excluded that a high level of accompanying flora is also present. Therefore, an acid treatment (pH 2.2 for 5 ± 0.5 min) or heat (50 ± 1 °C for 30 ± 2 min) treatment should be applied before plating out the *Legionella* to reduce the accompanying flora. In addition, the culture sample should be diluted 1:10 and 1:100 for high bacterial concentrations. Drinking water, on the other hand, usually shows lower values, so membrane filtration can be used for detection in order to concentrate the bacteria present in the sample. Inoculated agar plates are incubated at 35-37°C for 7 to 10 days. *Legionella* can be present in large concentration ranges for the inspection of industrial plants, so both the methods for the low detection limits and the high ones must be combined. Plates should be inspected on day 2, 3, 4 or 5 followed by a final inspection at the end of the incubation period. This can be used to detect

faster growing accompanying flora and to estimate whether further samples with a dilution are needed. *Legionella* is examined morphologically and presumptive colonies are confirmed by transfer to culture plate lacking L-cysteine and iron ("ISO 11731:2017 Water quality - Enumeration of Legionella," 2017). Here the weakness of the culture-based detection method with cultivation times of up to more than 10 days becomes apparent. In addition, cells in the VBNC are not able to detect by cultivation and the medium components enable also the growth of other bacteria such as *Acinetobacter haemolyticus*. These disadvantageous features of the culture method underline why alternative testing methods are needed.

1.5.2. Immunological methods

An urine antigen test is used for the diagnosis of community-acquired and travel-associated infections with *L. pneumophila* serogroup 1. The Enzyme-linked Immunosorbent Assay (ELISA) uses the property of labeled antibodies that specifically bind the target molecules (antigens) to be detected. Successful detection results in a color signal, either in the visible or fluorescent range. The antigen used for serological characterization of *L. pneumophila* serogroup 1 is the O-specific side chain of the LPS, which is excreted not only in urine but also in blood. In the latter, the concentration is usually too low for detection (Bibb et al., 1984; Lüch and Steinert, 2006). The antigen detection can be performed already 24 hours after the first symptoms appeared (Formica et al., 2001). However, it is not recommended for sole surveillance of hospital-acquired infections, since they are often also caused by strains of other serogroups or other species (Lüch and Steinert, 2006; Robert Koch Institut, 2019b).

Antibodies can also be applied in an ELISA to detect the pathogen from water samples. LPS can also serve as an antigen as in clinical assays as well as polyclonal antibodies generated by immunization with inactivated whole cell preparation of *Legionella*. Polyclonal antibodies bear the risk of binding unspecifically to other species, whereas monoclonal antibodies can bind specifically, the detection of only specific serogroups and not all *Legionella* strains are possible (Aurell et al., 2004; Kirschner et al., 2012).

In addition, a serological test can be used to detect an infection caused by *Legionella*. Here, the immune status of the diseased patient is examined with regard to the formation of antibodies against the bacterium and are detected by indirect immunofluorescence (Lüch et al., 2002). Pool antigens consisting of 4-6 individual antigens are used to test the increase in titer (Lüch and Steinert, 2006). In practice, it is therefore impossible to include all serogroup variants in one test. A serological diagnosis of *L. pneumophila* can also be performed using an ELISA with 5 purified proteins as coating antigens (H. Sun et al., 2015). Human antibodies directed against the bacterial cells can only be detected a few weeks after the onset of the disease and therefore often provide only a retrospective diagnosis (Cunha

et al., 2016; Robert Koch Institut, 2019b). Furthermore, 30 % of patients do not produce antibodies against *Legionella* and are therefore not suitable for this test (World Health Organization, 1993).

1.5.3. Polymerase chain reaction

PCR is possible with urine, respiratory and serum samples. After melting the DNA into two single strands, two short nucleotide strands bind to the outer ends of the gene segment to be detected and a polymerase completes the missing strand. Specific temperatures can be used to control the steps of denaturation, annealing and elongation to amplify the original sequence exponentially over several heating cycles. The advantage of PCR, besides its sensitivity, is its broad detection spectrum. Thus, genus- or species-specific primers can be used for the detection and differentiation of *Legionella* strains and are superior to an antibody-based detection. Gene sequences of the 5S (Ramirez et al., 1996) and 16S rRNA (Lisby and Dessau, 1994; Cloud et al., 2000) are used for the detection of *Legionella* spp. and the *mip* gene for the detection of *L. pneumophila* (Matsiota-Bernard et al., 1994). The detection limit of this technique depends on the sample type, extraction method and background of the sample and varies from 2 CFU to > 200,000 CFU/ml of clinical specimen (Rantakokko-Jalava and Jalava, 2001).

As with clinical detection, the gene segments of the 5 or 16S rRNA or the Mip protein can be targeted to detect *Legionella* in water samples (Miyamoto et al., 1997). Primers specific for *lacZ* and *lamB* genes are used for the detection of coliform bacteria and those associated with human fecal contamination (Bej et al., 1990; Mahbubani et al., 1990). PCR is often considered as the most convenient and accurate method. A major difficulty by using this method is the cell calculation, as qPCR results are expressed as genetic units (GU) and most water related guideline refer to CFU. No general correlation factor is established yet and implemented in the guideline, leading to individual determination within ranges of 4-1000-fold higher qPCR results than CFU (Ditommaso et al., 2015; Joly et al., 2006; Lee et al., 2011; Toplitsch et al., 2018; Whiley and Taylor, 2016; Yaradou et al., 2007). As already mentioned cells in the VBNC-status are not detectable by cultivation and also genetic material released from dead cells is amplified by qPCR leading to higher values of GU than CFU (Toplitsch et al., 2021).

1.5.4. Flow cytometry

Fluorescently modified antibodies are used to label *Legionella* cells and to detect and quantify them cytometrically. The bacterial suspension is fed into a sheath stream which concentrates the stream until the cells are isolated. The samples are analyzed by excitation with a laser beam, where emission or scattering is detected and read out with a photomultiplier. The advantage of the Fluorescence activated Cell Sorting (FACS) lies in the potential for cell quantification, observation of heterogeneity

of the cell population and differentiation of dead and living cells as well as metabolic activities (Berney et al., 2008; Davey, 2011; Jepras et al., 1995). One protocol described can perform the detection of *L. pneumophila* within 180 min with a detection limit of around 500 cells/l and a recovery of *Legionella* cells of 52.1 % out of spiked tap water (Füchslin et al., 2010). Fluorescent dyes are used that can stain the intact membrane of living cells (Syto 9) or intercalate into the DNA of dead and membrane-perforated cells (Propidium iodide) for differentiation (Allegra et al., 2008).

1.5.5. Fluorescence *in situ* hybridization

Fluorescence *in situ* hybridization (FISH) is known as a technique using short fluorescent labeled DNA or RNA probes for the detection and visualization of specific DNA or RNA targets in samples (Frickmann et al., 2017). After the first *in situ* hybridization experiments were performed using radioactive labeled probes, the term FISH was formed after the radioactive labels were replaced by fluorescent labels in hybridization probes (John et al., 1969; Pardue and Gall, 1969; Rudkin and Stollar, 1977). With properties such as greater safety, stability, and ease of detection, FISH was first mainly used for the detection of gene loci on chromosomes (Shakoori, 2017). FISH offers the possibility of direct quantitative imaging, which makes it interesting not only for cell biological research, but also for species identification and medical diagnostics (Huber et al., 2018).

For the detection of *Legionella*, oligonucleotide probes complementary to specific regions of 16S rRNA were designed which allows the differentiation of *L. pneumophila* from other *Legionella* species (Deloge-Abarkan et al., 2007; Grimm et al., 1998; Manz et al., 1995). After the *Legionella* cells were concentrated and fixed on a filter, they were permeabilized and incubated with the labeled probe, washed and dried, and finally visualized by epifluorescence or laser scanning microscopy. FISH can also be used for the detection of *Legionella* in water sample, lung specimen, internalized in amoeba or biofilms (Buchbinder et al., 2004; Declerck, 2010; Moreno et al., 2019). In hybridization experiments based on a catalyzed reporter deposition (CARD-FISH), an enzyme, for example horseradish peroxidase (HRP), is coupled to the probe instead of a fluorophore and the target hybridization is detected by the addition of a fluorescent substrate (e.g., fluorochrome-labeled tyramides). This makes a signal enhancement possible, because several fluorescent molecules can be introduced and lead to a signal compared to a probe with only one single fluorophore (Pernthaler et al., 2002). Using this method a detection limit of 3.5×10^2 cells/100 ml within 24 hours was claimed (Kirschner et al., 2012). A challenge of the FISH technique is the diffusion of the large modified probes into the fixed cells which includes a carefully permeabilization step to ensure still the integrity of the investigated cells (Amann et al., 1992; Schönhuber et al., 1999). Of course also combinations of techniques arose for example

using oligonucleotide probes for real-time PCR or in context with a microbead quantum-dots detection system in flow cytometry (Templeton et al., 2003; Wu et al., 2016).

Besides linear probes, often molecular beacon probes are used in FISH-based assays, to obtain better discriminatory power by a low signal-to-noise ratio (Lenaerts et al., 2007). A single stranded (ss) molecular beacon structure consists of four parts as schematically illustrated in Figure 3. First, the loop domain which is the region that is complementary to the target sequence. The length of the loop can vary between 18-45 bp. Second the stem structure, 5-7 bp long oligonucleotides that are complementary to each other and attached to both ends of the loop region. The length of the loop should be at least twice the length of the stem to ensure a conformational change upon hybridization and sufficient distance between fluorophore and quencher for fluorescent excitation (Tyagi and Kramer, 1996). To one end of the stem structure a fluorophore of choice is attached and to the other terminus an appropriate quencher is positioned. The fluorophore and the quencher should be selected with respect to compatible emission and absorbance spectra, respectively. The loop region causes the recognition of the target sequence, whereas the stem structure leads to a self-hybridization resulting in a hairpin conformation of the probe. In a closed state the fluorophore and quencher are in close proximity and the quencher prevents fluorescent emission by absorbing the light of the fluorophore. After hybridization of the probe with the target DNA, the fluorophore is no longer next to the quencher and excitation of the fluorophore results in a detectable fluorescence emission.

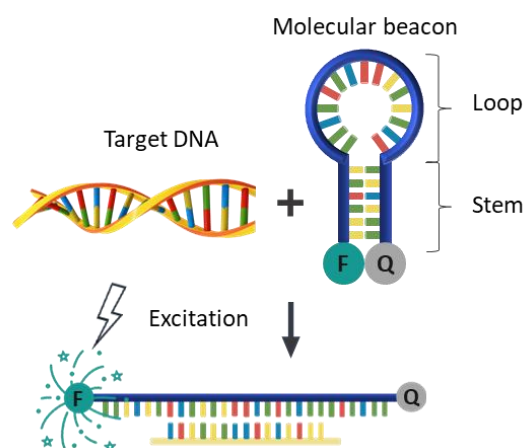


Figure 3: Schematic illustration of structure and detection principle of a fluorescently labeled molecular beacon probe. In absence of the appropriate target the probe is closed in a hairpin structure by self-hybridization of the stem structure. Fluorophore (green circle) and quencher (grey circle) at the ends of the probe are in close proximity leading to a suppression of the fluorophore emission. The presence of the target leads to an opening of the hairpin and fluorescence signal upon binding of probe and target.

1.6. Fiber-based microfluidic devices

In the last two decades enormous progress in the development of microfluidic systems for the application in biological and chemical research, as well as industry has been made. The need for miniaturized analytical systems using reaction volumes in dimensions from microliter to nanoliter scale and easily controlled physical processes and instrumental dimensions is increasing constantly (Berlanda et al., 2021; Wang et al., 2022). Rapid measurements can be obtained in fully-integrated and robustly operating microfluidic devices in diverse contexts (Chiu et al., 2017; Li et al., 2021). Besides utilization in a laboratory environment, microfluidic devices have the great advantage of being designed as on-site operational systems utilizable by the end-user (deMello, 2006; Sachdeva et al., 2021).

Paper-based microfluidics represent an important variant to traditional microfluidic devices made of silicon or polymer substrates (Convery and Gadegaard, 2019). The term microfluidic paper-based analytical device (μ PAD) was mainly defined by the Whitesides group in 2007 by pioneering work on a simple, low-cost but robust paper platform to detect glucose and bovine serum albumin (BSA) in artificial urine (Martinez et al., 2007). While most μ PADs were developed using cellulose filter papers, the term “paper-based” now covers also a variety of other porous materials with functional properties, such as nitrocellulose, chitosan or polyethersulfone (Hillscher et al., 2021; Magro et al., 2017; Noviana et al., 2021; Wang et al., 2022). Paper properties like flexibility, small diameter, light weight, hydrophilicity, high surface area and optional biocompatibility makes it an interesting candidate for microfluidic applications (Nishat et al., 2021). Affordable costs, simple and fast fabrication around the world combined with portability, disposability and simplicity of operation make μ PADs suitable for untrained people (Hoang et al., 2021). Further advantages of μ PADs include independence from expensive equipment, e.g. in less industrialized countries or in emergency situations, and applicability in home health care (Nie et al., 2013). Moreover diverse 3D-structures can be built by folding several paper layers (Liu and Crooks, 2011; Martinez et al., 2008b). The liquid transport is achieved by capillary forces without the need of external pumps. Furthermore functional groups depending on the material (e.g. accessible hydroxyl groups for cellulose-based papers) makes a distinct immobilization of molecules by chemical coupling possible (Tang et al., 2019). Rapid verification of μ PADs makes them an attractive candidate for environmental monitoring, food analysis or medical diagnosis. As μ PADs describe an innovative technology with potential for technically simple multiplexed assay and products for commercialization (Akyazi et al., 2018). Storage of chemicals on paper substrate in a dried state is a promising aspect to efficiently process and analyze molecular reactions independent of elaborate storage (Seok et al., 2017).

1.6.1. Fabrication techniques

Patterning and structuring capability of most papers by **cutting, photolithography, printing wax or inkjet, etching, laser treatment, flexography, lacquer spraying, screen-printing, ink stamping or plasma treatment** made it possible to create defined reaction areas e.g., channels in which concrete fluid transport is obtained. In the following, these methods are briefly described to provide some insight.

A convenient way for the integration of a structure in paper-based materials is by **printing** for example **ink** (Abe et al., 2008; Xu Li et al., 2010a) or **wax** (Carrilho et al., 2009a; Lu et al., 2010). For these methods a printer and an oven are needed. The printer applies the hydrophobic waxy polymer or ink directly on the paper substrate. By the application of heat the ink is dried or the wax is melted and penetrating the interspaces of the fiber material, resulting in a hydrophobic barrier after cooling to room temperature. Suitable inks for example are alkyl-ketene-dimer (Xu Li et al., 2010b) or an activatable acrylate mixture, the latter is fixed by the exposure to UV light instead of heat (Maejima et al., 2013).

The design of patterns onto paper by **photolithography** was developed by the Whiteside's group using a mask consisting of the design of interest, photoresist and a UV light source (Martinez et al., 2007, 2008c). The irradiated zones generate a polymeric boundary towards the interior of the channel. Unpolymerized photoresist is removed in most cases by rinsing the substrate in alcohol.

Lacquer spraying represent another mask using technique. An iron mask including the pattern of interest is placed on the paper and fixed by a magnetic plate on the opposite side. The uncovered areas are moisted by an acrylic lacquer upon spraying (Nurak et al., 2013).

For **screen printing** also melted wax or a polystyrene solution can be used for pouring through screen onto the below lying fiber material. The screen is containing the desired layout as negative image and blocking the not required areas for example with a photo emulsion.

Laser treatment can be used to cut hollow structures via a CO₂ Laser into the paper substrate preventing the fluid to pass beyond the burned border (Nie et al., 2013). As an alternative, the paper can be impregnated with a photopolymer and the pattern engraved by CO₂ laser illumination with the width of the laser. Un-polymerized regions are cleaned with isopropanol (Sones et al., 2014).

By using **etching** as a patterning method, the fiber material is immersed in trimethoxyoctadecylsilane followed by the alignment of a mask consisting of paper wetted with a sodium hydroxide (NaOH) solution. Consequently, the prior silanized paper is etched in the masked region and becomes hydrophilic again (Cai et al., 2014).

Flexography uses the roll-to-roll printing process found in many printing companies. Relief patterns in the printing plate are filled with a polystyrene solution in toluol and transferred to the paper by two other rolls resulting in hydrophobic barriers upon contact with the hydrophobic ink (Olkkonen et al., 2010).

Ink stamping is using a Polydimethylsiloxane (PDMS) stamp which is dipped first into an indelible ink and then on the paper substrate. This method is fast but the PDMS stamp requires several hours in preparation to ensure a constant ink volume to transfer (Curto et al., 2013).

For **plasma treatment** the fiber material is placed between two metal masks and exposed to a plasma. Either the paper was immersed with alkyl-ketene-dimer dissolved with n-heptane, dried and exposure to vacuum plasma (X. Li et al., 2008) or a direct polymerization without pretreatment using fluorocarbon plasma can be used (Kao and Hsu, 2014).

1.6.2. Detection principles and applications

With solid functionality comparable to conventional microfluidic devices, paper-based microfluidics already offers an attractive alternative in some diagnostic and analytical applications (Magro et al., 2017; Papatheodorou et al., 2022; Qin et al., 2021; Sachdeva et al., 2021; Tseng et al., 2021). It is important to mention that not all reaction steps are usually carried out on the fiber, but the fiber is often used only for detection or signal readout. A complete integration of an assay on a fiber-based material therefore means special challenges. However, μ PADs represent already an attractive alternative for analyte detection using especially **colorimetric, chemiluminescent, fluorescent and electrochemical methods**.

Colorimetric based detection systems in paper-based microfluidics are the best-known detection technique including, the lateral flow test for detecting pregnancy. In general, the detection reaction leads to a color change indicating qualitative or quantitative results. Colorful indicators which are oxidized upon specific oxidase enzymes can be used for the semi-quantitative detection of glucose, lactate and uric acid in urine and serum (Dungchai et al., 2010). A β -Galactosidase-based colorimetric paper sensor was developed for the determination of heavy metals for example copper, lead, silver, mercury, cadmium, chromium and nickel (Hossain and Brennan, 2011). Liver function could be detected by colorimetric paper-based assay using alkaline phosphatase (AST), aspartate aminotransferase (ALP), and total serum protein as markers and designed to require only a drop of blood from a patient's finger for detection (Vella et al., 2012). High levels of AST, ALP and low level of total serum protein indicate a liver dysfunction occurring from infections like hepatitis A-C or HIV,

abuse of alcohol or reaction to medication. Upon exposure to the substrate cysteine sulfinic acid, levels of AST can be measured by the generation of sulfite ions that cause a colorimetric indication of the sulfite-reactive dye triarylmethane (Maupin, 1993). ALP concentrations can be determined by measuring the p-nitrophenol formation upon hydrolysis of p-nitrophenyl phosphate (Wilkinson et al., 1969). The total serum protein was determined by the reaction with Coomassie Brilliant Blue G-250. The binding of the dye to alkaline and aromatic side chains of the amino acids result in a absorption shift from 465-595 nm causing a color change from reddish brown to blue (Bradford, 1976). Colorimetric detection in μ PADs were also developed for the detection of viruses e.g., the Zika virus. A pH indicator-based colorimetric assay for the detection of the Zika Virus in tap water, human urine, and blood plasma was developed in 2018. Upon a reverse transcription loop-mediated isothermal amplification (RT-LAMP) for increasing the target sequence to a detectable range, a color signal upon the conversion of phenol red in the master mix reagent of the amplification from red to yellow occurred after the target presence (Kaarj et al., 2018). For the pH dependent dyes it should be noted that high concentrations of cations like calcium and magnesium in tap water can generate false positive color output and also the reliability of primer annealing and amplification can be reduced by cations (Kaarj et al., 2018). Also the detection of food pathogens such as *E. coli*, *Salmonella* spp., and *Listeria monocytogenes* was achieved by a colorimetric assay. A color change from yellow to red-violet was used for the determination of *E. coli* upon the reaction of β -galactosidase with chlorophenol red- β -galactopyranoside. *L. monocytogenes* and *S. enterica* were determined by a color change from colorless to blue or purple, respectively, occurring from the reaction of phosphatidylinositol-specific phospholipase C with 5-bromo-4-chloro-3-indolyl-myo-inositol phosphate and esterase with magenta caprylate (Jokerst et al., 2012). Additionally, *E. coli* could be detected via a paper-based chip in combination with thermoresponsive hydrogels. The liquid release from the hydrogel reservoirs after a heat stimulus, dissolved and premixed the assay reagents and led to a colorimetric detection using a HRP-labeled antibody (Niedl and Beta, 2015).

Simultaneous detection of glucose and uric acid in artificial urine could be achieved by Yu et al., with the reaction of glucose and urate oxidase and was used to visualize the **chemiluminescent** reaction of rhodanine derivative and hydrogen peroxide (Yu et al., 2011). Monitoring blood glucose levels is important for patients with for example diabetes, high cholesterol or obesity (Miyashita et al., 2009). Uric acid on the other hand can be relate to a disease of kidney, heart or blood pressure failure (Gagliardi et al., 2009; Johnson et al., 2003; Yu et al., 2011). A chemiluminescence immunoassay based on a luminol hydrogen peroxide reaction catalyzed by silver nanoparticles could be established for tracking tumor markers to predict for example liver, germ cell, intestinal or pancreatic cancer in a origami folded paper-device (L. Ge et al., 2012; Li, 2001)

The equivalent of 96 and 385-well plates on filter paper combined with conventional microplate readers for measuring absorbance and **fluorescence** has been reported previously. A detection limit of 125 fmol of a fluorescein-labeled bovine serum albumin on a cellulose filter material showed great potential for the read-out of fluorescence-based assays (Carrilho et al., 2009b). Furthermore, a combination of a paper device with target specific aptamers for the recognition of cancer cells was reported. Bioconjugates consisting of silica nanoparticles coated with quantum dots and fluorescent labeled aptamers are adsorbed to graphene oxide. The signal occurred upon the binding of the aptamers to their respective cancer cells and caused the probe being unquenched by the graphene oxide and showing a fluorescence signal (Liang et al., 2016). Also a combination with isothermal DNA amplification was reported in the literature. The amplification of the *mip* gene for the identification of *Legionella* was performed at 38°C for 25 min using the endonuclease nfo provided in the TwistDx-Kit. The amplicon is labeled with Digoxigenin and Fluorescein after amplification and introduction of a fluorescently labeled probe. For read-out the amplification product was applied to a commercially available lateral flow strip leading to visible detection lines upon reaction with immobilized anti-digoxigenin antibodies on the stripe surface and gold nanoparticles conjugated with anti-6-Carboxyfluorescein (FAM) antibodies (Kersting et al., 2018). A fluorometric paper-based device was developed recently to quantify MRSA. The assay principle was based on amplification by Loop-mediated isothermal amplification (LAMP) with biotinylated primers and for the detection streptavidin immobilized on the paper strip was used to bind the amplified target. A SYBR Green-based read-out was chosen to detect the amplicon (Choopara et al., 2021). Also carbon dioxide can be measured fluorescently on paper by the formation of carbonic acid and protonation-induced fluorescence color shifting of a chromophore coated on the fiber and can act as a sensitive gas sensor in facilities and buildings (Wang et al., 2020).

Electrochemical sensors on paper-based substrates includes beside glucose, lactate and uric acid (Dungchai et al., 2009) also dopamine (Rattanarat et al., 2012), drugs (Shiroma et al., 2012) or cancer markers (S. Ge et al., 2012). A sensor system for the detection of acetaminophen and its nephrotoxic byproduct 4-aminophenol was developed by voltammetry and amperometry using gold sputtered electrodes on the cellulose paper strip. Screen-printed carbon electrodes on a ceramic substrate were connected to a cellulose filter paper, and the anionic surfactant sodium dodecyl sulfate (SDS) was used to detect an oxidation shift in dopamine levels, which, when it reaches abnormal levels, can lead to Parkinson's, Alzheimer's or schizophrenia, for example (Rattanarat et al., 2012).

Multiplexed analysis of several parameters are a promising detection possibility in combination with paper-based wearable sensors. The detection of metabolites e.g. glucose or lactate or chemicals such as chloride, as well as toxins, pH changes, rate of respiration, volume of sweat or pathogenic nucleic

acids signatures can be implemented in such kind of sensors (Ardalan et al., 2020; Colozza et al., 2019; Gao et al., 2018; Güder et al., 2016; Nguyen et al., 2021). In addition, μ PADs able to determine physical parameters for example heart rate or blood pressure were developed recently (Ardalan et al., 2020; Luo et al., 2015; Nguyen et al., 2021).

1.7. Electrophoresis

A popular method for the separation of DNA, RNA and protein containing molecular samples is electrophoresis, which is defined as the migration of charged particles in a viscous medium under the influence of an electric field. After separation of a sample mixture, the individual components can be visualized on the carrier material with the help of suitable reagents. Various matrices have been tested for separation. The most commonly used ones today are agarose gels for separation of DNA samples and polyacrylamide gels for the separation of proteins. However, fiber-based materials can also be used to achieve an electrophoretic separation.

Fiber-electrophoresis, also known as iconography, was first described in more detail between 1954-55 (Lederer, 1955; McDonald, 1955; Wunderly, 1954). Mainly sophisticated experimental setups were described, which usually consisted of a bridge of filter paper between two buffers and by applying the electric field the charged particles migrated from one to the other buffer reservoir on the strip. It has been predominantly used for the separation and identification of proteins, amino acids for example e.g. histidine and glutamic acid, serum albumin, and polyamines e.g. putrescine, spermidine and spermine or complex-ion formation (Fujita et al., 1980; McDonald et al., 1951; McLoughlin, 1961). After drying at high temperatures and labeling by spraying solutions containing ninhydrin, butanol or bromocresol-green on the filter paper, the migrated samples could be detected. A paper-based electrophoresis system for nucleic acids in order to separate purine, pyrimidine and nucleotide derivatives was investigated in 1967 (Smith, 1967). An electro-generated chemiluminescence under strongly alkaline conditions and at 330 V was used for the separation of serine, aspartic acid, and lysine on a cellulose filter (Ge et al., 2014). Also a low voltage paper-based origami device for the detection of fluorescent molecules and proteins was developed (Luo et al., 2014). BSA, calf serum and an antibody were labeled fluorescently and detected on this folded cellulose filter paper connected to plastic buffer reservoirs and Ag/AgCl electrodes. Recently the electrophoretic separation of synthetic RNA mimicking viral and human RNA in a capillary paper-based electrophoresis was reported (Na et al., 2021). Also isotachopheresis (ITP) was implemented on fiber-based substrates for the basic investigation of the electrophoretic migration of fluorescent dyes (Rosenfeld and Bercovici, 2014). ITP uses electrolytes with different mobilities, combining a fast migrating leading electrolyte and a

terminating electrolyte with slower electrophoretic mobility. After application of the electric field, the ions are concentrated in zones in the order of their mobility (Chen et al., 2006). Also a origami devices, consisting of 11 layers but with consistent fiber alignment was developed to pull a DNA sample across a cellulose channel using ITP (Li et al., 2015).

Instead of a cellulose-based matrix also a glass fiber was used for the electrophoretic separation of polysaccharides and for differentiating certain specimens of glycogen from various sources (Briggs et al., 1956; Lewis and Smith, 1957). The advantage of glass microfiber over cellulose was that complexing between polysaccharides and the fiber material were avoided (Bourne et al., 1956). Glass microfibers made of borosilicate glass show a high loading capacity, rapid flow rate and heat stability up to 500°C. Long strips of fiber were connected between two buffer filled tanks and after exposure to an electric field energy storing polysaccharides for example from calf liver, seaweed, rye flour or birch wood could be distinguished (Lewis and Smith, 1957). But the application was not as user-friendly as the further developed cellulose-based assays.

2. Material and methods

2.1. Instruments

Table 3: Instruments and manufacturer

Device	Company	Type
Analog-digital-converter	Adafruit Industries	ADS1115
Attune flow cytometer	Thermo Fisher Scientific	NxT
Autoclave	VWR	VAPOUR-Line
Biosafety cabinet	Telstar	Bio II Advance
Centrifuge	Hitachi Koki Co Ltd.	HFC 134a
Counting chamber	Marienfeld	Neubauer improved
Deep freezer -80°C	Fryka Kältetechnik	-
DNA workbench	VWR	PCR workstation
Gel chamber & power source	PerfectBlue L	VWR
Gel documentation system	VWR	Chemi Premium Imager
Heat press	Helo GmbH	T-shirtpresse 173777
Incubator	Lovibond	-
Microscope	Andonstar	Digital Microscope ADSM302
Microscope	Nikon	Eclipse Ci microscope bright field
Microscope	Olympus	DSX 500
Microwave	Moulinex	Compact Vario Grill Ep1
Multimeter	Conrad Electronics	Voltcraft VC820 multimeter digital
Opamps LT1056	Reichelt Elektronik	-
Oven	Binder	10-05517
Paste dispenser	Voltera	PCB Printer Voltera V-One
Pin electrodes	Hwato	Acupuncture needle
pH-Meter	Velp Scientifica	HSC IS2100L
Pipettes	Eppendorf	Research Plus
Raspberry pi	Reichelt Elektronik	Zero W V1.1 - 2016
Real-Time PCR Thermal Cycler	Analytic Jena GmbH	qTower ³
Scale	VWR	SMI245 Di
Screen printing machine	Siebdruckversand	FLAT-DX 300
Shaker	Grandbio	PSU-10i
Spectral photometer	Thermo Fisher Scientific	NanoDrop
Thermal cycler	VWR	peqSTAR
Thermoblock	VWR	Thermal Shake lite
Ultra-pure water system	VWR	Puranity TU 7 PU20
Vacuum pump	Integra	Vacusaft
Voltage source	Komerzi Elektronik	QJI 2001X
Voltera PCB printer	V-One	Voltera Inc
Vortexer	Velp Scientifica	ZX3 Advanced Vortex Mixer
Wax pinter	Xerox	ColorQube 8570

2.2. Materials

General consumables, such as serological pipettes, pipette tips for manual single- and multi-channel pipettes, disposable cuvettes, sterile filters, cryotubes, sterile syringes and reaction tubes were purchased from various companies, such as VWR, Brand, Eppendorf, Thermo Fisher and Neolab. All other electronic components e.g., board, resistors and cable were obtained from Reichelt Elektronik.

Chemicals were ordered from Carl-Roth, Sigma-Aldrich, VWR, GE Healthcare. Special consumables are listed in Table 4.

Table 4: Materials and manufacturer

Name	Company
1 x reaction buffer (diluted from Biozym Taq 10 x reaction buffer)	Biozym Scientific
2 x InnuMix qPCR SyGreen	Analytic Jena GmbH
50 x TAE	VWR
Adhesive foil	Simport Scientific
Overhead film	Office Tree
Agarose pure grade	PeqGOLD
BCYE + AB agar plates	Xebios
Bottle-top filter Polyester 0.2 µm	VWR
BseSI FD1444	Thermo Fisher Scientific
Carbon Paste C2000802P2	Sun Chemical
Cartridge Pack 1000030	Voltera
Cellulose paper A388 (average pore size 12-15 µm)	Ahlstrom-Munksjö
Cellulose paper MN 640 M (average pore size 4-12 µm)	Macherey-Nagel
Cellulose paper MN 640 W (average pore size 7-12 µm)	Macherey-Nagel
ChemChrome V6	Biomerieux
Chitosan fleece Vilmed 121-003-1	Freudenberg
Cooling rack	VWR
Copper varnish EMV 35	Conrad
Crocodile clamps SKS Hirschmann AGF 2	Conrad Elektronik
Cover glass	VWR
dNTPs	Thermo Fisher Scientific
Foil - Ziplock bag 40932	Storopack
GelRed Nucleic Acid Gel Stain 10,000 x in water	Biotium
Glass microfiber GF/A (average pore size 1.6 µm)	Whatman/GE Healthcare
Glass microfiber GF/B (average pore size 1.0 µm)	Whatman/GE Healthcare
Glass microfiber GF/D (average pore size 2.7 µm)	Whatman/GE Healthcare
Glass microfiber GF/F (average pore size 0.7 µm)	Whatman/GE Healthcare
Glass microfiber MN85/220 BF (average pore size 0.4 µm)	Macherey-Nagel
Gold coated contact fingers WE-SECF SMT EMI	Würth Elektronik
HaeIII R0108S	NEB
HhaI R0139S	NEB

Horseradish peroxidase	Alfa Aesar
HpaI R0105S	NEB
HpaII R0171S	NEB
Incoluation loop 90 % platinum, 10 % iridium	VWR
Kohrsolin FF	Hartmann Bode
Long Pass Filter (LED GreenModule)	VWR
Mouse-anti- <i>Legionella</i> serum A	New/era/mabs
Mouse-anti- <i>Legionella</i> serum B	New/era/mabs
Methylene blue	Sigma Aldrich
Midori Green Advance	Biozym Scientific
Mini-Bag Sealer	Amazon
Nozzle 1000375	Voltera
Nylon membrane Type FH	Merck Millipore
One-Step Blue protein stain	VWR
PEDOT:PSS 655201	Sigma-Aldrich
Polyethersulfone-Polyethylene-Fleece Vilmed 121-003-4	Freudenberg
Screen mesh PET 1500 61/156-70	Farben Frikell Berlin GmbH
SeramunBlue-fast	Seramun Diagnostica
Shaking flask	VWR
Silver conductive ink AG-500A	Applied Ink Solutions
Silver Nano Particle Ink NBSIJ-MU01	Mitsubishi Paper Mills Limited
SmlI R0597S	NEB
Taq DNA Polymerase (5 u/μl)	Biozym Scientific
Textile dye Novacron Brilliant Blue FN-G	Kremer Pigmente
Textile dye Orange F-BR	Kremer Pigmente
Voltera-software V-One V3.0.0	Voltera

Table 5: Strains

Name	Reference	Source
<i>Legionella pneumophila</i> subsp. <i>pneumophila</i> Philadelphia-1	DSM 7513; ATCC 33152; Brenner et al. 1979	Leibniz Institute DSMZ-German Collection of Microorganisms and Cell Cultures
<i>Legionella anisa</i>	DSM 17627; ATCC 35292; Gorman et al. 1985	Leibniz Institute DSMZ-German Collection of Microorganisms and Cell Cultures
<i>Legionella dresdenensis</i>	DSM 19488; NCTC 13409; Lück et al. 2010	Leibniz Institute DSMZ-German Collection of Microorganisms and Cell Cultures
<i>Escherichia coli</i>	DSM 1103; ATCC 25922; Migula 1895; Castellani and Chalmers 1919	Leibniz Institute DSMZ-German Collection of Microorganisms and Cell Cultures
<i>Pseudomonas aeruginosa</i>	PA500; DSM 24600; Schroeter 1872; Migula 1900;	Leibniz Institute DSMZ-German Collection of Microorganisms and Cell Cultures

<i>Escherichia coli</i>	Isolated from wild boar	New/era/mabs
<i>Sphingomonas paucimobilis</i>	Identified by MALDI-TOF analysis from the Ripac laboratory	Isolated from drinking water
<i>Acinetobacter haemolyticus</i>	Identified by MALDI-TOF analysis from the Ripac laboratory	Isolated from tap water sample
<i>Serratia marcescens</i>	Identified by MALDI-TOF analysis from the Ripac laboratory	Isolated from tap water

Table 6: Buffers and solutions

TAE-buffer	TRIS-Acetat-EDTA-buffer
40 mM 20 mM 1 mM	Tris Acetic acid EDTA pH 7.8

Elution buffer 1	
10 mM 0.1 mM 0.04 %	Tris EDTA NaN ₃ pH 8.3

Elution buffer 2	
10 mM 1 mM	Tris EDTA pH 8.0

Elution buffer 3	
50 mM 1 mM 1 mM	Tris EDTA NaCl pH 8.5

Elution buffer 4	Elution Buffer NE (Macherey-Nagel, 2008)
5 mM	Tris pH 8.5

Alkaline extraction buffer	
125 mM	NaOH
1 mM	EDTA
0.1 %	Tween 20

Neutralizing buffer	
125 mM	HCl
10 mM	Tris HCl

1 x PBS	Phosphate-buffered saline
137 mM	NaCl
2.7 mM	KCl
10 mM	Na ₂ HPO ₄
1,8 mM	KH ₂ PO ₄
	Dissolved in 1 l ultrapure water.

TMB solution	
120 mM	TMB
2.5 ml	DMSO
2.5 ml	EtOH (≥ 99.8 %)
	Stored at 4°C in the dark.

Gallatibuffer	
10.5 g	Citric acid monohydrate
	Dissolved in 250 ml ultrapure water.
	Adjusted to pH 3.95 with NaOH.

Kits:

The QIAamp DNA extraction Kit Mini from QIAGEN and GFX PCR DNA and Gel Band Purification Kit from GE Healthcare were used for the extraction of genomic DNA (gDNA). Bacterial DNA extraction was carried out according to the manufacturer's instructions for isolation of gDNA from bacterial plate cultures. The spin procedure was used for all extractions described in this work. The lysis step was performed at 56°C and 500 rpm in a thermoblock for 30 min. Elution volume was adapted to 100 µl in distilled Nuclease-free water or Tris buffer.

2.3. Microbiological methods

2.3.1. Bacterial cultivation and storage

Under sterile conditions some material of the cryocultured bacteria were taken by a sterile inoculation loop and distributed on the appropriate growth medium. All *Legionella* strains were incubated on Buffered Charcoal Yeast Extract (BCYE) agar plates from Xebios, containing antibiotics for selectivity, at 37°C in a humidity chamber for three days. Liquid cultures were inoculated in Yeast Extract Broth (YEB) and incubated at 37°C and 180-200 rpm on a shaker in an incubator. For this purpose, some bacterial material was taken from an agar plate with a sterile inoculation loop and added to a desired volume of YEB medium for example 25 ml in a 100 ml shaking flask.

E. coli, *P. aeruginosa*, *S. paucimobilis*, *A. haemolyticus* and *S. marcescens* were cultured on LB agar plates for one day. For a liquid culture, the bacterial cells were transferred from the agar plate into liquid LB medium using an annealed inoculation loop and are incubated for 24 h at 37°C and 200 rpm. To avoid spontaneous mutations, the bacterial culture should always be freshly prepared. The media required for the cultivation of bacteria are listed in Table 7.

For a long-term storage, the corresponding bacterial culture was spread out on an agar plate and incubated under standard conditions as described above. The bacterial material was collected by a sterilized inoculation loop and resuspended in 700 µl sterile 1 x PBS. Afterwards, the bacterial suspension was mixed with 500 µl of autoclaved 100 % glycerol in a cryotube and stored at -80 °C in the freezer. For inoculation the cryotubes can be removed from the -80°C, some material can be collected with a sterile inoculation loop and transferred to the appropriate growth medium.

Table 7: Bacterial growth media

YEB-medium	Yeast Extract Broth medium
10 g	ACES
10 g	Yeast Extract
0,4 g	L-cysteine
0,25 g	Iron pyrophosphate
	Dissolved in 1 l ultrapure water, adjusted to pH 6,9 with Potassium hydroxide and sterile filtered by a bottle-top filter (0.2 µm pore size) under vacuum.

LB-medium	Lysogeny Broth medium
10 g	Tryptone
5 g	Yeast Extract
5 g	Sodium chloride
	Dissolved in 1 l ultrapure water and sterilized by autoclaving.

LB-agar	Lysogeny broth agar
10 g	Tryptone
5 g	Yeast Extract
5 g	Sodium chloride
15 g	Agar
	Dissolved in 1 l ultrapure water and sterilized by autoclaving.

Table 8: Oligonucleotide sequences tested in this work were purchased from Sigma-Aldrich or Biomers.

Primer/probe	Sequence 5' - 3'	Gene target	Reference
Primer 910 bp (forward)	GGTAATACGGAGGGTGCGAG	<i>16S rRNA</i>	This work
Primer 910 bp (reverse)	ACTTCTGGTGCAACCCACTC	<i>16S rRNA</i>	This work
Molecular Beacon <i>Legionella</i> spp.	FAM- <u>CCGAGCGGTGAGTAACGCGTAGG</u> AATATGGCTCGG-DABCYL	<i>16S rRNA</i>	(Templeton et al., 2003)
Reverse complementary target to molecular beacon <i>Legionella</i> spp.	CATATTCCTACGCGTACTCACC	<i>16S rRNA</i>	(Templeton et al., 2003)
Non-target 1	ACTTCTGGTGCAACCCACTC	<i>16S rRNA</i>	This work
Non-target 2	GTCAACTTATCGCGTTTGCT	<i>16S rRNA</i>	(Rafiee et al., 2014)
Non-target 3	AATAGGTCCGCCAACGCTAC	<i>mip</i>	This work
Non-target 4	GCAATGTCAACAGCAA	<i>mip</i>	(Wilson et al., 2003)
Non-target 5	CATATTCCTACGCGTACTCACG	-	This work
Non-target 6	CATATTCCTACGCGTACTCAGG	-	This work
Non-target 7	CATATTCCTACCCGTTACTCACC	-	This work
Non-target 8	CATATTCCTAGCCGTTACTCACC	-	This work

2.3.2. Cell number determination

To determine a concentration of bacterial cells, the counting chamber Neubauer-improved (also known as Petroff chamber) was cleaned from dust and other residues with 70 % Ethanol and a Kim wipe. After the cover glass was placed on top of the cover glass support, the proper contact of the two glass surfaces was verified by the formation of the Newton's rings. After successful assembly, 1.5 µl cell suspension was pipetted to the upper and lower edge of the cover glass to be aspirated into the

chamber by capillary forces. This process was carried out under the safety cabinet, to reduce the risk of aerosol generation. The loaded counting chamber was placed under the Nikon Eclipse Ci microscope connected to a PC running the IC Capture software and pictures were taken using the 10 x objective in phase contrast. The grid of the chamber subdivided the area for counting. The main square in the center is subdivided into 16 large squares also called group squares. Each group square consists of 16 small squares with an area of 0.0025 mm² separated by triple lines, the middle one taken as boundary for counting. A picture of the chamber and the counting grid is shown in Figure 4. The number of bacterial cells was calculated by counting two squares of each of the two chambers and determining the mean value according to equation 1.

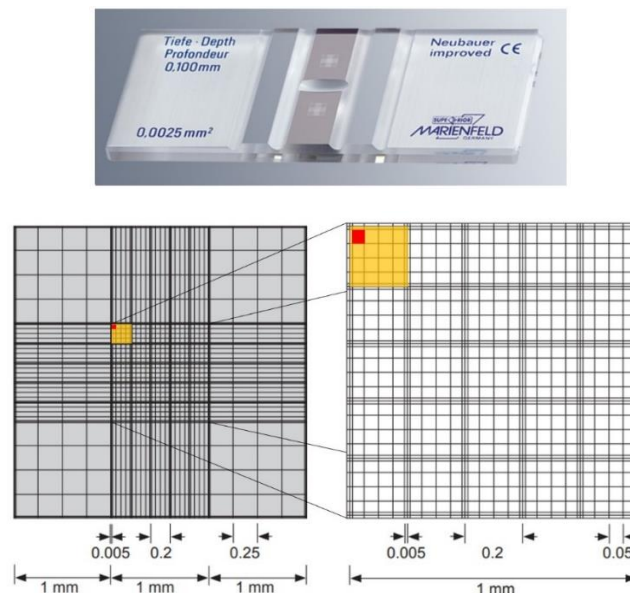


Figure 4: Image and drawings of the counting grid of the Neubauer improved counting chamber, modified illustration from Marienfeld-Superior (Paul Marienfeld GmbH & Co. KG, 2021). The left side shows one of the two counting areas in total. On the right hand side, the center square used for counting bacteria is depicted. A group square is highlighted in yellow, a small square in red.

Then the cell number was calculated using the following equation:

$$\frac{\text{Average counted cell number of group squares}}{0.01 \text{ mm} \times 0.0025 \text{ mm}^2 \times 16} \frac{\frac{\text{mm}^3}{\mu\text{l}}}{\text{mm}^3} = \frac{\text{cells}}{\mu\text{l}} \quad (1)$$

After counting the cover glass was removed and all glass surfaces were cleaned using 1.5 % Kohrsolin and 70 % Ethanol.

2.3.3. Growth curve and correlation of optical density to cell number

L. pneumophila Philadelphia was cultured on BCYE agar plates as described above and a liquid culture was prepared by inoculating some bacterial material taken from an already cultivated agar plate with an annealed inoculation loop and added to a 25 ml of YEB medium in a 100 ml shaking flask. Incubation was carried out at 37°C and 180 rpm for two days. The media required for the cultivation of *Legionella* are listed in Table 7. Two shaking flasks were spiked with an OD₆₀₀ of 0.1 using the inoculum from the agar plate and liquid culture respectively and incubated at 37°C and 180 rpm for about 4 days. The OD₆₀₀ was measured using the NanoDrop™ One every 8 or 16 hours, with 100 µl bacterial suspension transferred to a cuvette under sterile conditions. Each measurement of the optical density was followed by an image acquisition under the microscope and cell number determination as described in section 2.3.2.

2.3.4. Bacterial viability test

First, a *L. pneumophila* Philadelphia shaking culture was grown for 3 days in YEB and then inoculated into fresh medium in two flasks containing fresh medium. One flask was incubated without any further treatment, to the other culture 10 µl of ChemChrome V6 was added and the flask covered with aluminum foil to keep it dark. On the following day, 2 x 1 ml of the unstained and 1 x 1 ml of the stained culture were transferred to 1.5 ml reaction tubes respectively and centrifuged at 4000 g for 2 min. The elution fractions were removed and the pellets resuspended in 1 ml of sterile filtered 1x PBS pH 7.4 respectively. Besides the unstained and overnight stained cultures, a freshly stained culture was prepared, by mixing 890 µl 1 x PBS with 100 µl of the resuspended bacterial suspension and 10 µl ChemChrome V6. After an incubation for 30 min at 37°C in the dark, 100 µl of each sample was transferred to a 96 well plate and imaged under UV light with the Premium Chemi Imager.

In addition, a concrete cell number of 3.5×10^5 cells/µl *L. pneumophila* Philadelphia and *Legionella anisa* were also investigated with respect to staining with the metabolic dye followed by analysis with a flow cytometer. *L. anisa* was of interest in this experiment because it can serve as a negative control in the characterization of mouse anti-*Legionella-pneumophila* antibodies. The protocol was analogous to the freshly prepared staining described above but distilled water was used for the dilutions instead of 1 x PBS.

2.4. Molecular biological methods

2.4.1. Absorbance measurement

The microvolume UV-Vis spectrophotometer NanoDrop™ One was used for absorbance-based quantification. The instrument can be used to measure samples in droplets or in a cuvette. For droplet quantification, a minimal volume of 1 µl was required and for the cuvette a measurement of at least 100 µl was possible. Measurable wavelength ranged from 190-850 nm. In this work the NanoDrop™ One was used for the determination of DNA and protein concentrations, optical densities (OD₆₀₀) of bacterial cultures or absorbance of specific dyes e.g., methylene blue.

2.4.2. Bacterial lysis and DNA Extraction

For the lysis and extraction of gDNA from *L. pneumophila* Philadelphia, 400 µl of a cell suspension containing 2×10^6 cells/µl were prepared using the counting chamber Neubauer-improved. The bacterial suspension was mixed with 100 µl alkaline extraction buffer by inverting 10 times. Upon an incubation of 5 min at room temperature, 100 µl of neutralizing buffer was added and mixed by inverting 10 times again. To verify the lysis, 500 µl of the volume was pipetted on an BCYE+AB agar plate and distributed with a sterile Drigalski spatula. As a control the cell suspension mixed with 1 x PBS instead of lysis buffer was incubated on a separate agar plate. The agar plates were incubated at 37°C for 7 days. Pictures of the agar plates after incubation were taken under the biosafety cabinet using a smartphone camera. For determination of the colony forming units, the pictures were analyzed by ImageJ using the multi-Point tool for counting. Therefore, each colony was marked with the pointing tool and counted automatically.

To determine the extraction efficiency, a volume of 10 µl of the DNA extract was used for a 1:2 dilution series in ultrapure water. Afterwards, 10 µl of each dilution were loaded on a 1 % agarose gel casted with GelRed and gel electrophoresis was performed for 75 min at 125 V. In parallel the peqGold 1 kb ladder was diluted to total concentrations ranging from 125-16 ng. The extraction efficiency was determined after taking a picture with the gel documentation system and ImageJ. The sample bands were surrounded by horizontal lanes using the "Rectangular Selection" tool. The lane is selected by choosing Analyze → Gels → Select first lane. A next lane can be added by choosing Analyze → Gels → Select next lane. After selection the lane grayscale density is plotted by Analyze → Gels → Plot Lanes. To subtract the values from the background a baseline is drawn by using the line tool. In a next step the sample bands are isolated manually by using the line tool to connect the peaks to the base line.

Afterwards each peak corresponding to a sample can be identified choosing the wand (tracing) tool and clicking on each peak to be selected. Finally, a results window opens upon selecting Analyze → Gels → Label Peaks and outputs the area values of each peak. All values for the sample and reference bands are copied into an excel file and a standard curve was generated from the 1 kb ladder reference. The regression curve of the standard curve is used to recalculate the mass of the samples extracted by the alkaline extraction protocol.

2.4.3. PCR and real-time PCR

With the polymerase chain reaction, specific DNA segments were amplified exponentially with the help of two primers, a DNA polymerase and deoxyribonucleoside triphosphate (dNTPs) in several, repetitive heating cycles provided by the peqSTAR thermal cycler. At a temperature optimum of 72°C for the Taq-Polymerase, the extension of the new DNA strands was processed by incorporating dNTPs complementary to the DNA template strand. With the PCR, primarily qualitative statements could be made and the evaluation was carried out on an agarose gel upon gel electrophoresis to visualize the amplified target sequence. With real-time PCR, also a quantitative evaluation was possible through the addition of fluorescence markers and a continuous readout. SyGreen was used in this work to fluorescently label double-stranded (ds) DNA generated during amplification. With the InnuMix from Analytik Jena, annealing and extension steps were performed at the same temperature and detected by the qTower³ real-time PCR cycler. Tables 9 and 10 lists the PCR reaction mixtures for amplification of the gene sequences and the corresponding PCR program used in this work.

Table 9: Composition of the PCR-mixture for 1 reaction and thermal heating program for the peqSTAR thermal cycler.

Volume	Component
1 µl	10 x Taq reaction buffer
2 µl	8 mM dNTPs
0.4 µl	10 µM fwd. Primer 910 bp
0.4 µl	10 µM rev. Primer 910 bp
0.5 µl	Template DNA
0.1 µl	Taq-Polymerase
5.6 µl	Ultrapure water

Cycle	Temperature	Time	Cycle step
1 x	95°C	1 min	Initial denaturation
33 x	95°C	15 sec	Denaturation
	55°C	15 sec	Annealing
	72°C	15 sec	Extension

Table 10: Composition of the real-time PCR-mixture for 1 reaction and thermal heating program for the qTower³ real-time PCR cycler.

Volume	Component
10 µl	2 x InnuMix qPCR SyGreen
1 µl	10 µM fwd. Primer 910 bp
1 µl	10 µM rev. Primer 910 bp
0.5 µl	Template DNA
7.5 µl	Ultrapure water

Cycle	Temperature	Time	Cycle step
1 x	95°C	2 min	Initial denaturation
40 x	95°C	20 sec	Denaturation
	56°C	20 sec	Annealing and extension

2.4.4. Agarose gel electrophoresis

Agarose gel electrophoresis was used as an analytical method to separate DNA according to its size and charge. Agarose gels with different percentages (0.7 %, 1 %, 2 % and 2.5 % w/v) were casted directly in the tray of the “all-in-one” chamber, which combines pouring and electrophoresis of gels with a dimension of 12 x 14 cm. After resolving the agarose in 100 ml 1 x TAE buffer in a sterile beaker using a microwave and cooling to around 50°C, 8 µl 10,000 X GelRed was added and mixed properly by swiveling. The desired combs were inserted into the comb slots to form the sample pockets and the warm agarose was poured onto the gel tray. After solidification of the gel, the tray was lifted, turned about 90 degree and replaced in the chamber with the sample’s pockets directed to the black labeled cathode. As running buffer 1 x TAE buffer was poured around the gel until the fill line was reached. The combs were removed, the samples mixed with 1 x or 6 x loading dye and loaded into the pockets of the gel. After sliding the lid onto the chamber, the chamber was connected to the power source and voltage was applied. A voltage of 120 V for 75 min was chosen as standard conditions. After the gel electrophoresis was completed, the gel was transferred to the UV light table in the gel documentation system (Chemi Imager). Upon exposure to UV light the DNA samples stained by the intercalating dye became visible and can be photographed using the VWR Image Capture Software.

2.4.5. DNA ladders

Different DNA ladders were used as a reference to estimate the size of the DNA fragments separated by gel electrophoresis, or as a sample with a specific fragment composition in fiber electrophoresis. Figure 5 shows the band pattern of the DNA ladders used.

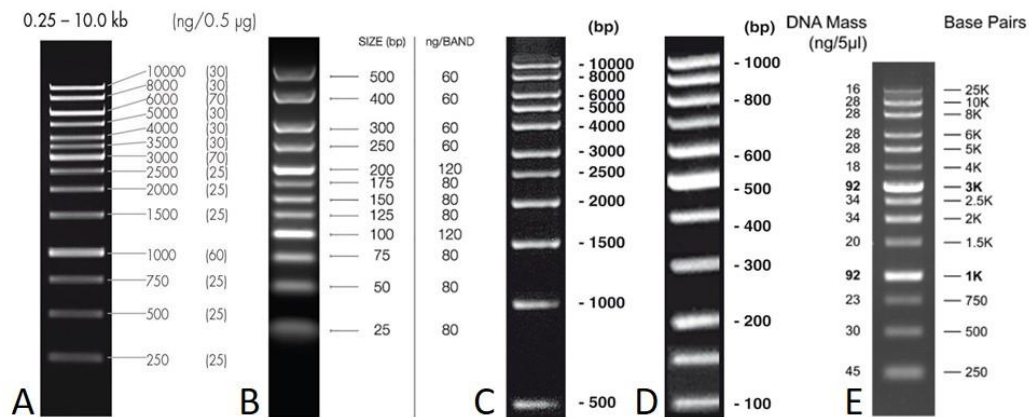


Figure 5: DNA ladders. A) peqGOLD 1 kb DNA ladder (VWR, 25-2030) on a 1 % agarose gel; B) Quantitas 25-500 bp DNA ladder (Biozym, 250216) on a 3.5 % agarose gel; C) 1 kbp DNA ladder, lyophilized (Carl Roth, Y014.1) on a 1.2 % agarose gel; D) 100 bp DNA ladder, equalized, lyophilized (Carl Roth, T833.1) on a 1.8 % agarose gel; E) 250 bp-25 kbp DNA ladder (GeneOn, 300007) on a 0.7 % agarose gel.

2.4.6. Fluorescence *in situ* hybridization

2.4.6.1. Rapid hybridization detection protocol

For a standard reaction 440 nM molecular beacon in 5 mM Tris buffer were mixed with 440 nM of the reverse complementary target DNA or non-target DNA in 5 mM Tris buffer. The sequences of the tested probe and DNA-target are listed in Table 8. A 10 µl reaction volume was either measured as liquid in a PCR tube or transferred to the glass microfiber pad by pipetting. Therefore, squares of 5 x 5 mm glass microfiber pads (Whatman GF/F) were cut by a scalpel from a round filter. The wetted filter pad was transferred to the inner wall of a PCR tube with a pair of tweezers. A short detection protocol was developed by incubating the fiber for 2 min at 95°C and 2 min at 55°C. After cooling down to 25°C (assumed to be room temperature) and incubation for 2 min, the fluorescence signals occurring from the hybridization were detected.

The heating protocol was programmed in the qTower³ real-time PCR cycler and the blue channel for the detection of the fluorescence occurring from the FAM excitation was chosen. Data acquisition was performed after the third temperature step at 25°C. After scanning of each sample position, the raw data was saved as a CSV file.

As an alternative detection method, the filter pads were transferred to the table of the Chemi Imager with a pair of tweezers after incubation in the peqSTAR thermal cycler at the temperatures described previously. The fluorescence of the hybridized probe-DNA complex was measured using UV light and the long pass filter (LED green module). The iris and focus were adjusted to values of 7.2 and 98, respectively, and 20.8 was defined as the lens control parameter. The captured images were saved as SGD, JPG and TIFF formats. For analysis of the fluorescence intensities, TIFF images were loaded to ImageJ. First, the images were transformed into 8-bit format. Secondly the threshold was set to exclude the background from the image (Image → Adjust → Threshold). Last, the parameters to be determined were set by adding each region of interest to the ROI manager (Analyze → Tools → ROI Manager; the tracing tool was chosen and each region of interest selected) and selecting measurement of area and intensity density.

2.4.6.2. Hybridization prediction and calculation of Gibbs free energy changes

The UNAFold web server (<http://www.unafold.org/>) was used for the predication of DNA hybridization and calculation of the Gibbs free energy changes (Markham et al., 2021). After the sequences of interest were loaded as FASTA format, the test conditions were adjusted by setting concentrations of sodium and magnesium, as well as a temperature. The self-hybridization of the molecular beacon probe under various conditions was predicted by using the DNA Folding Form of the mFold software package. For the hybridization prediction of the molecular beacon with the target and non-target sequences or the calculation of the Gibbs free energy change the DINAMelt software package with the application for hybridization of two different strands of DNA or RNA was used.

2.4.6.3. Cooling curve of hybridization

The cooling curve experiment was setup by adding the molecular beacon probe to a final concentration of 300 nM in a solution containing 1 x reaction buffer and 3 mM magnesium chloride (MgCl_2), with or without reverse complementary target DNA in the same molar ration in a total volume of 25 μl . The non-targets were tested in the same way as the target in separate reactions. The temperature was decreased from 95°C to 25°C in 1°C increments, each held for 15 sec. All fluorescence measurements were carried out with the qTower³ real-time PCR cycler from Analytik Jena using the FAM channel. The evaluation of the measurements to determine the melting or hybridization temperatures was carried out using the qPCRsoft 4.0 software from Analytik Jena.

2.4.6.4. Significance test

The significance levels were determined using the Medcalc Software based on the work of Altman, Kirkwood and Sterne which used the following equations. After calculation of the pooled standard deviation s (2.1), from the individual standard deviations s_1 and s_2 as well as the sample sizes n_1 and n_2 , the standard error se (2.2) between the two samples means \bar{x}_1 and \bar{x}_2 was determined. Finally, the significance level, or probability value (P-value) was calculated using the t-test, with the value t calculated with equation 2.3. The two-sided P-value was determined as the area of the t-distribution with $n_1 + n_2 - 2$ degrees of freedom that fell outside $\pm t$ after comparison with the t-distribution table. P-values below 0.05 ($P < 0.05$) indicated that the two samples could be differentiated in a significantly way (Altman, 1991; Kirkwood and Sterne, 2010; “MedCalc Software Ltd. Comparison of means calculator, Version 20.014,” 2021).

$$s = \sqrt{\frac{(n_1 - 1)s_1^2 + (n_2 - 1)s_2^2}{n_1 + n_2 - 2}} \quad (2.1)$$

$$se(\bar{x}_1 - \bar{x}_2) = s \sqrt{\frac{1}{n_1} + \frac{1}{n_2}} \quad (2.2)$$

$$t = \frac{\bar{x}_1 - \bar{x}_2}{se(\bar{x}_1 - \bar{x}_2)} \quad (2.3)$$

2.4.7. Fragmentation of gDNA by restriction enzymes

In general, 10-20 units of enzyme per μg gDNA are recommend and the enzyme volume should not exceed 10 % of the total reaction volume to avoid non-specific cleavage of sequences, known as star activity. A 25 μl reaction was used for the digestion of 0.5 μg gDNA. The recognition and cleaving sites for each enzyme, their isoschizomers, and the organism from which the enzyme was derived and where it was cloned are listed in Table 11. The protocol for each restriction enzyme used for fragmentation of gDNA in this work are listed in Table 12. After pipetting all components into PCR-tubes placed in a cooling rack, the samples were mixed by gently flicking with the fingers and centrifuged in a table centrifuge. The enzyme was kept cooled in a cooling rack after removal from the freezer and added last to the digestion mixture. Mixing by vortexing was prevented to preserve the enzyme activity.

Table 11: Restriction enzymes. Nucleotide code: A= Adenine; C=Cytosine; G= Guanine; T= Thymine; K= G or T ; M= A or C ; R= A or G ; Y= C or T.

Enzyme	SmlI	BseSI	HaeIII	HhaI	HpaI	HpaII
Isoschizomers	Smol	BaeGI	PhoI	HinP1I	KspAI	MspI
Cut site	5'...CTYRAG...3' 3'...GARYTC...5'	5'...GKGCM ⁺ C...3' 3'...CMCGKG...5'	5'...GG ⁺ CC...3' 3'...CC ⁺ GG...5'	5'...GCG ⁺ C...3' 3'...CGC ⁺ G...5'	5'...GTT ⁺ AAC...3' 3'...CAAT ⁺ TG...5'	5'...C ⁺ GGG...3' 3'...GGC ⁺ C...5'
Product source	An <i>E. coli</i> strain that carries the cloned SmlI gene from <i>Stenotrophomonas maltophilia</i> (T. Le).	An <i>E. coli</i> strain that carries the cloned BaeGI gene from <i>Bacillus aestuarii</i> GG790 (X. Pan).	An <i>E. coli</i> strain that carries the HaeIII gene from <i>Haemophilus aegypticus</i> (ATCC 11116).	An <i>E. coli</i> strain that carries the HhaI gene from <i>Haemophilus haemolyticus</i> (ATCC 10014).	An <i>E. coli</i> strain that carries the HpaI gene from <i>Haemophilus parainfluenzae</i> (ATCC 49669).	An <i>E. coli</i> strain that carries the HpaII gene from <i>Haemophilus parainfluenzae</i> (ATCC 49669).

Table 12: Digestion protocol of gDNA using restriction enzymes in a 25 µl reaction.

	SmlI	BseSI	HaeIII	HhaI	HpaI	HpaII
Restriction enzyme [units]	5	5	5	10	2.5	5
DNA [µg]	0.5	0.5	0.5	0.5	0.5	0.5
10 x NEB cut buffer [µl]	2.5	2.5	2.5	2.5	2.5	2.5
Nuclease-free water [µl]	to 25 µl	to 25 µl	to 25 µl	to 25 µl	to 25 µl	to 25 µl

All enzymes except of SmlI work at 30 min at 37°C, the latter one needed 55°C to be activated. The restriction enzymes HaeIII and HpaII required heat inactivation at 80°C and HhaI 65°C for 20 min to prevent DNA from further degradation. SmlI, BseSI and HpaI needed no heat inactivation. After the completion of the reaction, 3 µl of loading dye was added to a volume of 10 µl of each sample and loaded on a large 0.7 % agarose gel, casted with 10 µl GelRed and only on gel comb. After the gel electrophoresis was carried out at 25 V for 17.5 h, a picture was taken with the gel documentation system Chemi Imager under exposure to UV light. For a double digestion with HaeIII and HhaI as well as HpaI and HpaII respectively, the same volumes of DNA, cut buffer and enzyme were used as for a digestion with only one enzyme and the volume of water was adjusted to a total reaction volume of 25 µL. Each double digestion mix was followed by a heat inactivation at 80°C for 20 min. For the FISH experiments on glass microfiber, 2 µL of the digest was used.

2.4.8. Interaction of DNA molecules with different fiber substrates

As depicted in Figure 6 the ladder (4 µl VWR peqGold) was pipetted on a piece of fiber material. The fiber pad was placed on the inner wall of a PCR tube and was transferred to the peqStar PCR cycler for heating using the program described in Table 13 or as mentioned in the corresponding text of the

result section. Afterwards the fiber was removed using a pair of tweezers and was directly placed in a well of a casted agarose gel. As an option the fiber was treated with elution buffer first and the elution fraction was loaded onto the agarose gel. A volume of 20 μ l elution buffer was added to each fiber piece, mixed by vortexing for 5 sec and incubated for 15 min at room temperature. After squeezing the fiber at the bottom of the tube with a pipette, the elution fraction containing the sample of interest could be removed as supernatant and mixed with 2 μ l of 6X loading dye. Afterwards the samples were loaded onto a 1 % agarose gel poured with 6 μ l of Midori Green gel stain. Visualization was possible after gel electrophoresis.

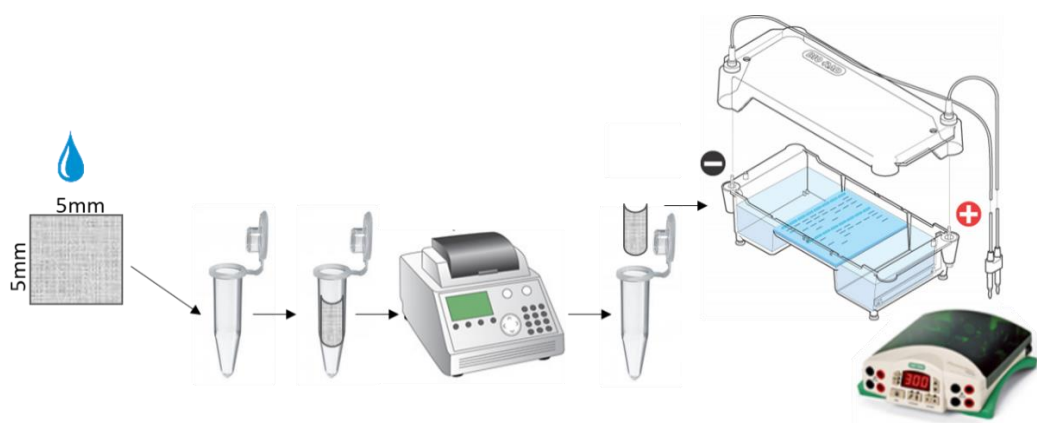


Figure 6: Experimental flowchart for studying the interaction of DNA samples with different fiber materials. A 5 x 5 mm fiber piece was cut out and placed into a PCR tube. Heat was applied by using a PCR cycler. To investigate the retention of the fiber substrates on DNA, the samples were exposed to various assay conditions and then visualized by transfer to an agarose gel and visualized after gel electrophoresis.

Table 13: Heating protocol for DNA samples loaded on fiber materials and placed in PCR tubes in the PCR cycler.

Cycle	Temperature	Time
33 x	95°C	15 sec
	55°C	15 sec
	72°C	15 sec

The average mass of a 5 x 5 mm cellulose filter piece was determined to 1.93 +/- 0.12 mg. For testing the substrate without the spatial structure, the same amount of microcrystalline cellulose was measured and used for the experiments with DNA samples. Moreover, samples with filter paper were occasionally overlaid by 20 μ l silicon oil to test whether DNA could be better recovered upon heat treatment. For detection, the silicone oil was removed with a pipette and the paper pieces were placed in the gel pockets. As an alternative, the fiber was sealed in foil using a bag sealer to protect the fiber

from drying out. For this purpose, a double-layered transparent sealing bag was cut to a size of 1 x 1 cm and the fiber was placed in between. After positioning the foil edges on the sealing wire and pressing the mini-sealer closed for approx. 2 sec, the two foils lying on top of each other were fused together. Three edges were sealed first, then the sample was pipetted through the fourth still open side onto the fiber, and finally sealed with the fourth foil seam.

2.4.9. Methylene blue labeling of DNA

A methylene blue (MB) stock solution was prepared with 20 μ M MB, 20 mM NaCl in 20 mM Tris-HCl buffer adjusted to pH 7.3 according to labeling protocols reported in the literature (Bifulco et al., 2013). The lyophilized 1 kb DNA ladder from Carl Roth (50 μ g) was resuspended with 500 μ l of the MB-stock solution and was incubated for 15 min in the dark. Unbound MB was removed by the QIAQuick PCR purification Kit and the samples were eluted in 100 μ l 5 mM Tris buffer at 17,000 g for 1 min.

2.5. Fabrication and characterization methods for paper-based materials

2.5.1. Long-term storage of detection reagents on glass microfiber

A 440 nM molecular beacon and target solution in 5 mM Tris respectively were dropped onto four glass microfiber pieces cut to 5 x 5 mm each, dried for 1 h under a DNA work bench and finally stored in a plastic petri dish. The dish was covered with aluminum foil to protect the samples from light. The samples were stored for 3 months at room temperature in a lab cupboard. Samples were analyzed after the addition of the respective missing component provided in 5 mM Tris at the same molar ratio, heated, documented and analyzed using the Chemi Imager and the ImageJ software as previously described. The control, consisting of a fresh solution of probe and target was prepared and measured in the same way as the samples.

2.5.2. Patterning of fiber materials

Fabrication of the paper-based DNA separator included at first the design of a structure using the LibreCAD software. A schematic illustration of the transfer printing processes is shown in Figure 7. For example, a rectangular shaped chip design with the dimension of 1 x 2 cm or a 96 well plate format was designed and exported as a PDF file. A structured fiber substrate was generated by the application

of a polymer mixture of resin and a thermoplastic mixed with different dyes by printing with a Xerox ColorQube 8570 solid ink printer and subsequent heat treatment. The application of the hydrophobic polymer material to the fiber depended on the fiber material. On the one hand, for sturdy fibrous materials like cellulose with a more solid texture, the polymer material was printed directly on the paper sheet using the adjustments manual paper feed and photo quality. On the other hand, for softer and rougher fiber materials like glass microfiber a transfer printing process. For this purpose, the polymer was first printed on an overhead transparency film using the same printing parameters. To penetrate the entire fiber depth, the polymer is melted by heat application and soaked into the fiber interspaces. For a homogenous heating process, a transfer press for imprinting fabrics was chosen. The printed cellulose paper was placed on the T-shirt press and the handle was brought down for 10 sec at 160°C. For the glass microfiber or nylon, the printed overhead film was placed face down on the fiber and both were soaked at 160°C for 30 sec, followed by the removal of the overhead film. In order to structure the glass microfiber in full depth, a second soaking step was required from the back side of the fiber. Therefore, the second soaking step was performed with the same settings, but the printed overhead film was aligned on the reverse fiber side with the already printed structure. Both processed, direct and transfer printing, resulted in a defined microchannel structure consisting of a hydrophilic fibrous sample area bounded by the hydrophobic barrier.

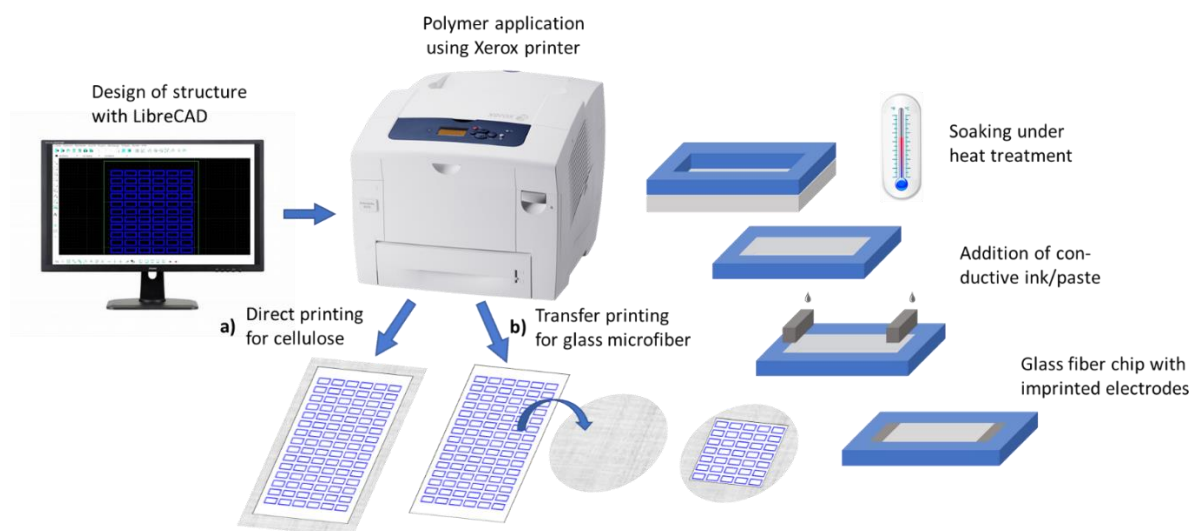


Figure 7: Schematic illustration of the transfer printing processes used for sturdy and soft fiber materials (modified from Heinsohn et al., 2022). The pattern is designed via LibreCAD and printed either directly on the cellulose sheet or on an overhead film using the Xerox polymer printer. For the transfer printing the overhead film was placed face down onto the glass microfiber. After heat application the polymer was melted and soaked into the fiber. Conductive inks or pastes can be applied at the ends of the fiber channel to generate imprinted electrodes.

2.5.3. Application methods for conductive materials on fiber

To create imprinted electrode structures the two ends of the microchannel were treated with a conductive material. Depending on the viscosity of the conductive material and the nature of the fiber, different methods of application were used for the fabrication of fiber-based electrophoresis chips. In this work, application by pipetting, spraying, screen printing, stamping and spotting were tested.

Pipetting:

Conductive inks such as silver and PEDOT:PSS, a conjugated polymer were pipetted gently to the intended areas at the end of the fiber chip. A volume of 4-8 μl of a 3-4 % PEDOT:PSS solution in ultrapure water or an undiluted silver nanoparticle suspension were used for one electrode area and dried for 20 min at room temperature.

Spraying:

First, a mask was made that had a cut-out area at the location of the electrodes. After placing the mask on the fiber material, a copper-based conductive varnish was sprayed from a distance of 15 cm for one second under a fume hood. The mask was removed and the electrode dried at room temperature.

Stamping:

A metal plate containing the engraved structure was filled by applying the conductive carbon paste on one side of the plate and scraping over the structure to the other end using a plastic scraper at a 45 degree angle. A silicone stamp was dipped onto the filled structure by a rolling motion from edge to edge to adsorb the conductive paste to the stamp. Afterwards the paste was applied to the fiber substrate in the same way by rolling from one side to the other while applying light pressure. After the stamp and metal plate were cleaned with isopropanol, a second stamping process could be performed.

Screen printing:

This printing technique can be used to transfer inks as well as pastes onto a substrate. In this work a polyester mesh was used, with a mesh size of 86 μm , a thread count of 61/cm and a sieve opening of 28 %. The frame where the mesh was mounted on consisted of aluminum with dimensions of 60 x 40 cm. The electrode design to be printed on the screen was created with a stencil using a negative image of the electrode. By placing the stencil on the screen and applying a resistant photo emulsion, the areas not belonging to the target structure were covered. The screen structure was then permeable to the pastes only on the desired areas. The screen was fixed into the screen printing machine and lowered onto the desired fiber material. After the conductive material was applied on

one edge of the screen, it was spread over the designated areas with a squeegee. For all substrate, the squeegee was passed over the mesh two times, once forwards and once backwards. In order to fix the conductive material to the substrate the screen printed fibers were dried for 5 min in an oven at 80°C. The screen was cleaned with acetone or propanol to remove any remaining paste from the interstices.

Dispensing:

The Voltera V-One PCB printer and all materials for dispensing were purchased from Voltera Inc (Kitchener, On, Canada). A cartridge was filled with the conductive material to be applied. Firstly, a piston was pushed down with a pen into the cartridge to be filled, allowing trapped air to flow past the edge of the piston. Secondly, a second cartridge was coupled by female-to-female luer fitting to the tip of the first cartridge. A volume of 5 ml of the carbon paste was filled into the second cartridge with a syringe and then sealed with a second piston. The first cartridge was filled after pressing the piston of the filled second cartridge gently down allowing the material to flow through the luer fitting. After bottomed out, the second and now-empty cartridge as well as the luer coupling were removed and a nozzle was screwed onto the tip of the filled cartridge. The nozzle consisted of polypropylene with an inner diameter of 0.23 mm. This type of filling process minimized the entry of air into the cartridge and thus prevented an irregular spotting result on the fiber substrate. Only intact cartridges could be used for further experiments because a rupture of the piston would prevent a constant ink pressure. Pictures of the cartridges as well as the correct filling are displayed in Figure 8 a) - e).

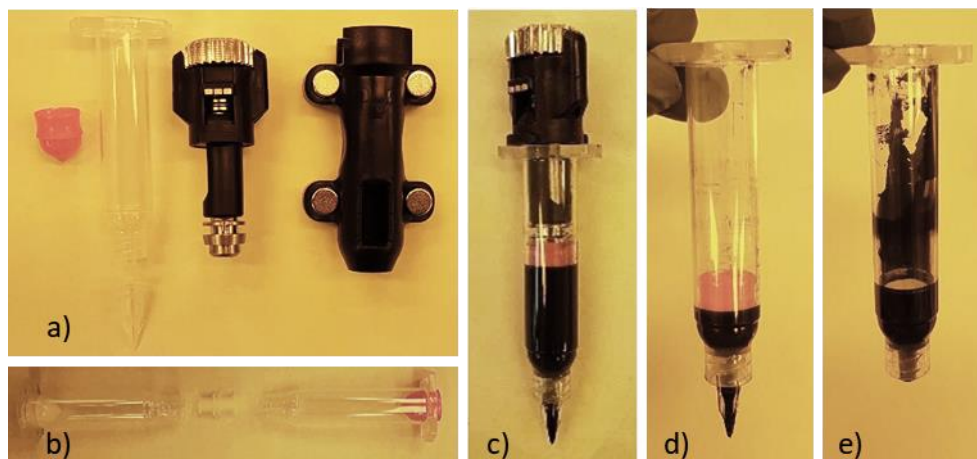


Figure 8: Components used for dispensing the carbon paste onto the glass microfiber. a) Red piston next to an empty cartridge, nozzle as well as inner and outer part of the dispensing unit. b) Female-to-female luer fitting of two cartridges. c) Assembly of the entire dispensing unit and the cartridge filled with black carbon paste. d) A tight cartridge with a piston pushed down without loss of material on the inner wall. e) Leaking cartridge that lost material during the printing process and does not ensure constant pressure during dispensing.

The design of the electrode structure was created with LibreCAD and saved as a Gerber file. The fiber was placed on the table of the dispenser and fixed with tape at the edges. After loading the file using the V-One software on a computer connected to the Voltera printer, a calibration step was performed to verify the alignment of the loaded design and the structured fiber material. By lowering the probe attached to the carriage system at several points of the designed structure, the height of the material could be measured. These parameters were then used for the dispensing process. After the calibration, the cartridge can be inserted into the dispenser and locked. For priming the dispenser, the gear on the dispenser was turned counter-clockwise to initiate the paste flow. When the paste came out of the nozzle the gear was turned one forth back by turning clockwise. Afterwards the cartridge was mounted to the printer by magnetically contacts on the carriage system and a control pattern from the manufacturer was printed that consisted of curved and parallel lines. The traces could be adjusted by changing the ink pressure and print height manually in the software if necessary. The paste was dispensed onto all selected areas after starting the conductive print process. The dispensing parameters for the carbon paste on glass microfiber were 0.33-0.36 mm as print height and 10-20 μm for the ink pressure. For fixation, the printed fibers were dried in the oven at 80°C for 5 min.

2.5.4. Characterization of the fiber-electrophoresis chip fabrication

For the characterization of the structured fiber-electrophoresis chips with imprinted electrodes, resistance measurements of the electrode and a microscopic evaluation of the penetration depth of the polymer pattern was carried out. The imprinted electrodes were tested regarding conductivity by measuring their resistance using a digital multimeter. The two needle point probes connected to the digital multimeter were placed at the ends of the imprinted electrode and the value in ohm (Ω) was recorded. Patterning of the fiber structures was checked by microscopic pictures using the digital microscope ADSM302. An adequate and uniform illumination had to be ensured by aligning the LED-lights of the microscope with the fiber structure, and a sharp image was captured after manual adjustment of the lens. The pictures were saved on an integrated SD-Card.

2.5.5. Experimental implementation of the fiber-based electrophoresis

The imprinted electrodes were connected to a voltage source via contact electrodes. After prewetting of the microchannel with 80 μl 5 mM Tris buffer pH 8.0, a sample volume of 1 μl was pipetted in front of the negatively charge electrode (cathode) and the voltage application was started. After the DNA movement was stopped by switching off the voltage, the fiber electrophoresis chip was cut into 4

pieces with a scalpel on a clean cutting mat. Each of these fiber pieces were transferred to a 0.2 ml tube using clean forceps and incubated with 25 μ l elution buffer 2 for at least 1 h. Afterwards the elution fractions were analyzed by agarose gel electrophoresis to visualize DNA fragments. As samples DNA ladders with fragments of several sizes, a single double-stranded DNA (dsDNA) fragment of 910 bp, a single-stranded DNA (ssDNA) of 23 bases or genomic DNA (gDNA) isolated from *L. pneumophila* Philadelphia were taken. As alternative to or in addition with elution, a fluorescent staining by an intercalating dye was used to visualize the migrated DNA samples directly on the chip area. Upon staining with a 6 x GelRed solution diluted in 20 mM sodium chloride (NaCl) for 3 min, images were taken under UV light using the Chemi Imager.

2.5.6. Measurement board

For the fiber electrophoresis, voltage was applied with two alternative contact modes. Either crocodile clamps or gold coated contact fingers were used for connecting the imprinted electrodes to a voltage source. Pictures of both experimental set ups are shown in Figure 9. For the measurement setup with the crocodile clamps, the current was tracked using a digital multimeter connected to the voltage source and the free software UT61E Interface Program Version 4.01 (x64) downloaded on a PC and connected to the digital multimeter. The height-limit was adjusted to 1000 and the lower limit was set to a value of -5. Recording parameters were set to repeat and limitless. After completion of measurements the data was saved as XLS and TXT formats.

In a High-Voltage-Analog-Digital-Converter (HVADC), developed as a prototype measurement device for future read-out by Dr. Alexander Anielski, the current and potential differences were recorded by a raspberry pi integrated to the electronic circuit connecting the electrodes and the voltage source. HVADC is an abbreviated designation defined by us which means that you can measure high voltages with this measuring device and these are then digitized. The main task of the circuit was to measure three voltages in the range of -100 to 100 V with a high impedance in the order of 10^{11} ohm. This allowed the measurement of potentials in low ion concentrations or in poor conductivity environment with lowest possible interaction between probe and sample, comparable with a potentiostat but without feedback. Further a current in the range of 1 μ A to 1 mA can be measured by a transimpedance amplifier. The high impedance of the inputs can be reached by the operational amplifier which are expanded with a bootstrap circuit to deal with a high input voltage. All analog signals are readable by a raspberry pi mini-computer with help of the analog-digital-converter. To supply samples with an electric field a voltage amplifier with buffer was placed on the measurement board. It was possible to read all analog inputs and to set an output voltage in the range of -100 to 100 V by software. A debian

linux was used on the raspberry pi and measurement and control scripts were written in octave. A schematic circuit diagram of all components and connections of the HVADC and the octave script are provided in the appendix of this work (see Figure A1 and section 6.12.).

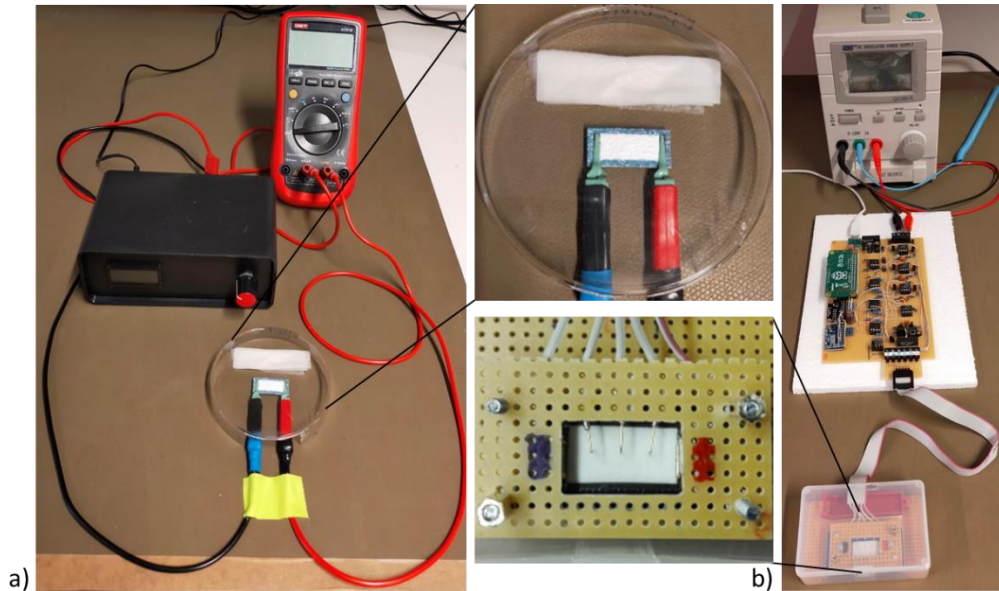


Figure 9: Images of the fiber-electrophoresis chips connected to the voltage and read-out-systems (modified from Heinsohn et al., 2022). a) The fiber-electrophoresis chip is placed between crocodile clamps and covered by a petri dish to avoid evaporation. The clamps are connected to a stabilized power supply and a digital multimeter was integrated for current tracking. b) Measuring board of High-Voltage-Analog-Digital-Converter (HVADC) designed and built by Dr. Alexander Anielski. The fiber electrophoresis chip is placed in a lockable box that contains a liquid reservoir (shown in red) to keep the environment moist. Gold coated contact electrodes integrated in the lid are used for the connection of the imprinted electrode to the voltage source and current measurement. Three gold coated pin electrodes are penetrating the fiber within the migration area were integrated for local measurement of potential differences.

2.5.7. Heating element

The cyler consists of a control unit, a heating element, as well as a temperature sensor and was designed and built by Dr. Alexander Anielski. A power bipolar transistor is used as the heating element, which has a metal surface of about 1 cm^2 on the back. Directly connected to the metal surface is a temperature sensor. The measuring, controlling and regulating is done by a program on the microcontroller. The transistor can be brought to the set temperature within a few seconds. The cooling is passive and, depending on the temperature difference, takes between half a minute up to a few minutes. Any temperature profiles from room temperature to 95°C can be run on this scale.

2.6. Protein biochemical methods

2.6.1. DNA-protein-mixture preparation

As an artificially prepared protein-DNA-mixture, 100 ng/ μ l HRP in phosphate buffer pH 7.0 were mixed with 120 ng/ μ l of a DNA fragment with a size of 910 bp amplified by PCR. The enzyme integrity can be detected via the oxidation of the chromogenic substrate tetramethylbenzidine (TMB) in the presence of hydrogen peroxide. In this work 40 μ l of SeramunBlue-fast, a premix containing both reagents, was pipetted onto the chip surface and the blue color occurring from the substrate conversion was documented via video using a smart phone camera.

2.6.2. Paper-based ELISA

On each spot of a polymer-structured 96 well paper plate (cellulose paper 640 M) 1 μ l of the bacterial suspension adjusted to 1.3×10^5 Z/ μ l respectively was pipetted and incubated for 1 h. Unspecific binding was blocked with 2 μ l/well 5 % ovalalbumin (OVA) + 0.1 % Tween for 15 min. The antibody sera to be tested were pipetted in dilutions ranging from 1:50 - 1:5,000,000 in 1 x PBS and a volume of 1 μ l/well. The antibody sera were generated by new/era/mabs on behalf of inventicsDx. After a 15 min incubation, the paper plate was placed on a paper towel and each well was rinsed two times by the addition of 2 μ l 1 x PBS. The paper towel draws the liquid from the structured paper plate by capillary forces. After removal of the paper towel, the second antibody goat-anti-mouse-HRP from dianova was diluted 1:5,000 and 1 μ l/well was added to each well and incubated for 1 h. The plate was placed on a new paper towel and each well was rinsed three times with 2 μ l of 1 x PBS. Finally, the TMB working solution was added in a volume of 2 μ l to each well and the signal was documented by a smart phone camera. For the TMB working solution 10 μ l of a 30 % hydrogen peroxide solution was mixed with 6 ml of the Gallati buffer and 60 μ l of the TMB solution described in table 6.

2.6.3. Flow cytometry

All experiments were performed with the Attune NTX Flow Cytometer, equipped with a blue laser, providing 50 mW at 488 nm and the standard filter set-up. An acquisition volume of 200 μ l at a flow rate of 25 μ l/min were chosen to display all events. The forward scatter and side scatter voltages were adjusted to 300 mV and 280 mV, respectively, to position the cell population on the scatter plot. The fluorescence channel voltage was adjusted to 350 mV to position the autofluorescence signal of the

unstained population. The forward scatter threshold was set to 25.0 (x 1000) to exclude unwanted noise signals. Green fluorescence of cells stained with ChemChrome V6 was collected in the BL1 channel (530±30 nm). All parameters were collected as logarithmic signals. All accessories and consumables such as the performance beads for calibration, focusing fluid, wash solution, shutdown solution or bleach solution were purchased from ThermoFisher Scientific.

3. Results and Discussion

3.1. Growth curve and correlation of optical density to cell number

Initially, a growth curve experiment of *L. pneumophila* Philadelphia was set up to learn about on-site cultivation conditions. In the present work, the wild-type strains of all organisms were used, since there was less interest in being able to cultivate the organism as fast as possible and follow specific genetic pathways than in being as close as possible to the naturally occurring pathogens. First, the optical density (OD₆₀₀) of two liquid cultures were measured every 8 and 16 hours, respectively, as shown in Figure 10 a). Upon a lag phase without cell division the bacteria pass over to the log phase, where exponential growth of the population takes place. Afterwards they enter the stationary phase, characterized by a plateau and equal numbers of cell dividing and dying because nutrients become limited. Finally, if the lack of nutrients becomes too high the cells start to die and the optical density declines. Of particular note in the tracked measurement is the difference between the inoculates. If the culture was inoculated from an already grown liquid culture, the bacteria can enter exponential growth after only 8 hours. If, on the other hand, the bacteria were transferred from a plate to a liquid culture, then the growth phase is delayed by 24 hours. This does not seem surprising from a microbiological point of view, since a change of media requires an adaptation of the metabolism to the condition, but it is certainly important for the preparation of the test suspension in following assays. The measured values for the liquid inoculum recorded here are consistent with those from the literature (Li and Faucher, 2016; Xiang-hui Li et al., 2010). Even more important was to determine the correlation between the measured OD₆₀₀ and the counted cells. Based on these results (see Figure 10 b), the following values could be determined. An OD₆₀₀ of 0.1 corresponds to an average cell number of 10⁴ cells/μl. Cell numbers of 10⁵-10⁶ cells/μl were counted for optical densities of 0.2-1 and OD₆₀₀ values of 2 and 3 followed cell concentrations of 10⁷ cells/μl and >10⁷ cells/μl. The higher the cell density, the less accurate the count becomes, as the individual cells cannot be differentiated from each other as well. The main aim was to know the decades of the cell numbers in order to be able to classify cell suspensions more quickly based on measurements of the optical density. For the determination of accurate cell numbers, counting via the counting chamber under the microscope was used in the following of this work.

Experiments were also performed to determine the vitality of the bacteria, based on the staining of metabolically active cells with the dye ChemChrome V6. The results of flow cytometry and measurement in a microtiter plate can be found in the appendix of this thesis (see section 6.11.).

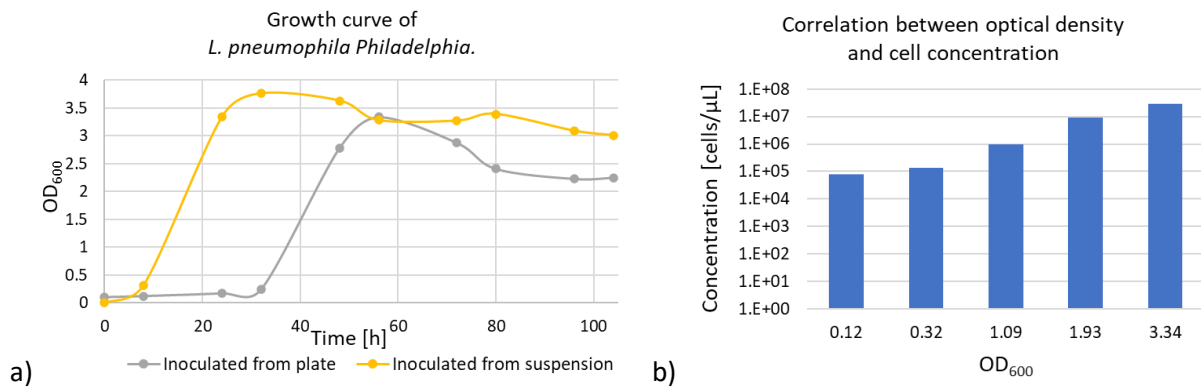


Figure 10: Growth curve and correlation of optical density to cell concentrations of *L. pneumophila Philadelphia*. a) Growth curve recorded of bacterial suspension inoculated with bacteria grown on an agar plate (grey) or in a liquid culture (yellow) and incubated in YEB at 37°C for 104 h. Cells inoculated from suspension reach the exponential growth after 8 h, while the culture inoculated from the agar plate enters the exponential phase after 24 h. After being in exponential phase for 24 h, both cultures reached their plateau corresponding to the lag phase and then begin to die, indicated by decreasing optical densities. b) Bacterial suspensions of different optical densities were counted using the Neubauer-improved counting chamber and a correlation of cell number to OD₆₀₀ (0.1 ~ 10⁴ cells/μl; 0.2-1 ~ 10⁵-10⁶ cells/μl; 2 ~ 10⁷ cells/μl and 3 >10⁷ cells/μl) could be determined.

3.2. Bacterial lysis and DNA extraction

The requirements for the bacterial sample preparation in this work were to find a simple, fast, inexpensive and feasible method without special equipment, while still being efficient in terms of lysis and DNA extraction. A simple extraction protocol, where the bacterial suspension is incubated with the reagents in a single-tube under ambient conditions was favored. Since *L. pneumophila Philadelphia* is robust against temperature, osmotic and oxidative variations (Xiang-hui Li et al., 2010), a lysis strategy just based on these stress conditions was no option. In the following a two-step protocol based on an alkaline extraction method was investigated concerning the inactivation and DNA extraction efficiency for *L. pneumophila Philadelphia*. The protocol is based on the work of Brewster and Paoli and was adapted for this work in terms of mixing, incubation time and temperature. In their work *E. coli* and *Listeria monocytogenes* were tested with the alkaline buffer for 15 min optional with heating to 65°C for 10 min (Brewster and Paoli, 2013). For experimental investigation in this work the protocol was reduced to a 1, 5 and 10 min incubation at room temperature. In addition, the bacterial suspension was not centrifuged, the elution fraction discarded and the pellet resuspended in lysis buffer by vortexing as previously reported, but the bacterial suspension was mixed directly with the lysis buffer by inverting. This procedure should be as simple as possible for a potential field application in future.

3.2.1. Lysis efficiency

First the extraction method was tested regarding the lysis efficiency of the bacteria. Since the parameters were changed to the protocol described in the literature, it must be ensured that the bacteria are still inactivated and there is no risk of infection. Figure 11 shows bacterial suspensions with and without treatment of the alkaline buffer and after incubation on the appropriate growth medium (BCYE-Agar). Without the addition of the lysis reagents, a bacterial lawn grew after 7 days of incubation. After the addition of the lysis buffer, no colonies were observed for the cell concentrations of 5×10^7 , 1×10^8 and 2×10^8 cells/ μl independently of the incubation time. Two colonies were able to grow at the highest cell concentration of 4×10^8 cells/ μl after treatment with the lysis buffer for 1 min. With an increased incubation time of the bacteria with this concentration to 5 or 10 min also no colonies were growing anymore. Even at high *Legionella* concentrations, a strong reduction in cell growth was observed by incubation with the modified alkaline lysis protocol only for 1 min. However, to ensure complete inactivation of the cells, an incubation time of 5 min is recommended based on these results.

Inactivation by inverting has worked well with prepared suspensions from the laboratory. In natural reservoirs, however, *Legionella* can also be found in biofilms or their hosts such as amoebae. Accordingly, they are not as accessible as the cells tested here and the lysis efficiency might be worse. In the future, such samples should also be tested in order to get as close as possible to the composition of real water samples.

The fact that alkaline lysis is more promising than thermal lysis can be supported by the example images of corresponding suspensions under the microscope. If a untreated bacterial cell suspension was viewed under the microscope as shown in Figure 12 a), the bacteria show their typical single cell and fibrous appearance. A temperature treatment, induced by an incubation in a heating block at 50°C for 20 min followed by an incubation in a freezer at -80°C for 20 min, resulted in no detectable change according to the cell number (see Figure 12 b). Only the morphological cell structures were in a smaller range compared to the untreated cells with less long bacterial filaments. Probably small numbers of cells were also disrupted already, which was not detectable at this magnification. A visible change is accompanied after the incubation with the alkaline lysis buffer as can be seen from Figure 12 c). No cell structures could be identified under the microscope at this magnification, confirming the inactivation efficiency of the alkaline lysis method.

Incubation time [min]	0	1	5	10
Cell concentration $\left[\frac{\text{cells}}{\mu\text{L}}\right]$ 5×10^7				
1×10^8				
2×10^8				
4×10^8				

Figure 11: *L. pneumophila* Philadelphia at different concentrations (5×10^7 , 1×10^8 , 2×10^8 and 4×10^8 cells/ μL) and incubation times (0, 1, 5 and 10 min) with alkaline lysis buffer. Compared to the initial cell number without lysis buffer showing an overgrown agar plate, all bacterial suspensions were completely inhibited in growth after cultivation on BCYE-agar plates for 7 days at 37°C , except the highest cell number with 4×10^8 cells/ μL incubated for 1 min showed two colonies highlighted by yellow arrows.

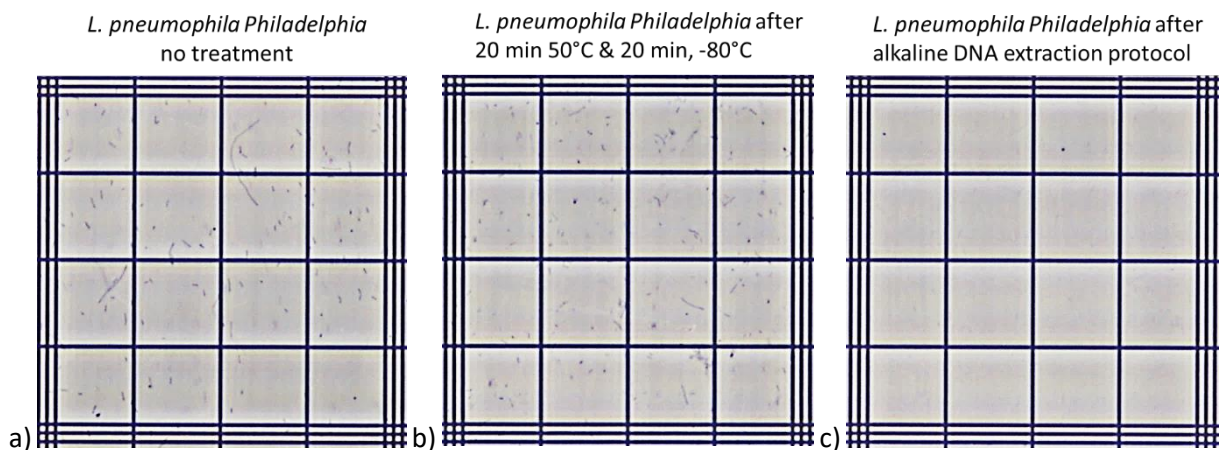


Figure 12: Microscopic pictures of *L. pneumophila* Philadelphia suspensions with and without treatment imaged in the Neubauer-improved counting chamber, placed under the Nikon Eclipse Ci microscope using the 10 x objective in phase contrast and the IC Capture software. a) Natural bacterial suspension shows single cells and fibrous structures. b) After incubation at 50°C and -80°C for 20 min respectively, less bacterial filament occur but cells can still be detected. c) After a 5 min incubation with the alkaline lysis buffer, no intact cells but only some cell debris can be detected.

3.2.2. Extraction efficiency

After ensuring lysis efficiency by inactivation of the bacteria, the second step was to examine the alkaline buffer with respect to DNA extraction. Since all cell components are still in the suspension after lysis, an absorbance measurement for concentration determination was not an option, since this does not provide reliable values due to the residual components. Instead, gel electrophoresis was used for visualization and quantification of extracted DNA. Different intense bands corresponding to the extracted gDNA could be detected according to the input cell number as shown on Figure 13. The higher the cell number the more intense was the band occurring at the top of the agarose gel. Since the genome of *Legionella* has a size of 3.4 Mbp (Chien et al., 2004) the DNA does not migrate through the whole gel, but ran slower than the largest fragment of the ladder, consisting of 1 kb. Interestingly the band intensity faded with increasing incubation time. Alkaline conditions can not only lead to cell disruption and denaturation, but also to DNA fragmentation at high concentrations (Crump et al., 1990; Sabriu-Haxhijaha et al., 2020). Especially for the lower cell numbers 5×10^7 and 1×10^8 cells/ μL an incubation for 5 or 10 min had an impact on DNA integrity, as indicated by the fading bands at the top of the agarose gel and smeared traces at the bottom.

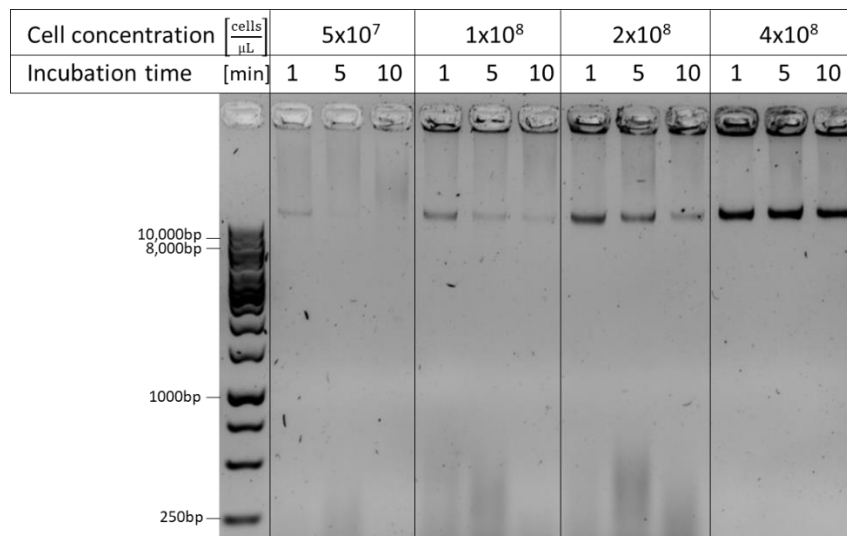


Figure 13: Verification of DNA extraction after incubation with alkaline lysis buffer by agarose gel electrophoresis. A volume of 10 μL of each lysis sample was loaded on a 1 % agarose gel and visualized after gel electrophoresis under UV light. A 1 kb ladder was loaded next to the samples as size reference. The extracted gDNA from *L. pneumophila* Philadelphia with a size of 3.4 Mbp can be seen at the top part of the gel. Band intensity correlates with increasing cell concentration. The longer the bacteria were incubated with the lysis buffer the less intense the DNA band could be detected, as the alkaline conditions also cause DNA degradation with prolonged exposure.

In the following, the alkaline lysis was evaluated with regard to its efficiency. For this purpose, extractions were carried out on three different days, each time with new bacterial suspensions to ensure independence of the experiments. By determining a standard curve of a sample with a known concentration, in this case the 1500 bp band of the 1 kb ladder, the intensity values on the gel could be used to conclude to the concentration in the original sample. Figure 14 a) shows the images of the agarose gels after gel electrophoresis of the diluted extraction samples as well as the corresponding standard curves. One *L. pneumophila* genome has a mean mass of 3.7 fg and was taken as a reference for the calculation of the extracted DNA amount per cell (Joly et al., 2006). The above described alkaline protocol with a 5 min incubation time for the DNA extraction from *L. pneumophila* Philadelphia, yielded in an average of 2.63 fg extracted gDNA per cell as shown in Figure 14 b), which corresponds to an average extraction efficiency of 64-77 % (see Figure 14 c). A possible explanation for the non-100 % yield and the variations between the experiments may be that bacteria were clustered together and the bacteria inside this conglomerate were therefore not or unequally reached by the lysis buffer. Also the determination of the cell number is not 100 % precise and may contribute to differences between the experiments.

In comparison, standard DNA extraction methods based on spin columns or a phenol chloroform treatment for example, are consisting of multistep protocols where elaborated equipment such as centrifuges, heating block or shaking devices are needed. On the basis of the results obtained in this work, a fast two-step protocol using an alkaline and neutralizing buffer without the need of any laboratory devices could be performed under ambient conditions and was suitable for the effective lysis and extraction of the gDNA from *L. pneumophila* Philadelphia.

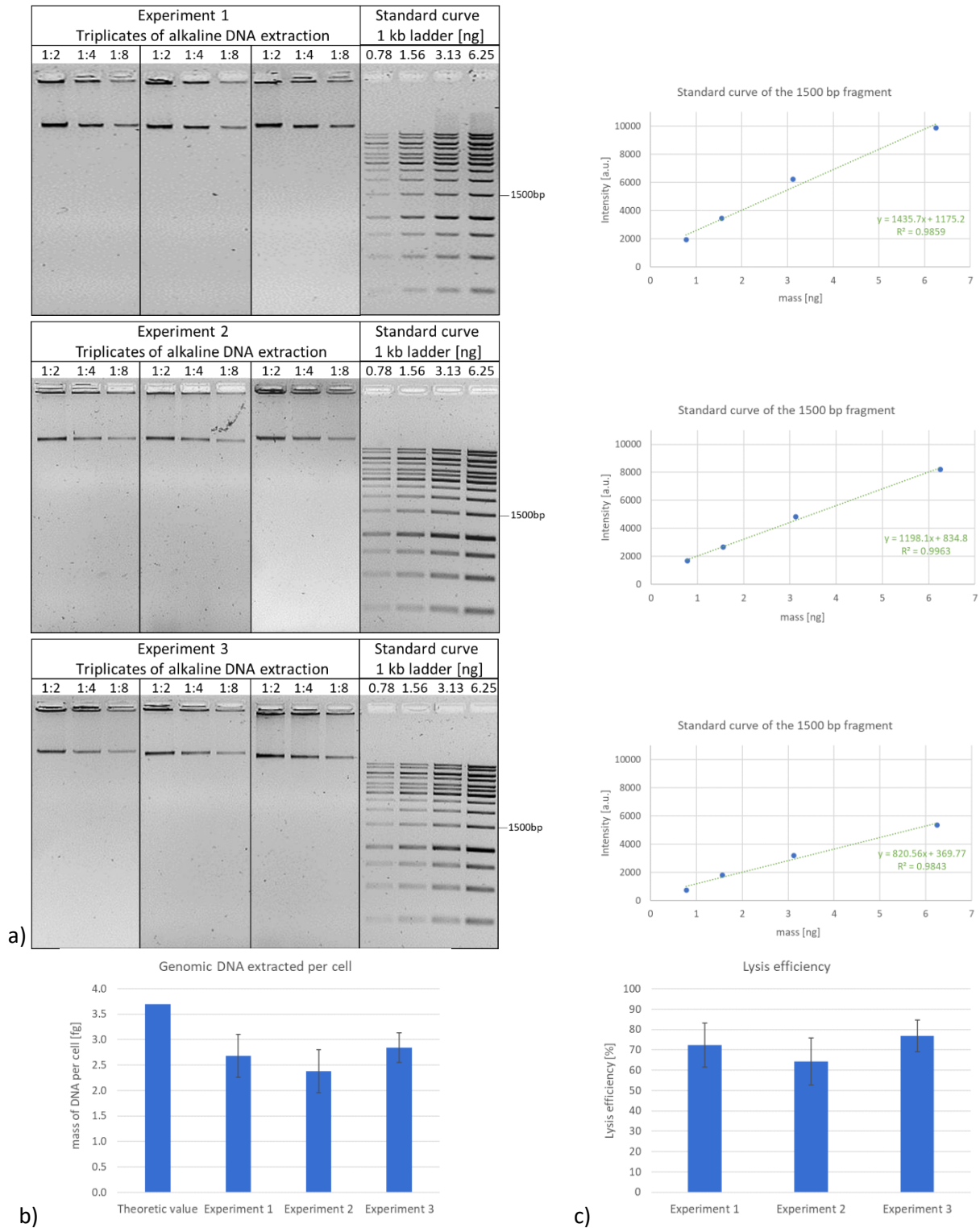


Figure 14: a) Dilution of the gDNA after alkaline extraction and visualization by agarose gel electrophoresis (1 % agarose gel, 120 V, 75 min) and comparison to standard curve, generated from the 1500 bp band of the 1 kb ladder also loaded onto the gel. Three independent experiments were performed with freshly prepared bacterial cultures and each experiment was tested in triplicates. The cell number of each repetition was determined by cell counting in the Neubauer-improved counting chamber. b) After analysis with ImageJ, it was shown that the alkaline lysis protocol with a 5 min incubation was able to extract an average of 2.63 fg of gDNA per bacterial cell, which corresponds. c) The extraction efficiency was determined by a comparison of the experimental values to the theoretic value reported in the literature and yielded in a lysis efficiency of 64-77 %.

3.3. Characterization of the fiber chip fabrication

Depending on the requirements of the fiber chip, different treatments of the fiber materials were needed. To create a hydrophobic boundary around a defined reaction space, a wax-like polymer mixture was tested for patterning different fiber materials by printing. For the development of a fiber-based electrophoresis unit, different electrically conductive materials were applied as electrodes and investigated together with the contact electrodes with respect to their quality and stability.

3.3.1. Patterning

Standard paper materials such as cellulose with a sturdy structure can be used directly for printing. The desired pattern is achieved by melting the printed hydrophobic mixture and penetrating the inter-fiber spaces. For patterning cellulose filters, material from two manufactures (Ahlstrom-Munksjö and Macherey-Nagel) and a blue polymer-resin mixture were used. The filter paper from Ahlstrom-Munksjö showed sharper edges of the channel compared to the filter paper from Macherey-Nagel. This shows that fiber materials from the same substrate can certainly differ in terms of structuring quality. Differences in the manufacturing process, such as the alignment or irregularity of the paper surface, can influence the patterning result.

For soft materials or filters with a geometry deviating from the standard that do not fit into the printer feed a two-step transfer printing process was established. First the designed structure was printed onto an overhead film and second this overhead film was faced down onto the fiber material and briefly pressed together while heating. The glass microfiber was patterned by this transfer printing process resulting in a blue channel barrier as can be seen from Figure 15 a). The transfer printing process made it possible to pattern other geometries e.g., round filter instead of DIN A4 paper sheets as shown for a nylon filter. The patterning in general also offered the opportunity to fabricate several fiber compartments at once for high throughput experiments as can be seen from the multipad layout. The penetration homogeneity and depth of the polymer-resin mixture was evaluated by microscopy. Figure 19 b) shows top views and cross sections of glass microfiber filter after patterning with the polymer-resin mixture. The amount of polymer transferred to the fiber and the heating duration influenced the penetration homogeneity and depth. Twice the amount of blue colored polymer led to a homogenous coverage of the whole fiber area. Application of double the amount was achieved by printing the overhead film twice on the same side and then transferring it to the underlying glass microfiber. Combined with 60 sec of heat application the entire glass microfiber depth is soaked resulting in a fully closed barrier. Half of the polymer amount and an incubation for only 30 sec left white, uncoated fiber areas. By varying the amount and heat duration, it is possible to generate closed

or semi-permeable channel structures. This is advantageous if a liquid velocity is to be influenced or reaction spaces should be sealed off to one side.

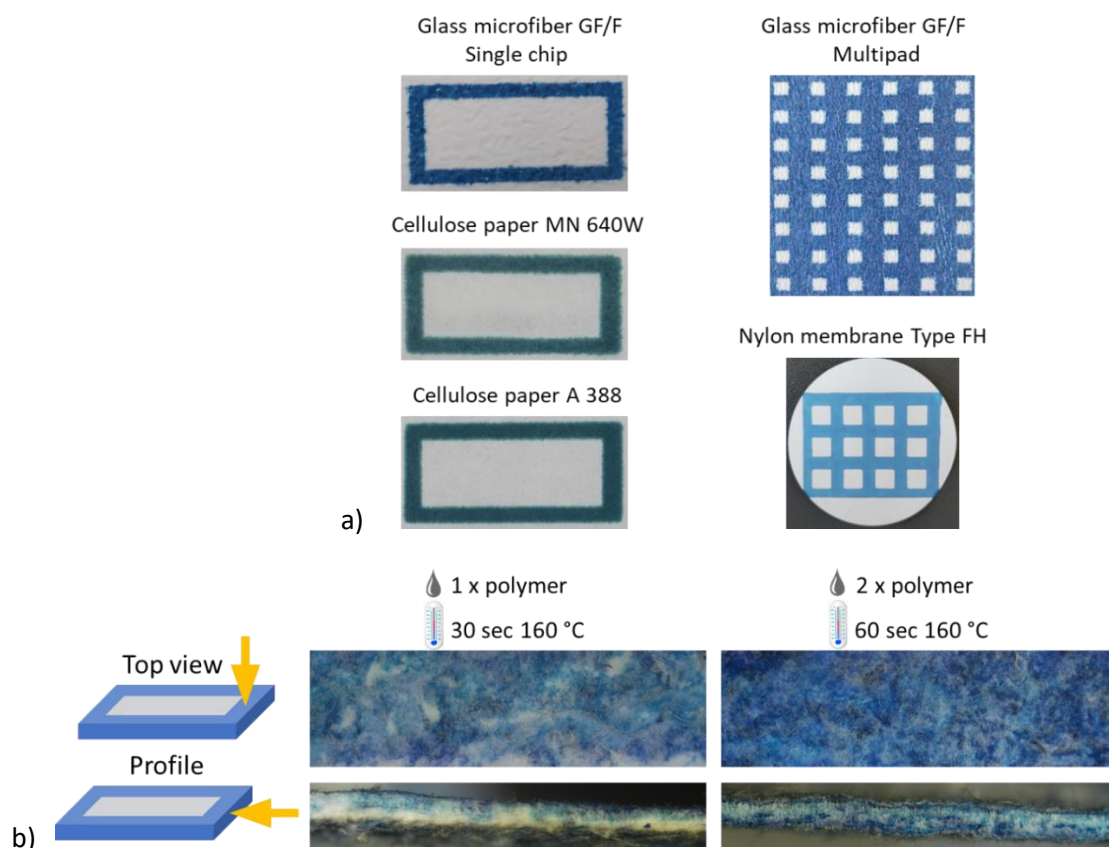


Figure 15: Filter paper after patterning with a polymer-resin mixture to generate channel structures. a) Single fiber chips of glass microfiber GF/F from Whatman, cellulose filter paper MN 640 W from Macherey-Nagel and A388 from Ahlstrom-Munksjö. Several reaction spaces generated by a multipad design on glass microfiber and nylon membrane Type FH from Merck Millipore. b) Penetration depth of patterned glass microfiber GF/F with a thickness of 420 μm (Heinsohn et al., 2022). Top view and profile of a channel barrier are shown with single and double amount of wax and 30 or 60 sec of heat application (160 °C) to the glass microfiber.

3.3.2. Characterization of imprinted electrodes

For the generation of imprinted electrodes on a fiber-based electrophoresis chips, PEDOT:PSS (a conductive polymer), copper varnish, silver ink and a carbon paste were tested as suitable conductive materials. A simple way to characterize the imprinted electrodes on the fiber chip was to measure the resistance over the whole electrode area using a circuit analyzer.

The highest electrical resistance (130 M Ω /cm) for an average distance of one centimeter has been measured at chips prepared with the copper-based varnish. PEDOT:PSS, a conductive polymer, and the carbon paste dispensed electrodes yielded mean values of 0.5 k Ω /cm and 1 k Ω /cm, respectively. The best conductivity was observed for the electrodes prepared of silver ink with a low average electric

resistance of 0.5 Ω /cm. Equally important besides high conductivity is a low variability of the conductivity between electrodes of the same fabrication batch. Reproducible values could only be generated for the silver electrodes. Both the copper varnish and the PEDOT:PSS fluctuated due to the manual application of the materials. Both methods, pipetting of viscous substances or spraying made it difficult to apply the same amount of material to the fiber. In addition, the whole chip surface discolored after a field was applied to the copper varnish electrodes and indicated that they were unstable.

Despite the excellent conductivities, the silver paste was not selected as electrode material for further experiments because also parts of the electrode were destroyed during electrophoresis and migrated together with the sample across the chip area. These interfering components were probably silver salts that dissolved from the electrode after voltage was applied. Since silver salts can be deposited as a by-product in front of the counter electrode, thus altering or inhibiting sample migration, as well as significantly overlaying the potential and current measurements, the silver electrodes tested here were unsuitable for further analysis.

The carbon paste was applied by an automated dispenser, consequently manual sources of error during the printing process could be excluded here. However, the values of the individual electrodes of a batch varied between 500-2000 Ω /cm. When printing several electrodes in series on a glass microfiber sheet, the conductivity was not dependent on the position of the electrode on the filter. Possible factors for the differences in conductivity may be due to inhomogeneities of the paste or the fiber surface. On the one hand, the paste was viscous, so that minimal differences in mixing before filling the cartridge could already lead to differences in conductivity. On the other hand, the unevenness of the fiber is challenging for the homogeneous paste application. The latter led to the fact that, in contrast to plane surfaces, the nozzle sometimes had too much or too little distance to the fiber substrate and therefore the nozzle was clogged or too little paste amount was applied. Especially for electrical parameter-based measurements, variations between electrode conductivities can have an influence on the results and make the acquisition of robust data difficult.

Several imprinted carbon paste electrodes were examined microscopically on the glass microfiber. An example is shown in Figure A2 in section 6.3. Partial penetration of the fiber matrix with penetration depths of 50-500 μ m was observed. The average height of the electrodes could be estimated in a range from 220-500 μ m. Despite the differences in the amount of electroconductive paste applied, a 3-D electrode was successfully generated within the fiber matrix. For the migration and separation of DNA samples, which was the focus of this work, the variations of the conductivity between batches of fiber electrophoresis chips were negligible, since a robust sample migration was detectable, as described in the following (see chapter 3.5.3.). Properties of the carbon paste electrodes such as good electrical conductivity, automated application by dispensing and chemical stability were important criteria for

further use. Figure 16 a) and b) shows images of the electrode manufacturing process by the Voltera dispenser and a fabricated chip next to a euro coin for size comparison (see Figure 16 c). From one glass microfiber roundfilter (\varnothing 14.2 cm), 18 fiber electrophoresis chips could be fabricated by dispensing the carbon paste within 15 min.

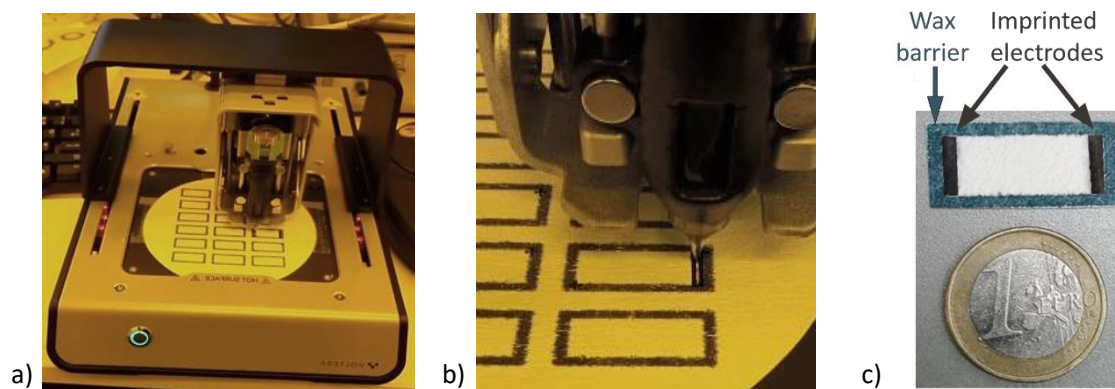


Figure 16. Images of the electrode manufacturing process (Heinsohn et al., 2022). (a) Carbon paste applied to the glass microfiber (Whatman GF/F) using the Voltera dispenser. (b) Nozzle dispensing the carbon paste in a rectangular movement from the out- to inside of the electrode area. (c) An individual fiber electrophoresis chip next to a euro coin.

3.3.3. Erosion of contact electrodes

The main electrochemical process occurring during aqueous electrophoresis is the electrolysis of water resulting in electrolysis products of hydrogen and oxygen. The gold coated copper electrodes, used in this work to connect the imprinted carbon paste electrodes on the fiber to the voltage source (see Figure 17 a), decomposed under electrochemical metal oxide formation. Microscopic images of the contact electrode surfaces as shown in Figure 17 b) indicated that the gold coating is noticeably peeled off the surface after 6 experiments which affected almost the entire electrode surface after 14 electrophoresis experiments. The cathode remained intact and showed no change in the surface coating with the same number of experiments. The corrosion of metals can occur due to metal interaction with acidic or oxygen-rich and moisture atmosphere (Chang, 1991). Furthermore, the electrolysis of water causes oxygen bubbles to settle on the surface of the electrode, which, since gold is a soft metal, could erode the coating in the form of cavitation (Dunsch, 1988). Due to these observations the gold coated electrodes are only suitable for a certain number of measurements and should not be used beyond 6 measurements.

Three gold coated pin electrodes can also be seen in Figure 17 a). These pin electrodes penetrated the fiber chip for voltage measurement in the center. The inputs of the HVDAC used had a high input resistance, as with a potentiostat. This prevented parasitic current flow through the meter from

affecting the measurement. Therefore, the three pin electrodes were only used to measure the electric potential differences between each other and to the contact electrodes, which were used in the later part of this work (see section 3.5.3.8.) to investigate whether the migrations of the sample could also be read out on the basis of locally propagating potential signals across the chip area.

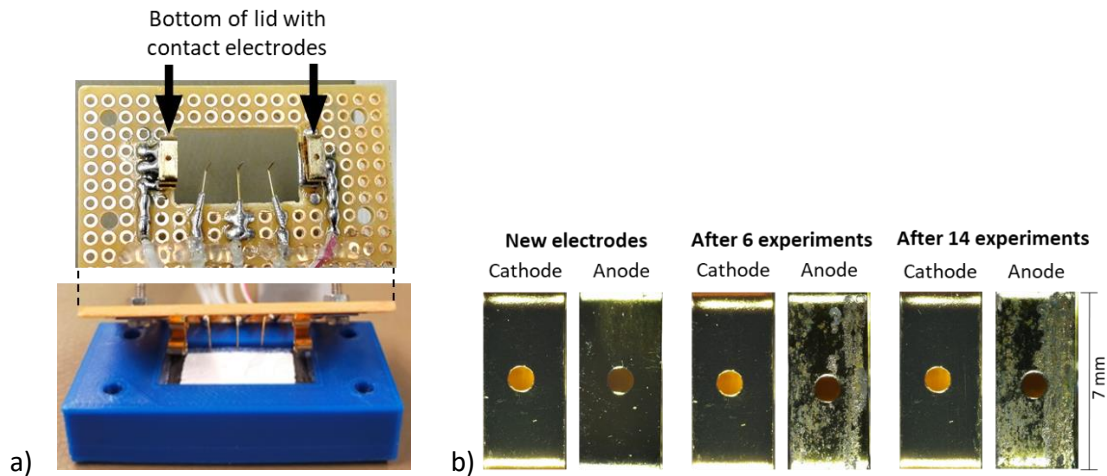


Figure 17: a) Bottom view of the gold coated electrodes contacting the imprinted carbon electrodes on the glass microfiber with the voltage source in the HVADC (modified from Heinsohn et al., 2022). b) Microscopic images of the contact electrodes after 0, 6 and 14 experiments. At the anode, destruction of the gold coating can be seen with increasing number of experiments, while the cathode remains intact.

3.4. Interaction of DNA with fiber materials under heat treatment

In a first step, basic experiments were performed to study the interaction of DNA with different fibrous substrates. Previous experiments regarding an amplification of DNA on a cellulose filter by PCR (data not shown) were difficult to implement and gave rise to the assumption that cellulose-based fiber materials captured DNA, especially upon heat treatment. Therefore, the interaction of DNA fragments with fiber substrates under different conditions was examined more closely. The initial investigations were aimed at clarifying whether the DNA-fiber interaction is temperature dependent. A commercially available 1 kb ladder, which is usually used as a size reference in gel electrophoresis, was taken as sample. For this work the ladder was used as a predefined DNA sample containing 14 fragments of different sizes ranging from 250 to 10,000 bp. The advantage using the fragment mixture is to test whether a size dependency of the interaction with the fiber occurs.

To address this question, DNA samples were pipetted onto the cut fiber pieces and heated using a PCR cycler, which was used only for heating and did not amplify the DNA. For recovery of the DNA two strategies were tested in parallel. The fiber pads were placed directly into the pockets of an agarose

gel to investigate whether DNA can be pulled electrophoretically from the fiber. The second approach should show if a sample recovery is possible in a liquid surrounding by treating the sample with four different elution buffers each. In addition to Tris and EDTA, the first and third elution buffer also contained sodium azide or sodium chloride in different concentrations and were adjusted to pH 8.5 or 8.3, respectively. The second elution buffer contained 1 mM EDTA and 10 mM Tris and was adjusted to a pH of 8.0. Elution buffer 4 was a commercially available buffer consisting according to manufacturer's instructions of 5 mM Tris at pH 8.5 (Macherey-Nagel, 2008).

Figure 18 a) shows the results after the samples were loaded on an agarose gel and electrophoresis and staining was performed to visualize the samples. The cellulose fiber heated with the DNA sample and placed directly into the gel is shown in lane 5 of the agarose gel (labeled as Cellulose). No band pattern could be observed indicating that the DNA was captured by the cellulose. The fiber pads treated with the elution buffer after incubation and heating with the DNA sample and placed directly into the gel pockets are shown on the left part of the gel (labeled as Cellulose). The corresponding elution fractions taken from these fiber pads were loaded on the left part of the gel (elution fractions from cellulose). No elution buffer composition tested made a recovery of the DNA fragments from the cellulose fiber possible, neither was it possible to electrophoretically force the DNA fragments after heating directly from the fiber piece into the agarose gel (see lane 5). The controls showed that the increase in temperature caused the DNA to adhere to the cellulose, as all DNA fragments from a paper without heat treatment could be visualized in lane 8 (labeled as Cellulose - heat). Moreover, it can be shown that the DNA fragments without the presence of fiber do not stick together under the influence of heat and can be separated electrophoretically in the same way as the original sample that has not been exposed to any influences and was also loaded in the middle of the gel (liquids from tube in lanes 6 and 7). The sample differs only in the intensity of the bands and, in addition, the band of the largest fragment is missing. This might be due to some DNA degradation occurring from the heat treatment.

In a second experiment the temperature applied to the DNA-containing fiber was reduced gradually from 95-72.7°C in separate approaches, to check whether a critical temperature for DNA retention exists. As lowest temperature 72.7°C was chosen here because the polymerase exhibits optimal enzymatic activity for DNA amplification at 72°C. After placing the cellulose pads into the pockets of the agarose gel, a slightly and smeared signal can be seen for all samples on the agarose gel but no distinct bands could be detected as shown in Figure 18 b). Three fragments can be visualized after gel electrophoresis of the fiber treated with 72.7°C and placed in the pocket of the gel but the signals are of poor quality. These results indicated a heat-dependent entrapment of the DNA sample on the cellulose fiber and that the temperature must be lowered below 72 °C to avoid irreversible retention of the DNA on the cellulose and to recover the sample.

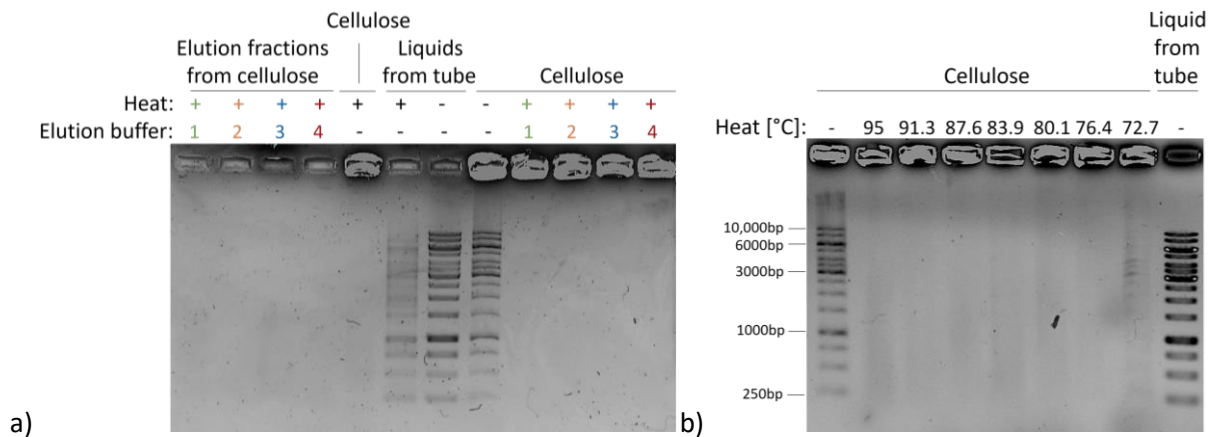


Figure 18: Investigation of the interaction of DNA fragments with cellulose filter paper A 388 after heat treatment with respect to sample recovery. a) DNA sample mixture (1 kb ladder) loaded on cellulose fiber pads, heated up to 95°C and treated with or without elution buffers afterwards. No DNA could be detected from a cellulose fiber heated with the sample (lane 5). The elution fraction of each cellulose pad, treated with the elution buffer 1-4 respectively, was taken and loaded on the left part of the gel (lanes 1-4) and the corresponding fiber pads were placed directly into the pockets of the right part of the agarose gel (lanes 9-12). Treatment with the elution buffers did not result in elution of DNA from cellulose after heating. The controls of the ladder loaded directly of the gel without heat treatment (lane 7), sample heated as liquid without fiber (lane 6) or a sample loaded on the fiber but without heat treatment (lane 8) showed the expected pattern of the DNA bands. b) Direct placement of fibers containing the DNA sample into agarose gel after heat treatment ranging from 72.7-95°C. Only at 72.7 °C a slightly band pattern could be observed, whereas the samples treated with higher temperatures only caused a faint smeared signal after gel electrophoresis. As control, the DNA ladder was loaded directly onto the gel (liquid from tube) or electrophoretically pulled from the cellulose if no heat was previously applied (lane 1).

3.4.1. Influence of substrate and 3D structure of cellulose on DNA retention

Another essential aspect that needed to be clarified was, whether the chemical nature of the substrate or the spatial structure leads to this temperature-dependent DNA retention. To address this question microcrystalline cellulose (Mc), consisting of the same chemical subunits than the cellulose fiber with an average particle size of 90 µm was tested for the retention of DNA fragments. The powder form of cellulose was mixed with the DNA sample and the whole suspension was pipetted directly into a pocket of the agarose gel or was treated with water or elution buffer and the elution fractions were loaded onto the gel as shown in Figure 19 a). From the lanes 2-4 of the agarose gel it can be seen that also the microcrystalline cellulose was binding the DNA fragments after heat treatment because only a faint signal was detectable after electrophoresis. If the whole suspension was loaded onto the gel (lane 2), especially the fragments larger than 3000 bp were missing after heating and could not be recovered by agarose gel electrophoresis. The elution fraction from microcellulose treated with water or elution buffer after heating (lanes 3-4) showed no positive effect regarding the recovery of the DNA fragments. On the contrary, sample recovery was even worse, showing only fragments of 250-1500 bp in size. The

same initial DNA sample incubated at room temperature in a tube (lane 1) or on microcrystalline cellulose and treated with or without elution buffers (lanes 5-7) allowed the detection of all fragments after gel electrophoresis.

From these experiments, it can be concluded that both the chemical nature of the organic saccharide and the fibrous 3D scaffold are responsible for the DNA adhering to the cellulose when exposed to heat, with the first aspect being more important, as shown by the experiment with microcrystalline cellulose. Nonspecific binding of DNA to cellulose under typical aqueous conditions and interference with some molecular applications has been reported in previous work and is consistent with the results observed here (Boese and Breaker, 2007). Moreover, cellulose as a network of fibrils also entraps DNA molecules physically by acting as microfilters (Su and Comeau, 1999), particularly well conceivable if the solvent is removed by evaporation because cellulose filter materials have microscopic swelling and shrinking properties. Adsorption to cellulose at high salt concentrations, in the presence of crowding agents such as polyethylene glycol, chaotropic salts or alcohol in purification of DNA samples is known (Zou et al., 2017). DNA is a negatively charged molecule and also cellulose carries a slightly negative charge, which should actually have a repellent effect (Whistler and BeMiller, 2009; Zhang et al., 2016). Increasing the ionic strength also increases the shielding effects which diminish repulsive conditions, allowing interactions to occur (Liang and Keeley, 2013). But also capturing of DNA by cellulose in pure water was observed (Zou et al., 2017).

The knowledge gained here that high temperatures led to retention of DNA on cellulose is consistent with reports in the literature that PCR on fiber materials is challenging due to several barriers, such as thermal control and inhibitory effects of paper (Seok et al., 2017). This is another aspect, why isothermal amplification methods at lower and constant temperatures may be preferred over conventional hot and cycling PCR in applications on paper-based materials. A constant and lower temperature for amplification like 60-65°C as used in LAMP or 37-42°C in Recombinase Polymerase Amplification (RPA) could reduce the DNA trapping within cellulose substrates.

3.4.2. Alternative filter materials for DNA recovery after heat application

To overcome these limitations, an alternative fiber material was sought in this work. Figure 19 b) shows the results of a glass microfiber, a 100 % chitosan fleece and a mixture of polyethersulfone and polyethylene (PES & PE) tested for the retention of DNA samples. Chitosan is the N-deacetylated form of chitin, a natural polysaccharide found in insects and crustaceans and was tested because of its alkaline nature occurring from the high nitrogen content (6.89 %) compared to synthetically substituted cellulose (1.25 %) (Ravi Kumar, 2000). The idea of using chitosan was to compare the interaction of cellulose and DNA with the adsorption of DNA to chitosan polymers, since the latter interaction is based on a charge dependence. Polyethersulfone and polyethylene were chosen because these synthetic fiber materials are usually derived petrochemically, have a high resiliency and, unlike cellulose fibers, they are produced by spinning and thus offer a higher degree of order. All fiber materials were placed directly into the pockets of the agarose gel. The chitosan fleece captured the DNA even without heat treatment and the PES & PE-mixture showed similar results as the cellulose fiber by trapping the DNA fragments after heat application.

Previous studies demonstrated that DNA can directly interact with membranes even with those that are designed to have low binding affinities. The PES-filters tested for the extraction of DNA from samples showed a moderate yield, so that retention of the DNA was already noticeable here as well (Hinlo et al., 2017; Liang and Keeley, 2013). In general, adsorption can also depend on the ionic strength and also on pH. The protonatable functional moiety of chitosan is resulting in a strong electrostatic interaction between chitosan and DNA at low pH and no charge at slightly higher pH (Cao et al., 2006). Since no alkaline buffer was used for testing the sample on the chitosan fleece, it can be assumed that the pH is too low, leading to electrostatic interaction between the DNA and chitosan. DNA incubated on the glass microfiber treated with or without heat was the only fiber material that showed signal after elution and subsequent agarose gel electrophoresis and was thus a candidate for further experiments. The glass microfiber consisted of pure borosilicate glass without any binder. In the following, the aim was to improve the dissolving of the DNA sample from the glass microfiber, since no clear band pattern was observed after heat incubation, only a smeared signal.

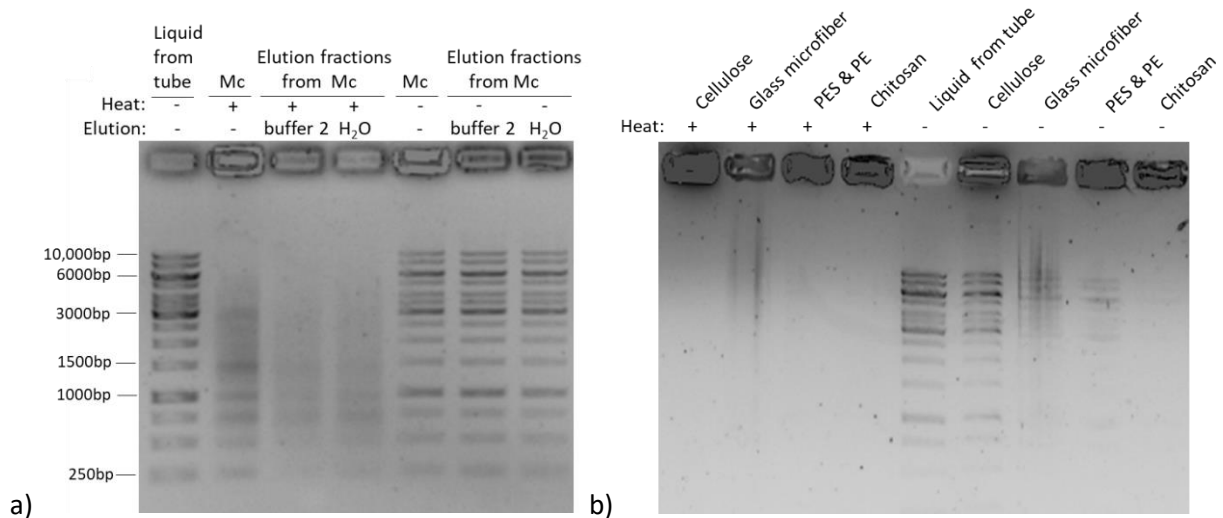


Figure 19: a) DNA sample mixture (1 kb ladder) added to microcrystalline cellulose (Mc) and incubated at 95 °C (+ heat) or room temperature (- heat). Direct placement of the samples into the pockets of a 1 % agarose gel or elution with water or elution buffer 2 and transfer of the elution fractions into the pockets of the agarose gel were compared. Sample recovery could be seen for all approaches tested without heat. Upon heat treatment a significantly reduction of DNA recovery is observed, especially in the elution fractions, with the larger fragments being retained by the microcrystalline cellulose. b) A glass microfiber GF/F, PES & PE-filter and a chitosan fleece were tested as alternative fiber materials to cellulose with respect to DNA interaction under heat application. Without heat the cellulose filter showed the best DNA recovery, followed by the glass microfiber and the PES & PE-filter. After heat treatment a smeared signal could be observed only from the glass microfiber. As controls the sample mixture was pipetted as liquid into one gel pocket in the middle of the gel.

3.4.3. Options for reducing the evaporation of liquids in glass microfibers

If the moisture content of the fibers decrease due to the heating process, the DNA molecules are likely to adsorb more strongly to the fiber and become more difficult to detach. One option to improve the DNA recovery quality was to reduce the evaporation of the sample solvent. In order to test this, the wetted glass fiber was sealed in foil or covered by silicon oil during heating. Figure 20 displays the results compared to a cellulose fiber treated in the same way and controls without evaporation protection. No DNA bands could be seen on the agarose gel of the tested cellulose samples, regardless if an evaporation reducing approach was used or not. In contrast to the cellulose fiber, DNA could be recovered from the glass microfiber in all tested samples. The glass fiber treated with silicon oil had a better yield regarding the DNA coming off from the fiber compared to the one sealed in foil or even no evaporation protection during heating. It was difficult to seal a small fiber piece of 5 mm in foil because it is either leaking or not tight enough around the fiber and evaporation can still occur. In contrast silicon oil is generating a hydrophobic compartment by surrounding the aqueous solution leading to a more efficient evaporation protection. Overall, glass fiber was shown to induce lower

nonspecific retention of DNA under heat compared to cellulose, which can even be slightly improved by protecting the liquid from evaporation with silicone oil.

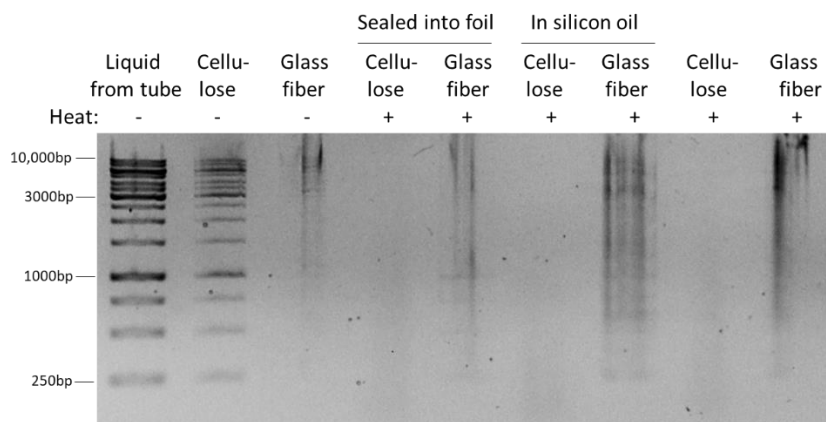


Figure 20: a) DNA sample mixture (1 kb ladder) heated on pieces of cellulose and glass microfibers and tested for sample recovery by reducing the solvent evaporation by sealing the fibers in foil or overlaying with silicon oil. After agarose gel electrophoresis using a 1 % agarose gel, no DNA bands from the cellulose filter could be recovered. Every glass microfiber showed DNA signals with the one covered with silicon oil being the best. Als controls the DNA sample mixture was pipetted directly into the first gel pocket or was tested on both fiber materials without heat treatment.

3.4.4. Test of different pore sizes and suitable elution buffers for DNA recovery from glass microfibers

A band pattern could already be detected by covering the glass microfiber with silicon oil, but the bands are still smeared. Also no band pattern could be seen, if no heat was applied to the glass microfiber containing the DNA sample. Subsequently, the glass microfiber was also tested with the previously described elution buffers (see Table 6 in Section 2.2.) to investigate whether they could lead to more efficient DNA recovery. Furthermore, glass microfibers with different average pore sizes ranging from 0.7 μm to 2.7 μm were compared to investigate whether a larger pore size might lead to a reduced sample retention (see Figure 21). After DNA application, heat exposure and incubation with the corresponding elution buffer, both the fiber from which the elution fraction was taken and the elution fraction itself were loaded next to each other onto the agarose gel.

All elution fractions of the glass fibers with an average pore size of 0.7, 1.6 or 2.7 μm , regardless of which elution buffer they were treated with, showed the original band pattern only in different intensities. The less signal came from the fiber directly placed in the gel, the better the fragments were visible in the corresponding loaded elution fractions. This implies a successful elution of the DNA from the fiber. A comparison of the different buffers tested for elution showed that the second one, containing 1 mM EDTA and 10 mM Tris-HCl at a pH of 8, was the most suitable one in terms of recovery

of the DNA fragments from the glass microfiber independently of their pore size, by yielding the most intense band pattern on the agarose gel. Based on this result, the elution buffer 2 was used exclusively in the following experiments of this work.

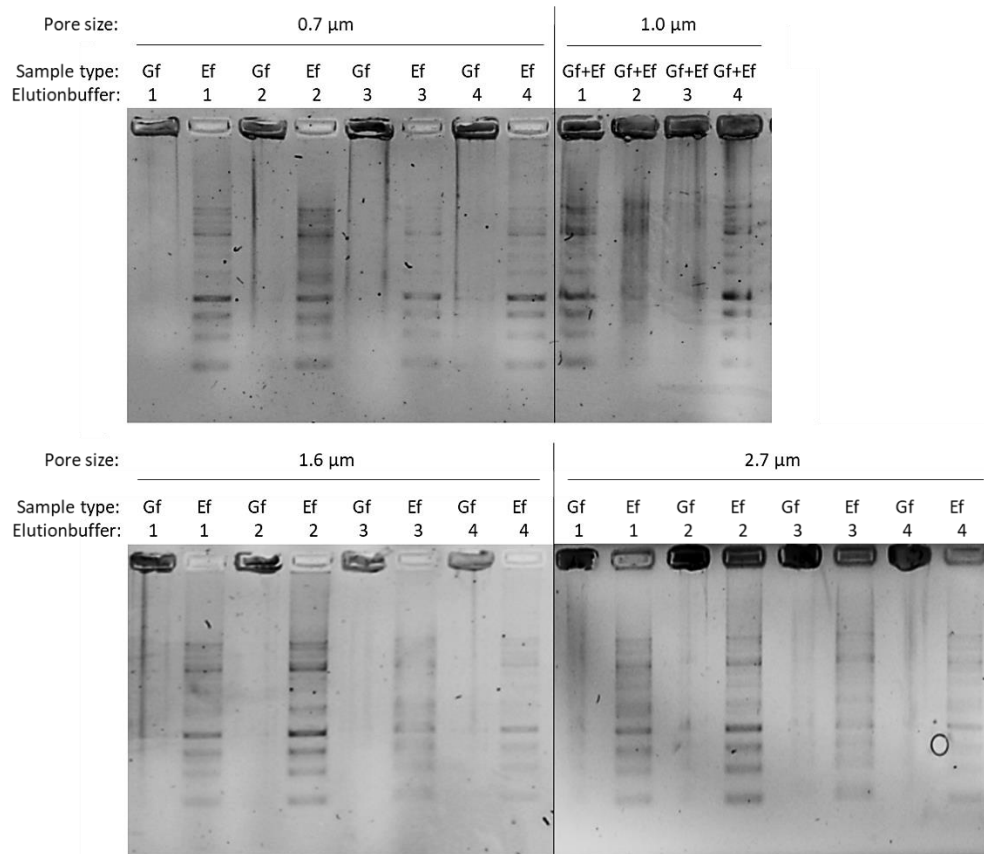


Figure 21: DNA sample mixture (1 kb ladder) tested for the recovery from glass microfibers with different average pore sizes (0.7, 1.0, 1.6 and 2.7 μm) upon heating and treatment with elution buffers 1-4. The glass microfiber (Gf) and the corresponding elution fractions (Ef) were loaded separately onto a 1 % agarose gel and compared with respect to the best band pattern after agarose gel electrophoresis. No elution was possible from the glass microfiber with an average pore size of 1.0 μm, consequently fibers and elution fractions were applied onto the gel together. Elution buffer 2 showed the best DNA recovery signal due to the most intense band pattern of all fragments.

For the glass microfiber with an average pore size of 1 μm it was not possible to gain any elution fraction, consequently only the wet fiber was transferred to the gel. This fiber type had the highest basis weight and a particularly fluffy texture compared to the other fiber types. Presumably, this is why the liquid was retained particularly well by the fiber and it was not possible to obtain an elution fraction. For this fiber type, the bands were still smeared and could only be better resolved by the addition of elution buffers 1 and 4.

The use of different pore sizes can be advantageous depending on the application. Using Elution Buffer 2, three glass fiber materials of different pore sizes with successful DNA recovery can be considered

for further applications. Chemicals like Tris and EDTA which were included in the elution buffer, kept the pH constant and prevent DNA degradation from nucleases (Panda et al., 2019). Slightly alkaline conditions have also been shown to be effective for the elution of DNA (Vandeventer et al., 2013).

3.5. Fiber electrophoresis

The migration of particles under the influence of an electric field is an important method for the analysis of biomolecules. DNA and protein mixtures are mostly separated by size in combination with charge using gel-based electrophoresis techniques such as agarose or polyacrylamide gels on a laboratory scale. The integration of such techniques into a miniaturized format is particularly advantageous when it comes to aspects such as portability, speed of measurement and analysis, disposability, decreased waste production, and low manufacturing costs. The aim of this work was, to investigate the behavior of DNA within a μ PAD under the influence of an electric field for future applications with biological samples e.g., water analysis with portable test systems. The question to be answered here was, whether a DNA sample can be reliably pulled across the fiber surface by the electric field between the imprinted electrodes. In the following, the first chapters cover the development steps towards a working fiber-based electrophoresis. Therefore, different fiber materials, cellulose and glass microfiber, as well as electrode materials, PEDOT:PSS and carbon paste were tested in combination with different measurement parameters and chips dimensions. Subsequently, the best variant will be characterized in more detail. Different artificial as well as biological samples will be tested and a statement about the time frame and robustness will be made. Additionally, these fiber electrophoresis experiments were carried out with simple and cost-efficient equipment.

3.5.1. Migration of DNA samples in cellulose with imprinted PEDOT:PSS electrodes

Due to the easy application of the polymer mixture without special equipment simply by pipetting, in combination with the reasonable resistances of the applied electrodes, the first fiber electrophoresis experiments were performed with PEDOT:PSS electrodes. The electrodes used in for the experiments described below consisted of 6 μ l of a 3-4 % PEDOT:PSS solution pipetted on the intended areas. PEDOT:PSS, a conductive polymer consisting of positively charged conjugated Poly(3,4-ethylenedioxythiophene) (PEDOT) and negatively charged saturated polystyrene sulfonate (PSS), is known as the most successful conductive polymer in terms of practical application. PSS acts as a surfactant by dispersing and stabilizing the PEDOT in water and other solvents. Good conductivity

properties (10^{-2} - 10^3 S cm⁻¹) and high work function (5.0-5.2 eV) can often induce spontaneous charge transfer with fast kinetics, thus providing PEDOT:PSS with catalytic properties (K. Sun et al., 2015). Furthermore, its flexibility and optical transparency in the visible range makes it an attractive candidate for optoelectronic devices (K. Sun et al., 2015; Xia and Dai, 2021).

First, electrophoretic DNA migration was tested within a patterned cellulose fiber. In the previous experiments (see section 3.4 Figure 18), cellulose showed high DNA retention when exposed to heat, whereas DNA was easily recovered from cellulose without heat exposure. The question arose whether the electrophoretic movement of the DNA molecules also causes retention of the sample on the cellulose filter or whether the electric field can even prevent a possible interaction. Subsequently, DNA migration and sample recovery from cellulose-based filter materials were tested under the influence of an electric field and are described in detail in section 6.4.

After the chip was prewetted, a volume of 1 µl of a 1 kb DNA ladder, containing 14 fragments of different sizes, was used as a representative DNA sample for these fiber electrophoresis experiments without constant fluid intake. Since the DNA ladder is not detectable by visible light, it was premixed with two dyes used as color indicators to track the progress of DNA migration as in conventional agarose gel electrophoresis without affecting the DNA samples. The dyes bromophenol blue and xylene cyanol do not bind the DNA, but migrate at the same rate as DNA of a given length in a polymer matrix such as an agarose gel. Visual tracking of the movement of the tracking dyes, suggested that the DNA also moved together with the dyes through the electrophoresis towards the counter electrode. However, sample recovery was not or barely possible with the patterned cellulose filters and thus no verification of this assumption was possible. An alternative cellulose material from another manufacturer or a reduction of the chip size to reduce the influence of evaporation due to long connection times did not lead to an improvement either (see results in section 6.4.1.).

When an untreated cellulose fiber was used, i.e., the patterning process with the wax-like polymer was omitted, DNA could be partially eluted from the surface in front of the anode and verified on an agarose gel. Since heat is also applied to the cellulose during patterning to melt the imprinted polymer and allow it to penetrate the fiber, the application of heat appears to alter the cellulose in a way that enhances nonspecific retention of DNA. However, even in the unpatterned fiber chip, only a fraction of the applied sample could be electrophoretically moved within the cellulose filters, and the rest of the sample remained at the sample application site (see Figure A6 in section 6.4.2.). Thus, it can be concluded that DNA applied to a heat-unmodified cellulose can be partially recovered by elution even after exposure to an electric field. However, the application of the electric field only caused the movement of a fraction of the sample, thus the cellulose retains DNA even under voltage application. The disadvantages just described led to the exclusion of cellulose as a material for fiber

electrophoresis. Consequently, an alternative fiber material had to be found to enable a successful DNA migration by fiber electrophoresis.

Since good results were obtained in the experiments with glass microfibers with respect to the non-specific retention of DNA under the influence of heat and, in combination with elution buffer 2, the DNA sample could be recovered well from the fiber, fiber-based electrophoresis with this glass microfiber was further investigated in the following.

3.5.2. Migration of DNA samples in glass microfiber with imprinted PEDOT:PSS electrodes

As mentioned earlier, different chip designs can be created via flexible patterning. In the next two sections, single and dual channel glass microfiber chips will be investigated with respect to fiber electrophoresis of DNA samples.

3.5.2.1. Single channel fiber electrophoresis chip

The glass microfiber with the smallest pore size (0.7 μm) was used to investigate a possible separation effect of DNA fragments by size. A picture of the experimental set up is shown in Figure 22 b). The sample chip was connected to the voltage source via crocodile clamps. In addition, a digital multimeter was integrated for current monitoring during fiber electrophoresis. The control chip was also equipped with crocodile clamps to apply the same pressure to the fiber as in the sample chip, but the connection to the voltage source was missing. Images of the glass microfiber chip (Whatman GF/F) during electrophoresis are shown in Figure 22 a). The blue spot corresponding to the DNA mixed with the tracking dyes started migrating already after 30 sec upon a voltage exposure of 90 V. After 1.5 min a bluish and elongated spot can be seen where the sample was loaded and after 3.5 min the blue color disappeared completely. In comparison, a control chip without voltage application was documented after the same time points. The blue sample spot remained in front of the cathode over 6 min without fading.

For verification of the DNA migration, the areas between the electrodes were cut into four equal parts. Each of these fiber pieces were incubated with 25 μl elution buffer overnight. Subsequently the elution fractions were loaded onto a 1 % agarose gel casted with GelRed to visualize DNA fragments under UV light. Figure 22 d) shows the elution fractions corresponding to their fiber position on the chip area. If no voltage was applied the ladder could be eluted from position 1, corresponding to the sample loading

zone, confirming that no DNA molecules diffused over the chip area and showed the same pattern as the sample control loaded directly onto the gel. Under the influence of the electric field, the DNA fragments migrated towards the anode in the sample chip. This could be demonstrated by a successful elution of the ladder from the end of the chip (position 3 and 4). It was noticeable that the ladder showed the same composition in the elution fractions than in the originally sample. Fragments of all sizes could be visualized in the elution fractions 3 and 4, suggesting that DNA molecules migrated through the fiber network but were not separated by size.

The average diameter of one DNA base pair is 0.34 nm (Martin, 1996), suggesting linear fragments of DNA ranging from 250-10,000 bp exhibit lengths of 85-3400 nm. Glass microfiber filters with an average pore size of 700 nm theoretically should retain 8 of the larger fragments from 2500-10,000 bp if only the length of the molecules is taken into account. Fibers act as sieving matrices restricting the lateral motion of the molecules. The possible motions of a single polymer chain through a surrounding polymer network was described as reptation model (de Gennes, 1971). When DNA is paving its way in a tunnel of the fiber network, two variants of motion can be distinguished, reptation with and without orientation, as depicted in Figure 22 c). If the DNA conformation is unchanged under the influence of the electric field, the mobility decreases approximately linearly with increasing molecular mass, described as reptation without orientation (Heller et al., 1994; Semenov et al., 1995; Southern, 1979; Viovy, 2000). For large DNA molecules or at high electric fields, the molecules become stretched and oriented in the direction of the electric field (Stellwagen and Stellwagen, 2009). Under these conditions, known as the reptation with orientation regime, separation by molecular mass is no longer possible (Semenov et al., 1995; Stellwagen, 1985). Since the voltage applied in this experiment is relatively high for the small migration distance, the reptation model with orientation probably applies to in this case and results in a longitudinal alignment of all DNA fragments, regardless of size, to make their way through the interstices of the fiber.

Sample migration appears to be much faster in glass microfiber (5 min) compared to a cellulose-based fiber electrophoresis chip (18-45 min) with the same chip length of 1.9 cm. This reduction of migration could be explained by a trapping effect of the cellulose towards the DNA molecules. Adsorption of DNA to cellulose has been observed previously although the concrete interaction of both molecules remains still unclear (Boese and Breaker, 2007; Bourne et al., 1956; Zou et al., 2017). Previous studies reported a negative surface charge for cellulose mainly due to the carboxyl groups (Dubitsky and Perreault, 1995; Sood et al., 2010). DNA also carries negative charge, due to the negatively charged phosphate backbone. According to this, a repulsive effect and no binding would actually seem logical. The repulsive force can be counteracted by salts leading to a binding event although cellulose could capture DNA also in pure water (Zou et al., 2017). Also in the electrophoresis, cellulose exhibits a trapping

feature reported especially for other polysaccharides e.g. amylose (Foster, 1957). A slightly slower migration of dsDNA compared to ssDNA by the probably stronger affinity for the cellulose was also described previously (Araújo et al., 2012; Li et al., 2015; Su et al., 2007). In this work, a new fiber-based electrophoresis system on the basis of glass microfiber with imprinted electrodes clearly had an advantage over cellulose-based filter paper concerning the migration of DNA through a patterned fiber channel. Glass microfiber was also preferred over cellulose paper because complexing between polysaccharides and the fiber were avoided and made the detection of carbohydrate easier (Bourne et al., 1956). Coaggregation or adsorption of DNA to cellulose in the presence of chemicals, high salt concentrations and/or crowding agents such as polyethylene glycol which destabilize the DNA structure and facilitate its interaction with the cellulose fibers have been reported, although the exact mechanism of nucleic acid binding remains unclear (Zou et al., 2017). Heat also seems to have an influence on adsorption of DNA binding affinity to cellulose. When exposed to heat, cellulose can be further broken down into sugars like glucose (Hoseney, 1984; Wyman, 1994). The partial change in chemical composition could promote interaction with DNA. The binding of carbohydrates to DNA is also already the subject of research with regard to antitumor antibiotics (Nicolaou et al., 1992; Walker et al., 1990). Here, however, the binding of carbohydrates to the small groove of DNA is usually referred to. In this work, a modification of the cellulose seems to take place, which promotes a non-specific retention of the oligonucleotides both during heating with DNA and before the application of DNA. However, the heat required to apply the polymer during the patterning process does not affect the sample migration in the case of the glass fiber.

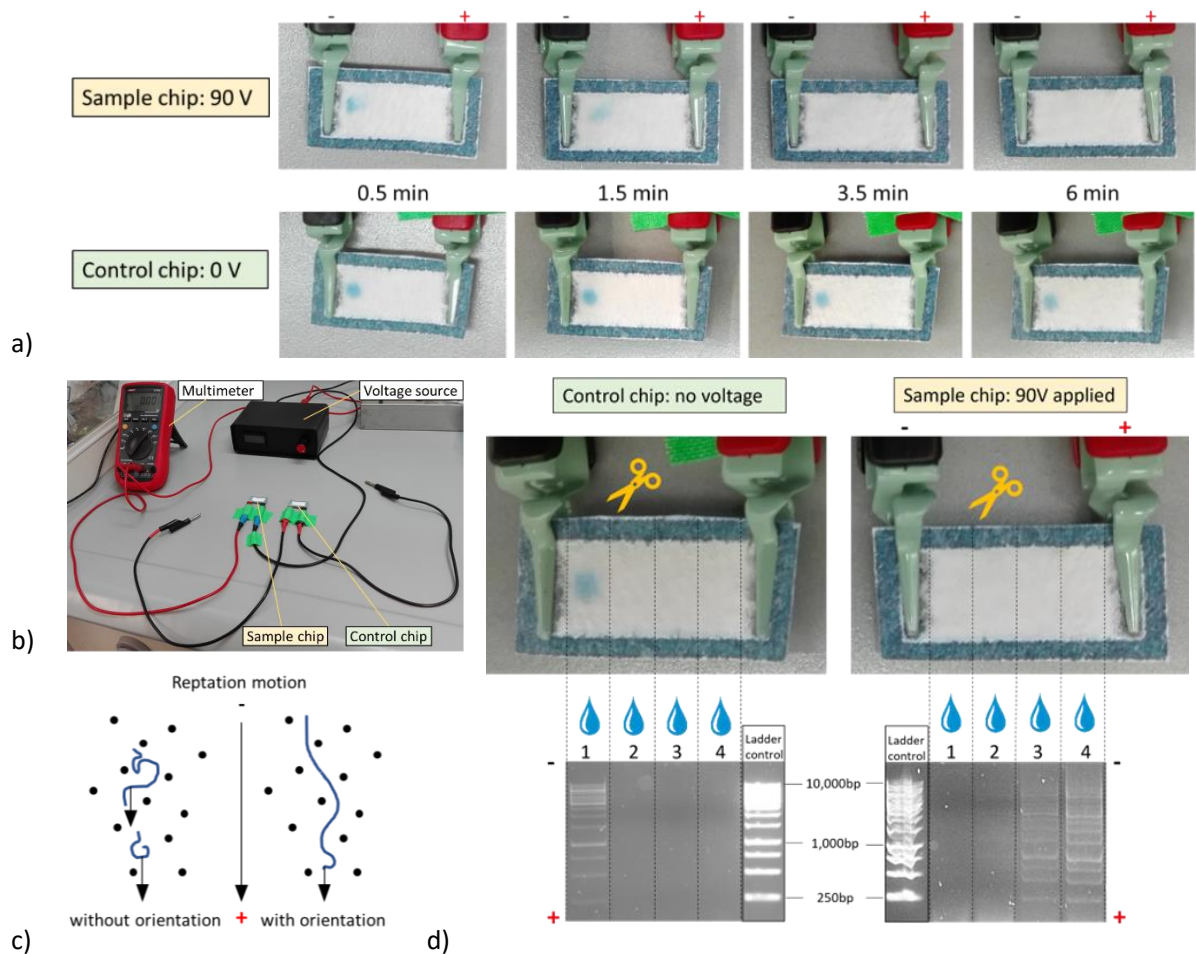


Figure 22: Glass microfiber-based electrophoresis with a sample and control chip (Whatman GF/F). a) A time series of images was recorded after 0.5, 1.5, 3.5 and 6 min. A sample chip was tested at 90 V and a chip without applied voltage was taken as a control. The sample mixture (1 kb ladder) with tracking dyes began to spread towards the anode after 1.5 min and was not longer detectable after 6 min. The sample stayed at the sample loading zone when no voltage was applied. b) The experimental setup shows the fiber chips with their imprinted electrodes connected to the crocodile clamps. Unlike the sample chip, the control chip was not connected to the voltage source. A digital multimeter was used to monitor the current during the experiment. c) Reptation model with and without orientation showed by blue DNA rods moving to the pores of a matrix indicated by the black circles. With increased electric field the DNA molecules become stretched and migrated to the counter electrode independent of their size. d) To verify sample migration the chips were cut into four pieces, treated with elution buffer (2) and the elution fractions were loaded for gel electrophoresis onto a 1 % agarose gel. Each column on the agarose gel represents the loaded elution fraction of one quarter on the chip area. A successful sample migration could be confirmed by elution of the ladder band pattern from position 3 and 4 of the fiber electrophoresis chip, whereas the control chip without electric field application showed the sample signal in position 1, corresponding to the sample loading zone. DNA fragments of all sizes could be detected, indicating a size independent migration. The sample mixture was loaded directly onto the gel as a ladder control and represents the original sample composition.

3.5.2.2. Dual channel fiber electrophoresis chip

An interesting question regarding a test device development was, whether two samples could be measured simultaneously on one electrophoresis chip. Therefore, a new chip design was prepared using the wax-like printing technique, in which the glass microfiber chip was split into two channels. For testing new patterns on fiber substrates in fiber electrophoresis, the use of textile dyes as sample material is particularly suitable without wasting rare and more expensive DNA samples. Textile dyes are already interesting candidates in replacing currently used tracking dyes as bromophenol blue due to their lower toxicity, fewer side effects and environment-friendly properties (Al-Awadi, 2013; Deka et al., 2015; Siva et al., 2008). As shown in Figure A7 in section 6.5. the textile dyes were successfully pulled across the fiber chip with two channels by electrophoresis. It was further shown that the highly visible orange dye could be electrophoretically moved a second time by rotating the fiber chip 180 degrees and again applying an electric field. This suggested that samples could be pulled away from their sample application site and back again.

In a second experiment the dual-channel fiber chip was tested with DNA samples using fiber electrophoresis. The lower channel (b) was loaded with the previously tested 1 kb ladder containing DNA fragments ranging from 250-10,000 bp as sample mixture. To the upper channel (a) a second ladder consisting of smaller DNA fragments ranging from 25-500 bp was added. In addition, the same experiment tested whether the PEDOT:PSS electrode material could be prevented from migrating with the DNA sample. For this purpose, a hydrophobic dashed line, made of the same polymer mixture as the outer channel boundary, was placed in front of the two electrode regions as a barrier. This was done during the patterning process of the chip with the wax-like polymer. The line was dashed to prevent complete shielding of the electrode and thus the electric field.

Each channel was prewetted and the samples were added immediately one after the other. Images of the agarose gels showing the eluted fractions from the corresponding channel positions, confirm the migration of both sample mixes in the sample chip by glass fiber electrophoresis as shown in Figure 23. After 6 min of connection time, the DNA fragments of both ladders could be detected mostly in respective position 4 a and b, corresponding to the area in front of the anode for both channels. In addition, low concentrations of the DNA bands can be found in position 3 a and b, indicating that not all of the sample has migrated to the anode yet. No DNA fragments ranging from 25-75 bp can be detected in the position 3 a of the upper channel of the sample chip. One possible explanation would be that the smaller fragment ran faster than the larger ones and already reached the counter electrode. Another reason for the missing fragments could be an inefficient elution of the sample. A chip tested without voltage served as a control and showed that all DNA fragments stayed at the

sample loading zones 1 (a) and 1 (b) if they were not electrophoretically pulled towards the counter electrode, as can be seen after treatment of the cut chip with the elution buffer and subsequent gel electrophoresis. The band below 250 bp corresponding to the conductive polymer PEDOT:PSS of the pipetted electrodes, as already shown in Figure A5 in section 6.9.1., can still be seen in the elution fractions from the lower channel positions of the control chip 1 (b) and the sample chip 1 (b) - 4 (b). Thus, the dashed polymer boundary in front of the imprinted electrodes does not affect the migration of the sample itself, but did not prevent the migration of the conductive ink across the chip.

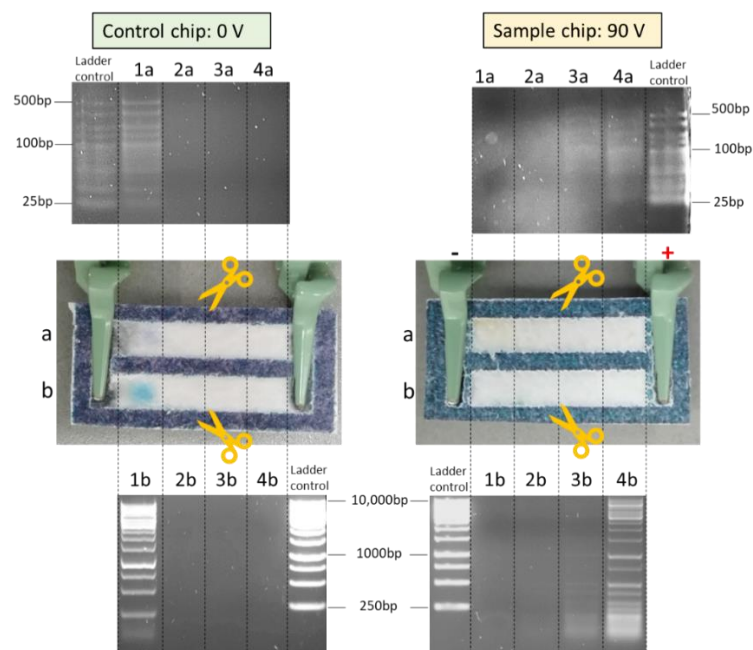


Figure 23: Dual-channel glass microfiber electrophoresis chip (Whatman GF/F) tested for sample migration with two DNA sample mixtures. A control chip without voltage was taken as control and verified that the samples (ladder with DNA fragments ranging from 25-500 bp in channel (a) and 250-10,000 bp in channel (b)) does not diffuse and remained at the sample loading zone. Sample migration by fiber electrophoresis could be verified by detecting the eluted DNA fragments from 25-500 bp on a 3 % agarose gel and the fragments from 250-10,000 bp on a 1 % agarose gel followed by gel electrophoresis. The blue indicator dye of the DNA samples disappeared upon exposure to the electric field (45 V). The samples could be successfully detected in both channels in front of the anode corresponding to the positions 4 (a) and 4 (b). Both sample mixtures were loaded separately as ladder controls directly onto the gel and represent the original sample composition.

To conclude, a small and simple glass microfiber electrophoresis chip with imprinted electrodes of PEDOT:PSS could be fabricated and used to move DNA molecules with a broad range of sizes (25-10,000 bp) upon the application of an electric field of 90 V. Since the pore size is large compared to the molecules and the samples are exposed to a high voltage within a short travel distance, the DNA strands probably elongated parallel to the fiber and thus migrate at the same speed regardless of their

size. If the tracking dyes are considered, migration was over 7 times faster in electrophoresis chips using glass microfiber than cellulose-based chips with same the chip length. However, the migration of DNA could not be tracked properly in cellulose-based sample chips. A successful DNA migration by fiber electrophoresis in combination with the elution protocol, determined in chapter 3.4.4. to verify the sample migration, could only be achieved using a glass microfiber. Alternative chip geometries, for example two channels in parallel, showed the same migration behavior of the DNA samples and offer the possibility to run multiple samples simultaneously.

The main drawback of PEDOT:PSS is the poor chemical and mechanical stability (Gueye et al., 2020; Kim et al., 2019). Swelling, cracking and breaking due to the connection to the voltage source and buffer addition could lead to a degradation of the imprinted electrode. Since the fiber chips with PEDOT:PSS as electrode material also fluctuated greatly in terms of the measured current values and parts of the ink itself were pulled over the chip distance, an alternative electrode material was sought and described in the following.

3.5.3. Migration of DNA samples in glass microfiber with carbon paste imprinted electrodes

Carbon provides good conductivity, electrochemical inertness and the ability to mix it with other compounds as additives, which makes it a preferred electrode material (McCreery and Cline, 1996; Rutledge, 2018; Vandaveer et al., 2004). The mixture of carbon powder and a liquid binder, mostly lipophilic organic substances, is defining carbon paste electrodes (Adams, 1958). During the 1960s carbon paste electrodes were used for electrochemical studies on redox pathways of numerous organic compounds (Švancara et al., 2009). The electrodes have shown low background currents, about 200 nA or lower, compared to solid graphite or noble metal electrodes over a wide potential range (Kalcher et al., 1995; Lindquist, 1973; Monien et al., 1967; Olson and Adams, 1960). As part of this work, the application by screen printing was tested first to apply the carbon paste to the glass microfiber as described in section 2.5.3. As an alternative to distilled water as running fluid, a 5 mM Tris-(hydroxymethyl)-aminomethane (Tris) buffer pH 8.0 was tested to check whether a more pH stable environment would improve the fiber electrophoresis results. Tris in combination with hydrochloric acid provides a strong pH buffering effect in a range of pH 7-9, while having low conductivity at relatively high concentrations (Aronsson and Gronwall, 1957).

Both running fluids were tested for migration of the DNA sample mixture (1 kb ladder) on fiber chips with carbon electrode at voltages of 90 and 45 V, as shown in Figure 24. Since the migration rate for the new electrode material was still unknown, the connection time was doubled in order

to reliably detect sample migration. The use of Tris buffer instead of distilled water causes a faster migration of the DNA fragments. After 10 min voltage exposure to 90 V, the DNA fragments could be detected already at position 4 corresponding to the area in front of the anode when wetted with Tris buffer, compared to a chip that was run in distilled water, which showed DNA fragments spread over the positions 1-3 but not in 4. Halving the voltage resulted in a decreased migration of all fragments. In distilled water the sample spread only from position 1 to 2. Samples with Tris buffer as running buffer run even until 3 but did not reach the end of the chip.

Nevertheless, 45 V seemed to be sufficient for a successful DNA transport through the fiber chip and was set as the standard voltage for subsequent experiments. The finding of improved migration distance of the sample in Tris buffer instead of water was used, so this running buffer was also applied in the following experiments.

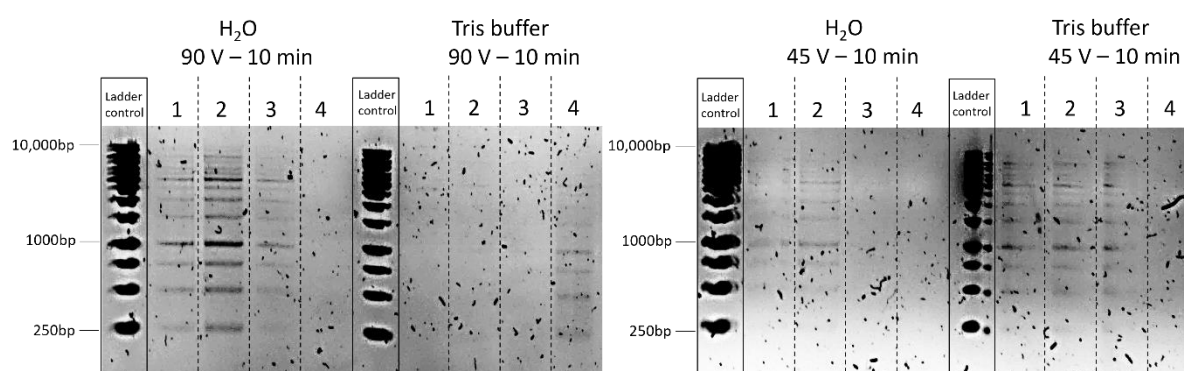


Figure 24: Glass microfiber-based electrophoresis chip (Whatman GF/F) with screen printed carbon paste electrodes tested for sample migration with DNA sample mixtures. Individual chips were pretwetted with 80 μ l water or Tris buffer and connected for 10 min to a voltage source providing 90 or 45 V. The migration distance was verified by elution of the sample after fiber electrophoresis, transfer to a 1 % agarose gel and agarose gel electrophoresis. Samples run in Tris buffer migrated faster than in water and reached the third quarter of the chip area after 10 min application to 45 V and the area directly in front of the electrode (position 4) if 90 V were applied. The sample mixture was loaded as ladder controls directly onto the gel representing the initial sample composition.

The automated dispensing of electrically conductive substances is attractive for a faster and easier production of the fiber electrophoresis chips. Therefore, dispensing of the carbon paste on the glass microfiber by the Voltera printer was used as an alternative application method to screen printing, as described in section 2.5.3. Parts of the following work were published by Heinsohn et al. in 2022.

The elution fractions of the corresponding chip areas showed no DNA sample on the agarose gel after 10 min fiber electrophoresis at 45 V. If the connection time was reduced to 5 min, the sample could be eluted from the position in front of the anode as can be seen from the agarose gel shown in Figure 25 a). These results indicate that DNA samples run faster in chips with carbon

electrodes applied by dispensing than by screen printing. The carbon paste is a suspension of conductive particles which, depending on the application method, may be applied more densely to the fiber material. In screen printing, less material is applied to the fiber than by using the dispenser, and it is therefore less conductive. This could also be determined from the measured resistances. The electrodes applied by screen printing had resistance values in the k Ω to M Ω range, whereas the carbon paste applied by dispenser showed values in the Ω to k Ω range.

As an alternative to the voltage source with the crocodile clamps, a new measurement setup was developed. The aim was to create a measurement setup that is closer to a later readout device. The glass microfiber chip was placed in a 3D-printed holder to achieve stable positioning, and gold-coated electrodes were used instead of crocodile clamps. It was found that with frequent use of the crocodile clamps, the fiber surface turned brownish, indicating that parts of the copper-based crocodile clamps decomposed and were also pulled over the fiber surface. For this reason, the gold coated electrodes were preferred to the crocodile clamps in the following, as they are more inert. These were mounted on a lid that can be turned down onto the printed electrodes. An illustration and description of the HVADC (High-Voltage-Analog-Digital-Converter) measurement setup can be found in section 2.5.6. With this setup, the connection time and the start of the measurement could be controlled digitally and the records of the measurement parameters were stored on the integrated Raspery-Pi. The experiments described before using the glass microfiber with the dispensed carbon paste were repeated several times with the new measurement setup to test their robustness.

Since it should be excluded that the tracking dyes of the DNA ladder affect the sample migration, only the 1 kb ladder without the tracking dyes and diluted in 5 mM Tris running buffer was used in the following experiments of this work. Figure 25 b) shows exemplary triplicates of the glass microfiber electrophoresis connected for 5 min at a voltage of 45 V. In all experiments, the sample mix was successfully pulled across the chip surface by fiber electrophoresis and subsequently detected by elution from the cut quarters, transfer to an agarose gel, and visualization under UV light after agarose gel electrophoresis. This showed on the one hand that the dispensed carbon paste electrodes led to reproducible results using the alternative measurement setup HVADC and supported the observed result that the electrode fabricated by dispensing reduced the migration time from 10 to 5 min compared to electrodes fabricated by screen printing.

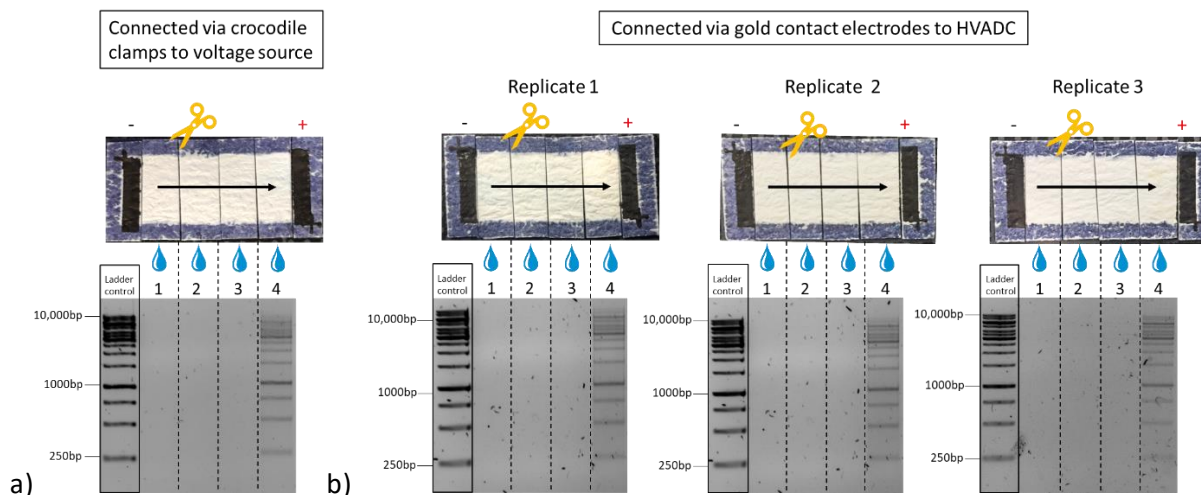


Figure 25. Glass microfiber-based electrophoresis chips with dispensed carbon paste electrodes tested for sample migration. a) Connection to a voltage source via crocodile clamps (Heinsohn et al., 2022). b) Connection to the HVADC measurement set up by gold coated contact electrodes. Upon the application of an electric field of 45 V all samples migrated to the opposite electrode, verified by dividing and elution of the chip area and visualization by gel electrophoresis using a 1 % agarose gel. Each column on the agarose gel represents the loaded elution fraction of one quarter on the chip area. As a control the 1 kb ladder was loaded directly onto the gel representing the initial sample composition.

3.5.3.1. Velocity of migration of DNA samples in glass microfibers

In order to observe the migration behavior of the sample in a time-dependent manner and to determine a rate of migration, the DNA samples were exposed to the electric field for different durations. Figure 26 shows individual fiber electrophoresis chips connected from left to right for one minute longer each with a maximum connection time of 5 min. Again, no size-dependent migration was observed. A slightly concentration dependent movement could be seen instead because the fragment pattern differs in intensity during spreading over the chip area. After 1 min, the sample has already spread to the chip center and after 2 min it has reached the second half of the glass microfiber chip, starting to collect in front of the anode. After 5 min all molecules have visibly migrated to the end of the chip with a migration distance of 1.9 cm using. The electric field strength could be determined to be 24 V/cm by considering the applied voltage (V) and migration distance (L) using equation 3.1. In comparison to previously reported work, the glass microfiber electrophoresis offers a fast method to migrate DNA sample while using a relatively low electric field. Higher electric fields (160-210 V/cm) were required for a similar migration time of 6-10 min in electrophoresis experiments of dsRNA or ITP of DNA on cellulose filter paper (Li et al., 2015; Na et al., 2021). A decrease in the electric field was accompanied by an significant increase in the connection time, as reported for the separation of various polysaccharides on glass fiber paper (Lewis and Smith, 1957).

Accordingly, a rate of migration or electrophoretic velocity of 6.3×10^{-3} cm/s can be determined from

these experiments using the migration distance (L) and migration time (t_m) in equation 3.2. This result can also be expressed in a physical quantity called electrophoretic mobility. It provides information on how fast a charged sample can move in dependence on the strength of the electric field surrounding it. The electrophoretic mobility can be calculated by dividing the observed electrophoretic velocity v by the electric field strength E using equation 3.3 (Charcosset, 2015).

$$E = \frac{V}{L} \quad (3.1)$$

$$v = \frac{L}{t_m} \quad (3.2)$$

$$\mu_{EP} = \frac{v}{E} \quad (3.3)$$

An electrophoretic mobility of $2.6 \times 10^{-4} \text{ cm}^2/\text{Vs}$ could be determined for the glass microfiber-based electrophoresis chip developed in this work. Compared to free solution mobilities of DNA in TAE-buffer, which were found to be $3.75 \times 10^{-4} \text{ cm}^2/\text{Vs}$ for DNA $\geq 400 \text{ bp}$ at 25°C (Stellwagen et al., 1997), the velocity deviated only by a factor of 1.4 even though the sample was in a fiber matrix and thus underlines the unhindered movement through the substrate.

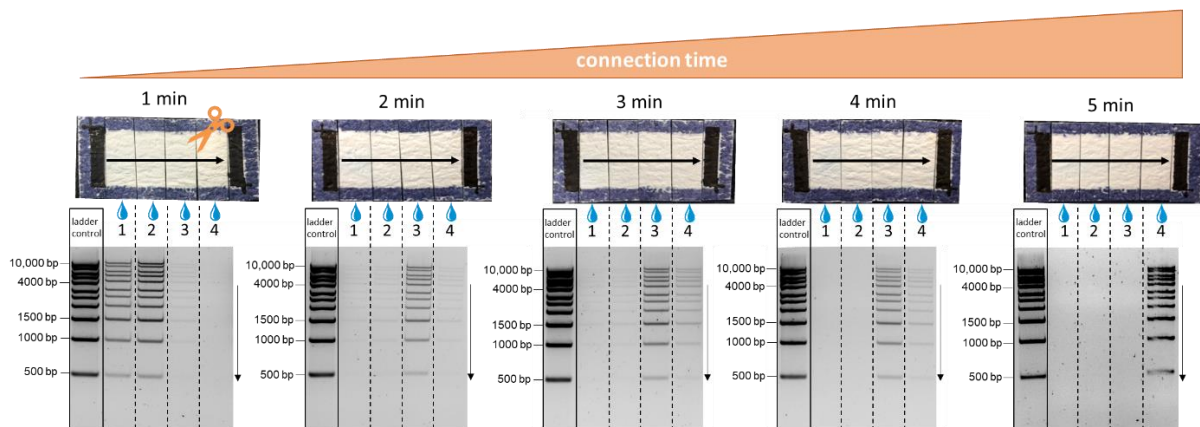


Figure 26: Glass fiber-based electrophoresis chips (Whatman GF/F) with dispensed carbon paste electrodes tested for different connection times to the HVADC (Heinsohn et al., 2022). From left to right, the individual chips were used for electrophoresis at 45 V for 1, 2, 3, 4 and 5 min. Sample migration was visualized by dividing and elution of the chip area and subsequent agarose gel electrophoresis using a 1 % agarose gel. Each column on the agarose gel represents the loaded elution fraction of one quarter on the chip area. With increased connection time, the sample was detected closer and closer to the counter electrode. As a control the 1 kb ladder was loaded directly onto the gel representing the initial sample composition.

3.5.3.2. Reduction of pore size and voltage

In the following it was tested whether a separation of the DNA fragments according to their size can be achieved with a reduction of the pore size and/or the voltage. The lowest pore size for glass microfiber which was commercially available at this time showed an average pore size of 0.4 μm . The voltage was tested with the 45 V, as previously applied to the fiber chips and also tested with a low voltage of 5 V, since 5 V power supplies are one of the most commonly used and applicable power sources.

But fiber electrophoresis for 5 min at 45 V and subsequent elution and visualization on an agarose gel showed, just like the fiber with a pore size of 0.7 μm , no size dependent migration of the DNA fragments of the 1 kb ladder (see Figure 27 a). A further reduction of the voltage to 5 V was tested with the glass microfiber with an average pore size of 0.7 μm at connection times of 10 and 20 min. Since the migration speed of the sample decreases with reduced voltage, the connection times had to be adjusted. As can be seen from Figure 27 b) the ladder migrated to the middle of the chip area upon an exposure to 5 V for 10 min and to the second half of the chip after 20 min. The velocity of the DNA sample pulled at 45 V in the glass microfiber with 0.7 μm could be determined to 6.3×10^{-3} cm/s. A reduction of the voltage from 90 V to 5 V resulted in a 4 times slower migration velocity (1.6×10^{-3} cm/s) of the sample. To summarize, neither a reduction of the pore size about 43 %, nor the 18-fold reduction of the voltage resulted in a separation of the DNA fragments by size.

However, the results also showed that the DNA samples can be pulled over the fiber at lower voltages. If lower voltages are used, the connection time must be extended accordingly and, in the case of long connection times, the chip must be prevented from drying out, otherwise the electrophoresis would come to a standstill. Since shorter connection times were preferred and no separation effect by size was visible at either 45 V or 5V, 45 V continued to be chosen as the connection voltage for the study of DNA migration in glass fiber. Short connection times are, on the one hand, advantageous for the later application and, on the other hand, the retarding effect of evaporation is avoided.

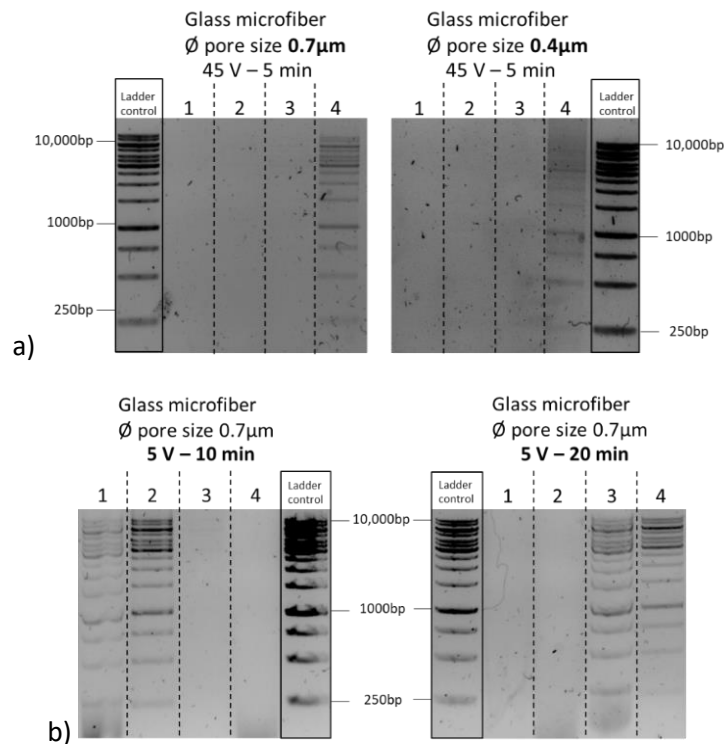


Figure 27: Reduction of pore size and electric field tested for size separation of a DNA sample mixture (1 kb ladder) in glass microfiber electrophoresis. a) The elution fractions of the fiber chips with an average pore size of 0.7 μm (Whatman GF/F) and 0.4 μm (Macherey-Nagel MN85/220 BF) treated with elution buffer (2) after fiber electrophoresis at 45 V for 5 min showed fragments of all sizes at position 4 (position in front of the anode) on the 1 % agarose gel upon gel electrophoresis. b) Decreasing the voltage to 5 V resulted in a decreased migration rate of the sample, as the first half of the glass fiber (Whatman GF/F; 0.7 μm) was reached after 10 min and the anode after 20 min, as seen when the elution fractions of the fiber pieces were transferred to the agarose gel and were visualized after gel electrophoresis. But again, no size-dependent movement was observed. The sample mixture was loaded directly onto the gel as a ladder control and represents the original sample composition.

3.5.3.3. Alternative detection of migrated DNA by staining via GelRed

An alternative detection method to visualize the DNA movement without destroying the fiber structure could be achieved by using an intercalating DNA dye. GelRed was chosen because of its high sensitivity to dsDNA, ssDNA and RNA. Furthermore it is described as non-cytotoxic and non-mutagenic and heat stable up to 50°C (Biotium, 2013). DNA fragments can easily be detected at different positions within the migration distance by the appearance of a fluorescent spot after incubation with GelRed (see Figure 28). To verify that the stained spots correspond to the migrated DNA, the samples were eluted afterwards again and visualized by agarose gel electrophoresis as described before. Figure 28 a) confirms that the fluorescent spots correspond to the DNA detected on the agarose gel, showing the band pattern of the sample mixture in the elution fraction 4. A control chip tested without DNA sample remained dark upon GelRed staining and UV excitation, and the agarose gel also showed no sample

after gel electrophoresis of the elution fractions (see Figure 28 b). Black shadows were visible around mainly in the last quadrant of the control chip and also around the bright fluorescent samples. These dark discolorations are probably components of the carbon paste that were released from the printed electrode surface after an electric field has been applied. They also migrate over the chip surface but appear dark after staining with GelRed, since less dye can be incorporated here than in the sample and in the remaining chip area. Despite these by-products, clear sample identification was possible with GelRed staining, which simplified the readout of sample migration.

Also the migration of a single DNA fragment could be detected as shown in Figure 28 c). A 910 bp DNA fragment, amplified from the gene coding for the 16S rRNA of *L. pneumophila* Philadelphia, has been used as a sample for the glass microfiber-based electrophoresis. Again, after 1, 2, 3 and 4 min, the sample could be stained using GelRed and corresponding to the fluorescent spots on the chip area, the fragment of the correct size could be detected via elution and visualization on the agarose gel. The single fragment showed a comparable velocity of migration as the sample mix. This is consistent with the observation that all fragments of the 1 kb ladder migrated with the same speed, including a DNA fragment with a comparable fragment size of 1000 bp.

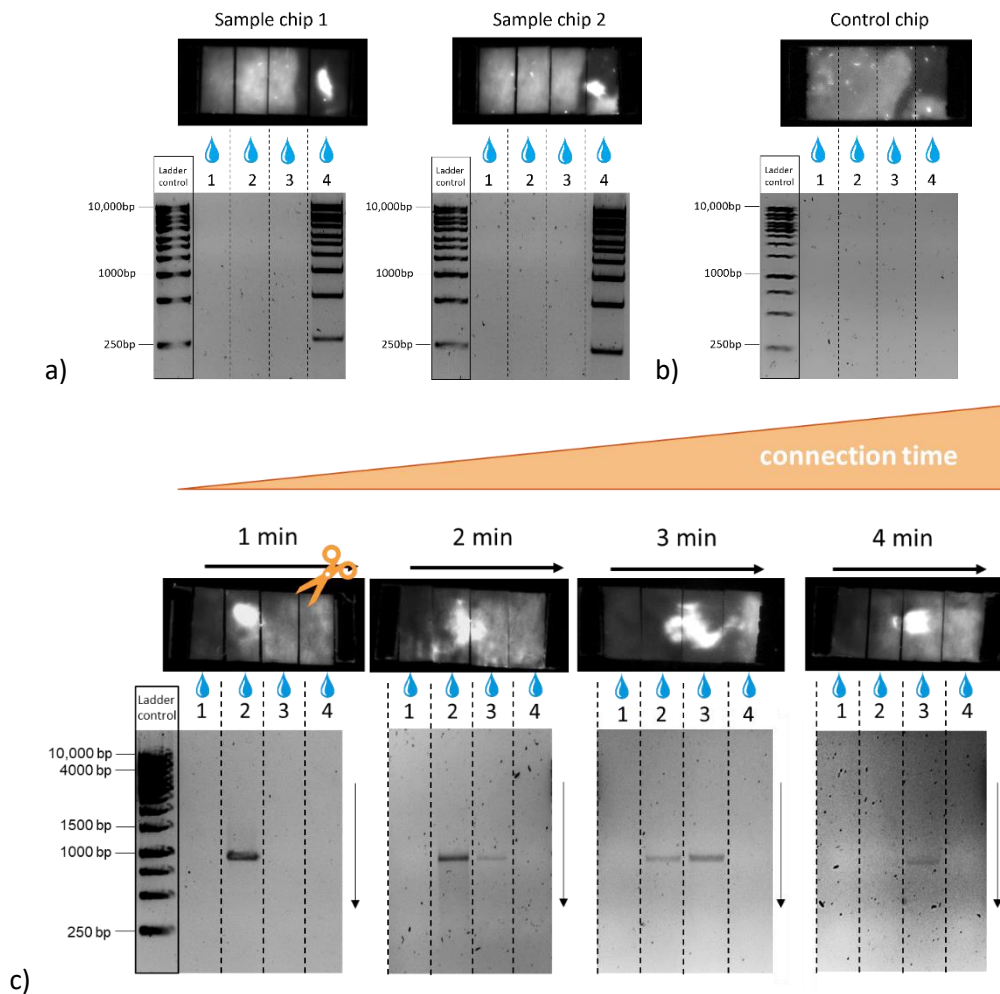


Figure 28: Alternative visualization of DNA samples by post staining with the intercalating dye GelRed and no interference with subsequent elution (modified from Heinsohn et al., 2022). a) Fluorescently stained sample mixture (1 kb ladder) in front on the anode upon fiber electrophoresis using a glass microfiber (Whatman GF/F) with dispensed carbon paste electrodes connected to the HVADC at 45 V for 5 min. Cutting and treatment of the fiber pieces with elution buffer 2 confirmed the fluorescent spot as the sample when visualized on a 1 % agarose gel after agarose gel electrophoresis. b) Control chips tested without sample showed no fluorescent spot on the chip and no bands on the agarose gel upon elution. c) Images of a 910 bp DNA fragment amplified from *L. pneumophila* Philadelphia and used as sample (100 ng) in fiber-based electrophoresis. From left to right the individual chips were used for electrophoresis at 45 V for 1, 2, 3 and 4 min and showed a time-dependent migration visualized by subsequent GelRed staining and elution. As a control the 1 kb ladder was loaded directly onto the gel representing the initial sample composition.

3.5.3.4. Test of DNA integrity

In addition to staining the DNA upon migration, it was essential to test if the described fiber electrophoresis method is compatible with downstream assays, for example PCR. This has been tested with the elution fractions after fiber electrophoresis by using them as templates for a PCR reaction as well as for real-time PCR. First, the fiber electrophoresis was performed using the 910 bp fragment. For this purpose, the glass microfiber chip was wetted with 80 μ l of 5 mM Tris buffer, 100 ng of the

910 bp fragment was used as a sample and the dispensed carbon paste electrodes were connected to the HVADC via the gold coated contact electrodes at 45 V, as previously described. In this case, the sample was electrophoretically pulled for 3 min to ensure that the sample was still detectable in the center of the chip area and had not possibly already run into the electrode.

After the sample has been recovered again by eluting with the elution buffer 2 from the quartered chip, a standard PCR was set up with primers for the 910 bp fragment and 1 μ l of each elution fraction was used as template DNA. After amplification, the PCR reactions were loaded next to 10 μ l of the remaining pure elution fractions onto the agarose gel, which is shown in Figure 29 a). An obvious increase in fragment concentration was observed after PCR amplification for all samples after comparison of the band width with the elution fractions without amplification. Even in the elution fractions 1 and 4, corresponding to the sample loading zone and the end of the chip, where no DNA bands could be detected directly after electrophoresis, a PCR product was amplified. This indicated that a small amount of sample is not moving with the major sample spot but the concentration is rather small. If the experiment had been extended in time, it is likely that all the sample would have been concentrated in front of the anode. An unspecific amplification can be excluded since the negative control containing all reaction compounds except the template DNA, showed not product.

The successful recovery by elution and amplification via PCR after the field-driven movement through the fiber strongly suggests that DNA integrity was maintained. Since the amplification product is highly concentrated and provided only an end-point result, also a real-time amplification with the same elution samples and same primers has been used for characterization. SyGreen was added to the Mastermix to track the generation of the amplified sequences over time. Signals obtained from real-time PCR correspond to the pure elution fractions as can be seen from Figure 29 b). The negative control without template showed no signal amplification. In contrast, the positive control, tested with the template DNA before fiber electrophoresis was carried out, showed a sigmoidal curve progression as expected. The fluorescent SyGreen dye intercalated into the dsDNA and generated a fluorescent signal. The increase in target DNA therefore correlates with the increase in fluorescence from cycle to cycle. Samples with higher initial target concentrations required less temperature cycles to generate a detectable fluorescence signal, which appeared earlier than lower concentrated samples. The fluorescence signals occurring first in real-time PCR (elution fractions 3 and then 2) correspond to the most intense bands of the elution fraction, in agreement with the amplified PCR reactions visualized on the agarose gel. Amplification signals of the remaining elution fractions that did not show a band on the agarose gel could also be detected by real-time PCR. Elution fraction 1 occurred as the third signal in real-time PCR followed by the amplification signal from elution fraction 4. These signals are also consistent with the results of the standard PCR, where the amount of sample that has already reached the anode is less concentrated than the amount that remains at the sample loading zone, as

indicated by the width of the bands on the agarose gel.

This underlines that small sample concentrations that were not detectable by elution stayed intact within the high electric field and were sufficient for amplification via PCR or real-time PCR.

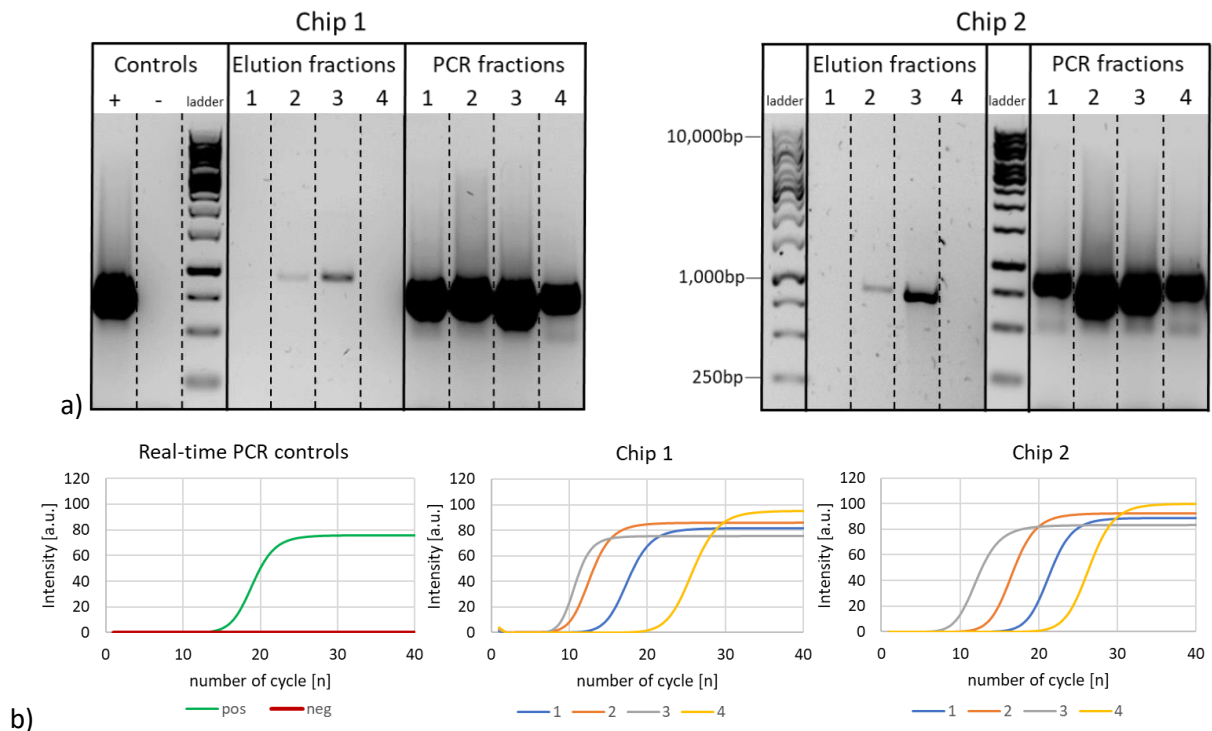


Figure 29: DNA samples eluted after fiber-electrophoresis and used as template for PCR and real-time PCR (modified from Heinsohn et al., 2022). a) Each column on the 1 % agarose gel represents 10 μ l of the loaded elution fraction of one quarter on the chip area, with the numbers 1-4 corresponding to the positions from left to right. A PCR with primers for the 910 bp fragment and 1 μ l of each elution fraction as template DNA was performed and run next to the elution fractions via agarose gel electrophoresis. b) The graphs depict the fluorescence intensities measured upon real-time PCR using the same primers and SyGreen. The signal of the positive control after real-time PCR with 100 ng of the 910 bp fragment, before fiber electrophoresis was carried out, is shown in green and the negative control without template DNA is shown in red. The sample curves appearing first in real-time PCR are consistent with the most intense band of the elution fractions and the PCR reactions. In both, PCR and real-time PCR, sample fragments can be amplified even if they were not seen in the elution fractions.

The duration of the connection time was further increased in the following to check whether the sample could possibly run into the electrode. Figure 30 a) shows the glass microfiber chips after 20, 30, 40 and 60 min fiber electrophoresis of the DNA sample mixture (1 kb ladder) connected to the HVADC at 45 V and stained with GelRed. A further extension of the connection time was not considered, since the chip surface would dry out completely due to evaporation, thus stopping any electrophoretic movement. As can be seen from the pictures, the sample does not migrate into the electrode area, but is still detectable in front of the anode. Also the elution and verification of the sample via subsequent agarose gel electrophoresis confirmed the integrity of the sample by detection

of all 14 DNA bands in the elution fraction, which corresponds to the fourth quadrant of the chip area in front of the anode (see Figure 30 b). These results exclude the possibility of the sample being lost or destroyed by an electrochemical reaction with the electrode and allow further detection reactions of the DNA sample after a successfully performed fiber electrophoresis. The second sample chip, which was connected for 30 min, showed that the sample spot had split. Uneven field lines emanating from the electrodes or minimal inclusions on the fiber surface can cause the sample to split during running. Nevertheless, the sample could be detected without any problems.

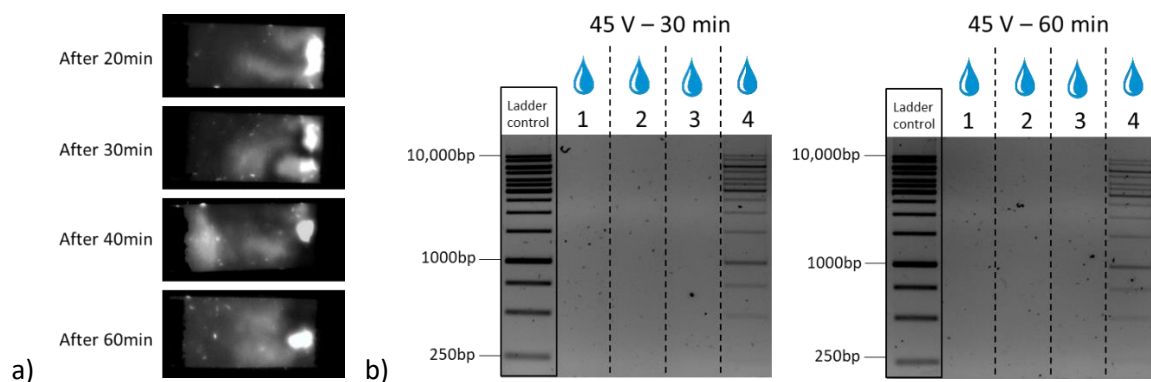


Figure 30: Extension of the connection time to check if the DNA sample migrates into the electrode. a) Fluorescently stained sample mixture (1 kb ladder) detected upon fiber electrophoresis using a glass microfiber (Whatman GF/F) with dispensed carbon paste electrodes connected to the HVADC at 45 V for 20, 30, 40 and 60 min in front of the anode (modified from Heinsohn et al., 2022). b) Fiber chips tested for 30 and 60 min in fiber electrophoresis were cut and each individual fiber pieces incubated with elution buffer (2). After transfer to a 1% agarose gel and gel electrophoresis the migrated and still intact DNA fragments were detected at position 4 of the fiber chip (position in front of the anode). As a ladder control the 1 kb ladder was loaded directly onto the gel representing the initial sample composition.

3.5.3.5. Cross-layer chip arrangement for targeted DNA separation

Another important aspect of characterizing the DNA movement involved studying the DNA migration through multiple fiber layers. In this more complex DNA transport, three layers of glass microfiber were placed on top of each other, with the cathode remaining in the first layer and the anode in the third layer as illustrated in Figure 31 a). For this experiment, the crocodile clamps were used again so that the imprinted anode in the third layer, now placed at the bottom instead of the top of the fiber, could also be contacted. After voltage application, the electric field runs across the layers from the upper left to the lower right. Experiments using the 1 kb ladder and corresponding elution fractions loaded on an agarose gel showed that the sample can be pulled through all layers and concentrated in front of the anode in the third layer as shown in Figure 31 b) (see position 17). This result further demonstrated that the combination of glass microfiber with imprinted electrodes provides a simple

separation platform to move samples either in one or several layers, which could be useful if reactions in separate compartments are needed. Especially when detection platforms are planned on the basis of hybridization with a fluorescent probe in one layer, this may be of particular advantage because interference with other components can be critical. Moreover, a slight discrimination of fragment size could be observed in the first and second layer. Elution fractions from the corresponding segments of the chip showed that at the end of the chip in the lowest layer the two largest fragments with a size of 8000 and 10,000 bp appear to be missing. A concentration dependent retention of the larger fragments (5000, 6000, 8000 and 10,000 bp) was also observed in the first (see no. 3) and second layer (see no. 9 and 10). Especially the DNA fragment with 6000 bp can be seen as a prominent band in the traces because it was 2.3 times higher concentrated in the original sample than the other fragments ranging from 5000-10,000 bp.

In conclusion by stacking several layers of glass fiber filters not only a targeted migration but also a size-dependent separation of the fragments might be feasible. Preliminary work in this field focused primarily on DNA samples tested in a low-voltage isotachopheresis (ITP). This technique is using different mobilities of electrolytes, a leading electrolyte with high electrophoretic mobility and a terminating electrolyte with slower electrophoretic mobility. Upon voltage exposure, the sample ions concentrate into zones in order of their mobility (Chen et al., 2006). A cellulose-based origami device folded into 11 layers was tested for the migration of a DNA ladder ranging from 100-1517 bp with a voltage of 18 V for 10 min (Li et al., 2015). They could not observe a size-dependent migration verified by elution and agarose gel electrophoresis. The cellulose paper had a 15 times larger pore size, was 2.3 times thinner and was defined to have a filtration speed reduced by more than half compared to the glass microfiber used in this work. The folded paper origami resulted in several layers, but the fiber orientation remained the same. Interestingly, the oblique field lines resulting from the experimental set up developed here in combination with up to 10 times longer DNA-fragments showed that an increased interaction as a result of a higher collision probability of the DNA molecules with the fibers can end in a slight retention of the larger DNA-fragments.

To the best of our knowledge an electrophoretic approach instead of ITP was only used for proteins so far (Luo et al., 2014). Consequently, the findings reported in this work can be seen as an addition to previous work and will serve as a basis for further experiments. It is plausible that testing fiber materials with smaller pore sizes strongly influence the separation results. Another beneficial distinction from the ITP experiments is the larger dimension of the glass fiber chip. Typically, ITP is performed on small dimensioned channels of 1-1.5 mm width allowing only the addition of small sample volumes. The fiber chip fabricated here offers the opportunity to analyze larger sample volumes while providing still a small and user-friendly platform.

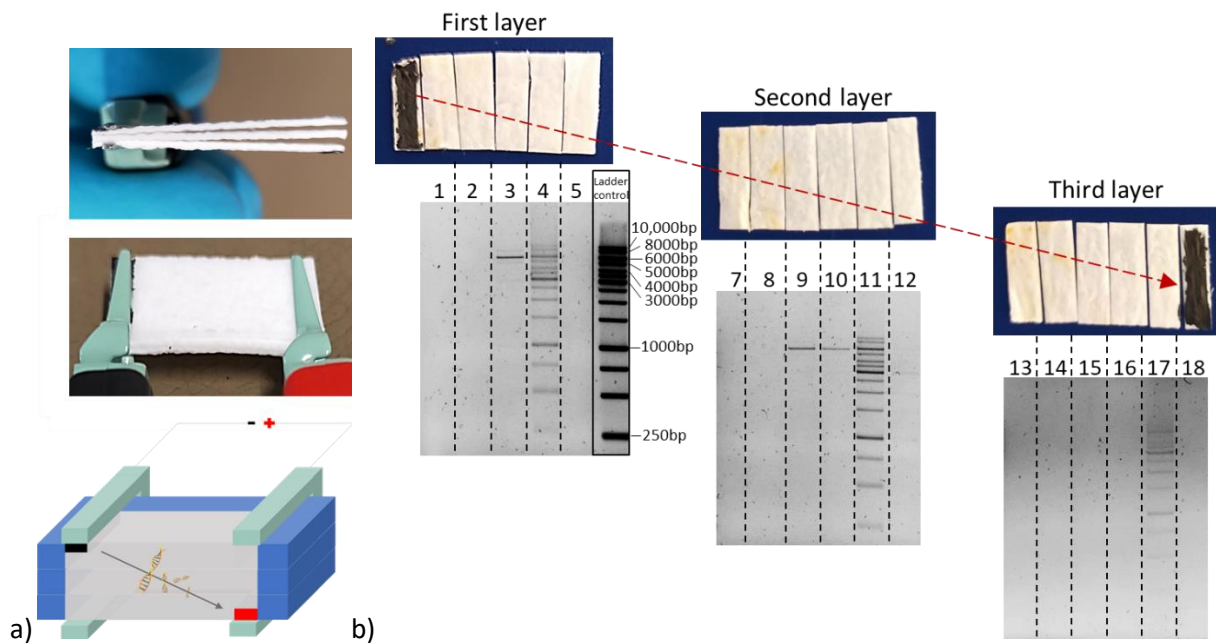


Figure 31: Cross-layer chip consisting of three layers of glass microfiber (Whatman GF/F) connected via the upper left and lower right electrode to generate an oblique migration direction through all layers (modified from Heinsohn et al., 2022). a) Pictures and illustration of the cross-layer chip connected by crocodile clamps. b) Elution fractions of each layer after agarose gel electrophoresis using a 1% agarose gel. The sample mixture migrated successfully to the anode in the third layer (position 17) after a voltage application of 45 V for 20 min. A slight size dependent migration can be observed for the higher concentrated fragments 5000-10,000 bp.

3.5.3.6. Separation of DNA from HRP as an exemplary protein

In order to test if the electrophoretic movement of DNA can also be used for purification of DNA from a biological sample, experiments with DNA-protein mixtures were carried out in the following. In a first step the 910 bp DNA-fragment from *L. pneumophila* Philadelphia and the horseradish peroxidase (HRP), a medium sized protein (44 kDa) at a neutral pH was used as a representative DNA-protein mixture. The position of the protein after electrophoresis can be visualized by the application of the Tetramethylbenzidine (TMB) substrate and hydrogen peroxide. Upon oxidation of the substrate a blue color occurs, indicating the integrity of the enzyme. Figure 32 shows the color changes induced by the enzyme. The position of the coloration clearly indicates that the HRP was not moving over the chip area during electrophoresis. Simultaneously, the DNA fragment migrated as intended in the electric field as can be seen from the elution fractions loaded on an agarose gel. Also a combination of the separation with DNA staining on the same chip was possible. After the HRP was visualized via TMB addition, GelRed can be used for the DNA detection as shown in Figure 32 b). This highlights the possibility of simultaneous detection on a chip without the need for a washing step between the two reactions. Staining directly on the fiber provides a quick way to demonstrate successful separation of

the DNA sample. In addition, elution makes the samples accessible to any other downstream processing for further analysis, such as PCR.

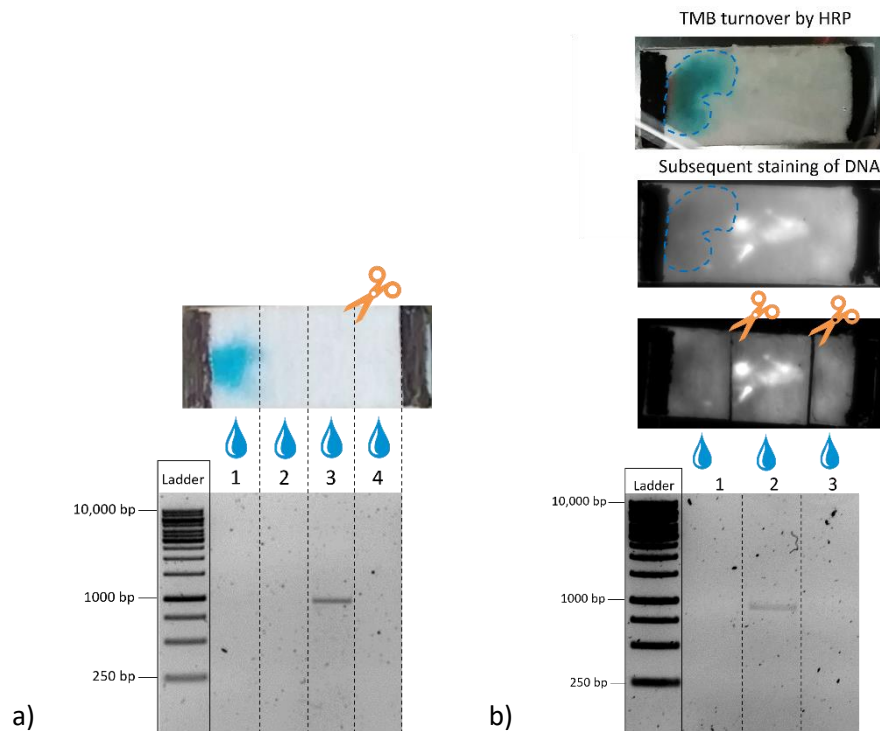


Figure 32: Separation of a DNA-fragment from an exemplary DNA-HRP-mixture (modified from Heinsohn et al., 2022). a) Detection of the HRP after fiber-electrophoresis by TMB substrate oxidation to a blue color at the sample loading zone and detection of the migrated 910 bp fragment by elution and subsequent agarose gel electrophoresis from the third quadrant of the chip area (Heinsohn et al., 2022). b) The immobile HRP was detected by TMB addition and turnover. The DNA-fragment pulled through the fiber substrate can be both stained with GelRed on the same chip where the HRP detection was performed and additionally eluted if desired. The dashed line outlines the area where the TMB previously reacted with the HRP. As a control the 1 kb ladder was loaded directly onto the gel representing the initial sample composition.

3.5.3.7. Separation of DNA from a bacterial cell lysate

In a second step, the performance of the fiber electrophoresis chip was investigated with an even more complex sample mixture, in order to separate gDNA from a bacterial cell lysate. More complex sample compositions e.g. native DNA-protein mixtures needed a longer separation time than purified DNA samples. The longer the voltage lasts, the greater the effect of evaporation on the migration time. To overcome this limitation, first an approach keeping the chip moist during fiber electrophoresis was required. One option would be to enclose the fiber channel by tape or seal it in foil. Both ideas were successful regarding reduction of evaporation but had the drawback that the soft fiber texture was disrupted after removing the adhesive tape or that the foil was not in enough proximity to the substrate, leading to condensate at the underside of the foil. As a promising alternative to ensure

constant hydration, a chip format with wings was identified. Two wings in the middle of the chip were bent down at a right angle and immersed in running buffer, which can be seen in Figure 33 a) and b). This geometry was chosen because it provided the liquid perpendicular to the direction of sample migration, thus ensuring electrophoretic migration instead of a capillary-driven movement. Figure 33 c) and d) show samples after fiber electrophoresis and staining with GelRed using the winged chip format. The sample could be detected on two independent chips in the last quarter of the chip as a concentrated fluorescent spot, proving an effective migration without being stopped by a dried fiber area or influenced by the perpendicular buffer addition. The subsequent elution from the cut fiber area confirmed the fluorescent spots to be the sample mixture. After agarose gel electrophoresis, the ladder bands were seen in the elution fractions 5 and 6 (see Figure 33 e) corresponding to the end of the chip. During the migration, the sample spot was split into two. Again, non-uniform field lines or minimal heterogeneities on the fiber surface may have caused the sample to split during running. In this case, one spot ran faster than the other. After successful elution, however, the spots did not differ in sample composition. Consequently, winged chip design allowed electrophoretic sample migration independent of fiber drying, resulting in longer, more stable connection times.

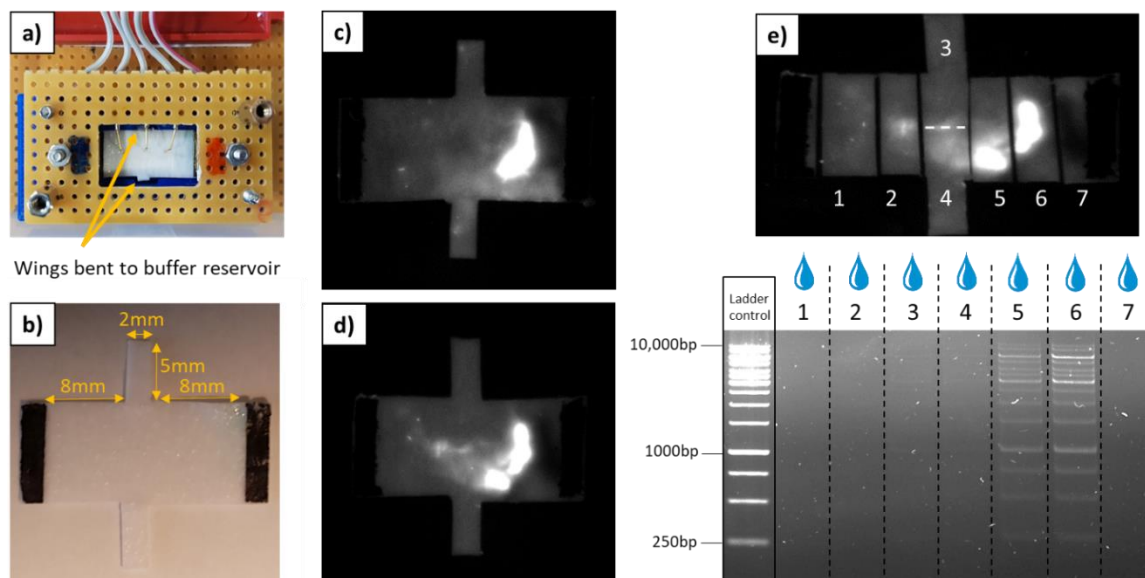


Figure 33: Test of a winged glass microfiber chip for fiber electrophoresis. a) Top view of the winged fiber chip placed in the 3D-printed plastic holder and connected to the HVADC via the lid containing the gold coated contact and pin electrodes. The wings are bent down to the buffer reservoir of the holder providing vertical wetting of the fiber area during horizontal conducted fiber electrophoresis. b) Dimensions of the winged glass microfiber chip with carbon paste electrodes applied by dispensing. c) & d) Two chips after fiber electrophoresis using the HVADC at 45 V for 10 min and post-staining of the DNA sample mixture (1 kb ladder) with GelRed confirmed a successful migration to the end of the fiber chip. e) Fiber chip shown in d) was cut and eluted after staining and elution fractions were loaded on a 1% agarose gel and detected after gel electrophoresis under UV light. Fluorescent spots correspond to the sample mixture because the ladder could be eluted from the positions 5 and 6. As a control the 1 kb ladder was loaded directly onto the gel representing the initial sample composition.

This chip assembly was then used to test the lysate of *L. pneumophila* obtained by the simple, fast and effective alkaline lysis and DNA extraction previously described in section 3.2. Upon an electric field-driven movement lasting 10 min, the gDNA can be visualized on the sample chips 1-3 by fluorescence occurring after staining with GelRed in the middle of the chip area (see Figure 34 a). Compared to distinct DNA fragments shown in the previous experiments, gDNA seems to migrate slower. Considering the multitude of other components in the sample, such as cell debris, proteins and lipids instead of only one protein, this was expected. After 25 min the gDNA could be fluorescently stained at the end of the chip (sample chip 4). In parallel the lysate containing proteins remained at the sample loading zone. This was verified using a general protein dye (One-Step Blue) as shown in Figure 34 b). In contrast to other well-known protein dyes such as Coomassie Blue, this dye was used to detect proteins in a single step without washing. A control chip without DNA again remained unstained by the GelRed. This finding showed the efficient separation of DNA from a complex biological sample.

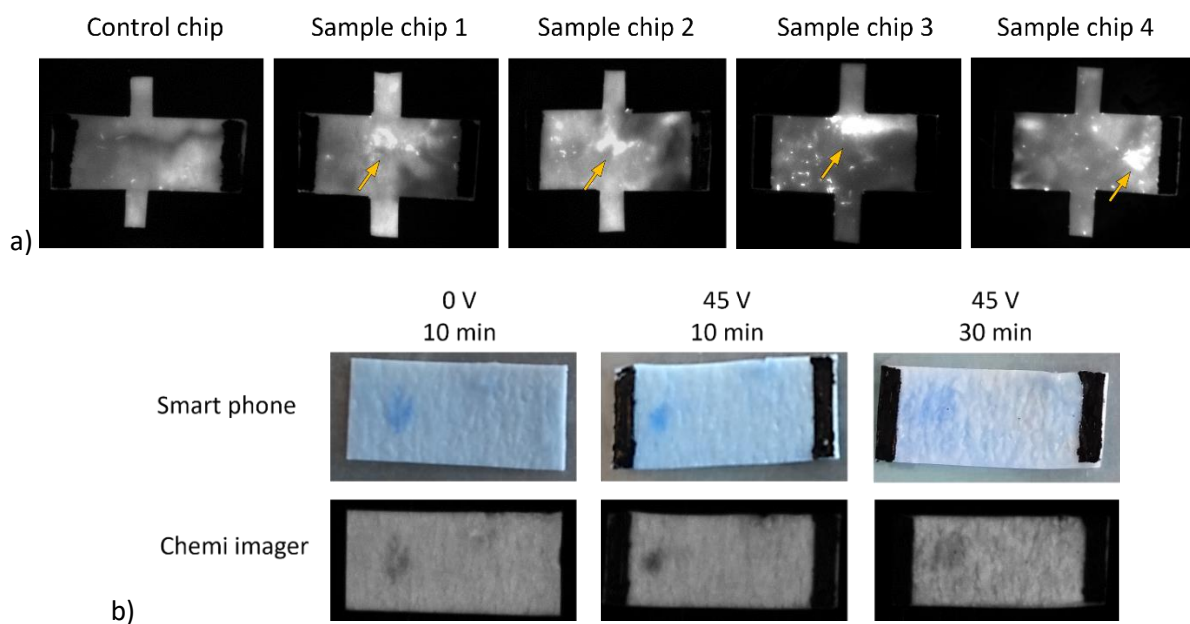


Figure 34: Purification of gDNA from bacterial cell lysate (modified from Heinsohn et al., 2022). a) Staining of a control chip, tested without DNA, with GelRed showed no fluorescent spots. Fluorescent spots corresponding to gDNA after fiber-electrophoresis of a cell lysate from *L. pneumophila* Philadelphia are indicated by yellow arrows. Sample chips 1-3 were connected at 45 V for 10 min and sample chip 4 for 25 min. b) Detection of remaining proteins from the cell lysate after fiber electrophoresis. After staining with OneStep Blue, blue spots occurred at the sample loading zone. The spots were still detectable at the sample loading zone after 10 and 30 min, indicating that proteins did not migrate towards the anode.

3.5.3.8. Current and potential based read-out of DNA sample migration

In order to investigate whether information about the nature of the DNA, e.g., the length, can be read during the migration of the sample in the fiber electrophoresis, the current signal during the migration of the sample in the electric field was followed and analyzed in the following chapter. From a biophysical point of view, DNA is not only carrier of the genetic code but can also be seen as a conductor of charge based on the π - π -interaction of the incorporated nucleic bases (Wagenknecht, 2006). Conveniently, the same electrodes can be used in this experimental setup to provide the electric field and simultaneously measure the current to study the DNA motion.

First results were obtained with glass fiber electrophoresis chips with electrodes made of PEDOT:PSS and can be found in the appendix (section 6.6. Figure A8). Here, an increase in current in the presence of the sample could be assumed, but the measurements were subject to fluctuations. These first measurements were also performed with the DNA ladder still containing the tracking dyes, so that an influence of these on the measurement could not be excluded.

Since the imprinted carbon paste electrodes were more advantageous in terms of fabrication, migration speed, and stability compared to the PEDOT:PSS-based electrodes, the current measurement with the carbon paste electrodes was considered in terms of possible characterization of the sample during migration through the fiber. To eliminate the possibility that the remaining sample buffer of the purchased DNA ladder, which was previously diluted in running buffer, would affect the signal during measurement, a lyophilized 1 kb ladder resuspended exclusively in 5 mM Tris running buffer was used for this experiment. The current signals tracked by the raspberry pi, included in the measurement set up of the HVADC, were analyzed by octave. As a negative control, electrophoresis chips with only running buffer instead of sample were analyzed.

The current characteristics of each individual chip are shown in Figure 35 a) and b). After connection to the voltage source at 45 V, every fiber chip showed a transient response in form of an increase of the current signal up to 350-450 μ A followed by a decrease to 250 μ A within 200-250 sec after voltage application. Based on this observation, 1 μ l of the 1 kb ladder resuspended in 5 mM Tris running buffer (5 μ g/ μ l) as sample was added after this initial increase in current in order not to lose any measurement signal from the sample in the background. The sample application after reaching the value of 250 μ A is marked with a black line in Figure 35. The fiber chips loaded with DNA showed a current increase starting about 75 sec after sample addition. The signal intensity varied between individual chips probably due to deviations in the quality of the imprinted electrodes, but they were still well distinguishable from chips without sample, where an exponential decrease of the current signal to 50 μ A was observed. Further replicates from other test days, which support this observation, can be

found together with the measurement curves already shown here in the appendix of this thesis (section 6.7. Figure A9).

Unfortunately, lower sample concentrations could not be reproducibly detected and varied widely, both in current and potential differences. It can be concluded that, if the sample concentration is sufficient, the current signal generated on the electrophoresis chip can be used as an indicator for the presence of DNA. These results show the potential of this measurement technique if the experimental conditions were further optimized. At this time, such a measurement setup would be difficult to integrate, since samples of this concentration do not naturally occur. It would be an option if sample is concentrated prior to the measurement or if lower concentrations are increased by amplification. It would be even better if the chip could be optimized to detect smaller amounts of DNA. Besides taking a different electrode or fiber materials into account, an extension of the printed electrodes should also be considered, so that the contact to the voltage source can be made outside the chip surface to reduce the influence on the measurement.

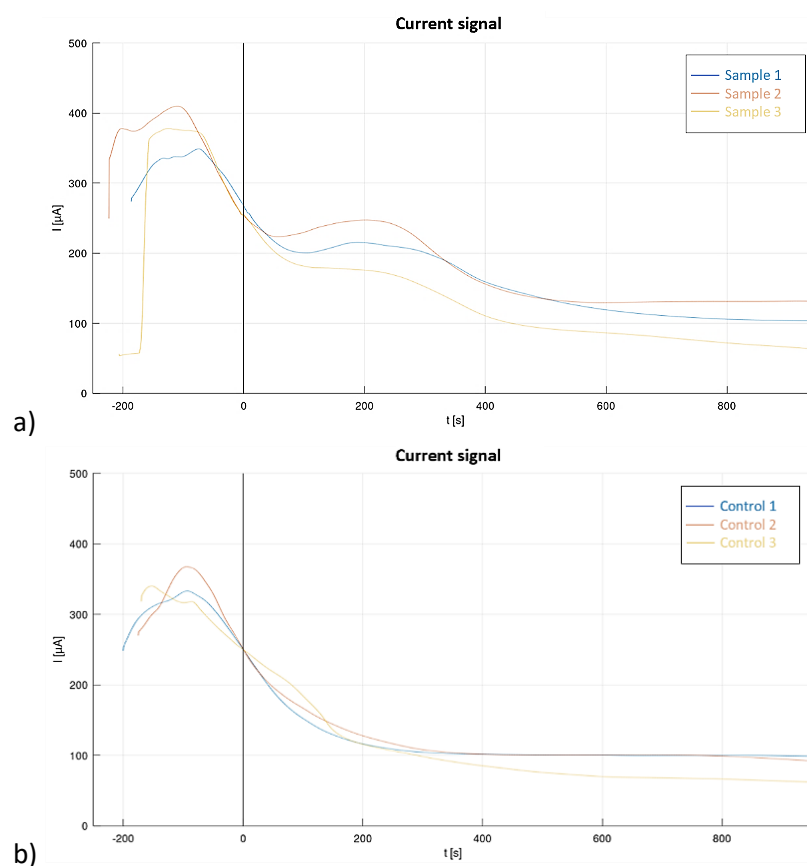


Figure 35: Current signals of fiber electrophoresis chips upon sample or buffer addition. a) The curves of chips with $5 \mu\text{g}$ of the 1 kb ladder as sample showed an increase in current signals between 50-400 sec after sample addition. b) Triplicates of control chips without sample but 5 mM Tris running buffer addition instead showed an exponential decrease of the current signal. Sample and buffer addition are marked with a black line in the corresponding graphs.

Another option to amplify a DNA signal is sample labeling with an electroactive dye for example methylene blue (MB). The positively charged MB contains an planar aromatic structure that can be inserted between two adjacent base pairs or interact with the grooves of the DNA double helix structure by electrostatic interaction (Castaño-Álvarez et al., 2007; Rohs and Sklenar, 2004). This organic dye have been used in previous studies as a ligand for DNA with good electrochemical properties (García-González et al., 2014). Upon incubation with the electroactive molecule the labeling was examined by taking UV/Visible (UV/Vis) absorbance spectra of the dye itself, of DNA prior to labeling, of DNA after labeling with MB and of DNA after separation of unbound MB as shown in Figure 36 a).

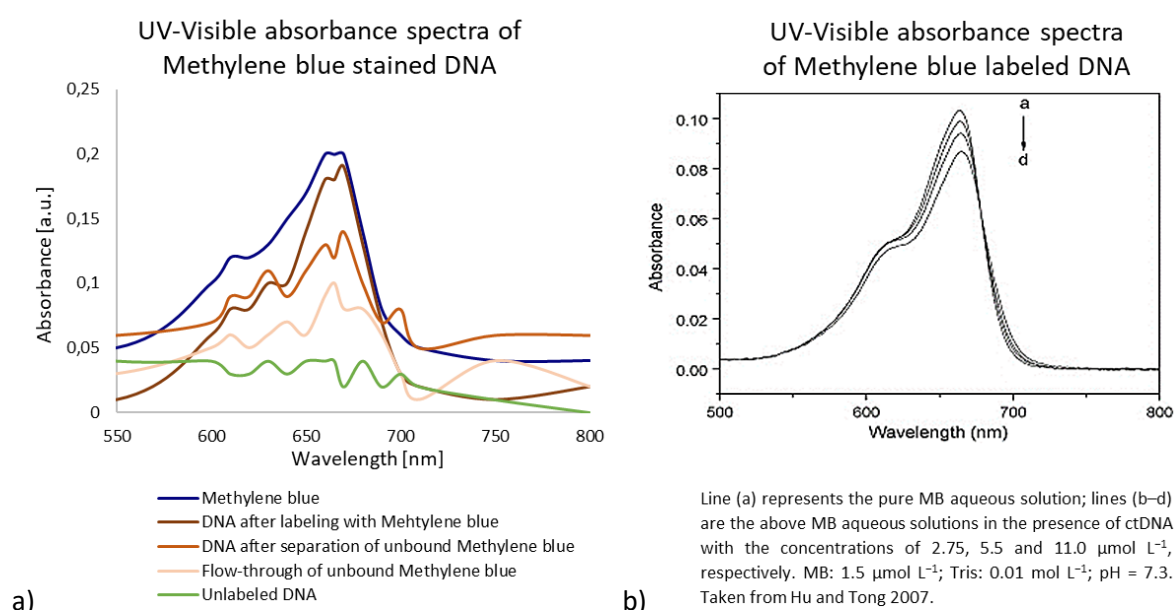


Figure 36: UV/Visible absorbance spectra of methylene blue (MB) stained DNA baseline-corrected using the absorbance value at 750 nm. a) In blue the MB dye without DNA is shown, the dark brown line represents the DNA after labeling with MB and light brown after separation of unbound MB from the stained sample. Two absorption peaks at 615 nm and 664 nm are seen due to the dimeric character of the MB in aqueous solutions. Unlabeled DNA (green) showed no signal and the flow-through of the separation step is depicted in nude. b) Absorbance spectra of MB taken from the literature confirming the experimental determined spectrum (Hu and Tong, 2007).

The UV/Vis spectrum of the MB agrees with the peak reported in literature showing a maximum at 664 nm as shown in Figure 36 b) (Hu and Tong, 2007; Utami et al., 2019). Additionally, a second peak at about 615 nm occurred in aqueous solutions of MB representing the dimeric form of the dye (Zuo et al., 2014). DNA prior to incubation with MB showed no signal at the measured wavelengths. Separation of the unbound MB resulted in an intensity decrease but the stained DNA sample was still clearly discernible with the corresponding peak pattern. The sum of the signal from the unbound MB measured in the flow-through and the signal from the labeled DNA sample after MB removal nearly equals the signal from the MB-labeled DNA before the unbound dye was removed. This indicated a

successful incorporation of MB into the sample and removal of excess dye. The absorbance decrease of MB upon binding to DNA can be explained by a so-called hypochromic effect. This effect is caused by a perturbation of the π -electrons of the chromophore upon interaction with DNA π -electrons, which leads to a drop in energy levels (Qi and Lei, 1999; Tong et al., 2010).

With the HVADC measurement setup, three measurement electrodes (E1-E3) were integrated, which penetrated the fiber one after the other arranged centrally over the chip surface as can be seen in Figure 17 a). These pin electrodes were used to measure the potential differences between each individual electrode without effecting the sample migration as described earlier (section 3.3.3.). These measurements should enable local signal resolution in addition to current measurement over the entire chip area. The DNA mix labeled with MB was used as a sample for fiber electrophoresis in the following steps. Since the current signal can only be recorded over the entire chip area but the spatially resolved measurement would provide more information about the sample migration during fiber electrophoresis, the potential differences between the five electrodes of the HVADC measurement set up (see Figure 37 middle) were considered.

Figure 37 shows the recorded potential signals of sample chips with MB labeled DNA (a & b) and control chips with either only MB without DNA (c) or just pure, unstained DNA (d). After comparison of the signals, recurring peaks can be identified in the sample chips. As can be seen from Figure 37 a), these signals spread both spatially and temporally, so that a small peak in the signal can be seen in the first quadrant after about 120 sec (red), in the second quadrant after 145 sec (green), in the third quadrant after 170 sec (blue), and in the last quadrant about 217 sec (yellow) after application of the sample. Interestingly, the signals do not coincide with the arrival of the sample at the anode. Contrary to the expectation, all signals occur already in the first 3.6 min. Since it has already been shown that a concentration-dependent migration takes place and the sample can spread over several quadrants, a minimal amount could have already reached the anode and triggered these signals. However, it is surprising why no change in potential signal can be detected when the majority of the sample migrated. A possible explanation could be that only the arrival of the first DNA molecules can be measured and the system is already saturated afterwards and further changes can no longer be detected.

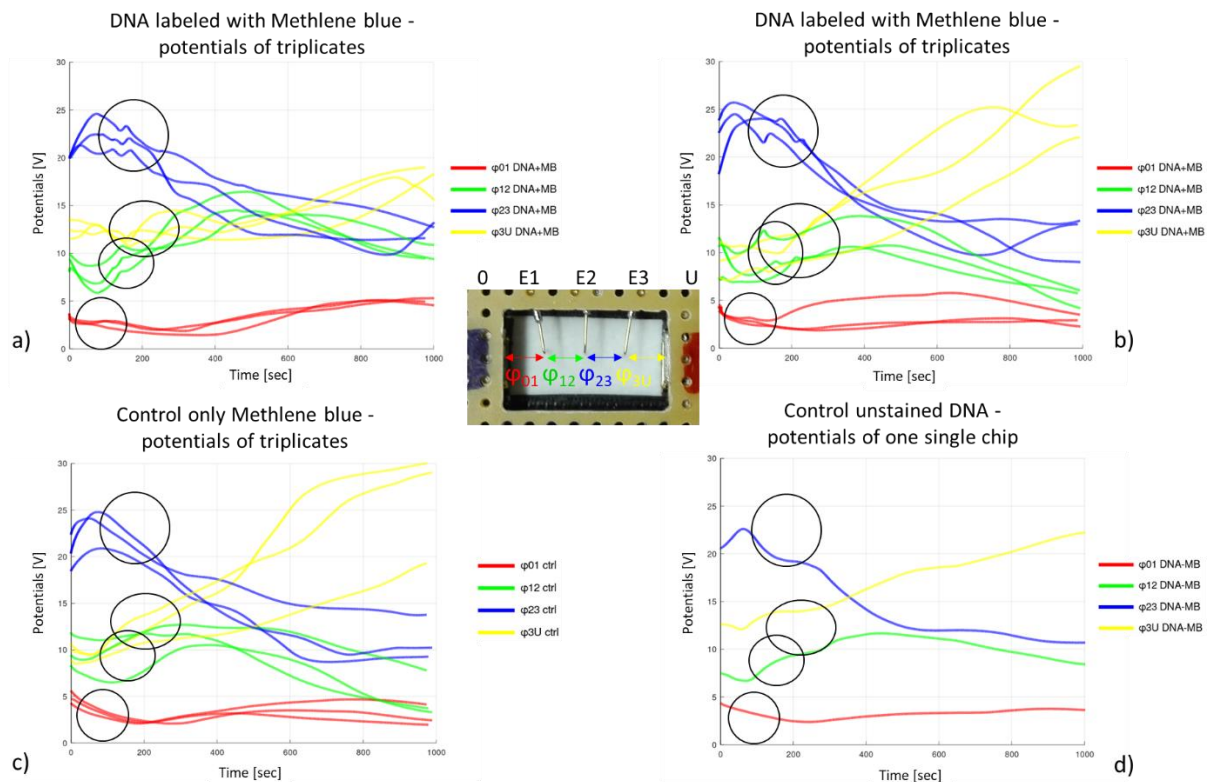


Figure 37: Potential signals recorded by the HVADC during fiber electrophoresis with methylene blue stained DNA. In the middle: Top view of the glass microfiber electrophoresis chip placed in the 3D-printed plastic holder and connected to the HVADC via the lid containing the gold coated contact and pin electrodes. Potential signals between the anode and the first pin electrode are shown in red, followed by the signals between the first and second pin electrode in green, the second and third in blue and the third pin electrode and the anode in yellow. a) & b) Triplicate measurements of DNA labeled with MB in fiber electrophoresis with carbon paste electrodes dispensed on the glass microfiber chip (Whatman GF/F). Measurements were performed on different days but showed all potential signal peaks (marked with black circles) occurring sequentially within 3.6 min after sample addition. c) Triplicates of only MB without DNA tested in fiber electrophoresis resulted in no potential peaks at the appropriate times marked with black circles. d) Also a measurement with unstained DNA was missing the signal peaks detected in the MB stained sample.

The difference in electric potential between the individual electrodes showed different initial values. Non-equidistant electrodes could lead to such potential differences. If the distance between two electrodes is smaller than between two others, this leads to a lower resistance or higher conductivity, which then also affects the other potentials, since these add up to the total voltage. Also the chip positioning could lead to minimal differences in the degree of moisture of the fibers. If the fiber is minimally skewed or if fiber sections are oriented differently from each other due to the contact pressure of the lid with the contact electrode, differences in the accumulation of the running buffer and thus in the local moisture can occur. More liquid leads to more charge carriers per area and consequently to a smaller potential difference. Sample application can also result in such a fluid difference and could explain the small potential ϕ_{01} . In contrast, ϕ_{3U} showed an increase of the potential over time. Possibly the formation of bubbles in front of the anode led to the fact that the

liquid quantity decreased and thus resulted in a higher resistance. The potential differences φ_{12} and φ_{23} should be similar with respect to their progression. However, φ_{23} showed a higher signal than φ_{23} . A possible explanation could be that minimal amounts of the gold coating have been removed from the pin electrode or anode contact electrode (U) during use, causing a change in the electrodes and measure different signals than the other electrodes. Nevertheless, the results shown here suggest that readout of DNA-containing samples is generally possible but will require further optimization and characterization in the future to understand the exact processes involved and to become useful for possible applications.

3.6. Fluorescence *in situ* hybridization (FISH)

At the time of this work, the regulations of the Drinking Water Ordinance in Germany required the detection not only of strains that lead to infections particularly frequently, but all *Legionella* spp. As already described, *Legionella* can be detected by antibodies in an ELISA. An example of a paper-based ELISA is described in section 6.10. The main focus of this work was placed on the FISH technology to detect *Legionella*-DNA from water samples using a rapid read-out on a glass microfiber. The question should be addressed whether a fast detection on a glass microfiber matrix would be possible only on the basis of hybridization, without prior amplification by device-intensive PCR.

Therefore, a molecular beacon probe for the detection of a 23 base long, characteristic region within the 16S rRNA gene sequence of *Legionella* spp. was characterized in the following. A published sequence of a molecular beacon probe directed against a part of the coding DNA sequence for the 16S rRNA was taken (Templeton et al., 2003). Their work was based on a classical real-time PCR assay with two fluorescently labeled probes for the detection of *L. pneumophila* and *Legionella* spp. simultaneously in one sample. Up to date, discrimination between *L. pneumophila* and other *Legionella* spp. was obtained by melting curve analysis of the primer pairs (Reischl et al., 2002) or separate reactions (Wellinghausen et al., 2001). The probe for the detection of *Legionella* spp. consists of a molecular beacon structure covalently labeled with FAM as a fluorophore and DABCYL (4,4-Dimethylaminoazobenzene-4-carboxylic acid) as a quencher. FAM is an isomer derivative of fluorescein with an absorption wavelength of 494 nm and an emission wavelength of 520 nm (biomers.net GmbH, 2021). It is one of the most commonly used fluorescent dyes attached to oligonucleotides. The combination with DABCYL as a dark quencher makes it possible to absorb the energy in the green range of the visible light spectrum that is emitted by the FAM upon excitation. Consequently, if no appropriate target is available for hybridization, the molecular beacon is in its closed state, the fluorophore and quencher are located in short distance from each other and the quenching prevents a fluorescent signal. In comparison, a hybridization of the complementary

sequence by the loop region of the molecular beacon causes a separation of the fluorophore and the quencher and a fluorescent emission of the fluorophore after illumination. In this work, the molecular beacon probe should be tested with regard to a possible target detection on the glass fiber without prior amplification. This could be used in future for the specific detection of *Legionella* DNA after successful separation by fiber electrophoresis.

3.6.1. Basic characterization of operating conditions and read out

In this work a short-detection protocol was established based on a denaturation step (95°C, 2 min) used to separate double-stranded target DNA and the stem-structure of the molecular beacon, a hybridization step (55°C, 2 min) in which the single-stranded molecular beacons could hybridize to their reverse complementary target sequence and a temperature step at room temperature (25°C, 2 min) followed by the detection with UV light. The latter was chosen because only correctly bound probe should be detected and unspecific detection of not hybridized but denatured probe should be avoided. The short experimental incubation time of only 6 min was sufficient to detect a fluorescent signal after DNA binding. As controls only the incubation buffer or a probe control without the DNA target were added to the fiber pads.

3.6.2. Buffer selection and fluorescence detection

To find an appropriate environment for the hybridization of the molecular beacon to the complementary sample sequence two buffers were compared. First experiments were tested in liquid and on the glass microfiber using the qTower³ real-time PCR cycler from Analytik Jena because it had the appropriate fluorescence unit for detection. The PCR 1 x reaction buffer was tested because buffer components can enhance the binding efficiency of DNA molecules. In comparison, the 5 mM Tris buffer was tested because it provided good conditions in prior fiber electrophoresis experiments. Usually, reagents like potassium chloride and magnesium chloride (MgCl₂) are used for an enhanced enzyme activity and primer binding efficiency. MgCl₂ acts as a cofactor for the catalytic reaction of enzymes like polymerases. Furthermore, the potassium- and magnesium ions bind to the DNA backbone and support DNA strand elongation during hybridization events of complementary sequences. Using detergents, such as Triton X-100 can suppress the activity of contaminants. Tris is commonly used in saline because it is an isotonic and non-toxic chemical and maintains a constant pH in buffer solutions between 7-9.

The buffers themselves, the probe diluted in the respective buffers as well as the probe mixed with the 100 % reverse complementary target diluted in both buffers respectively, were tested in three independent experiments. Two basic experimental procedures were used. In one, the components were mixed by pipetting in a reaction tube and placed in the cycler. In the other, the same procedure was followed with the additional transfer of the reaction mixture onto a cut piece of glass microfiber and placed in a PCR tube at an angle of 45 degree. The heating steps were programmed for the Real-Time PCR Cycler and the signal monitored in the FAM channel. After data acquisition the results were saved as raw data to obtain the absolute fluorescence intensity after each heating step and not corrected values by the qPCRsoft 4.0 software. To ensure an excess of target molecule for the probe to bind, the target DNA was first tested in double the amount compared to the probe. The results of the tested FISH experiments after the temperature ramping in the qPCR cycler and cooling down to room temperature (25 °C) are shown in Figure 38. With the 1 x reaction buffer in liquid, the signal of the molecular beacon increased 1.7-fold in the presence of the target (see Figure 38 a), whereas the mean values of the probe alone and the probe with target for the same approach in Tris buffer did not allow any distinction between both reactions (see Figure 38 b). The probe diluted in 1 x reaction buffer and tested on the fiber yielded a signal increase of 1.2-fold after binding of the beacon to its target as can be seen from Figure 38 c). The mean values of the hybridization of the probe in the Tris buffer yielded in a 1.5 times higher fluorescence signal if the target sequence is present and was tested on fiber (see Figure 38 d). Overall, the Tris buffer, showed the expected difference between target and non-target control on the fiber, although a high standard derivative was obtained for target detection. In general, variabilities can occur to the different arrangement of the fibers in the PCR tubes. Due to the manual placement of the filter pads in the PCR tube, the angle at which the light of the LEDs for the fluorescence measurement hits the fiber is not well controlled and thus a potential source of error. Furthermore, the heat transfer will be better if the fiber is not placed horizontally as chosen for the read out (see Figure 39 a) but vertically onto the inner wall of the tube (see Figure 39 b). To overcome these limitations, an alternative for signal readout was needed.

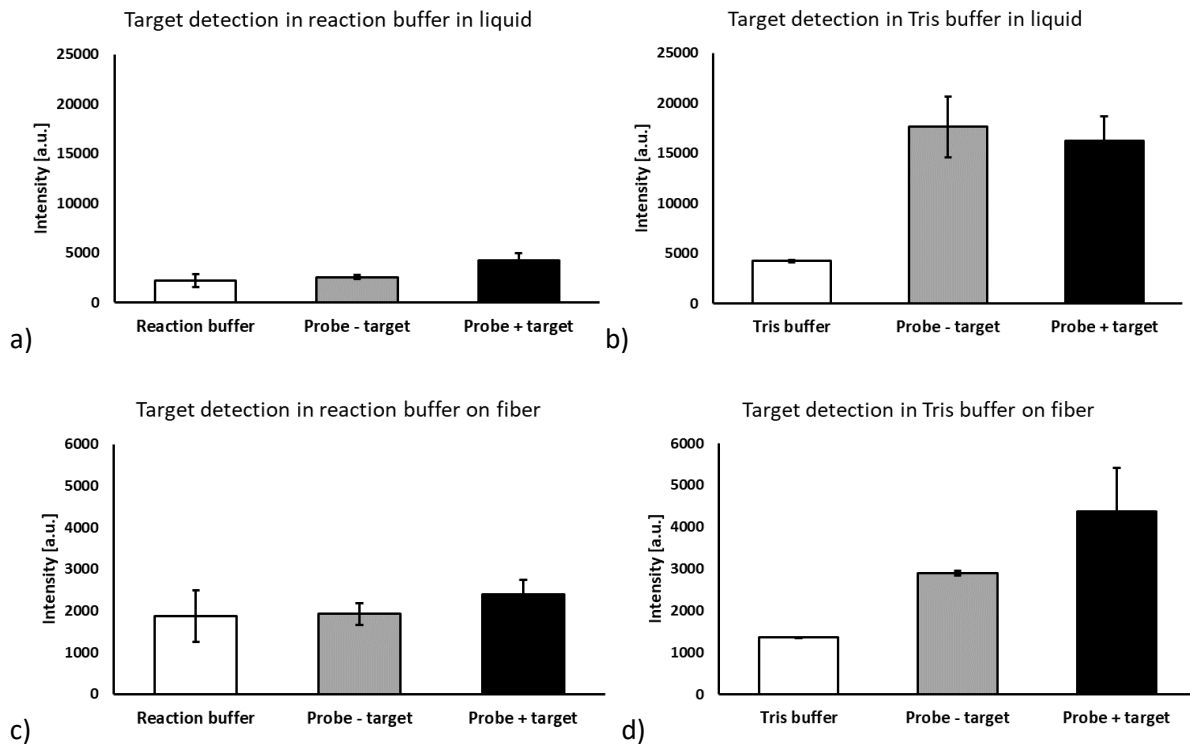


Figure 38: FISH of 440 nM molecular beacon probe and 880 nM reverse complementary target tested in 1 x reaction buffer (a) and 5 mM Tris buffer (b) as liquid approach in an reaction tube and on 5 x 5 mm glass microfiber pads placed in PCR reaction tubes (c & d). The samples were tested in duplicates and the fluorescence was measured after hybridization with the real-time PCR cyclor at 25°C. The fluorescence signals were higher in the 5 mM Tris buffer than in the 1 x reaction buffer and higher tested on the fiber than in liquid. The hybridization reaction in 5 mM Tris tested on fiber showed the clearest difference between the probe without target and the probe with the hybridized target sequence.

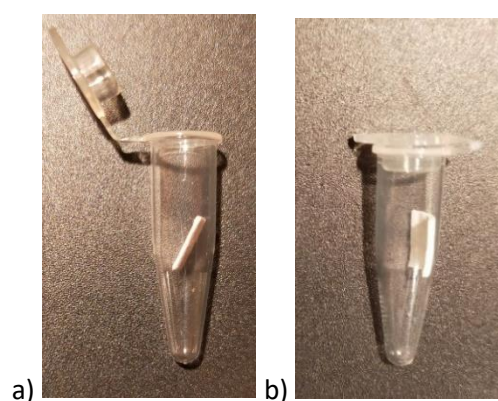


Figure 39: Placement of the 5 x 5 mm glass microfiber pad in the reaction tube for incubation. a) The fiber pad was placed at a 45-degree angle in the tube to allow heating and fluorescence read out of the fiber by the qTower³ real-time qPCR cyclor. b) The fiber pad was placed against the wall of the reaction tube to improve the heat transfer from the metal block of the cyclor to the fiber. For fluorescence readout, the fibers were transferred on the UV-table of the Chemi Imager and photographed.

In the following, the gel documentation system was tested for the detection of the hybridization reactions on the fiber. Molecular beacon and reverse complementary target were tested in an equal molar ratio of 440 nM and the glass fiber pad was placed vertically onto the inner wall of a PCR tube to ensure heat transition from the tube wall to the fiber. After heating, the fiber pieces were transferred to the UV-table with a pair of tweezers and documented using the Gel documentation system Chemi Imager (see Figure 40 a). This ensures homogeneous illumination of the fiber samples during fluorescence detection. A documentation of the fiber material in the lid of the PCR tube was not possible due to the autofluorescence of the plastic material. For analysis of the fluorescence intensities, ImageJ was used and the values are depicted in the graphs of Figure 40 b). In presence of the complementary DNA sequence, the probe showed a 25 % higher fluorescence signal in the 1 x reaction buffer compared to the mixture in Tris buffer. However, the standard deviation of the background signal was 23 % higher in the reactions diluted in 1 x reaction buffer compared to the ones in 5 mM Tris buffer. Background fluorescence occurs due to the fact that the loop is opened after the melting step and a small percentage of the probe rehybridized incorrectly or attached to the fiber. The signal does not appear to be homogeneously distributed over the surface and is highest at the edge. This can be attributed to several reasons. On the one hand, the manual pipetting of the reaction mixture plays a role, which is not always added accurately in the center of the fiber, and on the other hand, the drying of the liquids during heating essentially contributes to differences in intensity. There is a faster evaporation at the edges of the fiber compared to the center that induces a liquid transport towards the edges and consequently a higher amount of fluorescent dyes being transported and detected there. Also the fibers are slightly different in geometry because they have been cut manually, and differences in fiber density also occur due to the nature of the fibers themselves. These differences contribute to the fact that the reactants are distributed differently in the fiber network and lead to intensity variations over the area.

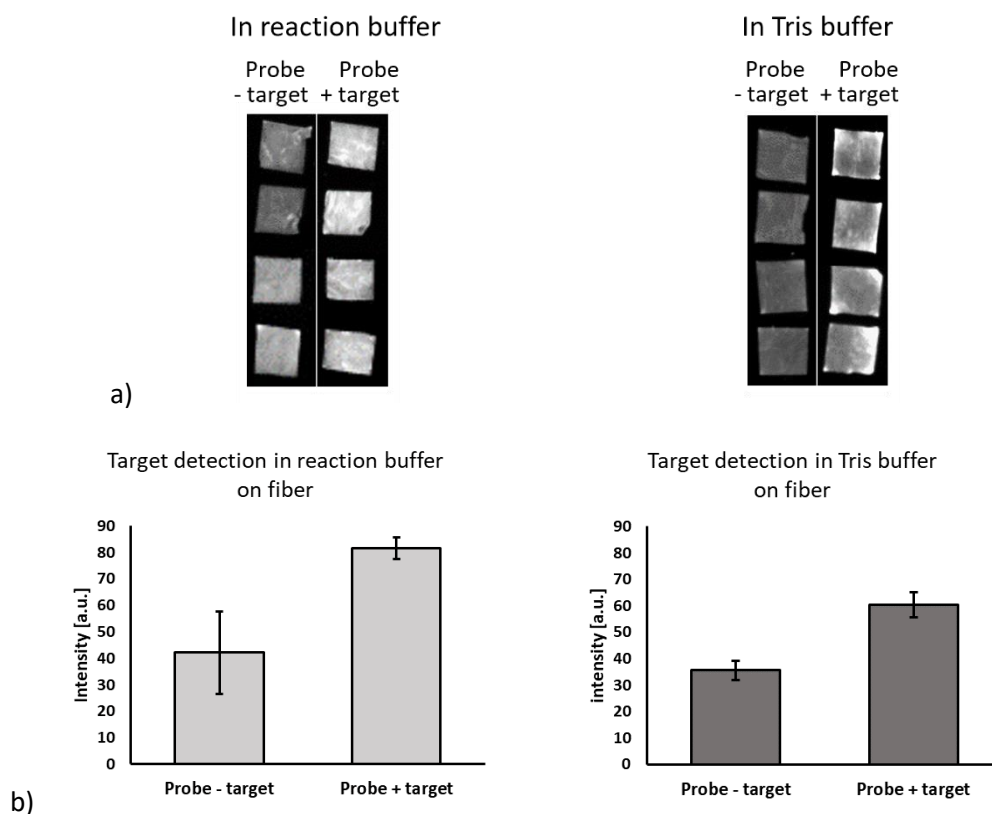


Figure 40: a) FISH of molecular beacon probe and reverse complementary target tested in the same molar ratio of 440 nM diluted in 1 x reaction buffer and 5 mM Tris buffer respectively and tested on 5 x 5 mm glass microfiber pads placed in reaction tubes for heating and hybridization. The fluorescence was measured after transfer to the Chemi Imager and excitation with UV light. b) The mean of four samples shows that the signal intensity is higher for the assay tested in 1 x reaction buffer but the background signal of the probe without target has a high standard deviation. The reverse complementary target detected by the molecular beacon in Tris buffer showed a distinguishable signal with low fluctuation that is almost twice as high as the probe itself.

In the following paragraphs, the influence of ions on the formation of hybridization structures will be addressed to understand the signal differences observed in the FISH experiments. For the physicochemical hybridization of DNA sequences, counterions such as sodium-, potassium-, magnesium or Tris cations play a role. The stabilization occurs on the one hand through the interaction with the bases and on the other hand through binding to phosphate groups of the DNA backbone. This reduces electrostatic repulsion between the phosphate groups and underpins favored hybridization (Every and Russu, 2008; Liubysch et al., 2015; Várnai and Zakrzewska, 2004). Often these ions are added to reaction buffers to take advantage of this positive effect. In the experiments tested in liquid, the low number of Tris ions in the buffer did not seem to be sufficient, helping the melted probe to close again after cooling and resulted in a background signal of the probe without target that was almost as high as the sample signal (see Figure 38 b). On the fiber, the background signal from the probe without

target diluted in Tris buffer is lower and a signal increase is seen in the presence of the target (see Figure 38 d and 40 b).

It is likely that ions on the fiber contribute to the specific binding of the probe to the target. The blank values of trace elements in several filter material by Inductively Coupled Plasma-Mass Spectrometry were already determined (Berg et al., 1993). A borosilicate filter material from the same manufacturer, only with a larger pore size and dimension was also taken into account. In the following, the values for sodium and magnesium from their work were adjusted to the fiber volume of the glass fiber used here. The results were 16.3 mM sodium and 0.371 mM magnesium.

The DNA Folding Form of the mFold application of the UNAFold (Unified Nucleic Acid Folding and hybridization package) web server was used to predict the possible hybridization structures of the probe and target under the influence of different concentrations of counter ions (Peyret, 2000; SantaLucia, 1998; Zuker, 2003). At 25°C and in the absence of counterions, five structures were predicted as shown in Figure 41 a)-e). Structures b) and c) folded in such a way that the 5' end with the fluorophore and the 3' end of the quencher were far enough apart to give a signal even without the presence of a target. This could explain the background signal of the Tris buffer in liquid.

Using this software, only sodium and magnesium concentrations can be entered, it was not possible to specify other ions. Monovalent Tris ions also contribute to DNA stabilization and should be considered for DNA structures (Owczarzy et al., 2008). A concentration of 10 mM Tris was stated to be equivalent to approximately 5 mM sodium. Since a 5 mM Tris buffer was used in this work, the structures were predicted with 2.5 mM sodium (corresponding to only 5 mM Tris buffer), 16.3 mM sodium and 0.371 mM magnesium (corresponding to ions coming from the fiber) and 18.8 mM sodium and 0.371 mM magnesium (corresponding to ion concentrations of the fiber plus the Tris buffer) respectively and are depicted in Figure 41 g)-i). Regardless of the three concentrations tested here, the hairpin structure of the molecular beacon probe is formed. For the probe tested here, a minimal concentration of only 0.26 mM sodium was required to exclusively form the desired hairpin structure (see Figure 41 f). At lower sodium concentrations, a second competing structure option arises with an open oligonucleotide sequence that can contribute to a non-specific signal.

In conclusion, it is confirmed here that the addition of ions affects the structure formation of the probe and too low concentrations can lead to a non-specific opening of the probe. Since the value for the Tris buffer was only assumed and not measured in this experiment, the actual concentration of Tris could be lower and explain the high background signal of the probe's background signal in pure Tris buffer in Figure 38 b). The ion concentrations coming from the fiber are sufficient to ensure the closed form of the beacon in the absence of its target.

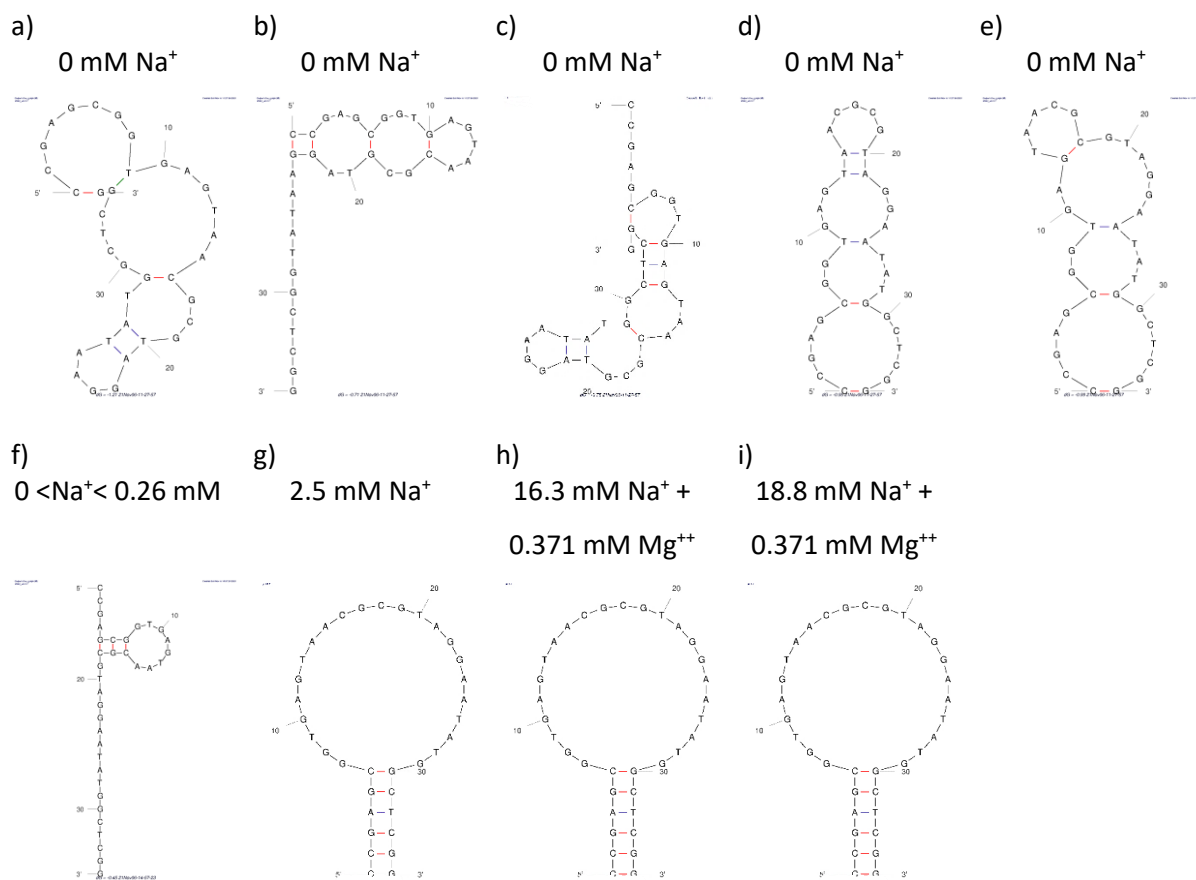


Figure 41: Prediction of the structure for the molecular beacon probe with different ion concentrations using the DNA Folding Form of the mFold application of the UNAFold web server. At 25°C and 0 sodium ions (Na^+) five options of folding the probe sequence were calculated, three ones (a, d and e) with the 5' and 3' end being in close proximity and two (b and c) with an open structure with the 5' end being separated of the 3' end. At sodium concentrations above 0 but below 0.26 mM only one structure was predicted with the small self-hybridizing part of the sequence but overall an open molecular beacon probe. At 2.5 mM Na^+ , 16.3 mM Na^+ and 0.371 mM magnesium ions (Mg^{++}) as well as 18.8 mM Na^+ and 0.371 mM Mg^{++} only the closed molecular beacon sequence with the self-hybridizing stem sequence is predicted.

3.6.3. Sensitivity

Two key factors for the development of a good sensor are time and accuracy. In order to characterize the sensitivity of the hybridization detection for implementation in a sensor, one aim of this work was the determination of the minimum input of target DNA to create a detectable fluorescence signal upon probe detection.

In a first step, the minimum concentration for a significant difference of the 100% reverse complementary target sequence to the backgrounds signal without DNA was determined in a liquid reaction using the Real-time PCR Cycler. This experimental set up was chosen to determine the lowest

DNA amount that can be detected under ideal conditions, for example without competing sequences or structures and impurities with other components like chemicals or cell debris. While the probe was kept constant at 440 nM, the complementary strand was diluted from 440 to 3.5 nM. Figure 42 shows the results of four independent experiments. A significant differentiation is possible from a concentration of 110 nM.

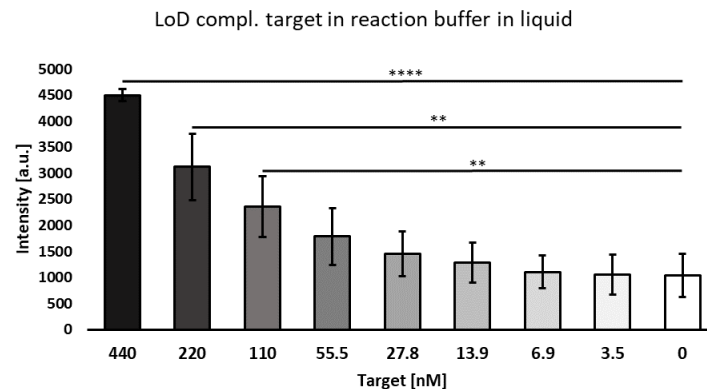


Figure 42: Dilution series of the reverse complementary target ranging from 440-3.5 nM in 1 x reaction buffer with a constant molecular beacon concentration of 440 nM was tested in liquid reactions. After heating and hybridization of the molecular beacon and the reverse complementary target, the samples were measured by the real-time PCR cycler and the fluorescence intensities evaluated using Excel. A significantly distinguishable sample signal to the background was determined using the student's t-test ($n=4$; **** $p<0.0001$; ** $p<0.01$).

For the FISH-based detection on fiber, the same dilution series of the target DNA was tested and again the 1x reaction buffer and the Tris buffer were compared. The dilution effect is not as strong on the fiber as in liquid but nevertheless the dilution trend is still clearly visible. The intensity values of the molecular beacon diluted in 1 x reaction buffer and tested for hybridization with the reverse complementary target and fluorescence readout on glass microfibers were higher overall (e.g., 25% at the highest concentration of 440 nM) compared to the same reaction diluted in 5 mM Tris buffer.

A significant differentiation of the molecular beacon hybridized with the reverse complementary target, diluted in 1 x reaction buffer and tested on glass microfibers from the probe without target, was possible from 220 nM, as shown in Figure 43 a). The background signal is caused by a non-specific signal of the probe without target, probably due to a non-specific retention of the molecular beacon by the fiber. In comparison, a reliable detection of the target hybridized with the probe diluted in Tris buffer and tested on the fiber is possible from 3.5 nM (see Figure 53 b). The fluctuations of the background value upon hybridization in reaction buffer contribute significantly to the fact that the concentrations for significant discrimination differ so much between the two buffers. Overall, it can be

concluded that the FISH-based detection in Tris buffer on glass microfiber is possible even at lower concentrations.

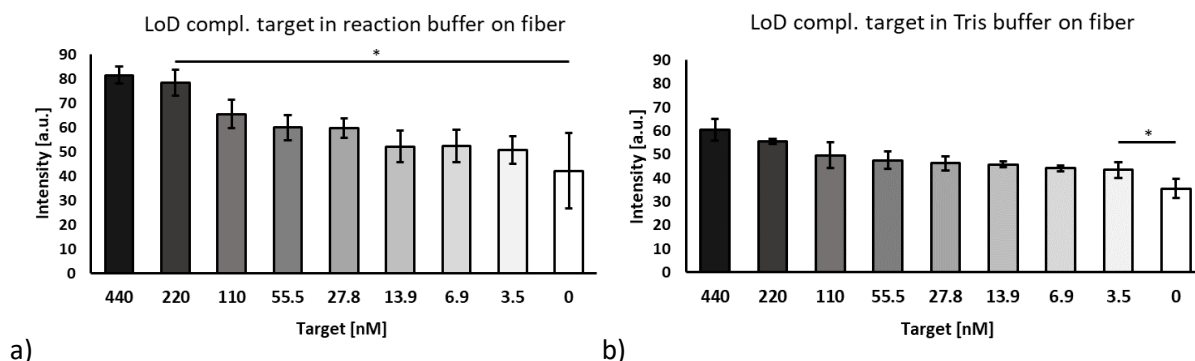


Figure 43: Dilution series of the reverse complementary target ranging from 440-3.5 nM with constant molecular beacon concentration of 440 nM 1 x reaction buffer (a) and in 5 mM Tris (b) were tested on glass microfiber, respectively. After heating and hybridization of molecular beacon and the reverse complementary target, the fibers were imaged under UV light and the fluorescence intensities evaluated using the ImageJ program. A significantly distinguishable signal of the target dilutions (n=4) to the background signal, measured as probe without target (n=9), was determined using the student's t-test (* $p \leq 0.05$).

Based on the structural predictions, the low standard deviation of the probe without target and the lower detection limit of the reverse complementary target in Tris buffer compared to the 1 x reaction buffer, the following experiments were performed in the Tris buffer. In addition, the composition of the 1 x reaction buffer is not known, since the manufacturer does not specify the exact composition. It is described containing 6 mM magnesium chloride and further enhancer and stabilizers. In order to investigate the effects of specific additives on the hybridization reaction, the use of an unknown mixture should be avoided and instead the concrete determination of environmental conditions should be possible. Another reason for using the Tris buffer is its compatibility with fiber electrophoresis. If the experiments are going to be combined into a complete assay, possible problems with the background signal can be excluded or the need to change the buffer of the sample can be avoided.

3.6.4. Specificity

For further characterization, the specificity of the probe with respect to various other oligonucleotides should be examined. For this purpose, eight ssDNA oligonucleotides were tested with different similarity to the target sequence of the molecular beacon probe.

3.6.4.1. Test of non-target sequences

First, oligonucleotide sequences were tested that were certain to be present in native samples. For this purpose, primer sequences were selected that are normally used for the detection of *Legionella* in PCR. Three of these sequences were 20 bases long and the fourth 16 bases. The tested oligonucleotide sequences are listed in Table 8. The test of the non-targets was carried out under the same experimental condition like the testing of the 100 % reverse complementary target, where probe and DNA were used in the same molar ratio (440 nM). The results after mixing of the reagents, transfer to the glass microfiber, heating for target hybridization and read out using excitation with UV light are pictured in Figure 44. From left to right, the buffer control is followed by the probe without target accompanied by the probe with reverse complementary target and the four non-targets hybridized with the probe. In three independent experiments (corresponding to 44 a), b) and c) including ten samples in total, only the fibers treated with the 100 % reverse complementary sequence showed a fluorescent signal. All non-targets remain as dark as the probe control containing neither DNA target nor non-target. After evaluation of the intensity values it was found, that a statistically highly significant discrimination between the reverse complementary target and the background as well as the tested non-targets was possible (see Figure 44 d).

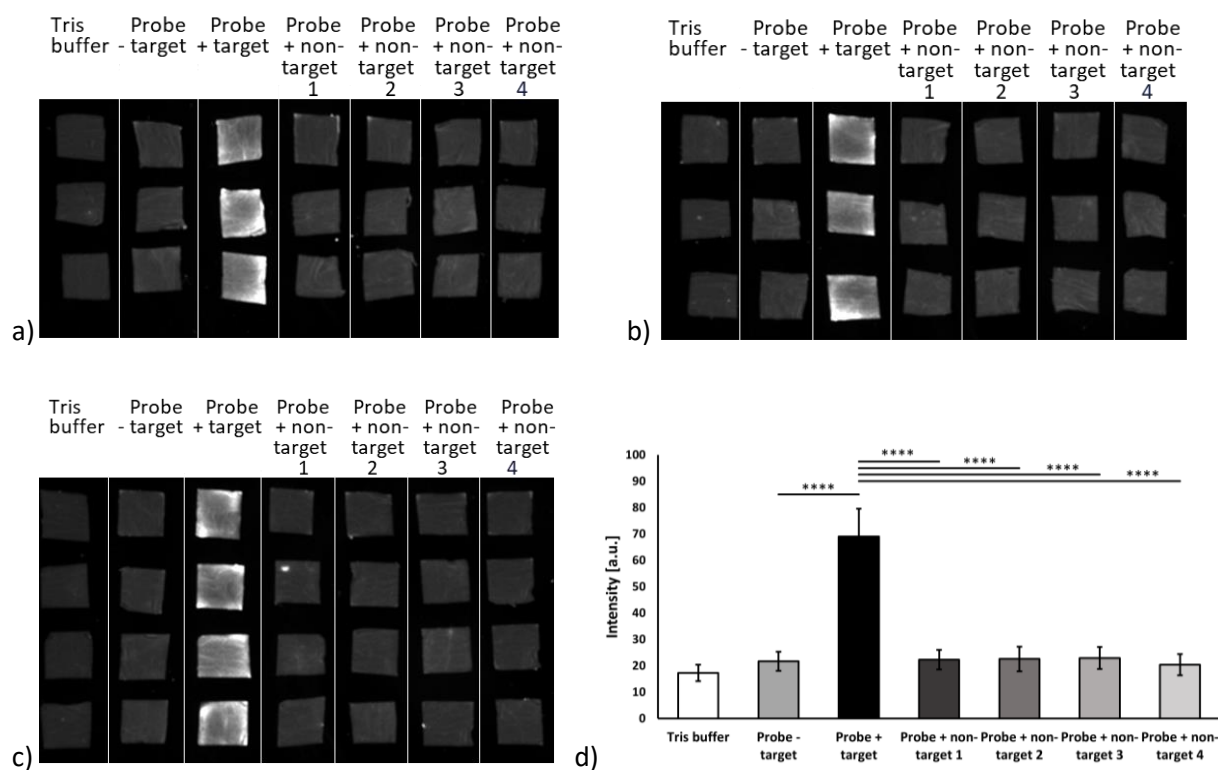


Figure 44: Hybridization of molecular beacon with the reverse complementary target and non-target DNA sequences on glass microfiber. a)-c) From left to right: Triplicate and quadrupole measurements of Tris buffer, probe without target, probe and reverse complementary target and probe with 4 different non-targets (1-4) were added to 5 x 5 mm pads of glass microfiber. After heating (95°C 2 min, 55°C 2 min, 25°C 2 min) the fibers were imaged under UV light. d) The fluorescence intensities were measured using the ImageJ program. The fluorescence from hybridization of probe and reverse complementary target was significantly higher than the probe background and each tested non-target sequence (n=10; **** p<0.0001; student's t-test).

3.6.4.2. Influences of single- and double nucleotide variations

In addition, other oligonucleotides very similar to the target sequence were tested to verify whether hybridization is also suitable for the detection of point mutations. Furthermore, it was to be examined whether the position of the base exchange shows a difference in the signal detection. For this purpose, one or two bases were exchanged at the end or in the center of the reverse complementary target of the probe as can be seen in Figure 46. Figure 45 shows the hybridized samples, the molecular beacon with the reverse complementary target and the four non-targets differing in one or two bases, on the glass microfiber after excitation with UV light. Testing of the single and double mutants regardless of their position in the target sequence resulted in the same fluorescent signal as the target sequence after hybridization with the probe. It is only possible to distinguish all samples to the probe control without any further oligonucleotide added.

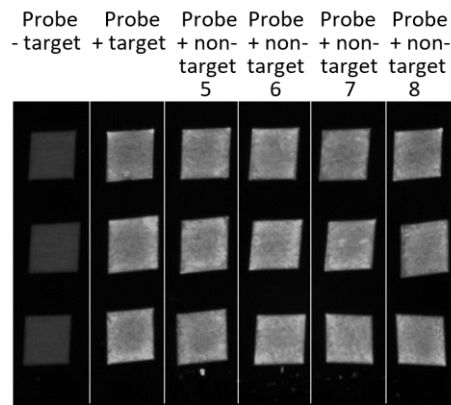


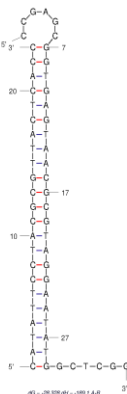
Figure 45: Hybridization of the molecular beacon with reverse complementary target and non-target DNA sequences differing in one or two bases on glass microfiber. The mutations were selected at the edge of the target sequence as well as in the center. While no signal occurred from the probe alone the intensities from the sequences incorporating single and doubled point mutations, independently from the position of the mutation, showed a comparable signal than the target recognized by the molecular beacon probe.

The DINAMelt (DI-Nucleic Acid hybridization and melting prediction) application was used to predict folding and hybridization of two different strands of DNA. Hybridization is characterized by a free energy difference, the Gibbs free energy changes (ΔG), which measures the binding affinity for the two strands to form a duplex (Hooyberghs et al., 2009). A negative free energy indicates that this is a thermodynamically favorable reaction (Davis, 2014). Sequences that cannot fold are given a positive folding energy (Zuker, 2003).

The results from this prediction are shown in Figure 46. The free energies of probe and reverse complementary target could be determined to -28.3 kcal/mol at 25°C and the hybridized structure is shown in Figure 46 a). For all non-targets more positive values were calculated but the single and double mismatches already came close to the value of ideal hybridization with energy changes of -20 to -26.7 kcal/mol.

The other non-targets, which differ in more than two bases, hybridize at significantly fewer sites. As can be seen in Figures 46 b)-e), the probe hybridizes with non-target 1 at only 3 bases, with non-targets 2 and 3 at 6 bases each, and with non-target 4 at 4 bases. Accordingly, non-targets 1 and 4 had 8 times higher free energies which corresponds to an 88 % increased Gibbs free energy differences compared to the target. Non-targets 2 and 3 showed 3-4 times higher values respectively than the target sequence which corresponds to a 75-69 % increase in Gibbs free energy differences.

a) Molecular beacon and reverse compl. target



	Molecular beacon with	Sequence	$\Delta G_{25^\circ\text{C}}$ [kcal/mol]
a)	Reverse compl. target	CATATTCCTACGCGTTACTCACC	-28.3
b)	Non-target 1	ACTTCTGGTGCAACCCACTC	-3.5
c)	Non-target 2	GTCAACTTATCGCGTTTGTCT	-8.9
d)	Non-target 3	AATAGTCCGCCAACGCTAC	-7.2
e)	Non-target 4	GCAATGTCAACAGCAA	-3.4
f)	Non-target 5	CATATTCCTACGCGTTACTCACC G	-26.7
g)	Non-target 6	CATATTCCTACGCGTTACTCAG GG	-24.8
h)	Non-target 7	CATATTCCTAC CC GTTACTCACC	-21.8
i)	Non-target 8	CATATTCCTA G CGTTACTCACC	-20

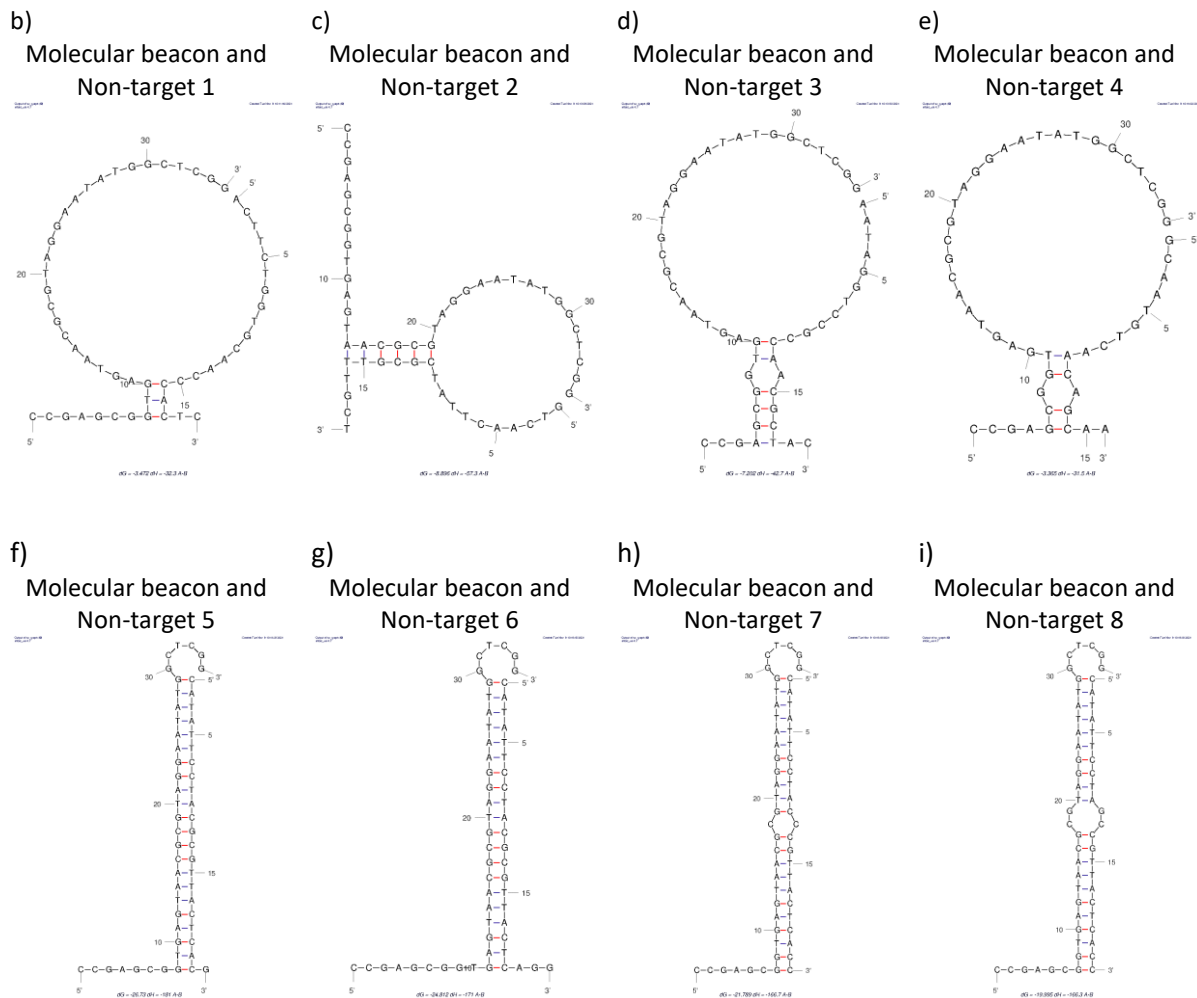


Figure 46: Base sequences, Gibbs free energy differences and prediction of the hybridization structures of the molecular beacon with the reverse complementary target and 8 non-targets. Single and double base mutations compared to the reverse complementary (compl.) target are highlighted in red. The Gibbs free energy differences and the hybridization structures were predicted using the DINAMelt application with hybridization conditions $T=25^\circ\text{C}$, 18.8 mM Na^+ , 0.371 mM Mg^{2+} and 0.44 μM sample concentration.

One or two mutations at the edge of the target binding site had less influence on the free energy than one or two base changes in the middle of the sequence, as indicated by the energy values of the edge variations being more consistent with the target energy. Two mutations in the center increased the free energy about 30 % and one mutation about 23 % compared to the target binding. Two mutations at the edge of the sequence on the other hand increased the energy only about 12 % and one mutation only about 5 % compared to the target binding. The hybridization structures of the probe with non-targets 1-4 respectively are shown in Figure 46 f)-i). Although the free energy is reduced by 30 %, the sequence with the two mutations in the center can still bind to 21 bases of the binding region of the molecular beacon, that led to an opening of the probe and a fluorescence signal upon excitation. A loop is built around the two non-hybridizing bases, whereas the rest of the bases hybridized as before as shown in the predicted structure of Figure 46 i).

It can be concluded that, binding of non-target molecules with more than two divergent base sequences is energetically insufficient for the formation of a stable hybridization structure that would cause permanent opening of the beacon. These sequences presumably have sufficient flexible free space for the quencher to be spatially close enough to the fluorophore to quench its emitted fluorescence. Therefore, non-targets 1-4 in the FISH experiment with the molecular beacon on the glass microfiber remained dark as shown in Figure 44. In contrast, sequences with one or two divergent bases opened the probe and thus a fluorescent signal was generated on the glass microfiber as shown in Figure 45. A difference in the fluorescence signal indicating a deviation of one or two bases and at which position this occurs is obviously not visible on the glass microfiber.

No detection of the single and double mutants was possible on the fiber, however, the structures can be distinguished to the actual target sequence if a temperature profile is recorded. Similar to a melting curve, which is usually used to characterize DNA hybrid structures, a cooling curve from 95°C to 25°C was recorded here to be as close as possible to the previous experiments of the probe hybridization. Figure 47 a) illustrates the transition state of the molecular beacon probe with and without the target sequence. The fluorescence intensities measured in the qPCR cyclers are shown in Figure 47 b). As the temperature was increased to 95°C the stem of the beacon dissociates and a fluorescence signal can be measured. At high temperatures the molecular beacon unravels into a fluorescent randomly coiled oligonucleotide and due to the high thermal energy impact, there is an increased molecular motion that causes the fluorophores partially fall apart and be adjacent to the quencher, leading to a medium fluorescence signal. Furthermore the frequency of intermolecular collisions and their average energy increases, releasing more and more excitation energy of the fluorophores through radiation-free collision processes (Pingoud et al., 2002). The further the probe is cooled, the more frequent the closed hairpin structure is formed and no fluorescence signal occurs, as the quencher eliminates the

fluorescence of the fluorophore due to its close proximity. In the presence of the target, the signal increases again after cooling to about 65°C, as hybridization with the target sequence begins here. The fluorescence intensities of the single and double mutants also increased after further cooling. The sequences with one or two base mismatches at the end of the sequence followed the target first and finally the sequences with one or two base mismatches in the middle of the sequence showed a fluorescence increase.

If the first derivative was formed from these measured values, the melting temperatures of the respective duplex structures can be determined as shown in Figure 47 c). A peak indicated the maximum intensity change of the samples. The melting temperature refers to the temperature at which half of the DNA molecules are in a double-helical state and half are in a random coil state (SantaLucia, 1998). Two peaks can occur after the derivation is formed, indicating that the molecules can not only exist in two phases, fully open and closed, but also an intermediate state can occur. In this case, partial sequences already begin to hybridize while the remaining ones are still open (Dwight and Wittwer, 2016). Therefore, the highest maximum is selected for the determination of the melting temperature. Based on these values, it is also possible to distinguish the target and non-targets with one or two base deviations. The target forms the most stable duplex structure with the probe and thus shows the highest melting temperature at 62.3°C. The base exchange at the end of the target sequence resulted in the duplex melting already at 61.6°C or in other words, from a cooling point of view, starts to bind in to the probe in a stably way below 61.6°C. Accordingly, the target can hybridize with the probe already at a temperature 0.7°C higher than the most similar non-target that was tested here (non-target 5) and thus forms the most stable structure. Two base mutations at the end already caused a melting temperature difference of 6.8°C between the target or the non-target hybridized to the probe and the base variations in the middle of the target sequence led to a difference of 9°C for one mutation and 14°C for two. This agrees with the results from the calculated free energies of the respective structures. The more stable a hybridized structure of two oligonucleotides is built, the higher the melting temperature. The most stable structure in this case is the sample-probe duplex, which is already formed at higher temperatures compared to the non-targets, when it is cooled down after melting. This analysis represents only a snapshot and is intended to show that detection methods other than hybridization, such as melting curve analysis, can be used to distinguish between individual mutations. At the same time, it turned out that DNA sequences that only differ in one base at the end are also difficult to distinguish with regard to the melting point. In particular, a difference of less than one degree in the melting temperature may be subject to fluctuation in several measurements. For a valid statement, the measurement would have to be repeated and the standard deviation of the measured values would have to be taken into account.

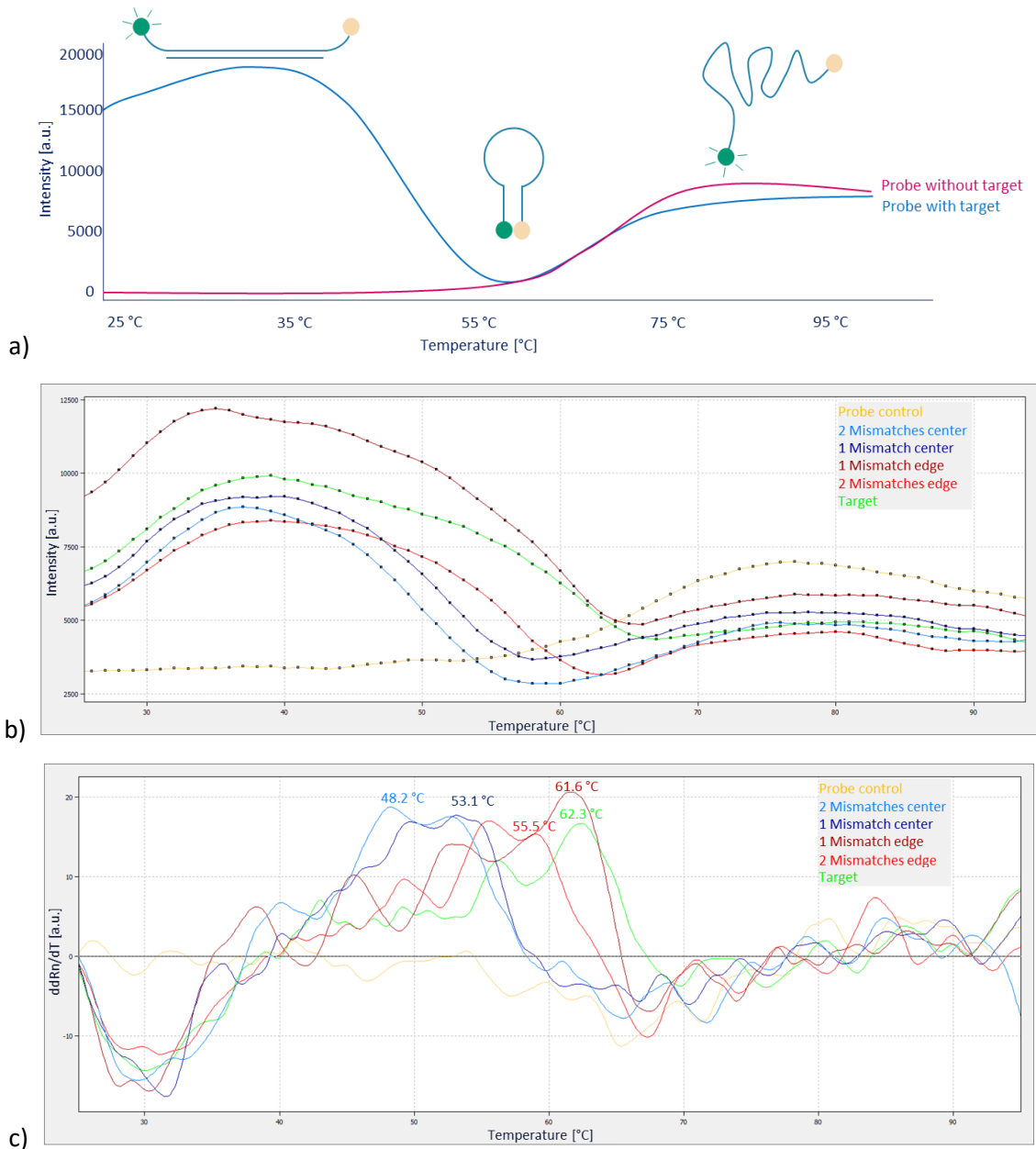


Figure 47: a) Illustration of the fluorescence signals and structures of the probe with and without target over a temperature gradient. The fluorescence intensities indicate that the molecular beacon exists as a hybrid with its reverse complementary target sequence, exhibiting high fluorescence at low temperatures (blue line), or in its free state without target in the form of a stem-loop structure with fluorescence quenched (red line). At higher temperature, the stem sequence melts and the molecular beacon arranges in a random coil structure in both cases. b) Fluorescence measurements during a cooling curve ranging from 95°C-25°C of the molecular beacon probe in the presence of the reverse complementary target sequence (green line), non-target 5 (1 mismatch at the edge, dark red), non-target 6 (2 mismatches at the edge, bright red), non-target 7 (1 mismatch in the center, dark blue), non-target 8 (2 mismatches in the center, bright blue) or in the absence of any target (probe control, yellow line), respectively were generated using the qPCR cyclor Dr. Klaus Hellmuth. c) The melting temperature was determined by forming the first derivative of the fluorescence curves (dR_n/dT : magnitude of the generated fluorescence signal at each time point) and the maxima of the forming peaks using the qPCRsoft 4.0 software from Analytik Jena. A melting temperature of 62.3°C for the probe and reverse complementary target, 61.6°C for the probe hybridizing with non-target 5, 55.5°C for non-target 6, 53.1°C for non-target 7 and 48.2°C for non-target 8 in the center could be determined.

3.6.5. Combination of glass microfiber electrophoresis and detection with FISH

In order to combine the detection by the molecular beacon based hybridization with fiber electrophoresis, the following results will show the migration of the single-stranded reverse complementary target of the molecular beacon probe. As described for other DNA samples in chapter 3.5., also the single-stranded reverse complementary target could be electrophoretically pulled across the fiber chip area upon exposure to a voltage of 45 V for 5 min. Triplicates of the described experiment with fluorescent spots in front of the anode, as expected for a successful target detection, are shown in Figure 48 b). The spots were less intense and focused than the spots observed for dsDNA. This can be explained by GelRed being two times more sensitive for dsDNA than for ssDNA. The more diffuse sample spots may occur if the samples have diffused in width after pipetting in front of the cathode and then electrophoretically pulled across the entire chip area. Another reason could be that the field lines of the electrodes did not run straight down the center between the electrodes as one would theoretically expect and led to deviating sample migration. Control chips tested only with buffer and missing the target DNA showed no fluorescence upon GelRed incubation as can be seen from Figure 48 b).

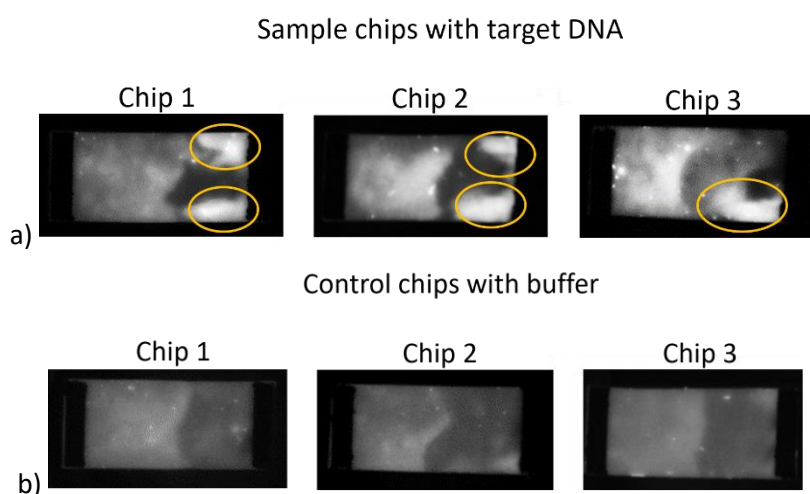


Figure 48: a) Glass microfiber electrophoresis with carbon paste dispensed electrodes and 440 nM of the reverse complementary target sequence to the molecular beacon probe as sample. After fiber electrophoresis at 45 V for 5 min and subsequent staining with GelRed, the fiber chips were documented under UV light using the Chemi Imager. Triplicates of the sample chip showed a diffusely stained sample at the end of the chip area, in contrast to control chips that were tested without sample and with 5 mM Tris running buffer only as shown in b).

In a second experiment the target was detected by hybridization with the molecular beacon which had the complementary binding sequence incorporated into its loop structure (see Figure 49 a). Both molecules were used in the same molar ratio of 440 nM. In contrast to electrophoresis fiber chips tested with the non-target sequence 2, shown in Figure 49 b), the reverse complementary target can

be detected upon hybridization with the molecular beacon by a fluorescent spot. Although the chips were connected to the voltage source for the same duration, the target DNA has not yet reached the anode here. A possible explanation for this is that the electrodes came from a different printed sheet and therefore not from the same batch as in the experiment before. Unfortunately, batch-related differences can occur as a result. Compared to GelRed the fluorescence intensity generated by the molecular beacon was more intense and offers the specific detection of the target of interest.

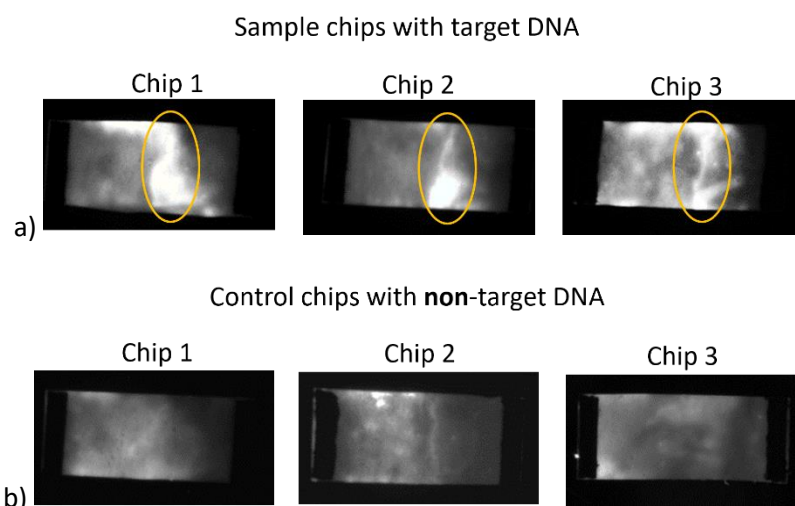


Figure 49: a) Glass microfiber electrophoresis with carbon paste imprinted electrodes and 440 nM of the reverse complementary target sequence to the molecular beacon probe as sample. After fiber electrophoresis at 45 V for 5 min and subsequent detection via FISH using the molecular beacon probe for hybridization, the fiber chips were documented under UV light using the Chemi Imager. Triplicates of the sample chip showed a fluorescent sample spot in contrast to control chips tested with a mismatched DNA sequence (non-target 2) instead as shown in b).

3.6.6. Long-term storage of detection reagents on glass microfiber

Another critical aspect in the development of detection systems is the testing of storage conditions. Fiber materials are suitable for the absorption of liquids containing biomolecules, subsequent drying and storage at room temperature. Storage under ambient conditions is attractive because no instruments, for example to maintain a cold chain, are needed. In the following, the storage capability of the probe on the glass microfiber was tested by an air dry preservation for three months and then investigating the fluorescence signal by adding the target dissolved in buffer. In addition, the target oligonucleotide was also stored on additional filter pieces in parallel. This should be representative of the target sequences that have been extracted from potential environmental samples and stored on the fiber to be used for measurement at a later time. Hybridization was carried out as previously described after either the probe or the target freshly prepared in Tris buffer was added to the filter piece with the dry-stored reaction counterpart. Compared to the freshly pipetted solution of target

and probe, the fluorescence signal of the target sample is reduced by 30 % as shown in Figure 50. The fluorescence signal of the stored probe differs by 44 % from the signal of the freshly pipetted one. Although storage results in some signal loss, the probe is not completely destroyed and able to detect the target sequence. It is important to remember that the filters were not produced under sterile conditions. Nucleases may be present due to the manual handling process that caused degradation of the stored oligonucleotides. Temperature can also have an influence on the stability of the biomolecules. Biomolecules that are stored refrigerated are generally stable over a longer period of time. In addition to damage of the oligonucleotide chain, the fluorophore also lost some of its activity. Photobleaching can be excluded as a possible source of damage in this work since the fibers were kept in the dark by covering them with aluminum foil. However, the fluorophore FAM is also sensitive to acidic environments. The fluorescence signal decreases as the dye becomes protonated and stable buffer conditions cannot be guaranteed in dry state as in solution (Integrated DNA Technologies, 2022).

In conclusion, the results obtained in this work showed the promising possibility of dry storage on the same fiber material, which also serves as the substrate for the analysis. No elaborated equipment for storage and application of the probe by pumps would be necessary. Since the current conditions are not yet optimal, further conditions such as temperature, humidity and sterility as well as the addition of additives should be tested to ensure a stable long-term storage and to obtain a comparable signal to the freshly prepared solutions. Trehalose could be a promising candidate for stabilizing DNA at room temperature. The disaccharide stabilizes biomolecules due to its ability to form tight hydrogen bonds to the phosphate groups, which leads to shielding of the large phosphate-phosphate repulsion (Zuo et al., 2014). It is likely that a similar process occurs in the case of DNA, with trehalose replacing the water molecules in the folded chain and keeping the DNA in a hydrated state (Smith and Morin, 2005; Zhu et al., 2007). Trehalose showed already stabilizing effects for a glucose assay stored on a paper-based device for 30 days. Without addition of trehalose the assay activity was reduced (Martinez et al., 2008a). Trehalose has also already been tested for dry storage of DNA samples at room temperature and is therefore promising to work on fiber as well (Smith and Morin, 2005).

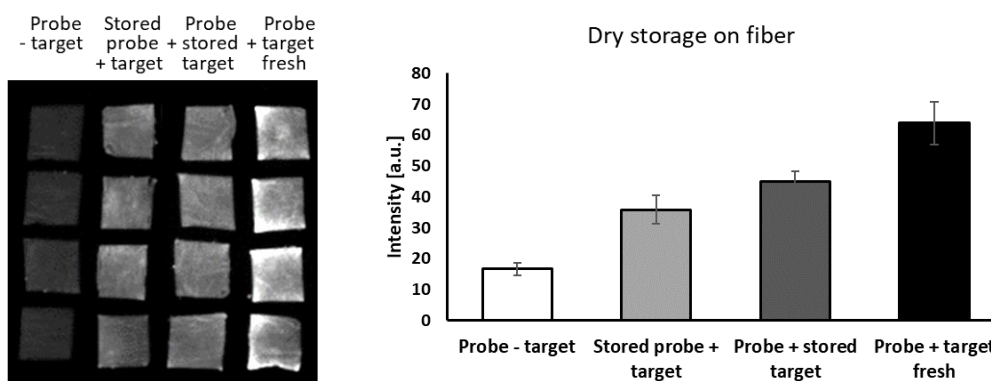


Figure 50: Fluorescence detection of the hybridization of probe and reverse complementary target after 3 months of dry storage at room temperature. Left) Quadrupole measurement of from left to right, freshly prepared probe control without target, freshly prepared probe and reverse complementary target stored, probe stored with freshly diluted target and probe and target freshly prepared at the day of measurement. Each reaction was added to a 5 x 5 mm pad of glass microfiber and after heating (95°C 2 min, 55°C 2 min, 25°C 2 min) the fibers for hybridization, images were taken under UV light. Right) The fluorescence intensities were measured using ImageJ. Stored probes showed higher loss in signal intensity than the stored target sequences compared to a freshly prepared solution of both. Without any treatment of the fiber or biomolecules before storage, 66 % of the hybridization signal was possible.

To take the first steps towards an application outside of the laboratory, the hybridization of probe and target was investigated using an in house developed heating cycler (see Figure 51 a). Here, the fiber pieces were sealed in foil, as shown in Figure 51 b), to provide protection from evaporation and contamination. Heating in this case was accomplished from below and after cooling to room temperature, the detection was again carried out under UV light of the Chemi Imager. As can be seen in Figure 51 b), a little condensate forms between the fiber and the bottom of the foil upon heating. Figure 51 c) shows that a clear fluorescence signal could be detected when the probe was kept opened by the target sequence after hybridization compared to the control without target DNA. The fluorescence distribution was inhomogeneous, but the fluorescent spots were more intense than the signal coming from the fibers that were heated in the reaction tubes was shown in the experiments before. This showed, on the one hand, that the degree of moisture of the fiber can have a decisive influence with regard to the fluorescence intensity and, on the other hand, that uneven drying effects can occur if the fiber is not covered tightly enough.

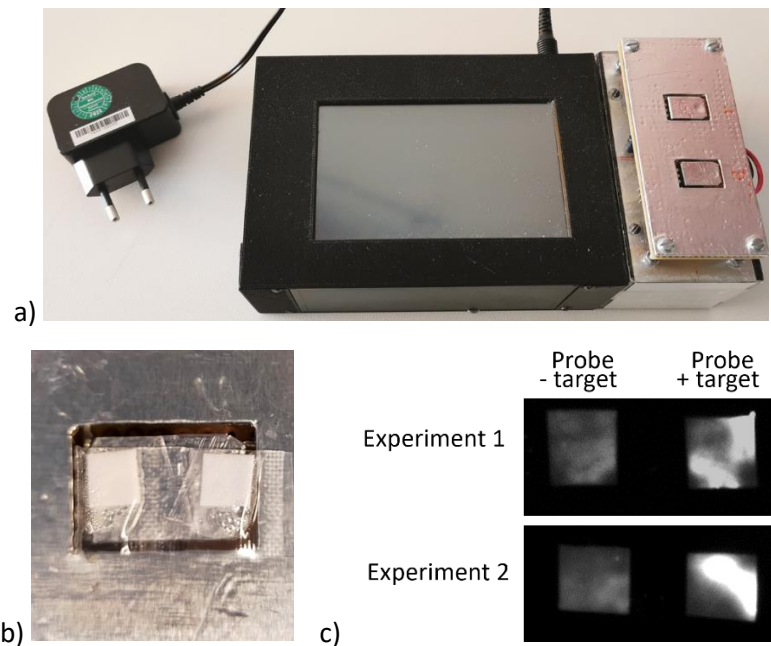


Figure 51: FISH with a self-built heating device by Dr. Alexander Anielski. a) Picture of the cyclor prototype. b) The 5 x 5 mm glass microfiber pads containing either the molecular probe without or with target were sealed in foil and placed onto the heating element. The same temperature steps were controlled as in the previous experiments (95°C 2 min, 55°C 2 min, 25°C 2 min). c) Detection under UV light reveals a fluorescent signal upon binding of the molecular beacon probe to its target sequence. The experiment was tested in duplicates.

3.6.7. Test of bacterial DNA

A further step of characterizing the molecular beacon-based detection on a fiber material included the test of native bacterial DNA. To verify that the beacon is also able to bind the complementary sequence in a *Legionella* contaminated environmental sample, gDNA of *L. pneumophila* Philadelphia was extracted at first via a standard laboratory-based extraction using a commercial Kit from QIAGEN. A molarity of 440 nM complementary DNA target with a molar mass of 6956,6 g/mol referred to an amount of 3 ng of the reverse complementary target, which was previously used in a standard reaction for detections by the molecular beacon. Figure 52 a) represents the hybridization tested with 2.3 ng of gDNA extracted from *L. pneumophila* Philadelphia. Compared to the reverse complementary target, no fluorescent signal can be observed for the gDNA. The fiber with the genomic *Legionella* DNA (middle) showed only low fluorescence signals like the control with the probe without target (left). Since the gDNA contained not only the target of interest, but predominantly other genomic sequences, the amount of DNA was increased in the following experiments. The amount of gDNA was first increased 20-fold in the experiment shown in Figure 52 b). After this increase to 46 ng, still no fluorescence signal could be detected after hybridization with the molecular beacon. Figure 52 c) shows the results of FISH experiments with a further increase in the inserted amount of gDNA. From

left to right the amount of gDNA was tripled starting from 127 ng to 1.14 μg . The first fiber piece was containing 50-fold increased concentration compared to the first experiment but still no fluorescence signal could be detected. A nearly 500-fold increase in gDNA showed a slightly brighter spot in the middle of the fiber material in comparison to the lower concentrated samples on the left side. In conclusion, even at high concentration, no reliable detection of extracted gDNA from *L. pneumophila* Philadelphia was possible using the molecular beacon probe.

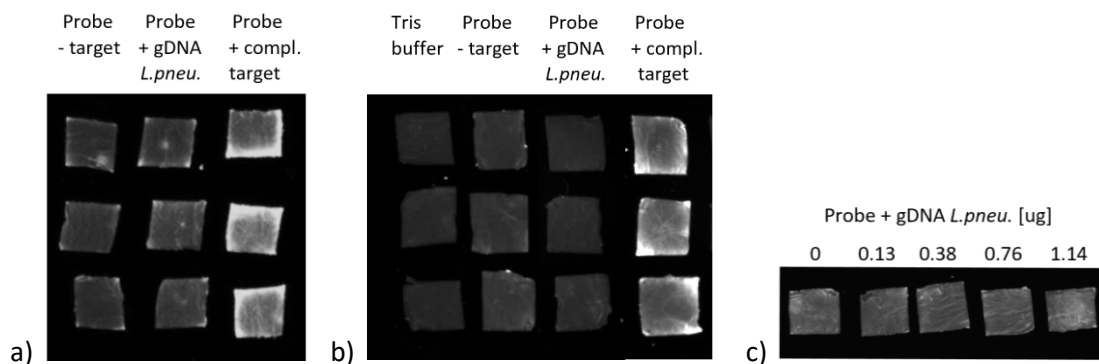


Figure 52: FISH of the molecular beacon (440 nM) with gDNA isolated from *L. pneumophila* Philadelphia on glass microfiber. a) Triplicates of buffer, probe without target, probe and gDNA as well as probe and reverse complementary target, respectively, were added to 5 x 5 mm pads of glass microfiber. After heating (95°C 2 min, 55°C 2 min, 25°C 2 min) the fibers were imaged under UV light. No signal for the native target in the gDNA could be detected compared to the complementary oligonucleotide sequence. b) A 20-fold increase of gDNA concentration (46 ng) compared to a) resulted in no fluorescence detection upon incubation with the molecular beacon probe. c) An increase of the gDNA amount up to 1.14 μg resulted only in a barely visible signal after hybridization with the molecular beacon.

3.6.7.1. Fragmented gDNA from *L. pneumophila* Philadelphia

The transfer from a sample of pure ssDNA to a native sample consisting of gDNA was not possible without further adjustment. In native cells, DNA occurs predominantly in a supercoiled state. The spatial twist of the double strands causes DNA packing in a condensed and particularly space saving manner. Even after extraction, the gDNA can be seen as a molecule of gigantic size, forming a crowded and coiled 3D structure. It was assumed that the region of interest for the FISH recognition was not accessible to the molecular beacon probe because of steric limitations. A strategy to overcome this limitation was an appropriate fragmentation of the gDNA by the use of restriction enzymes. DNA can be cleaved by restriction enzymes at specific recognition sites. These fragment mixes were then tested again for FISH with the molecular beacon probe on the glass microfiber to investigate whether the *Legionella* specific target sequence is recognized.

First several enzymes were tested for the fragmentation of genomic *L. pneumophila* Philadelphia DNA and the results verified by agarose gel electrophoresis. Prior to the start of the experiments, it was verified that the restriction enzymes did not have a cutting site within the target sequence or the probe. This ensured that the desired target DNA would remain intact during fragmentation of the gDNA and would be available for detection. Restriction enzymes SmaI and BseSI tested first did not result in satisfactory fragmentation of the gDNA as shown in Figure A10 and described in section 6.8.

Distinct restriction fragments were received after the digestion of 0.5 µg genomic *L. pneumophila* Philadelphia DNA with the enzymes HaeIII, HhaI, HpaI or HpaII as shown in Figure 53. After comparison with the untreated gDNA loaded in lane 5 and 11 the digestion with HaeIII resulted in bands from 750 to more than 10,000 bp as could be visualized on the agarose gel in lane 2. The digestion mix with HhaI in lane 3 showed smaller fragments ranging from 450 to about 6500 bp. The digestion with both enzymes showed the smallest fragments ranging from 250 to 4800 bp (see lane 4). The enzyme HpaI cleaved the gDNA in larger sequences compared to the other enzymes ranging from 1800 to over 10,000 bp as can be seen in lane 8. The restriction fragments occurring after treatment with HpaII showed smaller fragments than HpaI, approximately 375 bp to 7500 bp as shown in lane 9. The span of fragments of the double digestion with HpaI and HpaII was comparable with the single digestion with only HpaI (see lane 10). After a closer comparison, it became apparent that some fragments such as the fragment with 4800 bp or two fragments about 5000 bp and below for example were missing from the double digest. Also a double digestion with HaeIII and HpaI was possible as shown in lane 7. The largest fragment comprised 8000 bp and was in the middle of the largest fragments with digestion using either HaeIII (over 10,000bp) or HpaI (6500 bp) in comparison. The fragments sizes ranged from 500-8000 bp in total.

By using the Restriction Analyzer, a software tool for comprehensive restriction analysis of a DNA sequence, the experimentally obtained fragmentation patterns could be compared to a simulated DNA digest electropherogram as shown in Figure 54 (Čermák, 2021). The results shown here agree well with those predicted theoretically. The gradation in terms of fragment sizes from HaeIII to HhaI and the double restriction digestion with HaeIII and HhaI is well discernible. After the restriction digestion with HaeIII, another fragment larger than 10,000 bp was detected experimentally, which was not included in the theoretical prediction. However, the 9 largest fragments were found to be between 4000-10,000 bp in both, the theoretical prediction and the experimental fragmentation. The largest fragment of the HhaI digest was 6266 bp in size and the double digest with HaeIII and HhaI resulted in fragments starting at 4634 bp in both, the theoretical prediction and experiments. The combination of HaeII and HpaI showed fragment sizes of 8192 bp and smaller, whereas cutting with HpaI lead to much larger fragments starting at 36,548 bp and consequently the bands are above the largest fragment of

the ladder at 10,000 bp. The experimental data from digestion with HpaI and HpaII were also consistent with this prediction. According to the prediction of the program, HpaII cuts fragments of 7098 bp and smaller and a double restriction digestion together with HpaI produced 74 more fragments with the largest band corresponding to 6994 bp. Comparable to the experimentally obtained data, the fragment pattern between the single digest and the double digest looks similar, except that the double digest does not include certain band sizes such as the fragments below 5000 bp. The prediction includes one fragment around 7000 bp more for the single digest compared to the experimentally determined results. In summary, the experimental data of the restriction digestion tested in this work on *L. pneumophila* Philadelphia agreed well with the predicted ones from the software and, accordingly, the incubation conditions do not need to be changed.

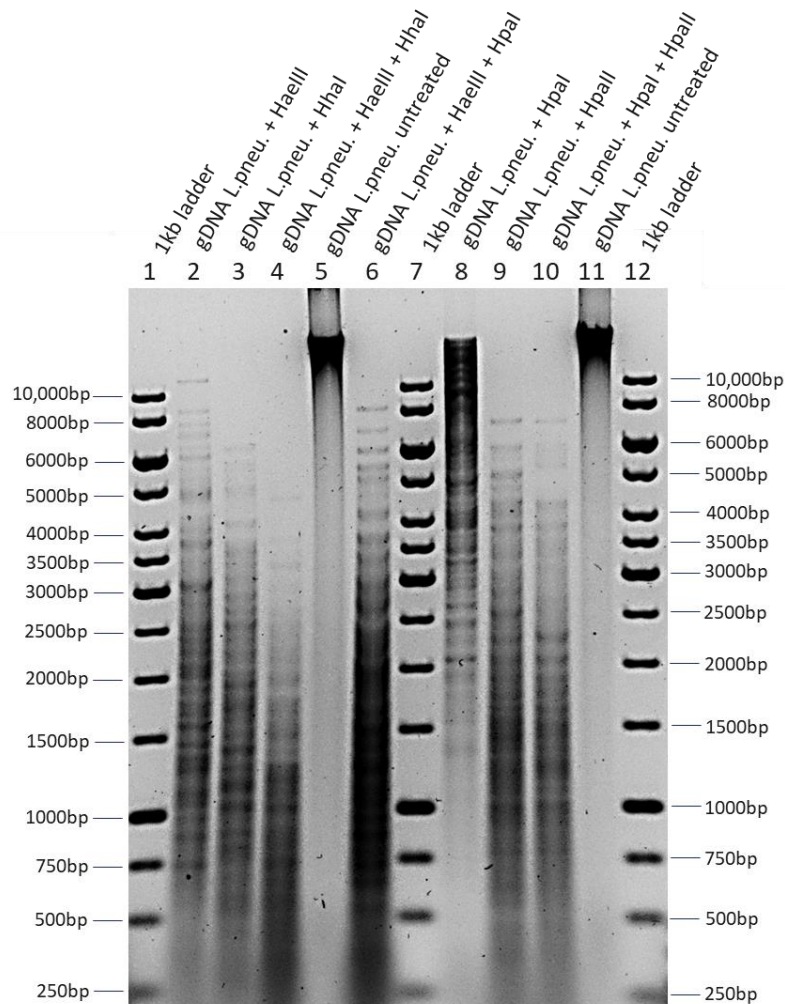


Figure 53: Digestion pattern of gDNA using restriction enzymes HaeIII, HhaI, HpaI and HpaII. Digestion reactions with HaeIII and HpaI, separately and in combination (lanes 2-4) were incubated at 37°C for 2 h and fragmentation with HpaI and HpaII, separately, and in combination for 6 h (lanes 8-10). A mix of HaeIII and HpaI was also incubated for 6 h with gDNA (lane 6). After heat inactivation at 80°C for 20 min the samples were visualized on a 0.7 % agarose gel after gel electrophoresis for 17.5 h. A 1 kb ladder was loaded as size reference (lanes 1, 7 and 12) and untreated gDNA from *L. pneumophila* Philadelphia was loaded on column 5 and 11 for comparison.

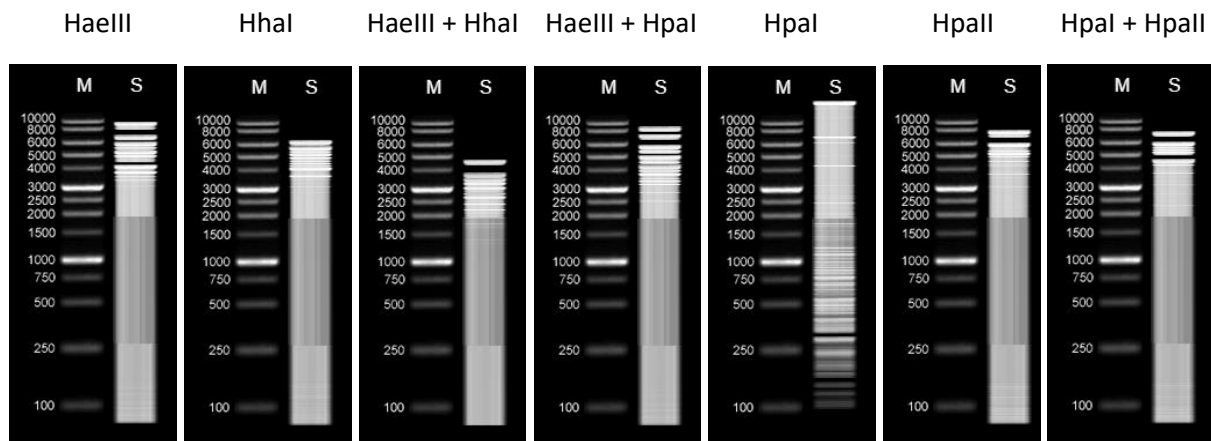


Figure 54: Prediction of the band patterns using the Restriction Analyzer software tool (Čermák, 2021). Restriction digestion of the *L. pneumophila* Philadelphia genome with the restriction enzymes HaeIII, HhaI, HpaI, and HpaII, alone or together, and visualized on a 1% agarose gel.

In the following section, the results of the FISH experiments of the molecular beacon to detect the fragmented gDNA on glass microfibers will be discussed. The double digestion mix of gDNA from *L. pneumophila* Philadelphia with HaeIII and HhaI was selected first because it yielded the smallest DNA fragments. In addition to the probe without target DNA to determine the background signal in column 1, the molecular beacon was incubated with untreated gDNA as shown in column 2 and fragmented DNA in column 3 as shown in Figure 55 a). To ensure that the restriction enzyme itself do not lead to an unspecific fluorescence signal, the enzymes were also incubated at the same temperature but without DNA and were tested on the fiber as well (column 4). As a positive control the 100 % reverse complementary target was taken (see column 5). The undigested DNA did not show a fluorescence signal after incubation with the probe and the signal intensity is again similar to the background value of the probe tested without target. If the DNA was cut using the restriction enzymes HaeIII and HhaI, a fluorescent signal could be detected. The intensity values can be evaluated using ImageJ and are shown in Figure 55 b). The intensity of the cut DNA can be clearly distinguished from the probe background, as the signal is twice as high when the DNA fragments are used for detection instead of the untreated DNA. These results underline the assumption that the probe cannot bind to its corresponding target sequence when detecting pure gDNA due to steric limitations. If the 3D structure is interrupted by fragmentation, the DNA target is accessible to the probe and can be detected. The fact that the probe could not be influenced by the restriction enzyme alone, was shown in column 4. Here the intensities are similar to those of the background signal of the probe without target and thus confirm no unspecific signal after addition of the enzyme inactivated by heat treatment.

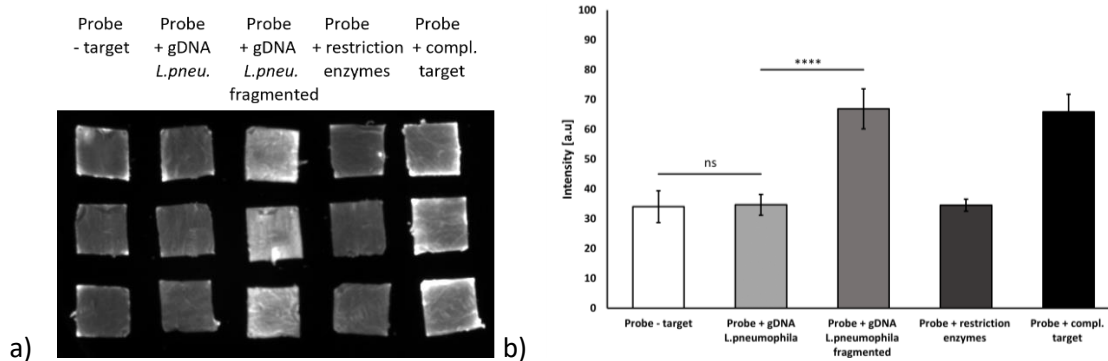


Figure 55: FISH of the molecular beacon with fragmented gDNA from *L. pneumophila* Philadelphia on glass microfiber. a) Triplicates of probe without target, probe and gDNA from *L. pneumophila* Philadelphia untreated and fragmented with HaeIII and HhaI, respectively, the enzymes without DNA and the probe with reverse complementary target sequence were added to 5 x 5 mm pads of glass microfiber. After heating (95°C 2 min, 55°C 2 min, 25°C 2 min) the fibers were imaged under UV light. b) The fluorescence intensities were evaluated using the ImageJ program. The fluorescence occurring from hybridization of the probe and fragmented DNA was significantly detectable in comparison to untreated gDNA (n=8; **** p<0.0001; ns not significance; student's t-test).

3.6.7.2. Fragmented gDNA from other bacterial strains

In a next step, the ability of the probe was tested to specifically detect gDNA from *Legionella*. For this purpose, the restriction digestion protocol was also applied to other bacterial strains. Besides *L. pneumophila* Philadelphia also *E. coli*, *P. aeruginosa*, *S. paucimobilis*, *A. haemolyticus* and *S. marcescens* were taken into account because these are also pathogens potentially found in water samples.

The restriction digestions with *E. coli* and *P. aeruginosa* with HaeIII or HhaI resulted in much smaller fragment sizes, predominantly smaller than 500 bp or 250 bp, compared to the fragmentation pattern of *L. pneumophila* Philadelphia as shown in Figure A11 and described in section 6.9. No differentiation between *L. pneumophila* Philadelphia and the other strains was possible after each fragmented gDNA was incubated with the molecular beacon probe on glass microfiber as shown in Figure A12. Fragmentation using restriction enzymes can also have the effect of creating additional target sequences, thus generating a false positive signal. Staggered cuts of dsDNA by the enzymes HhaI and HpaII generate sequences with overhanging bases on each strand after cutting. Those sticky ends can religate with other complementary overhangs of other restriction fragments, generating new sequences. The enzymes HaeIII and HpaI, on the other hand cleave both DNA strands at once, yielding in fragments with blunt ends. Another consideration was made towards the origin of the enzymes. They were all produced within *E. coli*, perhaps increasing their effectiveness in cutting their strain of

origin. Consequently, a new digestion mix containing HaeIII or HpaI was tested and *E. coli* was omitted as an alternative organism to *Legionella* for the digestion and FISH experiments.

Figure 56 shows the results of the adapted digestion reaction of HaeIII or HpaI with gDNA from *L. pneumophila* Philadelphia, *P. aeruginosa*, *S. paucimobilis*, *A. haemolyticus* or *S. marcescens*. Adaptation involved a decrease in incubation time of the DNA with the enzyme from 2 h to 15 min, in order to investigate if fragmentation into very small sequences could be prevented. HaeIII treated reactions were heat inactivated again after incubation with the enzyme to ensure termination of the cutting. Lanes 8-11 show the gDNA of the bacterial strains after extraction and without treatment of any restriction enzymes again as an intense black band on top of the agarose gel.

The restriction fragments of *P. aeruginosa*, *S. paucimobilis* and *S. marcescens* cut by HaeIII are again relatively small as shown in lane 2, 3 and 5. In contrast, *S. paucimobilis* could not be cleaved by HpaI as can be seen from lane 13 because a single thick band, similar to the untreated DNA, is still seen on top of the agarose gel. HaeIII as well as HpaI were suitable for the fragmentation of *A. haemolyticus* (see lane 4 and 14). Lane 15 shows that HpaI could be also used for the fragmentation of *S. marcescens* into moderate sized DNA fragments. The enzymes used for the restriction digestion were also loaded onto the gel as controls (see lanes 6 and 16), to show that only the DNA but not the enzymes generate stained signals on the agarose gel.

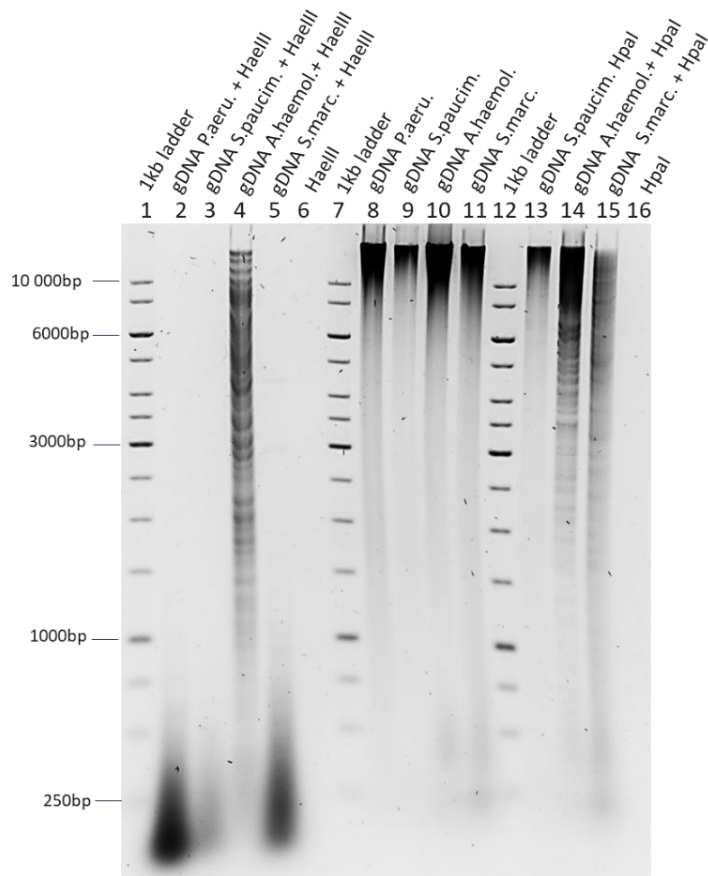


Figure 56: Fragmentation using restriction enzymes HaeIII and HpaI on gDNA of different bacterial strains. Samples were loaded on a 0.7 % agarose gel and visualized after gel electrophoresis for 17.5 h. Untreated gDNA of *P. aeruginosa*, *S. paucimobilis*, *A. haemolyticus* and *S. marcescens* (lanes 8-11) used as template DNA for the digestion showed one band at the same height on top of the agarose gel. Digestion of the DNA isolated from *P. aeruginosa*, *S. paucimobilis* and *S. marcescens* with HaeIII resulted in small and smeared fragments (lanes 2,3 and 5). The digestion of *A. haemolyticus* with HaeIII (lane 4) and HpaI (lane 14) and *S. marcescens* with HpaI (lane 15) resulted in fragments of different sizes, ranging over the whole gel area. Genomic DNA of *S. paucimobilis* was not cut by HpaI (lane 13) showing a band comparable to the untreated gDNA. A 1 kb ladder was loaded as size reference (lanes 1, 7 and 12). The restriction enzymes without DNA were loaded as controls in lanes 6 (HaeIII) and 16 (HpaI).

In order to replicate these results and for a better comparability to *Legionella* DNA, samples of the restriction mixes with HaeIII or HpaI using gDNA of *L. pneumophila* Philadelphia, *A. haemolyticus* and *S. marcescens* were performed again and loaded on a second agarose gel as shown in Figure 57 a). Naturally the fragmentation pattern is not equal, because the distribution of the restriction site in each bacterial genome differs. Nevertheless, the fragmentation pattern after the digestion mixes of gDNA from *L. pneumophila* Philadelphia (lane 3), *A. haemolyticus* (lane 6) and *S. marcescens* (lane 8) were similar showing fragments ranging from over 10,000 bp to at least 2000 bp in size, if HpaI was used.

By comparison of the treatment of *L. pneumophila* Philadelphia DNA with HaeIII as shown in column 3 and *A. haemolyticus* DNA in column 4, DNA bands in several sizes ranging over the whole gel area can be observed but differed in the number of fragments of specific sizes. Digestion of *L. pneumophila*

Philadelphia DNA caused a higher number of fragments ranging from 3000 bp and below. In contrast the fragmentation of *A. haemolyticus* resulted predominantly in fragments showing sequence length of 1000 bp to over 10,000 bp. Since it has already been shown for *S. marcescens* that a digestion with HaeIII was not suitable because the fragments were too small and poorly differentiable (compare Figure 56 lane 5), it was not included in this experiment.

In addition, the same restriction protocol was tested on gDNA extracted via the alkaline lysis and extraction protocol described in section 2.4.2. No matter if the gDNA was extracted via the spin-column based Kit from QIAGEN or the simple and rapid alkaline extraction protocol, the fragmentation pattern was identical. The only difference between the samples is the concentration of initial template DNA, which can be determined after comparing the untreated DNA in lanes 4 and 9 of Figure 57 b) with lines 5 and 11 from Figure 53. Consequently, there is also a lower concentration of restriction fragments for DNA extracted by the alkaline extraction protocol. These results confirm the possibility of eliminating the need for laboratory equipment for lysis and extraction of DNA from bacteria. Furthermore, no purification of the gDNA from cell debris or change in buffer conditions is required prior to the restriction digestion. The sample can be used directly after alkaline lysis for fragmentation using the protocol developed here.

Finally, it was tested, whether a specific detection of the native *Legionella* target is possible with the probe, when comparing strains that have similar sized fragments after restriction digestion. The test of HpaI digested gDNA isolated from *L. pneumophila* Philadelphia and *A. haemolyticus* on glass microfiber using the molecular beacon for the detection of the specific region within the 16S rRNA gene sequence of *Legionella* spp. was taken as an example and is shown in the Figure 58. Another advantage of using HpaI was that less enzyme had to be used for digestion and no heat inactivation was required. As can be seen from columns 2 and 3, the fluorescence signal of the probe incubated with the DNA fragments of *L. pneumophila* Philadelphia showed a significantly higher signal compared to the fragmented *A. haemolyticus* DNA. In this experiment, the signal of the probe incubated with the untreated DNA is slightly higher than in the previous experiment. However, the signal of the DNA cut with only HaeIII is 1.5-fold more intense compared to the untreated gDNA. The standard variation of the background signal (only probe without DNA) was also higher in this experiment because one exposed fiber in the third sample resulted in a non-specific signal. This may be due to a contamination during the preparation step.

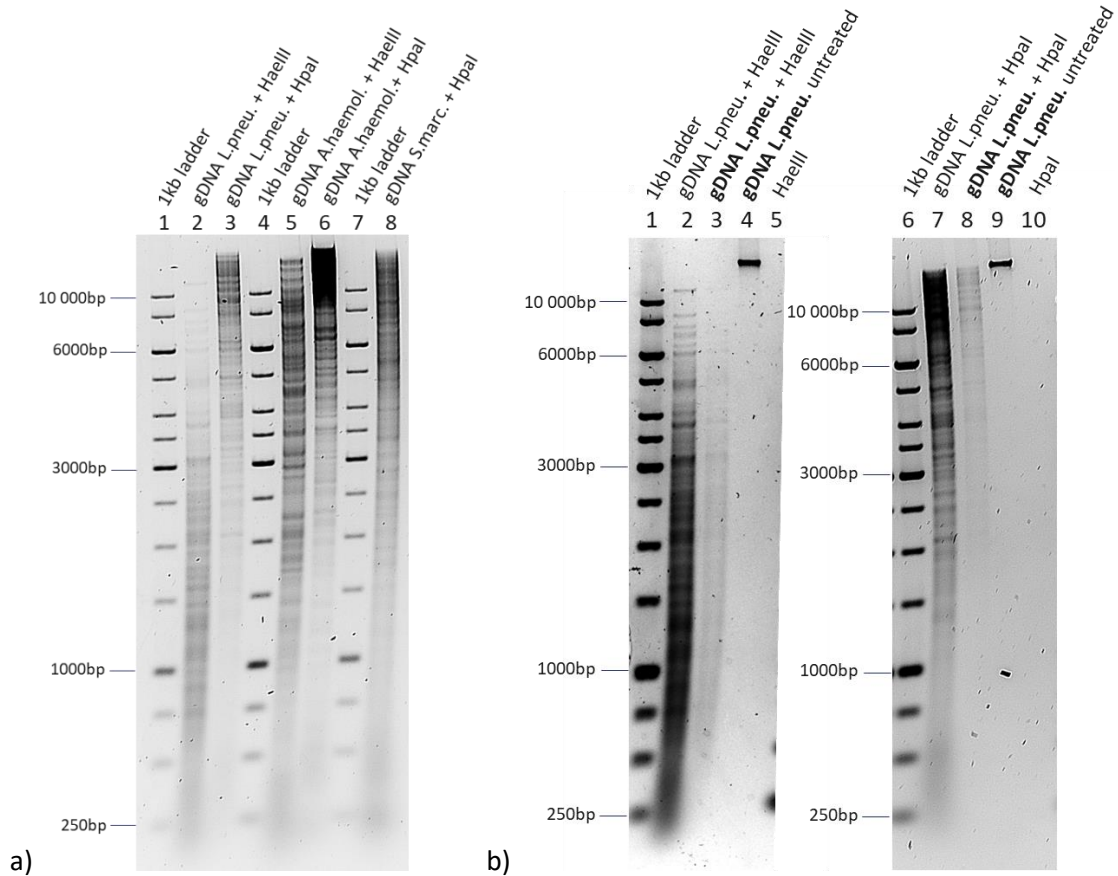


Figure 57: Comparison of the fragmentation patterns of gDNA isolated from *L. pneumophila* Philadelphia and *A. haemolyticus* via a spin-column based and alkaline extraction method upon digestion with the restriction enzymes HaeIII and HpaI. Samples were loaded on a 0.7 % agarose gel and visualized after gel electrophoresis for 17.5 h. a) *L. pneumophila* Philadelphia, *A. haemolyticus* and *S. marcescens* show similar fragmentation patterns after digestion with HaeIII and HpaI respectively. HaeIII cut gDNA in fragments of a broader range of DNA sizes than HpaI. b) Template *Legionella* DNA occurring from the alkaline extraction protocol (marked bold) showed the same fragmentation pattern only less concentrated as DNA isolated by the spin column based extraction. The restriction enzymes without DNA were loaded as controls in lanes 5 (HaeIII) and 10 (HpaI). A 1 kb ladder was loaded as size reference (lane 1).

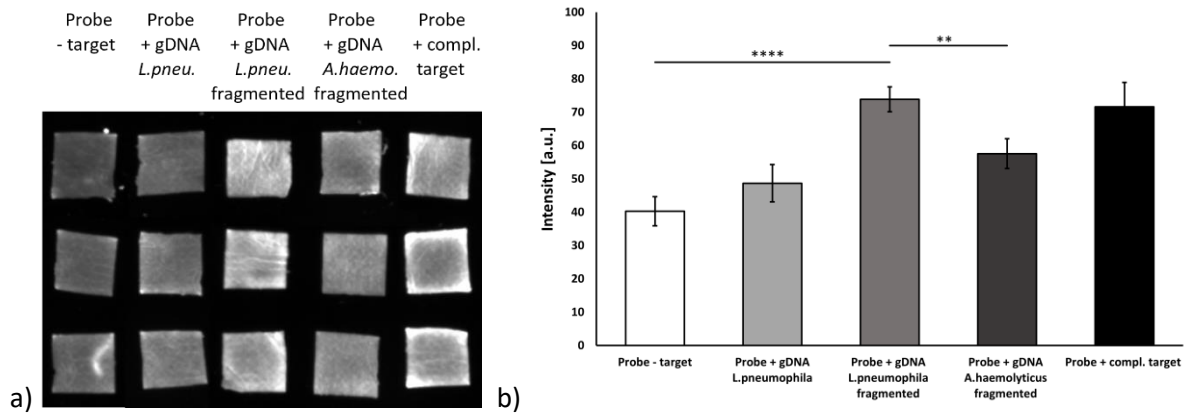


Figure 58: Hybridization of the molecular beacon with fragmented gDNA of *L. pneumophila* Philadelphia and *A. haemolyticus* on glass microfiber. a) Triplicates of probe without target, probe and gDNA from *L. pneumophila* Philadelphia untreated and fragmented with Hpa I, respectively. Digested gDNA from *A. haemolyticus* was tested as a negative control and the reverse complementary target sequence was tested as a positive control. All samples were mixed with the molecular beacon probe and added to 5 x 5 mm pads of glass microfiber, heated for hybridization (95°C 2 min, 55°C 2 min, 25°C 2 min) and imaged under UV light. B) The fluorescence intensities were measured using the ImageJ program. Fragments of *L. pneumophila* Philadelphia were detected by the molecular beacon significantly over fragmented gDNA isolated from *A. haemolyticus* (n=3; **** p<0.0001; ** p<0.01; student's t-test).

To put the results obtained here into context, in principle the molecular beacon probe recognized its complementary sequence specifically after a FISH experiment was performed on the glass microfiber. A significant detection of 3.5 nM reverse complementary target was possible using the molecular beacon in a FISH on fiber (Figure 43 b). A nanomolar detection limit has also been reported for molecular beacon based experiments (J. J. Li et al., 2008; Xi et al., 2003; Zhang et al., 2001). Consequently, the sensitivity obtained in this work for a FISH experiment of a glass microfiber agrees well with the values from the literature, which mainly reporting reactions in liquid.

However, if this detection limit is set in relation to the native target, reliable detection would only be possible with high cell numbers. In principle, successful detection via FISH is possible, but considering the results of the FISH experiments with bacterial DNA and the determination of the sensitivity, a cell number of about 10^8 - 10^{10} cells would be required if a molecular beacon-based detection without prior amplification of the target sequence is performed. Although detection of *Legionella* has the advantage of using filters that concentrate the bacteria prior to detection from the water sample, this number of cells is still difficult to achieve. Accordingly, exponential amplification prior to detection would be useful to increase the target concentration in future.

The autofluorescence of glass fiber is lower than that of cellulose and thus offers an advantage for fluorescence-based detections (Danielson et al., 2003; Zhang et al., 2020). Cellulose-substrates excited with UV light generate a blue/green emission. Cellulose as a skeletal component of plants is provided

as pulp and can remain a content of lignin, which has been attributed to the cellulose's autofluorescence (Castellan et al., 1992). The glass microfiber had a slightly positive effect on the robustness of the fluorescence signal detection compared to the detection as liquids in reaction tubes (compare Figure 42 and 43). Consequently, an enhanced sensitivity could be determined for the fiber-based FISH detection. The fiber matrix provides, due to its structural geometry many micro compartments at which the molecules are limited in their diffusion. Thus, an enrichment of the fluorescence signal by the local concentration of the probe can be assumed as an effect of probe density on DNA hybridization was already investigated for microarray format (Peterson et al., 2001; Wei et al., 2005).

4. Summary and outlook

The aim of this work was to develop a sensor for the rapid detection of *Legionella* on a fiber-based platform and to characterize the individual steps. Figure 59 shows how the laboratory prototype might look when all the steps developed are merged, even if they are not yet applicable without adaptation. The first step consisted of the gDNA extraction from the bacteria using an instrument-independent alkaline lysis. The DNA is then fragmented by the addition of restriction enzymes, without prior purification of the sample and can be separated from the cell debris by fiber electrophoresis on a glass microfiber chip with imprinted electrodes. Specific detection was performed using a molecular beacon probe directed against a specific region within the 16S rRNA gene of *Legionella* spp., resulting in a fluorescent signal upon successful detection. If the individual steps are added together in terms of time, a 5-min lysis and a 30-min fragmentation, followed by a subsequent electrophoretic separation of 10-25 min and a final hybridization of 6 min, resulted in a total detection time of about one hour. The results of each step are summarized below.

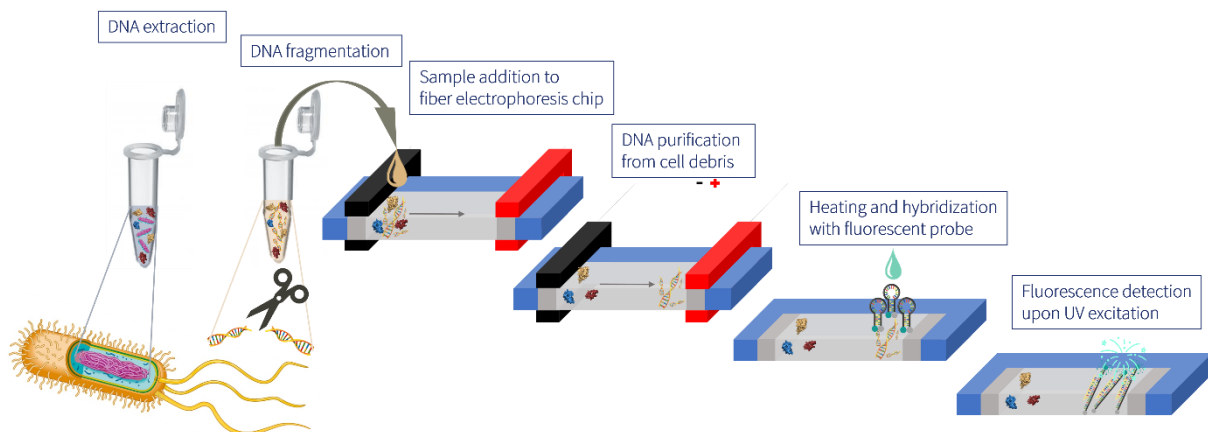


Figure 59: Possible sequence of steps for a fiber-based sensor platform for the detection of *Legionella*. After extraction of the gDNA from the bacteria using an instrument-independent alkaline lysis, the DNA was fragmented by the addition of restriction enzymes and could be separated from the cell debris by fiber electrophoresis on a glass microfiber chip with imprinted electrodes. After addition of a molecular beacon probe directed against the specific gene sequence within the 16S rRNA gene of *Legionella*, a FISH based detection was performed.

An optimized, simple and efficient alkaline lysis can be used to inactivate even high concentrated *Legionella* from water samples and release the gDNA. In only two steps consisting of the addition of buffers and without any devices, this method is easy to apply, cost-effective and suitable even for untrained personnel. But after neutralization of the alkaline chemicals, salts remain in the buffer, that could interfere with detection reactions, such as amplification, that may be integrated in the future. Therefore, also alternative DNA extraction methods, e.g., based on an enzymatic principle, should be

tested in the future and compared with respect to their efficiency. In particular, if other pathogens should become the focus of detection, heat treatment could also serve as a DNA extraction method in contrast to the heat-tolerant *Legionella*. However, thanks to a wide range of enzymes, there are salt-tolerant polymerases that can be used to amplify the extraction samples described here.

With respect to fibers, the interaction of DNA samples with fiber materials under the influence of heat was first investigated. This included the temperature dependence, chemical and structural properties, an evaporation protection and different elution buffers to investigate the recovery of the sample from the fiber. Cellulose-based fibers were the starting point, as frequently described in the literature. However, glass fibers were found to be superior to cellulose in terms of non-specific DNA retention and low autofluorescence in this work, so they were used as the main basis for fiber chip development. To provide a self-contained fiber area, it was possible to develop a patterning protocol for glass microfibers based on the principle of the offset printing technology. In this process, a wax-like polymer resin was printed in any design on an overhead film, comparable to a conventional laser or inkjet printer. When the printed overhead film was pressed together with the glass fiber under heat, the molten polymer penetrated into the fiber interstices and created the desired pattern on the fiber. This method was also applied for other soft and smooth fiber materials such as nylon or other geometries that deviate from common printer formats, e.g., small round filters. The penetration depth of the hydrophobic barriers could be controlled by the amount of the applied polymer mixture and the duration of heat exposure. This has made flexible patterning of almost any fiber material possible.

For the development of a fiber-based electrophoresis system in a miniature format, cellulose and glass microfiber filter paper were tested in combination with conductive materials and application methods to introduce imprinted electrodes. By applying a conductive carbon paste using a dispenser, electrodes could be reliably printed directly on the fiber material at the ends of the fiber chip. These electrodes were used to induce the migration of DNA samples within the fiber-based on the principle of electrophoresis. Starting with 115 V, the voltage could be successively reduced to 45 V. Migration at only 5 V was also successfully tested, but was accompanied by an increase in run time to at least 20 min. Despite variations in the penetration depth of the paste into the fiber, as well as in the resistances of the electrodes, this electrode setup could be used to reproducibly pull DNA samples across the fiber surface in a short time window of 5 min and at a low field strength of 24 V/cm. Direct staining of the DNA on the fiber surface using an intercalator (GelRed) or a molecular beacon probe was possible, as was subsequent elution and verification of the sample by agarose gel electrophoresis. Even with connection times of up to one hour, the DNA did not run into the electrode surface, but remained concentrated in front of it and could still be detected by staining or elution without any problems. The DNA also remained intact during fiber electrophoresis and could subsequently be eluted

and used for further detection methods, e.g. PCR, as shown in this work. This robust and reproducible electrophoresis on glass microfiber was similarly applicable to DNA single fragments, to a mix on different sized fragments as well as to gDNA. The latter was tested to provide an option for purification of bacterial lysates by fiber electrophoresis. In this process, DNA could be separated from the cell debris after alkaline lysis. Since the connection time may need to be increased for the purification of complex samples, a fiber chip with two wings perpendicular to the center of the chip was developed that were immersed into a buffer reservoir during electrophoresis and to prevent the chip from drying which would terminate migration.

The design of the chip structure could also be chosen in such a way that two channels separated from each other were present on the same chip surface and thus two DNA samples of different composition could be moved across the fiber surface in parallel with the same imprinted electrodes.

Targeted movement through several layers was also possible with this type of fiber electrophoresis chip. This may become particularly interesting if different detection reactions are planned to take place in different layers at a later time. In addition, a moderate size-dependent migration could be achieved by an arrangement of three stacked fiber layers. Thereby, the larger DNA fragments, despite the comparatively large pore size of the fiber material compared to the DNA molecules, could be retained probably because of the fiber alignment.

In the next steps, it should be investigated whether this separation process can be further improved by adding more layers or combining different fiber materials. A combination of glass microfiber with materials that have smaller pore sizes ($< 0.7 \mu\text{m}$) such as membranes would be conceivable. In addition, coating the fiber could lead to a reduction in pore size, or induce a charge-based retardation of the sample.

Initial experiments have shown that, in addition to fiber electrophoresis, the imprinted electrodes can also be used simultaneously as measuring electrodes. An increase in the electric current signal indicated the presence of DNA samples. Since the DNA concentrations required for this detection were high, it will be necessary in the future to find a combination of fiber and electrode materials that allow this detection even at lower concentrations. Enhanced detection using an electroactive dye can also help to obtain information about the progress of the sample already during migration. In this work, the first experiments using methylene blue as an electroactive dye were performed and it was shown that temporally sequential potential signals can be recorded and indicate possible sample migration.

Stable electrodes in terms of conductivity, alignment on the fiber and integrity after voltage exposure are prerequisites for a homogeneous E-field in which the charged sample can migrate always in the same way. With regard to the development of a robust fiber-based electric current or potential sensor,

which could be part of future work, the electrode material and printing method need to be improved, as different conductivities make it difficult to search for signal characteristics in the measurement data.

In addition to the results just described, a successful combination of the molecular beacon-based detection with fiber electrophoresis could be shown and thus offers the possibility of a specific DNA detection on the basis of fluorescence. Possible applications for this would be, for example, DNA detection after successful purification of cell extracts or the targeted movement of analytes in other layers of a stacked fiber chip for subsequent verification.

The probe tested here targeted a specific region within the 16S rRNA gene sequence of *Legionella* spp., which can be used for the phylogenetic classification of the bacterium into its genus. A short hybridization protocol for a successful detection of the reverse complementary target on the glass microfiber was developed. A dilution series of the reverse complementary target showed that significant detection was possible up to a dilution of 3.5 nM with the molecular probe on the glass microfiber. Structure-stabilizing ions such as sodium or magnesium, which are already present as ions on the fiber, are sufficient to stabilize the hairpin structure of the probe at 25°C, as confirmed by software-based structural observations.

First attempts were made to test the hybridization on fiber sealed in foil with a self-made heating cycler and the storage capability of the fluorescence-labeled probe for a period of three months. Both series of tests showed that in principle hybridization by a simple heating device and air-dried storage was successful, however, optimization is still required if the detection should take place outside the laboratory in the future.

Specificity studies with the probe showed that non-targets differing in more than two bases can be distinguished from the sample. Subsequent specific detection of the target DNA sequence was also demonstrated after migration through the glass fiber chip by electrophoresis, indicating the promising option to combine both methods in the future and to detect the desired target sequence immediately after purification of the gDNA.

In case of deviations of 1 or 2 bases, a differentiation from the actual target sequence was only achieved if a melting or cooling curve is recorded to distinguish the melting temperatures of the different hybridized sequences. The more accurate the base sequence, the more stable the hybridization to the probe and thus the higher the melting temperature. The effect of a base mismatch of one or two bases also depended on the position of the mismatch and had a stronger impact on the melting temperature of the hybridized sequence in the middle of the sequence, making it more easily distinguishable from the target sequence than at the edge.

In principle the molecular beacon probe can be used to detect also gDNA from *Legionella* on the glass microfiber just by FISH without prior amplification. Without pretreatment, detection of genomic *Legionella* DNA by the probe was not possible. Only after successful fragmentation of the DNA with restriction enzymes leading to a similar fragmentation pattern, the detection by the molecular beacon became possible. The specificity and sensitivity must be improved considerably in the future, since only high titers could be detected and these would only be present in the case of strong contamination by *Legionella* e.g., in biofilms.

An amplification step would be recommended in the future to enhance the sensitivity of the detection. In order to avoid the need of extensive laboratory equipment, an isothermal amplification method would be desirable, since the technical implementation of a constant heat supply is much easier than controlling temperature cycles. Methods that also operate at low constant temperatures, such as RPA at 37-42°C, are therefore particularly attractive for amplification in the fiber matrix, since it was already shown at the beginning of this work that extensive heat input can lead to unspecific retention of DNA on certain fiber materials. To increase specificity, a DNA target region can be chosen for the probe design that would be more specific to the bacterial species. In the case of the mostly legionellosis-causing strain *Legionella pneumophila*, the virulence factor Mip would be suitable here. In the future, other *Legionella* strains should be tested in addition to other water pathogens to test for a genus- and species-specific detection.

Another subject of subsequent work to improve the limitations of the FISH detection could be a local immobilization of the probe on the fiber followed by continuous sample migration over the immobilized sample. In this way, the local concentration of the target could be increased and the detection possibly enhanced. For this purpose, coatings of the fiber with avidin and specific binding of a biotinylated probe could be considered. In addition, a covalent coupling method would be conceivable, e.g., with an epoxide-based crosslinker such as BDDE, which can bind both the hydroxyl groups of the glass surface and amino tags of a modified molecular probe in a pH-dependent manner.

Textile dyes were used in this work to demonstrate back-and-forth movement of molecules upon electrophoresis and polarity reversal. In the future, this can be tried with DNA samples to allow flexible and multiple sample movement when needed, e.g., to first pull a sample to an immobilized probe and then recover it.

Pre-storage of the probe on the fiber in a dry state is a possible scenario with respect for future assay production. Without further pretreatment of the fiber nor the addition of any stabilizers, the probe could be stored in a dried state on the glass microfiber for over three months at room temperature and was still capable of reliably detecting the target sequence. To optimize storage in the next stability

assay to achieve activity comparable to a fresh probe solution, the fibers can be sterilized to minimize exposure of DNA to DNases. For stabilization of DNA, also additives such as Trehalose would be conceivable. Refrigerated storage, e.g., at 4°C, may also be considered in the future to reduce the effects of degradation.

For any kind of fluorescence readout in future applications of the described reactions, a mobile readout unit is still needed. The imager used in this work provided initial evidence that fluorescence-based readout on glass fiber is very feasible. However, the signal might be read out even better and more robustly if better filters and fine-tuned exposure times were incorporated into a self-developed device. In the detection unit for fluorescence, compatibility with a heating element should also be considered to improve readout during a heat dependent reaction, if necessary.

5. References

- Abe, K., Suzuki, K., Citterio, D., 2008. Inkjet-Printed Microfluidic Multianalyte Chemical Sensing Paper. *Anal. Chem.* 80, 6928–6934. <https://doi.org/10.1021/ac800604v>
- Abu Kwaik, Y., Gao, L.Y., Stone, B.J., Venkataraman, C., Harb, O.S., 1998. Invasion of protozoa by *Legionella pneumophila* and its role in bacterial ecology and pathogenesis. *Appl. Environ. Microbiol.* 64, 3127–3133. <https://doi.org/10.1128/AEM.64.9.3127-3133.1998>
- Adams, R.N., 1958. Carbon Paste Electrodes. *Anal. Chem.* 1.
- Ahlstrom-Munksjö, 2018. LABORATORY FILTRATION CATALOG.
- Akyazi, T., Basabe-Desmots, L., Benito-Lopez, F., 2018. Review on microfluidic paper-based analytical devices towards commercialisation. *Anal. Chim. Acta* 1001, 1–17. <https://doi.org/10.1016/j.aca.2017.11.010>
- Al-Awadi, S., 2013. Food dyes as an alternative tracking dye for DNA gel electrophoresis | Baghdad Science Journal. *Baghdad Sci. J.*
- Allegra, S., Berger, F., Berthelot, P., Grattard, F., Pozzetto, B., Riffard, S., 2008. Use of Flow Cytometry To Monitor *Legionella* Viability. *Appl. Environ. Microbiol.* 74, 7813–7816. <https://doi.org/10.1128/AEM.01364-08>
- Alleron, L., Merlet, N., Lacombe, C., Frère, J., 2008. Long-Term Survival of *Legionella pneumophila* in the Viable But Nonculturable State After Monochloramine Treatment. *Curr. Microbiol.* 57, 497–502. <https://doi.org/10.1007/s00284-008-9275-9>
- Alli, O.A., Gao, L.Y., Pedersen, L.L., Zink, S., Radulic, M., Doric, M., Abu Kwaik, Y., 2000. Temporal pore formation-mediated egress from macrophages and alveolar epithelial cells by *Legionella pneumophila*. *Infect. Immun.* 68, 6431–6440. <https://doi.org/10.1128/IAI.68.11.6431-6440.2000>
- Altman, D.G., 1991. *Practical statistics for medical research* Chapman and Hall. Lond. N. Y.
- Amann, R.I., Zarda, B., Stahl, D.A., Schleifer, K.H., 1992. Identification of individual prokaryotic cells by using enzyme-labeled, rRNA-targeted oligonucleotide probes. *Appl. Environ. Microbiol.* 58, 3007–3011. <https://doi.org/10.1128/aem.58.9.3007-3011.1992>
- Amtsblatt der Europäischen Union, 2020. Richtlinie (EU) 2020/2184 des Europäischen Parlaments und des Rates über die Qualität von Wasser für den menschlichen Gebrauch, 435.
- Araújo, A.C., Song, Y., Lundeberg, J., Ståhl, P.L., Brumer, H., 2012. Activated Paper Surfaces for the Rapid Hybridization of DNA through Capillary Transport. *Anal. Chem.* 84, 3311–3317. <https://doi.org/10.1021/ac300025v>
- Ardalan, S., Hosseinfard, M., Vosough, M., Golmohammadi, H., 2020. Towards smart personalized perspiration analysis: An IoT-integrated cellulose-based microfluidic wearable patch for smartphone fluorimetric multi-sensing of sweat biomarkers. *Biosens. Bioelectron.* 168, 112450. <https://doi.org/10.1016/j.bios.2020.112450>
- Aronsson, T., Gronwall, A., 1957. Improved separation of serum proteins in paper electrophoresis: a new electrophoresis buffer. *Scand. J. Clin. Lab. Invest.* 9, 338–341. <https://doi.org/10.1080/00365515709079983>
- Aurell, H., Catala, P., Farge, P., Wallet, F., Le Brun, M., Helbig, J.H., Jarraud, S., Lebaron, P., 2004. Rapid Detection and Enumeration of *Legionella pneumophila* in Hot Water Systems by Solid-Phase Cytometry. *Appl. Environ. Microbiol.* 70, 1651–1657. <https://doi.org/10.1128/AEM.70.3.1651-1657.2004>
- Bartram, J., Chartier, Y., Lee, J., Bond, K., Lee, S., 2007. *Legionella* and the Prevention of Legionellosis. World Health Organization.
- Bej, A.K., Mahbubani, M.H., Miller, R., DiCesare, J.L., Haff, L., Atlas, R.M., 1990. Multiplex PCR amplification and immobilized capture probes for detection of bacterial pathogens and indicators in water. *Mol. Cell. Probes* 4, 353–365. [https://doi.org/10.1016/0890-8508\(90\)90026-v](https://doi.org/10.1016/0890-8508(90)90026-v)

- Bellinger-Kawahara, C., Horwitz, M.A., 1990. Complement component C3 fixes selectively to the major outer membrane protein (MOMP) of *Legionella pneumophila* and mediates phagocytosis of liposome-MOMP complexes by human monocytes. *J. Exp. Med.* 172, 1201–1210. <https://doi.org/10.1084/jem.172.4.1201>
- Berg, T., Røyset, O., Steinnes, E., 1993. Blank values of trace elements in aerosol filters determined by ICP-MS. *Atmospheric Environ. Part Gen. Top.* 27, 2435–2439. [https://doi.org/10.1016/0960-1686\(93\)90411-Q](https://doi.org/10.1016/0960-1686(93)90411-Q)
- Berlanda, S.F., Breitfeld, M., Dietsche, C.L., Dittrich, P.S., 2021. Recent Advances in Microfluidic Technology for Bioanalysis and Diagnostics. *Anal. Chem.* 93, 311–331. <https://doi.org/10.1021/acs.analchem.0c04366>
- Berney, M., Vital, M., Hülshoff, I., Weilenmann, H.-U., Egli, T., Hammes, F., 2008. Rapid, cultivation-independent assessment of microbial viability in drinking water. *Water Res.* 42, 4010–4018. <https://doi.org/10.1016/j.watres.2008.07.017>
- Bifulco, L., Ingianni, A., Pompei, R., 2013. An Internalin A Probe-Based Genosensor for *Listeria monocytogenes* Detection and Differentiation. *BioMed Res. Int.* 2013, e640163. <https://doi.org/10.1155/2013/640163>
- biomers.net GmbH, 2021. Modification : Fam (6-Isomer) [WWW Document]. URL <https://www.biomers.net/en/Catalog/Modifications/6-Fam/MOD5?lang=en> (accessed 11.10.21).
- Biotium, 2013. Product Information.
- Boese, B.J., Breaker, R.R., 2007. In vitro selection and characterization of cellulose-binding DNA aptamers. *Nucleic Acids Res.* 35, 6378–6388. <https://doi.org/10.1093/nar/gkm708>
- Bosshardt, S.C., Benson, R.F., Fields, B.S., 1997. Flagella are a positive predictor for virulence in *Legionella*. *Microb. Pathog.* 23, 107–112. <https://doi.org/10.1006/mpat.1997.0134>
- Bourne, E.J., Foster, A.B., Grant, P.M., 1956. 831. Ionophoresis of carbohydrates. Part IV. Separations of carbohydrates on fibreglass sheets. *J. Chem. Soc. Resumed* 4311–4314. <https://doi.org/10.1039/jr9560004311>
- Bozue, J.A., Johnson, W., 1996. Interaction of *Legionella pneumophila* with *Acanthamoeba castellanii*: uptake by coiling phagocytosis and inhibition of phagosome-lysosome fusion. *Infect. Immun.* 64, 668–673. <https://doi.org/10.1128/iai.64.2.668-673.1996>
- Bradford, M.M., 1976. A rapid and sensitive method for the quantitation of microgram quantities of protein utilizing the principle of protein-dye binding. *Anal. Biochem.* 72, 248–254. [https://doi.org/10.1016/0003-2697\(76\)90527-3](https://doi.org/10.1016/0003-2697(76)90527-3)
- Brewster, J.D., Paoli, G.C., 2013. DNA extraction protocol for rapid PCR detection of pathogenic bacteria. *Anal. Biochem.* 442, 107–109. <https://doi.org/10.1016/j.ab.2013.07.013>
- Briggs, D.R., Garner, E.F., Smith, F., 1956. Separation of Carbohydrates by Electrophoresis on Glass Filter Paper. *Nature* 178, 154–155. <https://doi.org/10.1038/178154b0>
- Brodhun, B., Buchholz, U., 2020. Entwicklung der Fallzahlen von Legionärskrankheit vor dem Hintergrund der COVID-19-Pandemie, Januar bis Juli 2020. <https://doi.org/10.25646/7195>
- Buchbinder, S., Leitritz, L., Trebesius, K., Banas, B., Heesemann, J., 2004. Mixed lung infection by *Legionella pneumophila* and *Legionella gormanii* detected by fluorescent in situ hybridization. *Infection* 32, 242–245. <https://doi.org/10.1007/s15010-004-2127-z>
- Buchholz, U., Stöcker, P., Brodhun, B., 2010. Legionnaires disease--reordered. *Infect. Control Hosp. Epidemiol.* 31, 104–105. <https://doi.org/10.1086/648664>
- Bundesamt der Justiz, 2001. Trinkwasserverordnung - Verordnung über die Qualität von Wasser für den menschlichen Gebrauch.
- Bundesamt für Justiz, 2000. Gesetz zur Verhütung und Bekämpfung von Infektionskrankheiten beim Menschen (Infektionsschutzgesetz - IfSG).
- Bundesministeriums der Justiz und für Verbraucherschutz, 2017. Zweiundvierzigste Verordnung zur Durchführung des Bundes-Immissionsschutzgesetzes (Verordnung über Verdunstungskühlanlagen, Kühltürme und Nassabscheider - 42. BImSchV).

- Bundesverband der Energie- und Wasserwirtschaft e.V., 2019. Täglicher Trinkwasserverbrauch pro Kopf in Deutschland bis 2019 [WWW Document]. Statista. URL <https://de.statista.com/statistik/daten/studie/12353/umfrage/wasserverbrauch-pro-einwohner-und-tag-seit-1990/> (accessed 7.9.21).
- Cai, L., Xu, C., Lin, S., Luo, J., Wu, M., Yang, F., 2014. A simple paper-based sensor fabricated by selective wet etching of silanized filter paper using a paper mask. *Biomicrofluidics* 8, 056504. <https://doi.org/10.1063/1.4898096>
- Cao, W., Easley, C.J., Ferrance, J.P., Landers, J.P., 2006. Chitosan as a Polymer for pH-Induced DNA Capture in a Totally Aqueous System. *Anal. Chem.* 78, 7222–7228. <https://doi.org/10.1021/ac060391l>
- Carrilho, E., Martinez, A.W., Whitesides, G.M., 2009a. Understanding Wax Printing: A Simple Micropatterning Process for Paper-Based Microfluidics. *Anal. Chem.* 81, 7091–7095. <https://doi.org/10.1021/ac901071p>
- Carrilho, E., Phillips, S.T., Vella, S.J., Martinez, A.W., Whitesides, G.M., 2009b. Paper Microzone Plates. *Anal. Chem.* 81, 5990–5998. <https://doi.org/10.1021/ac900847g>
- Castañó-Álvarez, M., Fernández-Abedul, M.T., Costa-García, A., 2007. Electroactive intercalators for DNA analysis on microchip electrophoresis. *ELECTROPHORESIS* 28, 4679–4689. <https://doi.org/10.1002/elps.200700160>
- Castellan, A., Nourmamode, A., De Violet, Ph.F., Colombo, N., Jaeger, C., 1992. Photoyellowing of Milled Wood Lignin and Peroxide-Bleached Milled Wood Lignin in Solid 2-Hydroxypropylcellulose Films After Sodium Borohydride Reduction and Catalytic Hydrogenation in Solution: an Uv/Vis Absorption Spectroscopic Study. *J. Wood Chem. Technol.* 12, 1–18. <https://doi.org/10.1080/02773819208545047>
- Čermák, V., 2021. RESTRICTION ANALYZER [WWW Document]. URL <https://www.molbiotools.com/restrictionanalyzer.php> (accessed 11.12.21).
- Chang, R., 1991. *Chemistry*. McGraw-Hill, Inc., New York, p. pp.801-804.
- Charcosset, C., 2015. Electrophoretic Mobility, in: Drioli, E., Giorno, L. (Eds.), *Encyclopedia of Membranes*. Springer, Berlin, Heidelberg, pp. 1–2. https://doi.org/10.1007/978-3-642-40872-4_208-2
- Chen, L., E. Prest, J., R. Fielden, P., J. Goddard, N., Manz, A., R. Day, P.J., 2006. Miniaturised isotachopheresis analysis. *Lab. Chip* 6, 474–487. <https://doi.org/10.1039/B515551G>
- Chien, M., Morozova, I., Shi, S., Sheng, H., Chen, J., Gomez, S.M., Asamani, G., Hill, K., Nuara, J., Feder, M., Rineer, J., Greenberg, J.J., Steshenko, V., Park, S.H., Zhao, B., Teplitskaya, E., Edwards, J.R., Pampou, S., Georghiou, A., Chou, I.-C., Iannuccilli, W., Ulz, M.E., Kim, D.H., Geringer-Sameth, A., Goldsberry, C., Morozov, P., Fischer, S.G., Segal, G., Qu, X., Rzhetsky, A., Zhang, P., Cayanis, E., De Jong, P.J., Ju, J., Kalachikov, S., Shuman, H.A., Russo, J.J., 2004. The genomic sequence of the accidental pathogen *Legionella pneumophila*. *Science* 305, 1966–1968. <https://doi.org/10.1126/science.1099776>
- Chiu, D.T., deMello, A.J., Di Carlo, D., Doyle, P.S., Hansen, C., Maceiczky, R.M., Wootton, R.C.R., 2017. Small but Perfectly Formed? Successes, Challenges, and Opportunities for Microfluidics in the Chemical and Biological Sciences. *Chem* 2, 201–223. <https://doi.org/10.1016/j.chempr.2017.01.009>
- Choopara, I., Suea-Ngam, A., Teethaisong, Y., Howes, P.D., Schmelcher, M., Leelahavanichkul, A., Thunyaharn, S., Wongsawaeng, D., deMello, A.J., Dean, D., Somboonna, N., 2021. Fluorometric Paper-Based, Loop-Mediated Isothermal Amplification Devices for Quantitative Point-of-Care Detection of Methicillin-Resistant *Staphylococcus aureus* (MRSA). *ACS Sens.* 6, 742–751. <https://doi.org/10.1021/acssensors.0c01405>
- Cianciotto, N.P., 2007. Iron acquisition by *Legionella pneumophila*. *Biometals Int. J. Role Met. Ions Biol. Biochem. Med.* 20, 323–331. <https://doi.org/10.1007/s10534-006-9057-4>
- Cloud, J.L., Carroll, K.C., Pixton, P., Erali, M., Hillyard, D.R., 2000. Detection of *Legionella* species in respiratory specimens using PCR with sequencing confirmation. *J. Clin. Microbiol.* 38, 1709–1712. <https://doi.org/10.1128/JCM.38.5.1709-1712.2000>

- Collier, S.A., Deng, L., Adam, E.A., Benedict, K.M., Beshearse, E.M., Blackstock, A.J., Bruce, B.B., Derado, G., Edens, C., Fullerton, K.E., Gargano, J.W., Geissler, A.L., Hall, A.J., Havelaar, A.H., Hill, V.R., Hoekstra, R.M., Reddy, S.C., Scallan, E., Stokes, E.K., Yoder, J.S., Beach, M.J., 2021. Estimate of Burden and Direct Healthcare Cost of Infectious Waterborne Disease in the United States. *Emerg. Infect. Dis.* 27, 140–149. <https://doi.org/10.3201/eid2701.190676>
- Colozza, N., Kehe, K., Dionisi, G., Popp, T., Tsoutsoulopoulos, A., Steinritz, D., Moscone, D., Arduini, F., 2019. A wearable origami-like paper-based electrochemical biosensor for sulfur mustard detection. *Biosens. Bioelectron.* 129, 15–23. <https://doi.org/10.1016/j.bios.2019.01.002>
- Convery, N., Gadegaard, N., 2019. 30 years of microfluidics. *Micro Nano Eng.* 2, 76–91. <https://doi.org/10.1016/j.mne.2019.01.003>
- Correia, A.M., Ferreira, J.S., Borges, V., Nunes, A., Gomes, B., Capucho, R., Gonçalves, J., Antunes, D.M., Almeida, S., Mendes, A., Guerreiro, M., Sampaio, D.A., Vieira, L., Machado, J., Simões, M.J., Gonçalves, P., Gomes, J.P., 2016. Probable Person-to-Person Transmission of Legionnaires' Disease. *N. Engl. J. Med.* 374, 497–498. <https://doi.org/10.1056/NEJMc1505356>
- Crump, P.W., Fielden, E.M., Jenner, T.J., O'neill, P., 1990. A comparison of the techniques of alkaline filter elution and alkaline sucrose sedimentation used to assess DNA damage induced by 2-nitroimidazoles. *Biochem. Pharmacol.* 40, 621–627. [https://doi.org/10.1016/0006-2952\(90\)90565-3](https://doi.org/10.1016/0006-2952(90)90565-3)
- Cunha, B.A., Burillo, A., Bouza, E., 2016. Legionnaires' disease. *The Lancet* 387, 376–385. [https://doi.org/10.1016/S0140-6736\(15\)60078-2](https://doi.org/10.1016/S0140-6736(15)60078-2)
- Curto, V.F., Lopez-Ruiz, N., Capitan-Vallvey, L.F., Palma, A.J., Benito-Lopez, F., Diamond, D., 2013. Fast prototyping of paper-based microfluidic devices by contact stamping using indelible ink. *RSC Adv.* 3, 18811–18816. <https://doi.org/10.1039/C3RA43825B>
- Danielson, T.L., Rayson, G.D., Anderson, D.M., Estell, R., Fredrickson, E.L., Green, B.S., 2003. Impact of filter paper on fluorescence measurements of buffered saline filtrates. *Talanta* 59, 601–604. [https://doi.org/10.1016/S0039-9140\(02\)00575-1](https://doi.org/10.1016/S0039-9140(02)00575-1)
- Davey, H.M., 2011. Life, Death, and In-Between: Meanings and Methods in Microbiology ∇. *Appl. Environ. Microbiol.* 77, 5571–5576. <https://doi.org/10.1128/AEM.00744-11>
- Davis, M., 2014. Excimer-Monomer Switching Molecular Beacon: The Study on Synthetic Cryptosporidium DNA Detection, Thermodynamics, and Magnesium Effects. *Grad. Theses Diss.* <https://doi.org/10.26076/2b52-74d3>
- de Gennes, P.G., 1971. Reptation of a Polymer Chain in the Presence of Fixed Obstacles. *J. Chem. Phys.* 55, 572–579. <https://doi.org/10.1063/1.1675789>
- Declerck, P., 2010. Biofilms: the environmental playground of Legionella pneumophila. *Environ. Microbiol.* 12, 557–566. <https://doi.org/10.1111/j.1462-2920.2009.02025.x>
- Deka, A., Chougule, B.S., Parveen, A., Lahan, J.P., Barooah, M., Boro, R.C., 2015. Natural pigment betacyanin as tracking dye for gel electrophoresis. *Indian J. Nat. Prod. Resour. IJNPR Former. Nat. Prod. Radiance NPR* 6, 23–26.
- Deloge-Abarkan, M., Ha, T.-L., Robine, E., Zmirou-Navier, D., Mathieu, L., 2007. Detection of airborne Legionella while showering using liquid impingement and fluorescent in situ hybridization (FISH). *J. Environ. Monit.* 9, 91–97. <https://doi.org/10.1039/B610737K>
- deMello, A.J., 2006. Control and detection of chemical reactions in microfluidic systems. *Nature* 442, 394–402. <https://doi.org/10.1038/nature05062>
- Deutscher Verein des Gas- und Wasserfaches e.V., 2015. Arbeitsblatt W 556 Wasser Hygienisch-mikrobielle Auffälligkeiten in Trinkwasser-Installationen; Methodik und Maßnahmen zu deren Behebung.
- Deutscher Verein des Gas- und Wasserfaches e.V., 2009. twin Nr. 05 - Informationen des DVGW zur Trinkwasser-Installation. Desinfektion von Trinkwasser-Installationen zur Beseitigung mikrobieller Kontaminationen.
- Dietersdorfer, E., Kirschner, A., Schrammel, B., Ohradanova-Repic, A., Stockinger, H., Sommer, R., Walochnik, J., Cervero-Aragó, S., 2018. Starved viable but non-culturable (VBNC) Legionella

- strains can infect and replicate in amoebae and human macrophages. *Water Res.* 141, 428–438. <https://doi.org/10.1016/j.watres.2018.01.058>
- Ditommaso, S., Ricciardi, E., Giacomuzzi, M., Arauco Rivera, S.R., Zotti, C.M., 2015. Legionella in water samples: How can you interpret the results obtained by quantitative PCR? *Mol. Cell. Probes* 29, 7–12. <https://doi.org/10.1016/j.mcp.2014.09.002>
- Dubitsky, A., Perreault, S., 1995. A model for binding of DNA and proteins to transfer membranes. Pall Corp. Tech Note.
- Dungchai, W., Chailapakul, O., Henry, C.S., 2010. Use of multiple colorimetric indicators for paper-based microfluidic devices. *Anal. Chim. Acta* 674, 227–233. <https://doi.org/10.1016/j.aca.2010.06.019>
- Dungchai, W., Chailapakul, O., Henry, C.S., 2009. Electrochemical Detection for Paper-Based Microfluidics. *Anal. Chem.* 81, 5821–5826. <https://doi.org/10.1021/ac9007573>
- Dunsch, L., 1988. Vom Ion zur Elektrode: Eine moderne Einführung in die Grundlagen der Elektrochemie, 2nd ed. Dt. Verlag für Grundstoffindustrie, Leipzig.
- Dwight, Z., Wittwer, C., 2016. Interpreting melt curves : An indicator , not a diagnosis.
- Edelstein, P.H., 2007. Urine antigen tests positive for Pontiac fever: implications for diagnosis and pathogenesis. *Clin. Infect. Dis. Off. Publ. Infect. Dis. Soc. Am.* 44, 229–231. <https://doi.org/10.1086/510394>
- England, A.C., Fraser, D.W., Mallison, G.F., Mackel, D.C., Skaliy, P., Gorman, G.W., 1982. Failure of Legionella pneumophila sensitivities to predict culture results from disinfectant-treated air-conditioning cooling towers. *Appl. Environ. Microbiol.* 43, 240–244. <https://doi.org/10.1128/aem.43.1.240-244.1982>
- Every, A.E., Russu, I.M., 2008. Influence of Magnesium Ions on Spontaneous Opening of DNA Base Pairs. *J. Phys. Chem. B* 112, 7689–7695. <https://doi.org/10.1021/jp8005876>
- Formica, N., Yates, M., Beers, M., Carnie, J., Hogg, G., Ryan, N., Tallis, G., 2001. The impact of diagnosis by legionella urinary antigen test on the epidemiology and outcomes of Legionnaires' disease. *Epidemiol. Infect.* 127, 275–280. <https://doi.org/10.1017/S0950268801005672>
- Foster, A.B., 1957. Zone Electrophoresis of Carbohydrates, in: *Advances in Carbohydrate Chemistry*. Elsevier, pp. 81–115. [https://doi.org/10.1016/S0096-5332\(08\)60205-2](https://doi.org/10.1016/S0096-5332(08)60205-2)
- Franco, I.S., Shuman, H.A., Charpentier, X., 2009. The perplexing functions and surprising origins of Legionella pneumophila type IV secretion effectors. *Cell. Microbiol.* 11, 1435–1443. <https://doi.org/10.1111/j.1462-5822.2009.01351.x>
- Fraser, D.W., Tsai, T.R., Orenstein, W., Parkin, W.E., Beecham, H.J., Sharrar, R.G., Harris, J., Mallison, G.F., Martin, S.M., McDade, J.E., Shepard, C.C., Brachman, P.S., 1977. Legionnaires' Disease. *N. Engl. J. Med.* 297, 1189–1197. <https://doi.org/10.1056/NEJM197712012972201>
- Frickmann, H., Zautner, A.E., Moter, A., Kikhney, J., Hagen, R.M., Stender, H., Poppert, S., 2017. Fluorescence in situ hybridization (FISH) in the microbiological diagnostic routine laboratory: a review. *Crit. Rev. Microbiol.* 43, 263–293. <https://doi.org/10.3109/1040841X.2016.1169990>
- Füchslin, H.P., Kötzsch, S., Keserue, H.-A., Egli, T., 2010. Rapid and quantitative detection of Legionella pneumophila applying immunomagnetic separation and flow cytometry. *Cytom. Part J. Int. Soc. Anal. Cytol.* 77, 264–274. <https://doi.org/10.1002/cyto.a.20858>
- Fujita, K., Nagatsu, T., Shinpo, K., Maruta, K., Teradaira, R., Nakamura, M., 1980. Improved analysis for urinary polyamines by use of high-voltage electrophoresis on paper. *Clin. Chem.* 26, 1577–1582. <https://doi.org/10.1093/clinchem/26.11.1577>
- Gagliardi, A.C.M., Miname, M.H., Santos, R.D., 2009. Uric acid: A marker of increased cardiovascular risk. *Atherosclerosis* 202, 11–17. <https://doi.org/10.1016/j.atherosclerosis.2008.05.022>
- Gao, B., Elbaz, A., He, Z., Xie, Z., Xu, H., Liu, S., Su, E., Liu, H., Gu, Z., 2018. Bioinspired Kirigami Fish-Based Highly Stretched Wearable Biosensor for Human Biochemical–Physiological Hybrid Monitoring. *Adv. Mater. Technol.* 3, 1700308. <https://doi.org/10.1002/admt.201700308>

- García-González, R., Costa-García, A., Fernández-Abedul, M.T., 2014. Methylene blue covalently attached to single stranded DNA as electroactive label for potential bioassays. *Sens. Actuators B Chem.* 191, 784–790. <https://doi.org/10.1016/j.snb.2013.10.037>
- Garduño, R.A., Garduño, E., Hoffman, P.S., 1998. Surface-associated hsp60 chaperonin of *Legionella pneumophila* mediates invasion in a HeLa cell model. *Infect. Immun.* 66, 4602–4610. <https://doi.org/10.1128/IAI.66.10.4602-4610.1998>
- Ge, L., Wang, S., Ge, S., Yu, J., Yan, M., Li, N., Huang, J., 2014. Electrophoretic separation in a microfluidic paper-based analytical device with an on-column wireless electrogenerated chemiluminescence detector. *Chem. Commun.* 50, 5699–5702. <https://doi.org/10.1039/C3CC49770D>
- Ge, L., Wang, S., Song, X., Ge, S., Yu, J., 2012. 3D Origami-based multifunction-integrated immunodevice: low-cost and multiplexed sandwich chemiluminescence immunoassay on microfluidic paper-based analytical device. *Lab. Chip* 12, 3150. <https://doi.org/10.1039/c2lc40325k>
- Ge, S., Ge, L., Yan, M., Song, X., Yu, J., Huang, J., 2012. A disposable paper-based electrochemical sensor with an addressable electrode array for cancer screening. *Chem. Commun.* 48, 9397–9399. <https://doi.org/10.1039/C2CC34887J>
- Gomez-Valero, L., Rusniok, C., Carson, D., Mondino, S., Pérez-Cobas, A.E., Rolando, M., Pasricha, S., Reuter, S., Demirtas, J., Crumbach, J., Descorps-Declere, S., Hartland, E.L., Jarraud, S., Dougan, G., Schroeder, G.N., Frankel, G., Buchrieser, C., 2019. More than 18,000 effectors in the *Legionella* genus genome provide multiple, independent combinations for replication in human cells. *Proc. Natl. Acad. Sci.* 116, 2265–2273.
- Grimm, D., Merkert, H., Ludwig, W., Schleifer, K.-H., Hacker, J., Brand, B.C., 1998. Specific Detection of *Legionella pneumophila*: Construction of a New 16S rRNA-Targeted Oligonucleotide Probe. *Appl. Environ. Microbiol.* 64, 2686–2690. <https://doi.org/10.1128/AEM.64.7.2686-2690.1998>
- Güder, F., Ainla, A., Redston, J., Mosadegh, B., Glavan, A., Martin, T.J., Whitesides, G.M., 2016. Paper-Based Electrical Respiration Sensor. *Angew. Chem. Int. Ed.* 55, 5727–5732. <https://doi.org/10.1002/anie.201511805>
- Gueye, M.N., Carella, A., Faure-Vincent, J., Demadrille, R., Simonato, J.-P., 2020. Progress in understanding structure and transport properties of PEDOT-based materials: A critical review. *Prog. Mater. Sci.* 108, 100616. <https://doi.org/10.1016/j.pmatsci.2019.100616>
- Harb, O.S., Gao, L.-Y., Kwaik, Y.A., 2000. From protozoa to mammalian cells: a new paradigm in the life cycle of intracellular bacterial pathogens. *Environ. Microbiol.* 2, 251–265. <https://doi.org/10.1046/j.1462-2920.2000.00112.x>
- Heinsohn, N.K., Niedl, R.R., Anielski, A., Lisdat, F., Beta, C., 2022. Electrophoretic μ PAD for Purification and Analysis of DNA Samples. *Biosensors* 12, 62. <https://doi.org/10.3390/bios12020062>
- Heller, C., Duke, T., Viovy, J.L., 1994. Electrophoretic mobility of DNA in gels. II. Systematic experimental study in agarose gels. *Biopolymers* 34, 249–259. <https://doi.org/10.1002/bip.360340211>
- Heuner, K., Steinert, M., 2003. The flagellum of *Legionella pneumophila* and its link to the expression of the virulent phenotype. *Int. J. Med. Microbiol.* 293, 133–143. <https://doi.org/10.1078/1438-4221-00259>
- Hilbi, H., Segal, G., Shuman, H.A., 2008. Icm/Dot-dependent upregulation of phagocytosis by *Legionella pneumophila*: *Legionella pneumophila*-upregulated phagocytosis. *Mol. Microbiol.* 42, 603–617. <https://doi.org/10.1046/j.1365-2958.2001.02645.x>
- Hillscher, L.M., Liebich, V.J., Avrutina, O., Biesalski, M., Kolmar, H., 2021. Functional paper-based materials for diagnostics. *ChemTexts* 7, 14. <https://doi.org/10.1007/s40828-021-00139-w>
- Hinlo, R., Gleeson, D., Lintermans, M., Furlan, E., 2017. Methods to maximise recovery of environmental DNA from water samples. *PLOS ONE* 12, e0179251. <https://doi.org/10.1371/journal.pone.0179251>

- Hoang, T.X., Phan, L.M.T., Vo, T.A.T., Cho, S., 2021. Advanced Signal-Amplification Strategies for Paper-Based Analytical Devices: A Comprehensive Review. *Biomedicines* 9, 540. <https://doi.org/10.3390/biomedicines9050540>
- Hoffman, P.S., Garduno, R.A., 1999. Surface-associated heat shock proteins of *Legionella pneumophila* and *Helicobacter pylori*: roles in pathogenesis and immunity. *Infect. Dis. Obstet. Gynecol.* 7, 58–63. <https://doi.org/10.1155/S1064744999000125>
- Hooyberghs, J., Van Hummelen, P., Carlon, E., 2009. The effects of mismatches on hybridization in DNA microarrays: determination of nearest neighbor parameters. *Nucleic Acids Res.* 37, e53. <https://doi.org/10.1093/nar/gkp109>
- Horwitz, M.A., 1988. Phagocytosis and Intracellular Biology of *Legionella Pneumophila*, in: Cabello, F.C., Pruzzo, C. (Eds.), *Bacteria, Complement and the Phagocytic Cell*, NATO ASI Series. Springer, Berlin, Heidelberg, pp. 231–237. https://doi.org/10.1007/978-3-642-85718-8_18
- Hosoney, R.C., 1984. Chemical changes in carbohydrates produced by thermal processing. *J. Chem. Educ.* 61, 308. <https://doi.org/10.1021/ed061p308>
- Hossain, S.M.Z., Brennan, J.D., 2011. β -Galactosidase-Based Colorimetric Paper Sensor for Determination of Heavy Metals. *Anal. Chem.* 83, 8772–8778. <https://doi.org/10.1021/ac202290d>
- Hu, Z., Tong, C., 2007. Synchronous fluorescence determination of DNA based on the interaction between methylene blue and DNA. *Anal. Chim. Acta* 587, 187–193. <https://doi.org/10.1016/j.aca.2007.01.050>
- Huber, D., Voith von Voithenberg, L., Kaigala, G.V., 2018. Fluorescence in situ hybridization (FISH): History, limitations and what to expect from micro-scale FISH? *Micro Nano Eng.* 1, 15–24. <https://doi.org/10.1016/j.mne.2018.10.006>
- Hussong, D., Colwell, R.R., O'Brien, M., Weiss, E., Pearson, A.D., Weiner, R.M., Burge, W.D., 1987. Viable *Legionella pneumophila* Not Detectable by Culture on Agar Media. *Bio/Technology* 5, 947–950. <https://doi.org/10.1038/nbt0987-947>
- Hwang, M.G., Katayama, H., Ohgaki, S., 2006. Effect of intracellular resuscitation of *Legionella pneumophila* in *Acanthamoeba polyphage* cells on the antimicrobial properties of silver and copper. *Environ. Sci. Technol.* 40, 7434–7439. <https://doi.org/10.1021/es060412t>
- Integrated DNA Technologies, 2022. Frequently asked questions [WWW Document]. *Integr. DNA Technol.* URL <https://eu.idtdna.com/pages/support/faqs/why-is-my-fam-labeled-oligo-not-as-bright-as-it-was-6-months-ago-> (accessed 2.12.22).
- ISO 11731:2017 Water quality - Enumeration of *Legionella*, 2017.
- Jankowski, S., 2013. Trinkwasser [WWW Document]. Umweltbundesamt. URL <https://www.umweltbundesamt.de/themen/wasser/trinkwasser> (accessed 7.9.21).
- Jepras, R.I., Carter, J., Pearson, S.C., Paul, F.E., Wilkinson, M.J., 1995. Development of a Robust Flow Cytometric Assay for Determining Numbers of Viable Bacteria. *Appl. Environ. Microbiol.* 61, 2696–2701.
- John, H.A., Birnstiel, M.L., Jones, K.W., 1969. RNA-DNA Hybrids at the Cytological Level. *Nature* 223, 582–587. <https://doi.org/10.1038/223582a0>
- Johnson, R.J., Kang, D.-H., Feig, D., Kivlighn, S., Kanellis, J., Watanabe, S., Tuttle, K.R., Rodriguez-Iturbe, B., Herrera-Acosta, J., Mazzali, M., 2003. Is There a Pathogenetic Role for Uric Acid in Hypertension and Cardiovascular and Renal Disease? *Hypertension* 41, 1183–1190. <https://doi.org/10.1161/01.HYP.0000069700.62727.C5>
- Jokerst, J.C., Adkins, J.A., Bisha, B., Mentele, M.M., Goodridge, L.D., Henry, C.S., 2012. Development of a Paper-Based Analytical Device for Colorimetric Detection of Select Foodborne Pathogens. *Anal. Chem.* 84, 2900–2907. <https://doi.org/10.1021/ac203466y>
- Joly, P., Falconnet, P.-A., André, J., Weill, N., Reyrolle, M., Vandenesch, F., Maurin, M., Etienne, J., Jarraud, S., 2006. Quantitative Real-Time *Legionella* PCR for Environmental Water Samples: Data Interpretation. *Appl. Environ. Microbiol.* 72, 2801–2808. <https://doi.org/10.1128/AEM.72.4.2801-2808.2006>

- Kaarj, K., Akarapipad, P., Yoon, J.-Y., 2018. Simpler, Faster, and Sensitive Zika Virus Assay Using Smartphone Detection of Loop-mediated Isothermal Amplification on Paper Microfluidic Chips. *Sci. Rep.* 8, 12438. <https://doi.org/10.1038/s41598-018-30797-9>
- Kalcher, K., Kauffmann, J.-M., Wang, J., Švancara, I., Vytrás, K., Neuhold, C., Yang, Z., 1995. Sensors based on carbon paste in electrochemical analysis: A review with particular emphasis on the period 1990–1993. *Electroanalysis* 7, 5–22. <https://doi.org/10.1002/elan.1140070103>
- Kao, P.-K., Hsu, C.-C., 2014. One-step rapid fabrication of paper-based microfluidic devices using fluorocarbon plasma polymerization. *Microfluid. Nanofluidics* 16, 811–818. <https://doi.org/10.1007/s10404-014-1347-5>
- Katz, S.M., Hashemi, S., Brown, K.R., Habib, W.A., Hammel, J.M., 1984. Pleomorphism of *Legionella Pneumophila*. *Ultrastruct. Pathol.* 6, 117–129. <https://doi.org/10.3109/01913128409018566>
- Kersting, S., Rausch, V., Bier, F.F., von Nickisch-Rosenegk, M., 2018. A recombinase polymerase amplification assay for the diagnosis of atypical pneumonia. *Anal. Biochem.* 550, 54–60. <https://doi.org/10.1016/j.ab.2018.04.014>
- Kim, T., Park, S., Seo, J., Lee, C., Kim, J.M., 2019. Highly conductive PEDOT:PSS with enhanced chemical stability. *Org. Electron.* 74. <https://doi.org/10.1016/j.orgel.2019.06.033>
- Kirkwood, B.R., Sterne, J.A.C., 2010. *Essential Medical Statistics*. John Wiley & Sons.
- Kirschner, A. k. t., Rameder, A., Schrammel, B., Indra, A., Farnleitner, A. h., Sommer, R., 2012. Development of a new CARD-FISH protocol for quantification of *Legionella pneumophila* and its application in two hospital cooling towers. *J. Appl. Microbiol.* 112, 1244–1256. <https://doi.org/10.1111/j.1365-2672.2012.05289.x>
- Knirel, Y.A., Rietschel, E.T., Marre, R., Zähringer, U., 1994. The structure of the O-specific chain of *Legionella pneumophila* serogroup 1 lipopolysaccharide. *Eur. J. Biochem.* 221, 239–245. <https://doi.org/10.1111/j.1432-1033.1994.tb18734.x>
- Lederer, M., 1955. *An introduction to paper electrophoresis and related methods*. Elsevier Pub. Co., Amsterdam; Houston.
- Lee, J. v., Lai, S., Exner, M., Lenz, J., Gaia, V., Casati, S., Hartemann, P., Lück, C., Pangon, B., Ricci, M. I., Scaturro, M., Fontana, S., Sabria, M., Sánchez, I., Assaf, S., Surman-Lee, S., 2011. An international trial of quantitative PCR for monitoring *Legionella* in artificial water systems. *J. Appl. Microbiol.* 110, 1032–1044. <https://doi.org/10.1111/j.1365-2672.2011.04957.x>
- Lenaerts, J., Lappin-Scott, H.M., Porter, J., 2007. Improved Fluorescent In Situ Hybridization Method for Detection of Bacteria from Activated Sludge and River Water by Using DNA Molecular Beacons and Flow Cytometry. *Appl. Environ. Microbiol.* 73, 2020–2023. <https://doi.org/10.1128/AEM.01718-06>
- Lewis, B.A., Smith, F., 1957. THE HETEROGENEITY OF POLYSACCHARIDES AS REVEALED BY ELECTROPHORESIS ON GLASS-FIBER PAPER. *J. Am. Chem. Soc.* 79, 3929–3931. <https://doi.org/10.1021/ja01571a091>
- Li, J.J., Chu, Y., Lee, B.Y.-H., Xie, X.S., 2008. Enzymatic signal amplification of molecular beacons for sensitive DNA detection. *Nucleic Acids Res.* 36, e36. <https://doi.org/10.1093/nar/gkn033>
- Li, L., Faucher, S.P., 2016. The Membrane Protein LasM Promotes the Culturability of *Legionella pneumophila* in Water. *Front. Cell. Infect. Microbiol.* 6, 113. <https://doi.org/10.3389/fcimb.2016.00113>
- Li, T.X., 2001. *Modern clinical immunoassay*. Military Medical Science Press 178–209.
- Li, X., Luo, L., Crooks, R.M., 2015. Low-voltage paper isotachopheresis device for DNA focusing. *Lab. Chip* 15, 4090–4098. <https://doi.org/10.1039/C5LC00875A>
- Li, Xu, Tian, J., Garnier, G., Shen, W., 2010a. Fabrication of paper-based microfluidic sensors by printing. *Colloids Surf. B Biointerfaces* 76, 564–570. <https://doi.org/10.1016/j.colsurfb.2009.12.023>
- Li, Xu, Tian, J., Garnier, G., Shen, W., 2010b. Fabrication of paper-based microfluidic sensors by printing. *Colloids Surf. B Biointerfaces* 76, 564–570. <https://doi.org/10.1016/j.colsurfb.2009.12.023>

- Li, X., Tian, J., Nguyen, T., Shen, W., 2008. Paper-Based Microfluidic Devices by Plasma Treatment. *Anal. Chem.* 80, 9131–9134. <https://doi.org/10.1021/ac801729t>
- Li, Xiang-hui, Yonglun, Z., Gao, Y., Zheng, X., Zhang, Q., Zhou, S.-N., Lu, Y., 2010. The ClpP protease homologue is required for the transmission traits and cell division of the pathogen *Legionella pneumophila*. *BMC Microbiol.* 10, 54. <https://doi.org/10.1186/1471-2180-10-54>
- Li, Z., Bai, Y., You, M., Hu, J., Yao, C., Cao, L., Xu, F., 2021. Fully integrated microfluidic devices for qualitative, quantitative and digital nucleic acids testing at point of care. *Biosens. Bioelectron.* 177, 112952. <https://doi.org/10.1016/j.bios.2020.112952>
- Liang, L., Su, M., Li, L., Lan, F., Yang, G., Ge, S., Yu, J., Song, X., 2016. Aptamer-based fluorescent and visual biosensor for multiplexed monitoring of cancer cells in microfluidic paper-based analytical devices. *Sens. Actuators B Chem.* 229, 347–354. <https://doi.org/10.1016/j.snb.2016.01.137>
- Liang, Z., Keeley, A., 2013. Filtration Recovery of Extracellular DNA from Environmental Water Samples. *Environ. Sci. Technol.* 47, 9324–9331. <https://doi.org/10.1021/es401342b>
- Lindquist, Jorgen., 1973. Carbon paste electrode with a wide anodic potential range. *Anal. Chem.* 45, 1006–1008. <https://doi.org/10.1021/ac60328a019>
- Lisby, G., Dessau, R., 1994. Construction of a DNA amplification assay for detection of *Legionella* species in clinical samples. *Eur. J. Clin. Microbiol. Infect. Dis. Off. Publ. Eur. Soc. Clin. Microbiol.* 13, 225–231. <https://doi.org/10.1007/BF01974541>
- Liu, H., Crooks, R.M., 2011. Three-Dimensional Paper Microfluidic Devices Assembled Using the Principles of Origami. *J. Am. Chem. Soc.* 133, 17564–17566. <https://doi.org/10.1021/ja2071779>
- Liubys, O.O., Vlasiuk, A.V., Perepelytsya, S.M., 2015. Structuring of counterions around dna double helix: a molecular dynamics study. *ArXiv150305334 Q-Bio*.
- Lu, Y., Shi, W., Qin, J., Lin, B., 2010. Fabrication and Characterization of Paper-Based Microfluidics Prepared in Nitrocellulose Membrane By Wax Printing. *Anal. Chem.* 82, 329–335. <https://doi.org/10.1021/ac9020193>
- Lück, P.C., Helbig, J.H., Schuppler, M., 2002. Epidemiology and Laboratory Diagnosis of *Legionella* Infections/Epidemiologie und Labordiagnose von *Legionella*-Infektionen. *LaboratoriumsMedizin* 26, 174–182. <https://doi.org/10.1515/LabMed.2002.023>
- Lück, P.C., Steinert, M., 2006. Pathogenese, Diagnostik und Therapie der *Legionella*-Infektion. *Bundesgesundheitsblatt - Gesundheitsforschung - Gesundheitsschutz* 49, 439–449. <https://doi.org/10.1007/s00103-006-1254-3>
- Lüneberg, E., Zähringer, U., Knirel, Y.A., Steinmann, D., Hartmann, M., Steinmetz, I., Rohde, M., Köhl, J., Frosch, M., 1998. Phase-variable Expression of Lipopolysaccharide Contributes to the Virulence of *Legionella pneumophila*. *J. Exp. Med.* 188, 49–60. <https://doi.org/10.1084/jem.188.1.49>
- Luo, L., Li, X., Crooks, R.M., 2014. Low-Voltage Origami-Paper-Based Electrophoretic Device for Rapid Protein Separation. *Anal. Chem.* 86, 12390–12397. <https://doi.org/10.1021/ac503976c>
- Luo, W., Zhou, D., Luo, D., Jiang, J., Xu, X., 2015. Melting temperature of molecular beacons as an indicator of the ligase detection reaction for multiplex detection of point mutations. *Anal. Methods* 7, 4225–4230. <https://doi.org/10.1039/C5AY00475F>
- Macherey-Nagel, 2008. PCR Clean-up User Manual NucleoSpin® 8 Extract II.
- Macherey-Nagel GmbH & Co.KG., 2019. Data sheet Filter paper MN640 w.
- Maejima, K., Tomikawa, S., Suzuki, K., Citterio, D., 2013. Inkjet printing: an integrated and green chemical approach to microfluidic paper-based analytical devices. *RSC Adv.* 3, 9258–9263. <https://doi.org/10.1039/C3RA40828K>
- Magro, L., Escadafal, C., Garneret, P., Jacquelin, B., Kwasiborski, A., Manuguerra, J.-C., Monti, F., Sakuntabhai, A., Vanhomwegen, J., Lafaye, P., Tabeling, P., 2017. Paper microfluidics for nucleic acid amplification testing (NAAT) of infectious diseases. *Lab. Chip* 17, 2347–2371. <https://doi.org/10.1039/c7lc00013h>

- Mahbubani, M.H., Bej, A.K., Miller, R., Haff, L., DiCesare, J., Atlas, R.M., 1990. Detection of Legionella with polymerase chain reaction and gene probe methods. *Mol. Cell. Probes* 4, 175–187. [https://doi.org/10.1016/0890-8508\(90\)90051-z](https://doi.org/10.1016/0890-8508(90)90051-z)
- Manz, W., Amann, R., Szewzyk, R., Szewzyk, U., Stenstrom, T.-A., Hutzler, P., Schleifer, K.-H., 1995. In situ identification of Legionellaceae using 16S rRNA-targeted oligonucleotide probes and confocal laser scanning microscopy. *Microbiology* 141, 29–39. <https://doi.org/10.1099/00221287-141-1-29>
- Markham, N.R., Zuker, L.S., Zuker, M., 2021. The UNAFold Web Server. <http://www.unafold.org/>.
- Martin, R., 1996. Elektrophorese von Nucleinsäuren. Spektrum Akad. Verlag, Heidelberg.
- Martinez, A. W., Phillips, S.T., Butte, M. J., Whitesides, G.M., 2007. Patterned Paper as a Platform for Inexpensive, Low-Volume, Portable Bioassays. *Angew. Chem. Int. Ed.* 46, 1318–1320. <https://doi.org/10.1002/anie.200603817>
- Martinez, A.W., Phillips, S.T., Carrilho, E., Thomas, S.W., Sindi, H., Whitesides, G.M., 2008a. Simple Telemedicine for Developing Regions: Camera Phones and Paper-Based Microfluidic Devices for Real-Time, Off-Site Diagnosis. *Anal. Chem.* 80, 3699–3707. <https://doi.org/10.1021/ac800112r>
- Martinez, A.W., Phillips, S.T., Whitesides, G.M., 2008b. Three-dimensional microfluidic devices fabricated in layered paper and tape. *Proc. Natl. Acad. Sci.* 105, 19606–19611. <https://doi.org/10.1073/pnas.0810903105>
- Martinez, A.W., Phillips, S.T., Wiley, B.J., Gupta, M., Whitesides, G.M., 2008c. FLASH: A rapid method for prototyping paper-based microfluidic devices. *Lab. Chip* 8, 2146–2150. <https://doi.org/10.1039/B811135A>
- Matsiota-Bernard, P., Pitsouni, E., Legakis, N., Nauciel, C., 1994. Evaluation of commercial amplification kit for detection of Legionella pneumophila in clinical specimens. *J. Clin. Microbiol.* 32, 1503–1505.
- Maupin, P.H., 1993. One-step test for aspartate aminotransferase. EP0523227A4.
- McCreery, R.L., Cline, K.K., 1996. Laboratory Techniques in Electroanalytical Chemistry, Kissinger, P. T., Heineman, W. R. (Eds.), 293–332.
- McDade, J.E., Shepard, C.C., Fraser, D.W., Tsai, T.R., Redus, M.A., Dowdle, W.R., 1977. Legionnaires' Disease. *N. Engl. J. Med.* 297, 1197–1203. <https://doi.org/10.1056/NEJM197712012972202>
- McDonald, H.J., 1955. Ionography, *Electrophoresis in Stabilized Media*, 1. Aufl. X, 268 S., 37. ed. The Year Book Publishers, Inc. Chicago.
- McDonald, H.J., Urbin, M.C., Williamson, M.B., 1951. Ionography: Some aspects of ion migration on paper in an electric field. *J. Colloid Sci.* 6, 236–244. [https://doi.org/10.1016/0095-8522\(51\)90042-6](https://doi.org/10.1016/0095-8522(51)90042-6)
- McLoughlin, J.V., 1961. Splitting of Serum Albumin during Electrophoresis on Paper. *Nature* 191, 1305–1306. <https://doi.org/10.1038/1911305a0>
- MedCalc Software Ltd. Comparison of means calculator, Version 20.014 [WWW Document], 2021. . MedCalc. URL https://www.medcalc.org/calc/comparison_of_means.php (accessed 10.28.21).
- Miyamoto, H., Yamamoto, H., Arima, K., Fujii, J., Maruta, K., Izu, K., Shiomori, T., Yoshida, S., 1997. Development of a new seminested PCR method for detection of Legionella species and its application to surveillance of legionellae in hospital cooling tower water. *Appl. Environ. Microbiol.* 63, 2489–2494. <https://doi.org/10.1128/aem.63.7.2489-2494.1997>
- Miyashita, M., Ito, N., Ikeda, S., Murayama, T., Oguma, K., Kimura, J., 2009. Development of urine glucose meter based on micro-planer amperometric biosensor and its clinical application for self-monitoring of urine glucose. *Biosens. Bioelectron.*, Selected Papers from the Tenth World Congress on Biosensors Shanghai, China, May 14-16, 2008 24, 1336–1340. <https://doi.org/10.1016/j.bios.2008.07.072>
- Molmeret, M., Bitar, D.M., Han, L., Kwaik, Y.A., 2004. Disruption of the phagosomal membrane and egress of Legionella pneumophila into the cytoplasm during the last stages of intracellular

- infection of macrophages and *Acanthamoeba polyphaga*. *Infect. Immun.* 72, 4040–4051. <https://doi.org/10.1128/IAI.72.7.4040-4051.2004>
- Molmeret, M., Horn, M., Wagner, M., Santic, M., Abu Kwaik, Y., 2005. Amoebae as Training Grounds for Intracellular Bacterial Pathogens. *Appl. Environ. Microbiol.* 71, 20–28. <https://doi.org/10.1128/AEM.71.1.20-28.2005>
- Molofsky, A.B., Swanson, M.S., 2004. Differentiate to thrive: lessons from the *Legionella pneumophila* life cycle. *Mol. Microbiol.* 53, 29–40. <https://doi.org/10.1111/j.1365-2958.2004.04129.x>
- Monien, H., Specker, H., Zinke, K., 1967. Über die Anwendbarkeit verschiedener Kohleelektroden zur inversen Voltammetrie von Silber. *Fresenius Z. Für Anal. Chem.* 225, 342–351. <https://doi.org/10.1007/BF00983679>
- Moreno, Y., Moreno-Mesonero, L., García-Hernández, J., 2019. DVC-FISH to identify potentially pathogenic *Legionella* inside free-living amoebae from water sources. *Environ. Res.* 176, 108521. <https://doi.org/10.1016/j.envres.2019.06.002>
- Na, H., Kang, B.-H., Ku, J., Kim, Y., Jeong, K.-H., 2021. On-chip Paper Electrophoresis for Ultrafast Screening of Infectious Diseases. *BioChip J.* 15, 305–311. <https://doi.org/10.1007/s13206-021-00034-z>
- National Center for Immunization and Respiratory Diseases, 2021. Legionnaires Disease History, Burden, and Trends | CDC [WWW Document]. URL <https://www.cdc.gov/legionella/about/history.html> (accessed 7.10.21).
- Nguyen, P.Q., Soenksen, L.R., Donghia, N.M., Angenent-Mari, N.M., de Puig, H., Huang, A., Lee, R., Slomovic, S., Galbersanini, T., Lansberry, G., Sallum, H.M., Zhao, E.M., Niemi, J.B., Collins, J.J., 2021. Wearable materials with embedded synthetic biology sensors for biomolecule detection. *Nat. Biotechnol.* <https://doi.org/10.1038/s41587-021-00950-3>
- Nicolaou, K.C., Tsay, S.C., Suzuki, T., Joyce, G.F., 1992. DNA-carbohydrate interactions. Specific binding of the calicheamicin γ .11 oligosaccharide with duplex DNA. *J. Am. Chem. Soc.* 114, 7555–7557. <https://doi.org/10.1021/ja00045a033>
- Nie, J., Liang, Y., Zhang, Y., Le, S., Li, D., Zhang, S., 2013. One-step patterning of hollow microstructures in paper by laser cutting to create microfluidic analytical devices. *The Analyst* 138, 671–676. <https://doi.org/10.1039/c2an36219h>
- Niedl, R.R., Beta, C., 2015. Hydrogel-driven paper-based microfluidics. *Lab. Chip* 15, 2452–2459. <https://doi.org/10.1039/c5lc00276a>
- Nishat, S., Jafry, A.T., Martinez, A.W., Awan, F.R., 2021. Paper-based microfluidics: Simplified fabrication and assay methods. *Sens. Actuators B Chem.* 336, 129681. <https://doi.org/10.1016/j.snb.2021.129681>
- Noviana, E., Ozer, T., Carrell, C.S., Link, J.S., McMahon, C., Jang, I., Henry, C.S., 2021. Microfluidic Paper-Based Analytical Devices: From Design to Applications. *Chem. Rev.* 121, 11835–11885. <https://doi.org/10.1021/acs.chemrev.0c01335>
- Nurak, T., Praphairaksit, N., Chailapakul, O., 2013. Fabrication of paper-based devices by lacquer spraying method for the determination of nickel (II) ion in waste water. *Talanta*. <https://doi.org/10.1016/j.talanta.2013.05.037>
- Olkkonen, J., Lehtinen, K., Erho, T., 2010. Flexographically printed fluidic structures in paper. *Anal. Chem.* 82, 10246–10250. <https://doi.org/10.1021/ac1027066>
- Olson, C., Adams, R.N., 1960. Carbon paste electrodes application to anodic voltammetry. *Anal. Chim. Acta* 22, 582–589. [https://doi.org/10.1016/S0003-2670\(00\)88341-5](https://doi.org/10.1016/S0003-2670(00)88341-5)
- Owczarzy, R., Moreira, B.G., You, Y., Behlke, M.A., Walder, J.A., 2008. Predicting Stability of DNA Duplexes in Solutions Containing Magnesium and Monovalent Cations. *Biochemistry* 47, 5336–5353. <https://doi.org/10.1021/bi702363u>
- Palusińska-Szyszk, M., Russa, R., 2009. Chemical structure and biological significance of lipopolysaccharide from *Legionella*. *Recent Patents Anti-Infect. Drug Disc.* 4, 96–107. <https://doi.org/10.2174/157489109788490316>

- Panda, B.B., Meher, A.S., Hazra, R.K., 2019. Comparison between different methods of DNA isolation from dried blood spots for determination of malaria to determine specificity and cost effectiveness. *J. Parasit. Dis. Off. Organ Indian Soc. Parasitol.* 43, 337–342. <https://doi.org/10.1007/s12639-019-01136-0>
- Papatheodorou, S.A., Tsironi, T., Giannakourou, M., Halvatsiotis, P., Houhoula, D., 2022. Application of microfluidic paper-based analytical devices (μ PADs) for food microbial detection. *J. Sci. Food Agric.* <https://doi.org/10.1002/jsfa.11822>
- Pardue, M.L., Gall, J.G., 1969. Molecular Hybridization of Radioactive DNA to the DNA of Cytological Preparations. *Proc. Natl. Acad. Sci.* 64, 600. <https://doi.org/10.1073/pnas.64.2.600>
- Paul Marienfeld GmbH & Co. KG, 2021. Informationen zu unseren Zählkammern - Paul Marienfeld | Neubauer-improved-dl [WWW Document]. URL <https://marienfeld-superior.com/informationen-zu-unseren-zaehlkammern.html> (accessed 11.4.21).
- Pernthaler, A., Pernthaler, J., Amann, R., 2002. Fluorescence In Situ Hybridization and Catalyzed Reporter Deposition for the Identification of Marine Bacteria. *Appl. Environ. Microbiol.* 68, 3094–3101. <https://doi.org/10.1128/AEM.68.6.3094-3101.2002>
- Peterson, A.W., Heaton, R.J., Georgiadis, R.M., 2001. The effect of surface probe density on DNA hybridization. *Nucleic Acids Res.* 29, 5163–5168. <https://doi.org/10.1093/nar/29.24.5163>
- Peyret, N., 2000. Prediction of nucleic acid hybridization: parameters and algorithms. UMI, Ann Arbor, Mich.
- Pingoud, A., Urbanke, C., Hoggett, J., Jeltsch, A., 2002. *Biochemical Methods: A Concise Guide for Students and Researchers* | Wiley-VCH.
- Qi, Z., Lei, W., 1999. Synthesis of Ruthenium Polypyridyl Complexes and the Steric Influence of the Intercalated Ligand on DNA Binding. undefined.
- Qin, X., Liu, J., Zhang, Zhong, Li, J., Yuan, L., Zhang, Zhiyang, Chen, L., 2021. Microfluidic paper-based chips in rapid detection: Current status, challenges, and perspectives. *TrAC Trends Anal. Chem.* 143, 116371. <https://doi.org/10.1016/j.trac.2021.116371>
- Rafiee, M., Jahangiri-Rad, M., Hajjarian, H., Mesdaghinia, A., Hajaghazadeh, M., 2014. Detection and identification of Legionella species in hospital water supplies through Polymerase Chain Reaction (16S rRNA). *J. Environ. Health Sci. Eng.* 12, 83. <https://doi.org/10.1186/2052-336X-12-83>
- Ramirez, J.A., Ahkee, S., Tolentino, A., Miller, R.D., Summersgill, J.T., 1996. Diagnosis of Legionella pneumophila, Mycoplasma pneumoniae, or Chlamydia pneumoniae lower respiratory infection using the polymerase chain reaction on a single throat swab specimen. *Diagn. Microbiol. Infect. Dis.* 24, 7–14. [https://doi.org/10.1016/0732-8893\(95\)00254-5](https://doi.org/10.1016/0732-8893(95)00254-5)
- Rantakokko-Jalava, K., Jalava, J., 2001. Development of Conventional and Real-Time PCR Assays for Detection of Legionella DNA in Respiratory Specimens. *J. Clin. Microbiol.* 39, 2904–2910. <https://doi.org/10.1128/JCM.39.8.2904-2910.2001>
- Rasch, J., Ünal, C.M., Klages, A., Karsli, Ü., Heinsohn, N., Brouwer, R.M.H.J., Richter, M., Dellmann, A., Steinert, M., 2019. Peptidyl-Prolyl-cis/trans-Isomerases Mip and PpiB of Legionella pneumophila Contribute to Surface Translocation, Growth at Suboptimal Temperature, and Infection. *Infect. Immun.* 87, e00939-17. <https://doi.org/10.1128/IAI.00939-17>
- Rattanarat, P., Dungchai, W., Siangproh, W., Chailapakul, O., Henry, C.S., 2012. Sodium dodecyl sulfate-modified electrochemical paper-based analytical device for determination of dopamine levels in biological samples. *Anal. Chim. Acta* 744, 1–7. <https://doi.org/10.1016/j.aca.2012.07.003>
- Ravi Kumar, M.N.V., 2000. A review of chitin and chitosan applications. *React. Funct. Polym.* 46, 1–27. [https://doi.org/10.1016/S1381-5148\(00\)00038-9](https://doi.org/10.1016/S1381-5148(00)00038-9)
- Reischl, U., Linde, H.-J., Lehn, N., Landt, O., Barratt, K., Wellinghausen, N., 2002. Direct detection and differentiation of Legionella spp. and Legionella pneumophila in clinical specimens by dual-color real-time PCR and melting curve analysis. *J. Clin. Microbiol.* 40, 3814–3817. <https://doi.org/10.1128/jcm.40.10.3814-3817.2002>

- Riboldi-Tunncliffe, A., König, B., Jessen, S., Weiss, M.S., Rahfeld, J., Hacker, J., Fischer, G., Hilgenfeld, R., 2001. Crystal structure of Mip, a prolyl isomerase from *Legionella pneumophila*. *Nat. Struct. Biol.* 8, 779–783. <https://doi.org/10.1038/nsb0901-779>
- Robert Koch Institut, 2021. Infektionsepidemiologisches Jahrbuch meldepflichtiger Krankheiten für 2020. ISBN 978-3-89606-306-9. <https://doi.org/10.25646/6948>
- Robert Koch Institut, 2020. Infektionsepidemiologisches Jahrbuch meldepflichtiger Krankheiten für 2019. ISBN 978-3-89606-306-9. <https://doi.org/10.25646/6948>
- Robert Koch Institut, 2019a. Infektionsepidemiologisches Jahrbuch meldepflichtiger Krankheiten für 2018. ISBN 978-3-89606-297-0. <https://doi.org/10.25646/5978>
- Robert Koch Institut, 2019b. RKI-Ratgeber Legionellose. <https://doi.org/10.25646/6248>
- Robert Koch Institut, 2019c. Falldefinitionen des Robert Koch-Instituts zur Übermittlung von Erkrankungs- oder Todesfällen und Nachweisen von Krankheitserregern 150.
- Robert Koch Institut, 2018. Infektionsepidemiologisches Jahrbuch meldepflichtiger Krankheiten für 2017. ISBN 978-3-89606-291-8. <https://doi.org/10.17886/rkipubl-2018-001>
- Robert Koch Institut, 2017. Infektionsepidemiologisches Jahrbuch meldepflichtiger Krankheiten für 2016. ISBN 978-3-89606-280-2. <https://doi.org/10.17886/rkipubl-2017-002>
- Robert Koch Institut, 2016. Infektionsepidemiologisches Jahrbuch meldepflichtiger Krankheiten für 2015. ISBN 978-3-89606-270-3.
- Rohs, R., Sklenar, H., 2004. Methylene Blue Binding to DNA with Alternating AT Base Sequence: Minor Groove Binding is Favored over Intercalation. *J. Biomol. Struct. Dyn.* 21, 699–711. <https://doi.org/10.1080/07391102.2004.10506960>
- Rosenfeld, T., Bercovici, M., 2014. 1000-fold sample focusing on paper-based microfluidic devices. *Lab Chip* 14, 4465–4474. <https://doi.org/10.1039/C4LC00734D>
- Rudkin, G.T., Stollar, B.D., 1977. High resolution detection of DNA–RNA hybrids in situ by indirect immunofluorescence. *Nature* 265, 472–473. <https://doi.org/10.1038/265472a0>
- Rutledge, N., 2018. Engineering Chemistry. Scientific e-Resources.
- Sabriu-Haxhijaha, A., Ilievska, G., Stojkovski, V., Blagoevska, K., 2020. A Modified SDS – Based Method Applied for Extraction of High-Quality DNA from Raw Corn and Roasted Soybean. *Maced. Vet. Rev.* 43, 61–67. <https://doi.org/10.2478/macvetrev-2020-0017>
- Sachdeva, S., Davis, R.W., Saha, A.K., 2021. Microfluidic Point-of-Care Testing: Commercial Landscape and Future Directions. *Front. Bioeng. Biotechnol.* 8.
- SantaLucia, J., 1998. A unified view of polymer, dumbbell, and oligonucleotide DNA nearest-neighbor thermodynamics. *Proc. Natl. Acad. Sci.* 95, 1460–1465. <https://doi.org/10.1073/pnas.95.4.1460>
- Sartorius Lab Instruments GmbH & Co.KG., 2021. Filter Papers for the Laboratory and Industry.
- Schönhuber, W., Zarda, B., Eix, S., Rippka, R., Herdman, M., Ludwig, W., Amann, R., 1999. In situ identification of cyanobacteria with horseradish peroxidase-labeled, rRNA-targeted oligonucleotide probes. *Appl. Environ. Microbiol.* 65, 1259–1267. <https://doi.org/10.1128/AEM.65.3.1259-1267.1999>
- Semenov, A.N., Duke, T.A.J., Viovy, J.-L., 1995. Gel electrophoresis of DNA in moderate fields: The effect of fluctuations. *Phys. Rev. E* 51, 1520–1537. <https://doi.org/10.1103/PhysRevE.51.1520>
- Seok, Y., Joung, H.-A., Byun, J.-Y., Jeon, H.-S., Shin, S.J., Kim, S., Shin, Y.-B., Han, H.S., Kim, M.-G., 2017. A Paper-Based Device for Performing Loop-Mediated Isothermal Amplification with Real-Time Simultaneous Detection of Multiple DNA Targets. *Theranostics* 7, 2220–2230. <https://doi.org/10.7150/thno.18675>
- Shakoori, A.R., 2017. Fluorescence In Situ Hybridization (FISH) and Its Applications, in: Bhat, T.A., Wani, A.A. (Eds.), *Chromosome Structure and Aberrations*. Springer India, New Delhi, pp. 343–367. https://doi.org/10.1007/978-81-322-3673-3_16
- Shiroma, L.Y., Santhiago, M., Gobbi, A.L., Kubota, L.T., 2012. Separation and electrochemical detection of paracetamol and 4-aminophenol in a paper-based microfluidic device. *Anal. Chim. Acta* 725, 44–50. <https://doi.org/10.1016/j.aca.2012.03.011>

- Siva, R., Mathew, G.J., Venkat, A., Dhawan, C., 2008. An alternative tracking dye for gel electrophoresis. *Curr. Sci.* 94, 3.
- Smith, J.D., 1967. [42] Paper electrophoresis of nucleic acid components, in: *Methods in Enzymology, Nucleic Acids, Part A*. Academic Press, pp. 350–361. [https://doi.org/10.1016/S0076-6879\(67\)12051-X](https://doi.org/10.1016/S0076-6879(67)12051-X)
- Smith, S., Morin, P.A., 2005. Optimal storage conditions for highly dilute DNA samples: a role for trehalose as a preserving agent. *J. Forensic Sci.* 50, 1101–1108.
- Söderberg, M.A., Cianciotto, N.P., 2008. A *Legionella pneumophila* peptidyl-prolyl cis-trans isomerase present in culture supernatants is necessary for optimal growth at low temperatures. *Appl. Environ. Microbiol.* 74, 1634–1638. <https://doi.org/10.1128/AEM.02512-07>
- Sones, C.L., Katis, I.N., He, P.J.W., Mills, B., Namiq, M.F., Shardlow, P., Ibsen, M., Eason, R.W., 2014. Laser-induced photo-polymerisation for creation of paper-based fluidic devices. *Lab. Chip* 14, 4567–4574. <https://doi.org/10.1039/C4LC00850B>
- Sood, Y.V., Tyagi, R., Tyagi, S., Pande, P.C., Tondon, R., 2010. Surface charge of different paper making raw materials and its influence on paper properties 69, 5.
- Southern, E.M., 1979. Measurement of DNA length by gel electrophoresis. *Anal. Biochem.* 100, 319–323. [https://doi.org/10.1016/0003-2697\(79\)90235-5](https://doi.org/10.1016/0003-2697(79)90235-5)
- Steinert, M., Emödy, L., Amann, R., Hacker, J., 1997. Resuscitation of viable but nonculturable *Legionella pneumophila* Philadelphia JR32 by *Acanthamoeba castellanii*. *Appl. Environ. Microbiol.* 63, 2047–2053.
- Steinert, M., Hentschel, U., Hacker, J., 2002. *Legionella pneumophila*: an aquatic microbe goes astray. *FEMS Microbiol. Rev.* 26, 149–162. <https://doi.org/10.1111/j.1574-6976.2002.tb00607.x>
- Stellwagen, N.C., 1985. Effect of the electric field on the apparent mobility of large DNA fragments in agarose gels. *Biopolymers* 24, 2243–2255. <https://doi.org/10.1002/bip.360241207>
- Stellwagen, N.C., Gelfi, C., Righetti, P.G., 1997. The free solution mobility of DNA. *Biopolymers* 42, 687–703. [https://doi.org/10.1002/\(SICI\)1097-0282\(199711\)42:6<687::AID-BIP7>3.0.CO;2-Q](https://doi.org/10.1002/(SICI)1097-0282(199711)42:6<687::AID-BIP7>3.0.CO;2-Q)
- Stellwagen, N.C., Stellwagen, E., 2009. Effect of the matrix on DNA electrophoretic mobility. *J. Chromatogr. A* 1216, 1917–1929. <https://doi.org/10.1016/j.chroma.2008.11.090>
- Stone, B.J., Abu Kwaik, Y., 1998. Expression of multiple pili by *Legionella pneumophila*: identification and characterization of a type IV pilin gene and its role in adherence to mammalian and protozoan cells. *Infect. Immun.* 66, 1768–1775. <https://doi.org/10.1128/IAI.66.4.1768-1775.1998>
- Su, S., Nutiu, R., Filipe, C.D.M., Li, Y., Pelton, R., 2007. Adsorption and Covalent Coupling of ATP-Binding DNA Aptamers onto Cellulose. *Langmuir* 23, 1300–1302. <https://doi.org/10.1021/la060961c>
- Su, X., Comeau, A.M., 1999. Cellulose as a matrix for nucleic acid purification. *Anal. Biochem.* 267, 415–418. <https://doi.org/10.1006/abio.1998.2987>
- Sun, H., Ma, H., Liu, L., Cao, X., Yang, Z., 2015. A new ELISA method for serological diagnosis of *Legionella pneumophila*: use of five purified proteins, FLA, MOMP, MIP, IP, and PILE, as diagnostic antigen. *Clin. Lab.* 61, 275–282. <https://doi.org/10.7754/clin.lab.2014.140908>
- Sun, K., Zhang, S., Li, P., Xia, Y., Zhang, X., Du, D., Isikgor, F.H., Ouyang, J., 2015. Review on application of PEDOTs and PEDOT:PSS in energy conversion and storage devices. *J. Mater. Sci. Mater. Electron.* 26, 4438–4462. <https://doi.org/10.1007/s10854-015-2895-5>
- Švancara, I., Vytrás, K., Kalcher, K., Walcarius, A., Wang, J., 2009. Carbon Paste Electrodes in Facts, Numbers, and Notes: A Review on the Occasion of the 50-Years Jubilee of Carbon Paste in Electrochemistry and Electroanalysis. *Electroanalysis* 21, 7–28. <https://doi.org/10.1002/elan.200804340>
- Tang, R.H., Liu, L.N., Zhang, S.F., He, X.C., Li, X.J., Xu, F., Ni, Y.H., Li, F., 2019. A review on advances in methods for modification of paper supports for use in point-of-care testing. *Microchim. Acta* 186, 521. <https://doi.org/10.1007/s00604-019-3626-z>
- Templeton, K.E., Scheltinga, S.A., Sillekens, P., Crielaard, J.W., van Dam, A.P., Goossens, H., Claas, E.C.J., 2003. Development and Clinical Evaluation of an Internally Controlled, Single-Tube

- Multiplex Real-Time PCR Assay for Detection of *Legionella pneumophila* and Other *Legionella* Species. *J. Clin. Microbiol.* 41, 4016–4021. <https://doi.org/10.1128/JCM.41.9.4016-4021.2003>
- Tesh, M.J., Morse, S.A., Miller, R.D., 1983. Intermediary metabolism in *Legionella pneumophila*: utilization of amino acids and other compounds as energy sources. *J. Bacteriol.* 154, 1104–1109. <https://doi.org/10.1128/jb.154.3.1104-1109.1983>
- Tong, C., Hu, Z., Wu, J., 2010. Interaction Between Methylene Blue and CalfThymus Deoxyribonucleic Acid by Spectroscopic Technologies. *J. Fluoresc.* 20, 261–267. <https://doi.org/10.1007/s10895-009-0549-9>
- Toplitsch, D., Platzer, S., Pfeifer, B., Hautz, J., Mascher, F., Kittinger, C., 2018. *Legionella* Detection in Environmental Samples as an Example for Successful Implementation of qPCR. *Water* 10, 1012. <https://doi.org/10.3390/w10081012>
- Toplitsch, D., Platzer, S., Zehner, R., Maitz, S., Mascher, F., Kittinger, C., 2021. Comparison of Updated Methods for *Legionella* Detection in Environmental Water Samples. *Int. J. Environ. Res. Public Health* 18, 5436. <https://doi.org/10.3390/ijerph18105436>
- Tseng, C.-C., Kung, C.-T., Chen, R.-F., Tsai, M.-H., Chao, H.-R., Wang, Y.-N., Fu, L.-M., 2021. Recent advances in microfluidic paper-based assay devices for diagnosis of human diseases using saliva, tears and sweat samples. *Sens. Actuators B Chem.* 342, 130078. <https://doi.org/10.1016/j.snb.2021.130078>
- Tyagi, S., Kramer, F.R., 1996. Molecular Beacons: Probes that Fluoresce upon Hybridization. *Nat. Biotechnol.* 14, 303–308. <https://doi.org/10.1038/nbt0396-303>
- Utami, F., Rahman, D., Margareta, D., Dany, H., Munir, R., Sustini, E., Abdullah, M., 2019. TiO₂ Photocatalytic Degradation of Methylene Blue Using Simple Spray Method. *IOP Conf. Ser. Mater. Sci. Eng.* 599, 012026. <https://doi.org/10.1088/1757-899X/599/1/012026>
- Vandaveer, W.R., Padas-Farmer, S.A., Fischer, D.J., Frankenfeld, C.N., Lunte, S.M., 2004. Recent developments in electrochemical detection for microchip capillary electrophoresis. *ELECTROPHORESIS* 25, 3528–3549. <https://doi.org/10.1002/elps.200406115>
- Vandevanter, P.E., Mejia, J., Nadim, A., Johal, M.S., Niemz, A., 2013. DNA Adsorption to and Elution from Silica Surfaces: Influence of Amino Acid Buffers. *J. Phys. Chem. B* 117, 10742–10749. <https://doi.org/10.1021/jp405753m>
- Várnai, P., Zakrzewska, K., 2004. DNA and its counterions: a molecular dynamics study. *Nucleic Acids Res.* 32, 4269–4280. <https://doi.org/10.1093/nar/gkh765>
- Vella, S.J., Beattie, P., Cademartiri, R., Laromaine, A., Martinez, A.W., Phillips, S.T., Mirica, K.A., Whitesides, G.M., 2012. Measuring markers of liver function using a micropatterned paper device designed for blood from a fingerstick. *Anal. Chem.* 84, 2883–2891. <https://doi.org/10.1021/ac203434x>
- Viasus, D., Gaia, V., Manzur-Barbur, C., Carratalà, J., 2022. Legionnaires' Disease: Update on Diagnosis and Treatment. *Infect. Dis. Ther.* <https://doi.org/10.1007/s40121-022-00635-7>
- Viovy, J.-L., 2000. Electrophoresis of DNA and other polyelectrolytes: Physical mechanisms. *Rev. Mod. Phys.* 72, 813–872. <https://doi.org/10.1103/RevModPhys.72.813>
- Voytas, D., 2001. Agarose Gel Electrophoresis. *Curr. Protoc. Mol. Biol.* 51, 2.5A.1-2.5A.9. <https://doi.org/10.1002/0471142727.mb0205as51>
- Wagenknecht, H.-A., 2006. Electron transfer processes in DNA: mechanisms, biological relevance and applications in DNA analytics. *Nat. Prod. Rep.* 23, 973–1006. <https://doi.org/10.1039/B504754B>
- Wagner, C., Khan, A.S., Kamphausen, T., Schmausser, B., Unal, C., Lorenz, U., Fischer, G., Hacker, J., Steinert, M., 2007. Collagen binding protein Mip enables *Legionella pneumophila* to transmigrate through a barrier of NCI-H292 lung epithelial cells and extracellular matrix. *Cell. Microbiol.* 9, 450–462. <https://doi.org/10.1111/j.1462-5822.2006.00802.x>
- Walker, S., Valentine, K.G., Kahne, D., 1990. Sugars as DNA binders: a comment on the calicheamicin oligosaccharide. *J. Am. Chem. Soc.* 112, 6428–6429. <https://doi.org/10.1021/ja00173a058>

- Wang, H., Vagin, S.I., Rieger, B., Meldrum, A., 2020. An Ultrasensitive Fluorescent Paper-Based CO₂ Sensor. *ACS Appl. Mater. Interfaces* 12, 20507–20513. <https://doi.org/10.1021/acscami.0c03405>
- Wang, X., Hong, X.-Z., Li, Y.-W., Li, Y., Wang, J., Chen, P., Liu, B.-F., 2022. Microfluidics-based strategies for molecular diagnostics of infectious diseases. *Mil. Med. Res.* 9, 11. <https://doi.org/10.1186/s40779-022-00374-3>
- Wei, C.-W., Cheng, J.-Y., Huang, C.-T., Yen, M.-H., Young, T.-H., 2005. Using a microfluidic device for 1 μ l DNA microarray hybridization in 500 s. *Nucleic Acids Res.* 33, e78. <https://doi.org/10.1093/nar/gni078>
- Wellinghausen, N., Frost, C., Marre, R., 2001. Detection of legionellae in hospital water samples by quantitative real-time LightCycler PCR. *Appl. Environ. Microbiol.* 67, 3985–3993. <https://doi.org/10.1128/aem.67.9.3985-3993.2001>
- Whiley, H., Taylor, M., 2016. Legionella detection by culture and qPCR: Comparing apples and oranges. *Crit. Rev. Microbiol.* 42, 65–74. <https://doi.org/10.3109/1040841X.2014.885930>
- Whistler, R.L., BeMiller, J.N., 2009. Starch: chemistry and technology, 3rd ed. ed, Food science and technology, International Series. Academic Press, London.
- Wieland, H., Goetz, F., Neumeister, B., 2004. Phagosomal acidification is not a prerequisite for intracellular multiplication of Legionella pneumophila in human monocytes. *J. Infect. Dis.* 189, 1610–1614. <https://doi.org/10.1086/382894>
- Wilkinson, J.H., Boutwell, J.H., Winsten, S., 1969. Evaluation of a New System For the Kinetic Measurement of Serum Alkaline Phosphatase. *Clin. Chem.* 15, 487–495. <https://doi.org/10.1093/clinchem/15.6.487>
- Wilson, D.A., Yen-Lieberman, B., Reischl, U., Gordon, S.M., Procop, G.W., 2003. Detection of Legionella pneumophila by Real-Time PCR for the mip Gene. *J. Clin. Microbiol.* 41, 3327–3330. <https://doi.org/10.1128/JCM.41.7.3327-3330.2003>
- World Health Organization, 1993. Guidelines for Drinking-water Quality. World Health Organization.
- Wu, T.-Y., Su, Y.-Y., Shu, W.-H., Mercado, A.T., Wang, S.-K., Hsu, L.-Y., Tsai, Y.-F., Chen, C.-Y., 2016. A novel sensitive pathogen detection system based on Microbead Quantum Dot System. *Biosens. Bioelectron.* 78, 37–44. <https://doi.org/10.1016/j.bios.2015.11.016>
- Wunderly, C., 1954. *Papierelktrophorese*, 1. Aufl. 128 S., 46. ed. Verlag H. R. Sauerländer u. Co., Aarau u. Frankfurt/M.
- Wyman, C.E., 1994. Ethanol from lignocellulosic biomass: Technology, economics, and opportunities. *Bioresour. Technol.*, Special issue: Biotechnology for the conversion of lignocellulosics 50, 3–15. [https://doi.org/10.1016/0960-8524\(94\)90214-3](https://doi.org/10.1016/0960-8524(94)90214-3)
- Xebios Diagnostics GmbH, 2022. Legionella-BCYE+AB Agar (Bulk) (BCYE+AB) 2.
- Xi, C., Balberg, M., Boppart, S.A., Raskin, L., 2003. Use of DNA and peptide nucleic acid molecular beacons for detection and quantification of rRNA in solution and in whole cells. *Appl. Environ. Microbiol.* 69, 5673–5678. <https://doi.org/10.1128/AEM.69.9.5673-5678.2003>
- Xia, Y., Dai, S., 2021. Review on applications of PEDOTs and PEDOT:PSS in perovskite solar cells. *J. Mater. Sci. Mater. Electron.* 32, 12746–12757. <https://doi.org/10.1007/s10854-020-03473-w>
- Xu, H.-S., Roberts, N., Singleton, F.L., Attwell, R.W., Grimes, D.J., Colwell, R.R., 1982. Survival and viability of nonculturable Escherichia coli and Vibrio cholerae in the estuarine and marine environment. *Microb. Ecol.* 8, 313–323. <https://doi.org/10.1007/BF02010671>
- Yaradou, D.F., Hallier-Soulier, S., Moreau, S., Poty, F., Hillion, Y., Reyrolle, M., André, J., Festoc, G., Delabre, K., Vandenesch, F., Etienne, J., Jarraud, S., 2007. Integrated real-time PCR for detection and monitoring of Legionella pneumophila in water systems. *Appl. Environ. Microbiol.* 73, 1452–1456. <https://doi.org/10.1128/AEM.02399-06>
- Yu, J., Ge, L., Huang, J., Wang, S., Ge, S., 2011. Microfluidic paper-based chemiluminescence biosensor for simultaneous determination of glucose and uric acid. *Lab. Chip* 11, 1286–1291. <https://doi.org/10.1039/C0LC00524J>

- Zähringer, U., Knirel, Y.A., Lindner, B., Helbig, J.H., Sonesson, A., Marre, R., Rietschel, E.T., 1995. The lipopolysaccharide of *Legionella pneumophila* serogroup 1 (strain Philadelphia 1): chemical structure and biological significance. *Prog. Clin. Biol. Res.* 392, 113–139.
- Zhang, H., Zhao, C., Li, Z., Li, J., 2016. The fiber charge measurement depending on the poly-DADMAC accessibility to cellulose fibers. *Cellulose* 23, 163–173. <https://doi.org/10.1007/s10570-015-0793-x>
- Zhang, L., Chen, K.S., Yu, H.-Z., 2020. Superhydrophobic Glass Microfiber Filter as Background-Free Substrate for Quantitative Fluorometric Assays. *ACS Appl. Mater. Interfaces*. <https://doi.org/10.1021/acsami.9b17432>
- Zhang, P., Beck, T., Tan, W., 2001. Design of a Molecular Beacon DNA Probe with Two Fluorophores. *Angew. Chem. Int. Ed Engl.* 40, 402–405. [https://doi.org/10.1002/1521-3773\(20010119\)40:2<402::AID-ANIE402>3.0.CO;2-I](https://doi.org/10.1002/1521-3773(20010119)40:2<402::AID-ANIE402>3.0.CO;2-I)
- Zhu, B., Furuki, T., Okuda, T., Sakurai, M., 2007. Natural DNA mixed with trehalose persists in B-form double-stranding even in the dry state. *J. Phys. Chem. B* 111, 5542–5544. <https://doi.org/10.1021/jp071974h>
- Zou, Y., Mason, M.G., Wang, Y., Wee, E., Turni, C., Blackall, P.J., Trau, M., Botella, J.R., 2017. Nucleic acid purification from plants, animals and microbes in under 30 seconds. *PLOS Biol.* 15, e2003916. <https://doi.org/10.1371/journal.pbio.2003916>
- Zuker, M., 2003. Mfold web server for nucleic acid folding and hybridization prediction. *Nucleic Acids Res.* 31, 3406–3415. <https://doi.org/10.1093/nar/gkg595>
- Zuo, R., Du, G., Zhang, W., Liu, L., Liu, Y., Mei, L., Li, Z., 2014. Photocatalytic Degradation of Methylene Blue Using TiO₂ Impregnated Diatomite. *Adv. Mater. Sci. Eng.* 2014, e170148. <https://doi.org/10.1155/2014/170148>

6. Appendix

6.1. Abbreviation

Table 14: List of abbreviations used in this work.

%	Percent
μ	Micro
A	Ampere
ACES	N-(2-Acetamido)-2-aminoethanesulphonic acid
ALP	Alkaline phosphatase
AST	Aspartate aminotransferase
BCYE	Buffered Charcoal Yeast extract
BCYE+AB	Buffered Charcoal Yeast Extract including antibiotics
bp	Base pair
BSA	Bovine serum albumin
CARD	Catalyzed reporter deposition
CFU	Colony forming units
cm	Centimeter
CO ₂	Carbon dioxide
DABCYL	4,4-Dimethylaminoazobenzene-4-carboxylic acid
DNA	Deoxyribonucleic acid
dNTP	Desoxynukleosidtriphosphat
dsDNA	Double-stranded DNA
E	Electric field strength
EDTA	Ethylendiamintetraacetate
ELISA	Enzyme-linked Immunosorbent Assay
f	Femto
FAM	6-Carboxyfluorescein
FISH	Fluorescence <i>in situ</i> hybridization
fwd	Forward
gDNA	Genomic DNA
h	Hour
HCl	Hydrocholric acid
HRP	Horseradish peroxidase
HVADC	High-Voltage-Analog-Digital-Converter
kb	Kilobases
KCl	Potassium chloride
KH ₂ PO ₄	Monopotassium phosphate
LAMP	Loop-mediated isothermal amplification
l	Liter
L	Migration distance
LB	Lysogeny broth
LPS	Lipopolysaccharide
m	Milli
MAL-A	Mouse-anti-Legionella serum A
MAL-B	Mouse-anti-Legionella serum B
M	Molar
Mb	Megabases

MgCl ₂	Magnesium chloride
Ultrapure water	Deionized and sterile water
min	Minutes
mm	Millimeter
mol	Mole
n	Nano
Na ₂ HPO ₄	Disodium phosphate
NaCl	Sodium chlorid
NaN ₃	Sodiumazide
NaOH	Sodium hydroxide
NASBA	Nucleic acid sequencebased amplification
OD	Optical density
OD ₆₀₀	Optical density measured at 600 nm
Ω	Ohm
π	Pi
PBS	Phosphate buffered saline
PCR	Polymerase chain reaction
PDMS	Polydimethylsiloxane
PEDOT:PSS	Poly(3,4-ethylenedioxythiophene) polystyrene sulfonate
PES	Polyethersulfone
pH	Potential of hydrogen
PP	Polyethylen
P-value	Probability value
rev	Reverse
RPA	Recombinase polymerase amplification
rpm	Rounds per minute
RT-LAMP	Reverse transcription loop-mediated isothermal amplification
sec	Seconds
spp	Species
ssDNA	Single-stranded DNA
TAE-buffer	Tris-Acetate-EDTA-buffer
tbd	To be determined
t _m	migration time
TMB	Tetramethylbenzidine
Tris	Tris-(hydroxymethyl)-aminomethane
v	Electrophoretic velocity
V	Volt
YEB	Yeast extract broth
YEB	Yeast Extract Broth medium
μPAD	Microfluidic paper-based analytical devices

6.2. Circuit diagram HVADC

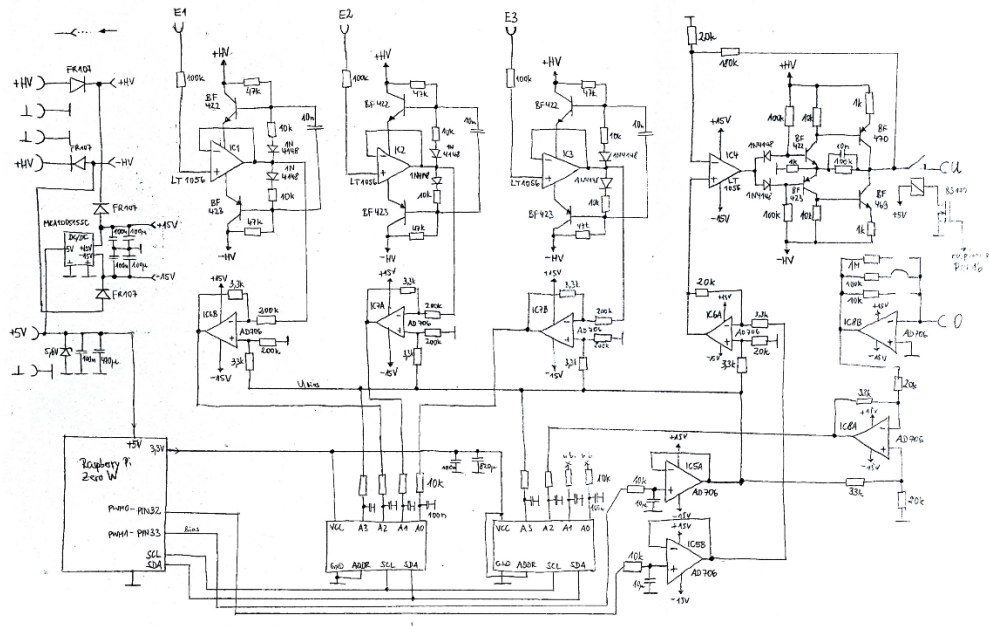


Figure A1: Circuit diagram. Schematic diagram of the electrical components and interconnections of the circuit in the High-Voltage-Analog-Digital-Converter (HVADC) designed and built by Dr. Alexander Anielski.

6.3. Microscopic determination of the layer thickness of a carbon paste electrode

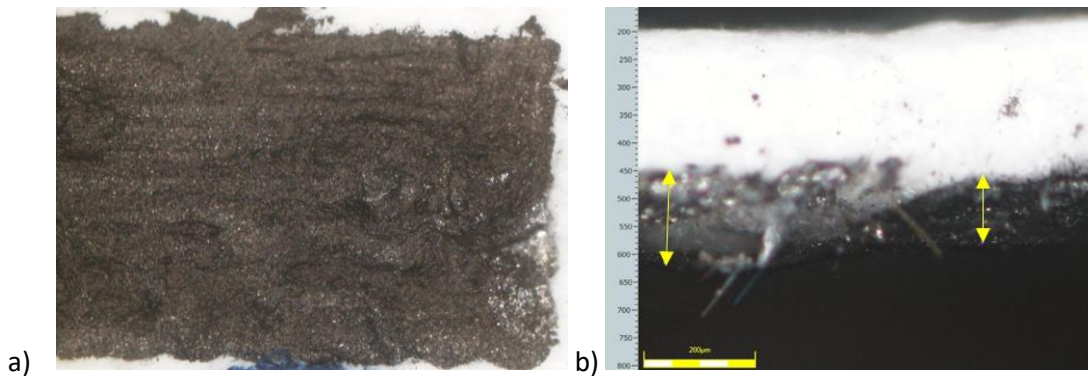


Figure A2. Microscopic determination of the layer thickness of a carbon paste electrode by Gero Göbel (Heinsohn et al., 2022). a) Top view of the measured electrode on glass microfiber GF/F with a thickness of 420 μm . b) Cross-section of the electrode showing here a layer thickness of 111 to 153 μm recorded with the Olympus DSX 500 optical microscope.

6.4. Electrophoretic migration of DNA samples in cellulose filters with imprinted electrodes consisting of PEDOT:PSS

A filter paper A388 from Ahlstrom-Munksjö with an average pore size of 12-15 μm was used to test whether a DNA containing sample could be pulled over a paper area towards the counter electrode after the application of an electric field. Each imprinted electrode was connected via a crocodile clamp to the voltage source and the interior surface was moistened with 50 μl distilled water. The chip interior measured an area of 1.2 x 3 cm. Bromophenol blue migrates in agarose gel electrophoresis approximately at the same rate as a dsDNA fragment of 300 bp and the turquoise appearing xylene cyanol follows the migration of DNA fragment of 4000 bp (Voytas, 2001). To be in a comparable range to the standard method of gel electrophoresis, a voltage of 115 V was chosen for the first fiber electrophoresis experiment. To keep the chip area wet, 20 μl distilled water was added after 0.6, 0.9 and 1.1 h, respectively, in four times 5 μl steps. To ensure that the sample migration occurred due to the electric field and not due to flushing of the sample over the fiber substrate, the fluid was added against the migration direction near the anode. Figure A3 shows pictures after several time points of the fiber-based electrophoresis chip under the influence of the electric field. The sample was added in front of the negatively charged electrode, the cathode, and can be easily identified by the blue spot. After 17 min the blue spot dissolved and a blue band was formed that moved about 3 mm towards the counter electrode. After 54 min this blue band had migrated one third of the chip area towards the anode and reached the counter electrode after 2.5 h. Up to 1.1 h after connection of the fiber chip, a blue coloration could also be detected at the site of sample application. It is difficult to determine whether this is bromophenol, the darker of the two dyes, or whether a residue of both dyes remained at the sample application site.

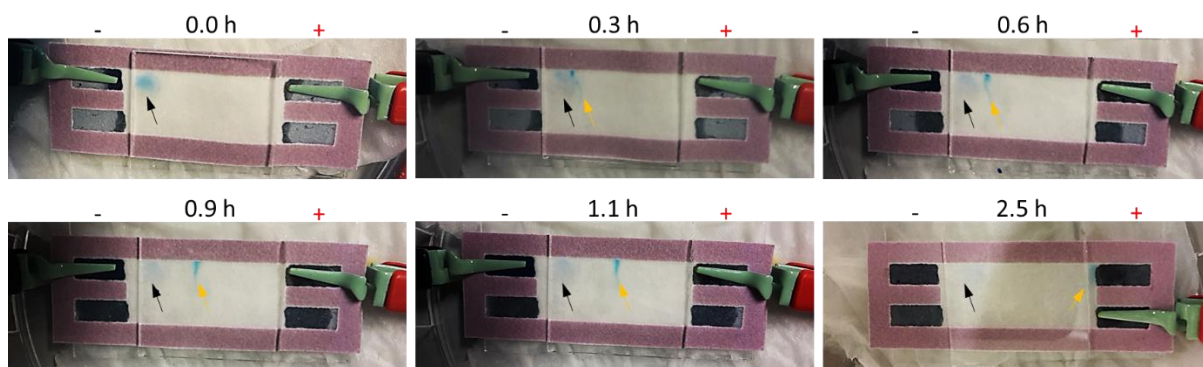


Figure A3: Cellulose fiber-based electrophoresis chip (Ahlstrom-Munksjö A388) with PEDOT:PSS electrodes was connected via crocodile clamps to a voltage source. Upon the application of an electric field of 115 V the blue sample spot migrated towards the positively charged electrode. A time series of images was recorded from the start of fiber electrophoresis until 2.5 hours after connection to the voltage source. The black arrow is pointing at the spot where the sample was applied and the yellow arrow follows the blue migrating sample spot. The fiber chip was covered by a cover glass to reduce evaporation during electrophoresis.

In order to test different electrode arrangements, the conductive polymer was added to the patterned cellulose sheet at the upper left and lower right, to test whether a diagonal migration direction is achieved after connection to the contact electrodes. As shown in Figure A4 a), the two dyes separated from each other during fiber electrophoresis. One dye was moving only a few millimeters away from the position where both were loaded and the other one migrated almost over the entire chip area towards the counter electrode at the lower right. After 30 min of voltage exposure, the blue spot was separated into two bands, which can be seen in the first picture. After 42 min, the faster running band was already pointing in the direction of the electrode at the bottom right and is pulled further towards the anode during the influence of the electric field. However, it could not completely detach itself from the upper chip surface, but extended over the entire chip width after 2 h. The second band, on the other hand, which has moved slowly, remains only in the upper half of the chip. After color comparison of the dyes loaded onto an agarose gel and the paper chip, it could be observed that the lighter blue band was pulled faster than the darker one. This suggests that instead of bromophenol blue, xylene cyanol is reaching the end of the electrophoresis chip first. Interestingly, the turquoise xylene cyanol band migrated instead of the bromophenol blue, although the latter corresponded to the migration behavior of smaller fragments and ran faster in agarose gel electrophoresis (see Figure A4 b). Assuming that the tracking dyes on the cellulose still run together with the DNA of the corresponding size, one could deduce from this result that the larger DNA molecules in the cellulose are electrophoretically attracted more strongly than the smaller ones and therefore arrive first at the chip end together with xylene cyanol. To investigate the sample size composition after fiber electrophoresis, the paper around the turquoise band was cut out and placed in a reaction tube with 10 μ l elution buffer 2. After vortexing and centrifugation to elute the DNA, the elution fraction was loaded onto an agarose gel for visualization. No DNA bands could be observed onto the gel after loading the elution fractions of the cellulose-based electrophoresis chip (see Figure A4 c). Either the DNA had not yet reached the end of the chip or it could not be recovered from the cellulose, similar to the situation after exposure to heat (as described in section 3.4). Also other different elution buffers containing sodium chloride or sodium azide were not suitable for eluting the DNA molecules from the cellulose scaffold.

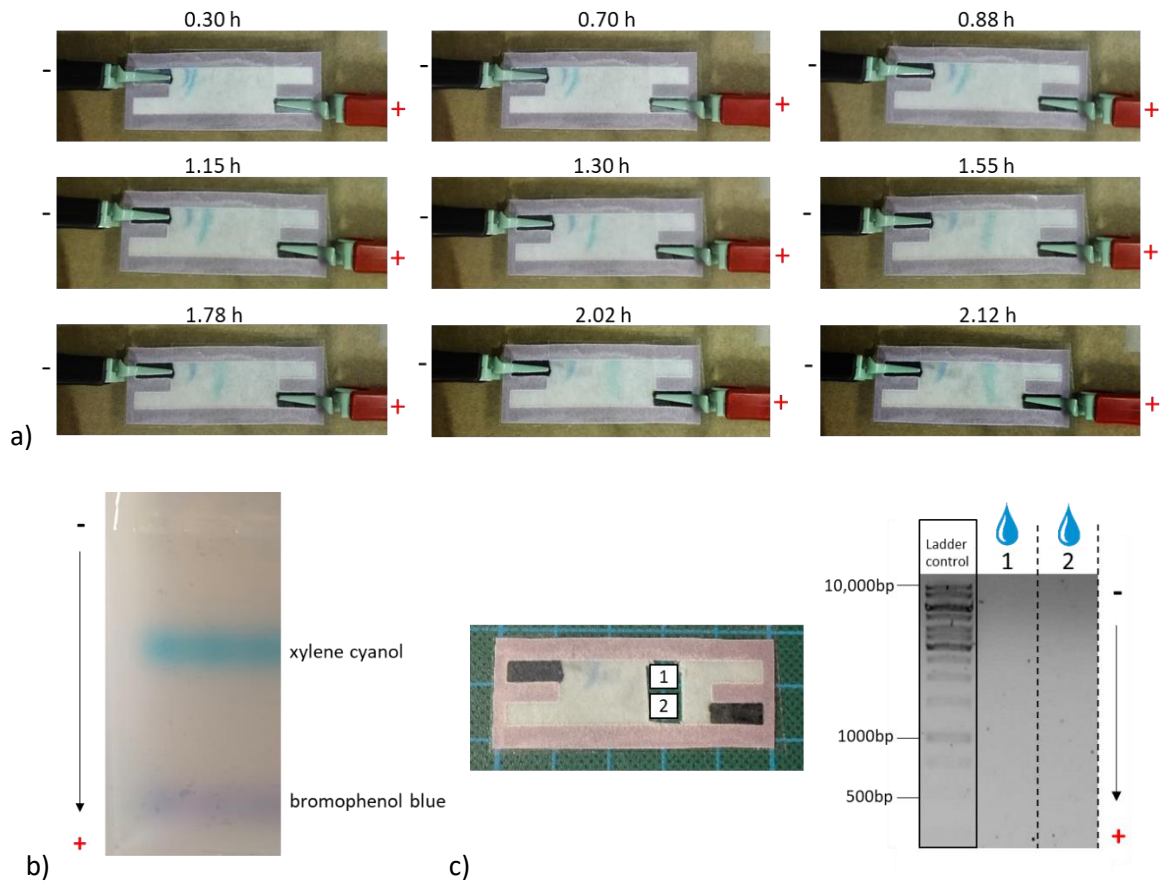


Figure A4: Cellulose fiber-based electrophoresis chip (Ahlstrom-Munksjö A388) connected by diagonally arranged PEDOT:PSS electrodes and crocodile clamps to a voltage source. a) A time series of images was recorded from the start of fiber electrophoresis until 2.12 h after connection to the voltage source. Upon the application of an electric field of 115 V the blue sample spot separated into two bands, with the turquoise xylene cyanole migrating to the opposite electrode. The fiber chip was covered by an adhesive foil to reduce evaporation during electrophoresis. b) The separation pattern of the tracking dyes on a 1 % agarose gel after electrophoresis at 115 V for 75 min and photographed in daylight. Bromophenol blue migrated faster than xylene cyanol and can be seen at the lower part of the agarose gel. c) Cut fiber area around the migrated band was treated with elution buffer 2 and the elution fractions were loaded onto a 1 % agarose gel for visualization after gel electrophoresis. No DNA samples could be eluted upon fiber electrophoresis on the cellulose filter paper. The sample mixture was loaded directly onto the gel as a ladder control and represents the original sample composition.

6.4.1. Alternative cellulose material and reduced chip geometry

In the following, it was investigated whether sample migration can be achieved by subsequent elution from a cellulose filter from another manufacturer. In addition, the chip geometry was reduced in order to reduce the possible effect that the long migration distance and drying of the fiber favors a retention of the DNA on the fiber.

Although the filters from both manufacturers are cellulose filters, they may differ in texture and residues, which could affect the experimental result. Both filter papers were treated with acid in the production procedure to remove any remaining organic and inorganic impurities and washed with

ultrapure water. In addition, both fiber types have low-ash grades of below 0.01 % and are therefore suitable for quantitative analyses where it must be ensured that no foreign substances are released (Sartorius Lab Instruments GmbH & Co.KG., 2021). The manufacturers do not disclose information on other residues. The filter paper from Macherey-Nagel differs slightly from Ahlstrom-Munksjö in terms of pores size, thickness, weight and filtration speed as can be seen from Table 14.

Table 14: Typical properties of the cellulose filter paper A338 from Ahlstrom-Munksjö and MN 640 W from Macherey-Nagel (Ahlstrom-Munksjö, 2018; Macherey-Nagel GmbH & Co.KG., 2019; Sartorius Lab Instruments GmbH & Co.KG., 2021).

	A338	MN 640 W
Average pores size	7-12 μm	12-15 μm
Thickness	0.21 mm	0.20 mm
Weight	85 g/m ²	85 g/m ²
Filtration speed	10 s/10 ml	9 s/10 ml

Since a smaller chip geometry resulted in shorter sample migration times and less evaporation surface, polymer structures with 1.2 x 2.3 cm dimensions were chosen in the following to pattern the fiber materials. Consequently, also the buffer volume and voltage were adjusted. After wetting the chip area with 80 μl distilled water and sample addition (1 μl 1 kb ladder VWR), the voltage was reduced to 90 V.

Using the MN 640 W cellulose filter of Macherey-Nagel, application of the electric field for 18 min was already sufficient to localize the turquoise tracking dye near the counter electrode as can be seen from Figure A5 a). This confirms the assumption that materials from different manufacturers, which differ slightly in their properties can have a great influence on the experiments. In this case, the larger pore size as well as differences during the manufacturing process (such as spreading over different sieves, compressing or drying of the filter paper) can lead to the faster sample migration across the Macherey-Nagel paper. In this experiment the chip area was cut into 5 pieces and the elution fractions were loaded onto the gel to verify whether the DNA sample was pulled across the fiber as shown in Figure A5 b). A faint band pattern could be seen in the lanes 3 and 4 corresponding to position 1 on the chip (1.1 and 1.2). No DNA patterns could be eluted at positions 2 and 3. This showed that some of the sample was still at the beginning of the chip after fiber electrophoresis. However, if the intensity of the elutions is compared with the sample originally applied on the chip and also loaded in column 1 on the gel, it can be seen that most of the sample could not be eluted and was probably still on the fiber. The closer to the anode, the more distinct a particular band with a size smaller than 250 bp became visible (elution fractions 2-3). It could also be detected from the area corresponding to the cathode (C1 and

C2). After comparison with PEDOT:PSS loaded onto the agarose gel it became clear that this band referred to some material of the imprinted electrode that was solved and migrated over the chip area (see Figure A5 c). After further tests, the elution result from the cellulose fiber could not be improved and was even fluctuating such that in some cases no bands could be detected at all.

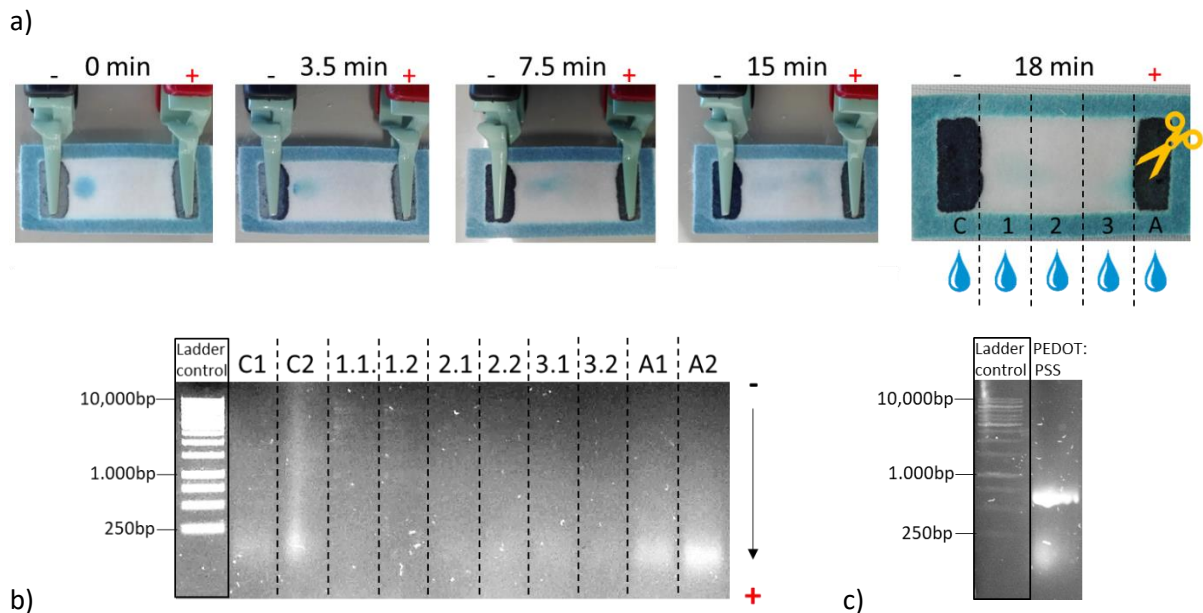


Figure A5: Cellulose fiber-based electrophoresis chip (Macherey-Nagel 640 W) connected by PEDOT:PSS electrodes and crocodile clamps to a voltage source. a) A time series of images was recorded from the start of fiber electrophoresis until the blue sample mixture (1 kb ladder) with blue tracking dyes reached the counter electrode upon 18 min exposure to an electric field of 90 V. Afterwards the chip area was cut into 5 pieces and each part was treated with elution buffer 2 separately. b) The elution fractions were loaded onto a 1 % agarose gel and visualized under UV light after agarose gel electrophoresis. An agarose with smaller pockets was used in this experiment and consequently the volume of the elution fractions was divided into two pockets indicated by 1 and 2 for each position. A faint signal of the ladder sample could be detected from the position 1.1 and 1.2 and a distinct band below 250 bp could be observed in the elution fraction of the area from the cathode (C) and anode (A) and the chip positions 2 and 3. The sample mixture was loaded directly onto the gel as a ladder control and represents the original sample composition. c) Loading of the PEDOT:PSS ink onto an agarose gel confirmed that the band below 250 bp corresponds to electrode material that detached from the imprinted electrode during fiber electrophoresis and ran along on the fiber chip.

6.4.2. Influence of cellulose patterning on DNA detection

Since patterning of the fiber chips with the blue wax-like polymer requires heat to briefly melt it and allow it to penetrate the fiber network, the surface properties of the cellulose paper may have changed. As shown in the previous chapter 3.4., nonspecific DNA retention on cellulose can be induced by heat application. To investigate whether the application of heat during the patterning of the paper affected the subsequent migration of the DNA sample and prevented detection by elution, the conductive ink was applied to a plain, not patterned piece of A388 cellulose paper. After 45 min of fiber electrophoresis at 90 V, the blue spot has migrated towards the anode as can be seen from Figure A6. Only one additional wetting step, consisting of 20 μ l distilled water after 20 min was carried out in this experiment. The missing boundary and probably oblique field lines caused that the tracking dye migrated to the upper edge of the paper. The chip area was divided into thirds and elution buffer was added to each piece. After the elution fractions were loaded onto an agarose gel and gel electrophoresis was performed, the DNA bands of the sample mixture were detectable. Most of the sample was still traceable at the site of sample application and thus did not migrate, with small concentrations of sample migrating towards the counter electrode. Consistent with the previous results of chapter 3.4. where the DNA molecules of the non-heat-treated cellulose fibers could be recovered, the absence of heat treatment during the patterning process seems to have a positive effect on sample elution in this case as well. However, these results also showed that unlike in an agarose gel electrophoresis, the tracking dyes in an electrophoresis performed on cellulose appeared to move independently of the main part of the DNA sample.

Contrary to expectation, no size-dependent migration is evident, as fragments of all sizes can also be detected upstream of the anode. The tracking dyes therefore seem to behave differently on cellulose fiber than in agarose gels. They do indicate the arrival of sample material, but not depending on their size. A possible correlation between the lack of sample separation and the pore size is discussed in section 3.5.2.1.

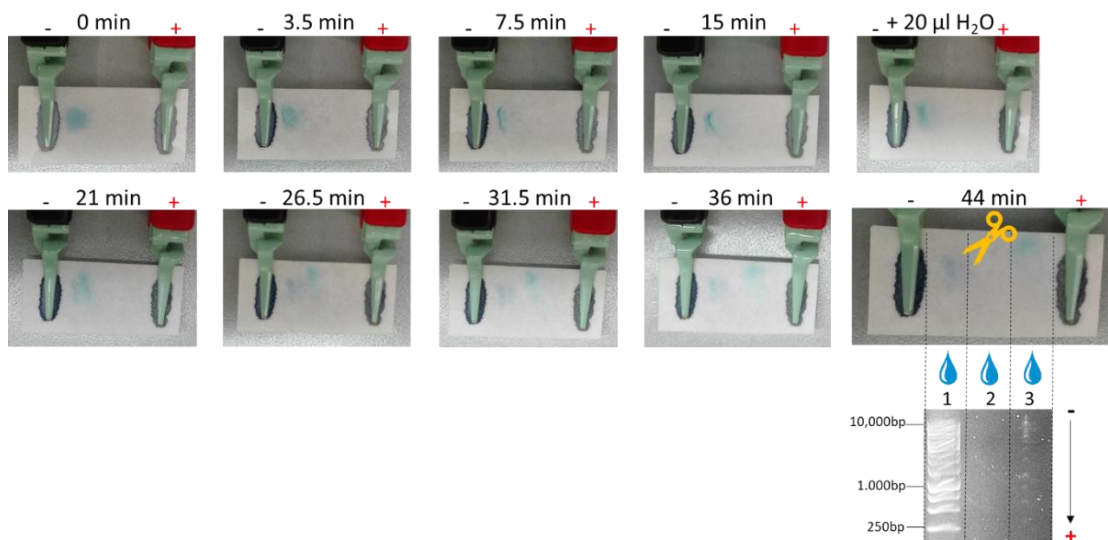


Figure A6: Cellulose fiber-based electrophoresis chip (Ahlstrom-Munksjö A388) without hydrophobic polymer outline, connected by PEDOT:PSS electrodes and crocodile clamps to a voltage source. a) A time series of images was recorded from the start of fiber electrophoresis until 44 min after connection to the voltage source. Upon the application of an electric field of 90 V the sample mixture (1 kb ladder) with two tracking dyes separated into two bands, with xylene cyanole migrating to the opposite electrode. After termination of the voltage exposure, the fiber area has been divided into thirds by cutting, treated with elution buffer 2 and the elution fractions were loaded for gel electrophoresis on a 1 % agarose gel. The majority of the sample remained in front of the cathode (position 1) but bands of all fragment sizes could also be eluted from the area in front of the anode (position 3) with lower concentration, confirming the successful migration of the DNA sample.

6.5. Test of a new channel pattern via fiber electrophoresis with textile dyes

Textile dyes instead of DNA samples were used in fiber electrophoresis to test a new pattern with two channels connected via the same imprinted electrode on glass fibers. For this purpose, 1 µl of a blue textile dye and 1 µl of an orange textile dye were each loaded on one of the channels on the glass microfiber chip (see Figure A7). The geometry of the imprinted electrode stayed unchanged, consequently both channels were connected through the same electrodes. While the blue dye loaded in channel a) disappeared during electrophoresis, as already seen before when the DNA mixture with the blue indicator dyes was tested in glass microfiber electrophoresis, the orange dye loaded in channel b) initially spread over the entire chip area and then accumulated in front of the counter electrode.

Reversal of polarity and a second fiber electrophoresis was also possible. In this case, the chip was rotated by 180 degrees and reconnected to the crocodile clamps. The second fiber electrophoresis showed the same running pattern, the orange textile dye in channel b) was distributed over the entire length of the channel and finally recovered at the channel end corresponding to the initial sample loading zone of the first run. The blue textile color no longer appeared. This result implies that more

than one sample can be processed at a time and multiple movements were also possible, for example, by moving the sample back and forth in the channel. If the use of tracking dyes during fiber electrophoresis is desired, light blue should not be considered because the contrast is insufficient to observe sample migration through the fiber.

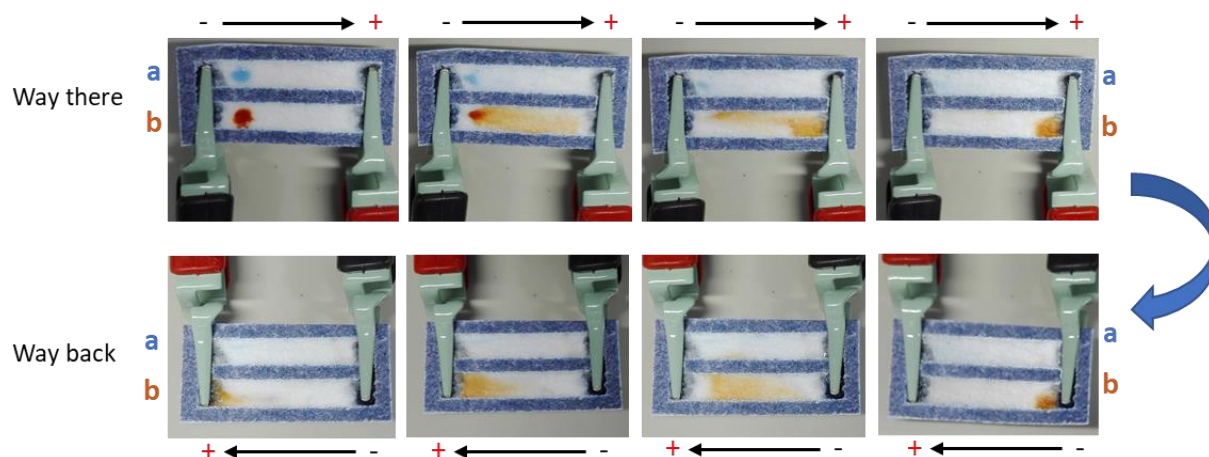


Figure A7: Two channelled glass microfiber-based electrophoresis chip (Whatman GF/F) tested for sample migration there and back with a blue and orange textile dye. Blue dye disappears upon exposure to the electric field (90 V) but the orange dye could be tracked during the movement along the chip channel. After the dye reached the end of the channel, the chip was rotated 180 degrees and reconnected to the voltage source. The orange dye also migrates here to the positively charged pole and is finally concentrated at the sample application site again.

6.6. Current based read-out of DNA sample migration on glass microfiber with imprinted electrodes consisting of PEDOT:PSS

A digital multimeter, connected to a computer, was placed between the connecting crocodile clamps and the voltage source and used to record the current values between the cathode and anode. Figure A8 a) shows the current signals for the ladder samples with DNA fragment mixtures of 25-500 bp (25 bp ladder) and 250-10,000 bp (1 kb ladder) in single-channel fiber chips. Also both mixtures together were tested regarding their current signals on a fiber chip with two channels. Each curve corresponds to one chip and all samples were tracked for 9 min after loading to ensure the arrival of the DNA sample at the end of the electrophoresis chip. The curves of all samples show a current increase in the first 3 min followed by a continuous signal drop to about 80-120 μA . The ladder containing smaller fragments (25-500 bp) showed a current increase about 50 μA after 80 sec of voltage exposure, whereas the current signal of the DNA fragments ranging from 250-10,000 bp increased about 300 μA with a maximum at 700 μA after 60 sec. Both sample mixtures applied on one chip led to an increase of about 360 μA , and resulted in the highest maximum at 750 μA after about

90 sec. It seems as if the values of the individual samples add up when both samples are measured simultaneously on one chip.

Compared to the observations just described, the current signals from fiber chips with electrodes fabricated on a different day differ as can be seen in Figure A8 b). Contrary to the results observed before, the sample mixture with the smallest fragments showed the highest current values. However, if all signals were normalized to a common starting point, the current signal of the ladder with fragments from 25-500 bp would again be the lowest. But even after normalization, the intensities and timing of the current signals of the 25 bp ladder and the 1 kb ladder were reversed compared to the previous experiment. Nevertheless, the increase was higher for all sample chips compared to control chips measuring just water as background signal. In this case, a volume of 1 μL water was applied instead of the sample to rule out the possibility of inducing a current signal due to the mere addition of liquid during the application of the sample.

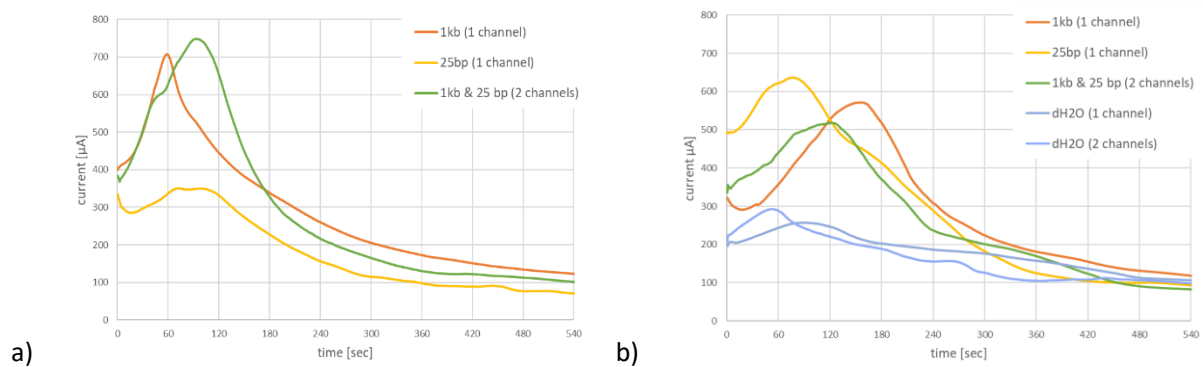


Figure A8: Current signals of glass microfiber electrophoresis chips with imprinted PEDOT:PSS electrode and voltage application of 90 V upon sample or water addition. a) Single-channel fiber electrophoresis chips show a current increase of 50 μA when a 25 bp ladder with tracking dyes (25-500 bp fragments in yellow) was added as sample and an increase of 300 μA after a 1 kb ladder with tracking dyes (250-10,000 bp fragments in orange) was tested. Both samples added to a chip with two channels led to a current increase of 360 μA . b) A current increase could be detected for all sample compared to the controls with just water (blue). The 25-500 bp sample mixture (yellow) showed the highest current peak followed by the 250-10,000 bp ladder (orange) and both sample mixtures loaded onto a dual-channel chip (green).

6.7. Repetitions of the current-based readout of DNA

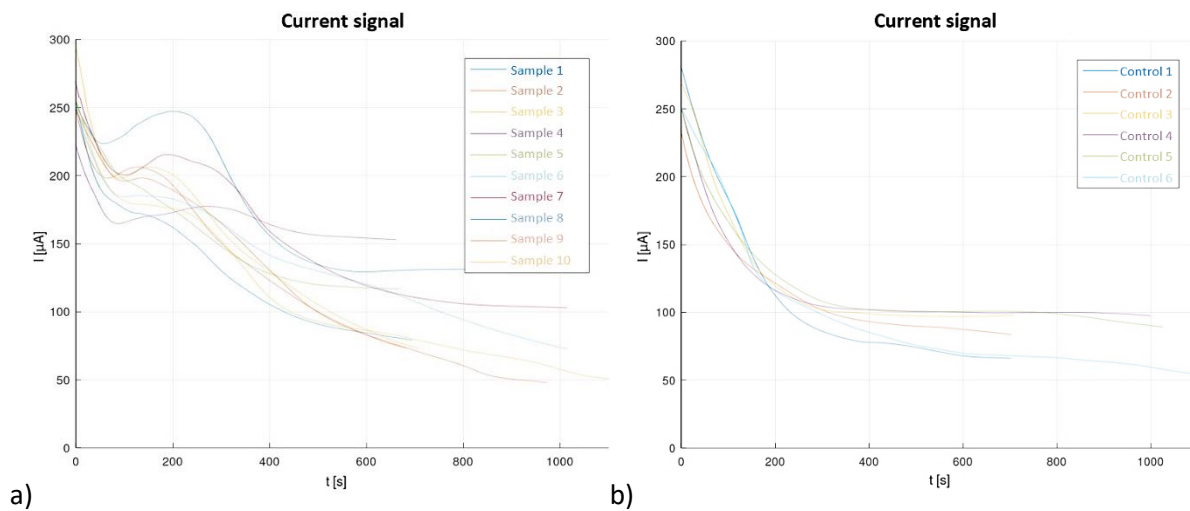


Figure A9: Current signals of fiber electrophoresis chips with imprinted carbon paste electrodes upon sample or buffer addition. a) The curves of 9 glass microfiber chips with 5 μg of the 1 kb ladder as sample showed an increase in current signals between 50-400 sec after sample addition. b) The 6 control chips without sample but 5 mM Tris running buffer addition instead showed an exponential decrease of the current signal. Both diagrams show the current signals after the application of the sample or buffer.

6.8. Restriction digestion of genomic *L. pneumophila* Philadelphia DNA by restriction enzymes SmlI and BseI

The gel image (see Figure A10 a) shows untreated and digested gDNA with SmlI after one hour loaded on a 1 % agarose gel and documented after electrophoresis at 120 V for 1 h. Untreated gDNA from *Legionella* has a size of 3.4×10^6 bp, as previously described, and appeared as an intense band at the upper part of the gel (see lane 1). For size estimation, the gel concentration is not suitable here and can only be detected as above 10,000 bp. But in the following the focus was on the detection of the fragments occurring upon restriction digestion and comparison to the uncut DNA sample. In comparison to the large gDNA, the DNA is reduced in size after incubation with the restriction enzymes (see lane 3), which can be transported further to the lower edge of the gel in the electric field of electrophoresis. Here, a clear reduction and thus successful fragmentation of the gDNA can be seen, but distinct bands corresponding to DNA fragments are difficult to detect. For improved visualization of the numerous fragments after cleaving, the digestion mix was loaded on an agarose gel with lower agarose concentration and electrophoresis was performed at low voltage of 25 V for 17.5 h. Different options for the fragmentation with SmlI, differing in enzyme amount and incubation time were tested and can be seen in columns 2 to 5 of Figure A10 b). In the first reaction, shown in column 2, 0.1 μl SmlI was tested with an incubation time of 1 h. In column 3, 4 and 5 the reactions tested with 0,5 μl

restriction enzyme were loaded. These reactions differ in incubation time of the gDNA with the restriction enzyme and were loaded after 1, 7 and 16 h. Furthermore, the samples shown in lanes 2 and 3 were loaded after heat inactivation of the enzyme whereas the samples 4 and 5 were loaded without heat inactivation. It can be observed that an increase of the enzyme amount resulted in a slightly increased band pattern. An increase of the incubation time from 7 to 16 h also increased the intensity of the band pattern, visible by darker bands, and showed the best results of these four tested reactions. BseSI, another restriction enzyme working at 37°C and tested in parallel, was not suitable for cutting the DNA from *Legionella* because only a broad smeared band instead of distinct bands could be seen after loading on an agarose gel as shown in lane 6. In principle, fragmentation of genomic *L. pneumophila* Philadelphia was then possible with SmlI but despite the optimized conditions, a satisfactory result was not yet obtained and further restriction enzymes were tested in the following.

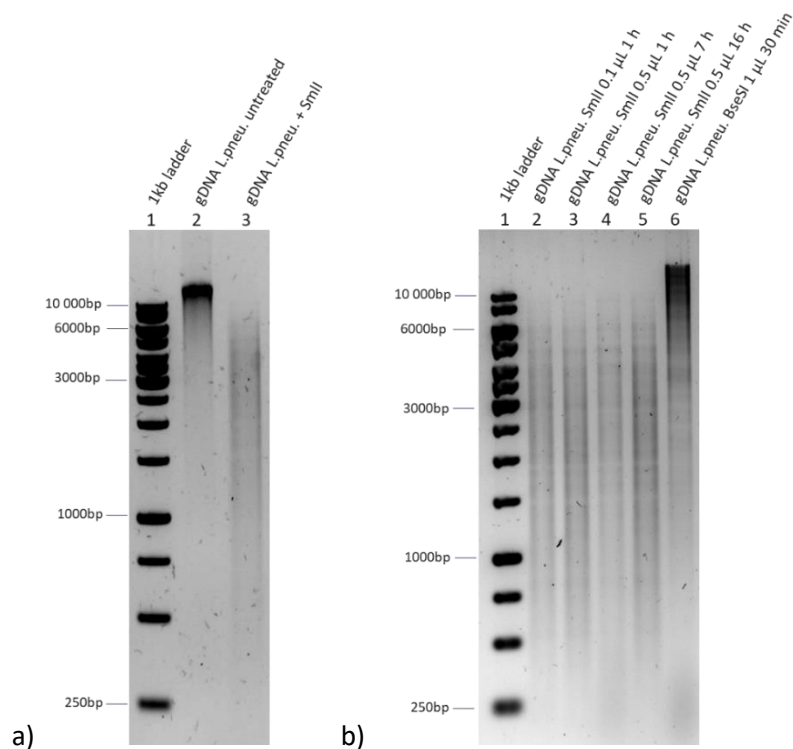


Figure A10: Fragmentation pattern of gDNA from *L. pneumophila* Philadelphia by restriction enzymes SmlI and BseSI. After incubation of extracted gDNA with SmlI at 55°C and BseSI at 37°C the digestion mixes were loaded on a 1 % agarose gel and gel electrophoresis was run at 120 V for 75 min. a) Comparison of the untreated gDNA (lane 2) and digested with SmlI (lane 3) led to a size decrease but smeared DNA band pattern. b) Test of different digestion conditions like enzyme volume (0.1-0.5 μl) as well as incubation duration (1-16 h) of SmlI with gDNA (lanes 2-5). BseSI restriction enzyme showed only a slightly fragmentation upon incubation at 37°C for 30 min (lane 6). A 1 kb ladder was loaded as a size reference in lane 1 of each gel.

6.9. Restriction digestion of gDNA from *L. pneumophila* Philadelphia, *E. coli* and *P. aeruginosa* by restriction enzymes HaeIII and HhaI

E. coli and *P. aeruginosa* were treated with the enzymes HaeIII and HhaI in the same way as *L. pneumophila* Philadelphia and the restriction patterns are shown in Figure A11. The untreated gDNA of those strains remained like the one of *L. pneumophila* Philadelphia on the top of the gel during agarose gel electrophoresis (compare lanes 5-7). The gDNA from *E. coli* and *P. aeruginosa* cut by HaeIII and HhaI resulted in much smaller fragment sizes compared to the DNA of *L. pneumophila* Philadelphia treated with the same enzymes. Since the majority of fragments were between 250 bp and 500 bp in length, they were collected as an undifferentiable cloud at the bottom of the gel instead of spreading as a banding pattern throughout the gel.

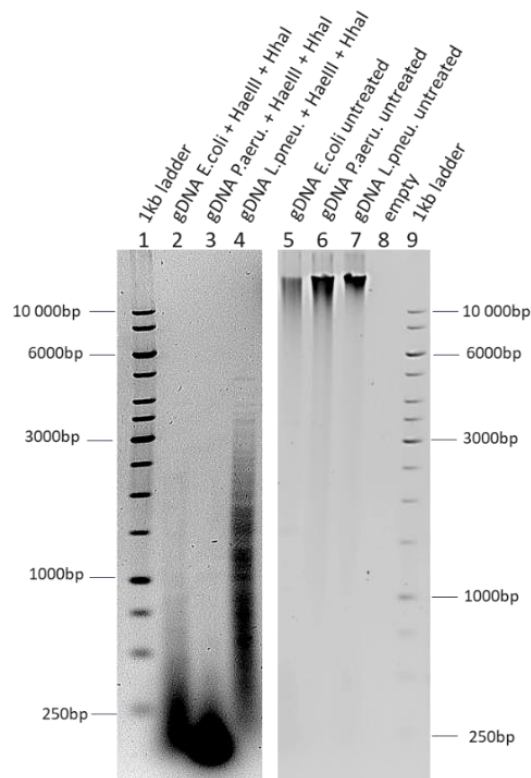


Figure A11: Fragmentation of gDNA from *L. pneumophila* Philadelphia, *E. coli* and *P. aeruginosa* with restriction enzymes HaeIII and HhaI. Samples were loaded on a 0.7 % agarose gel and visualized after gel electrophoresis for 17.5 h. Untreated gDNA of all strains (lanes 5-7) used as template DNA for the digestion showed one band at nearly the same height on top of the agarose gel. Digestion of DNA isolated from *E. coli* and *P. aeruginosa* with HaeIII and HhaI resulted in small and smeared fragments (lanes 2 and 3) compared to *L. pneumophila* Philadelphia (lane 4). A 1 kb ladder was loaded as a size reference (lane 1). No sample was loaded in lane 8.

Although the fragmentations turned out so differently, it was tested on the fiber incubated with the probe as shown in Figure A12. In contrast to the uncut DNA from *L. pneumophila* Philadelphia or *E. coli*, the fragmented DNA from *L. pneumophila* Philadelphia was well distinguishable in a significant manner from the background signal of the probe tested without target as seen before. The uncut DNA of

P. aeruginosa was not tested here in the FISH experiment because no difference was expected from the genomic DNA of *L. pneumophila* Philadelphia or *E. coli* based on the gel image. Also the comparison to the enzyme control in which the restriction enzyme was tested without DNA and just incubated with the probe showed lower mean signal intensities about 50 similar to the uncut DNA from *L. pneumophila* Philadelphia. The complementary target was taken as a positive control and showed again a 2.5-fold increase compared to probe without target. No differentiation between the fluorescence signals occurring from the probe incubated with the fragmented gDNA of *L. pneumophila* Philadelphia and *P. aeruginosa* or *E. coli* was possible. The mean intensity values were similar between 75 and 80 and showed large standard deviations which made a differentiation between the strains not possible.

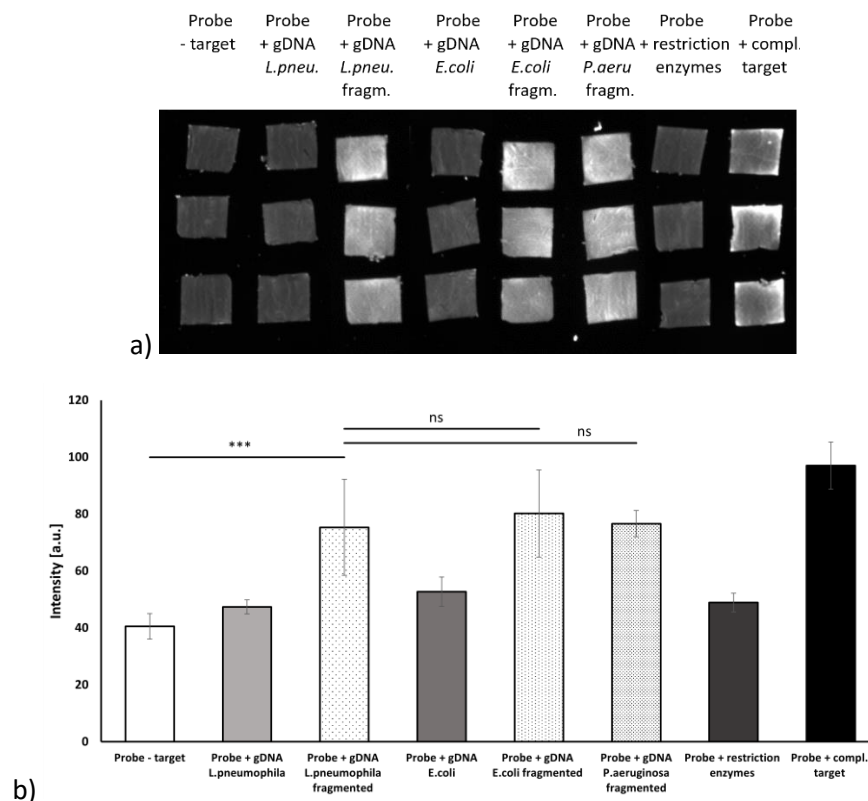


Figure A12: FISH of the molecular beacon with fragmented gDNA of *L. pneumophila* Philadelphia, *E. coli* and *P. aeruginosa* on glass microfiber. A) Measurements of probe without target ($n=6$), probe and untreated gDNA from *L. pneumophila* Philadelphia ($n=3$) and *E. coli* ($n=3$), and gDNA from *L. pneumophila* Philadelphia and *E. coli* and *P. aeruginosa* fragmented with HaeIII and HhaI ($n=6$). The enzymes without DNA ($n=3$) and the reverse complementary target sequence ($n=3$) were added after mixing with the molecular beacon probe to 5 x 5 mm pads of glass microfiber. After heating (95°C 2 min, 55°C 2 min, 25°C 2 min) the fibers were imaged under UV light. B) The fluorescence intensities were evaluated using the ImageJ program. The fluorescence from hybridization of the probe and fragmented DNA from *Legionella* was not distinguishable from fragmented DNA from *E. coli* or *P. aeruginosa* (***) $p < 0.001$; ns not significance; student's t-test).

6.10. Paper-based ELISA

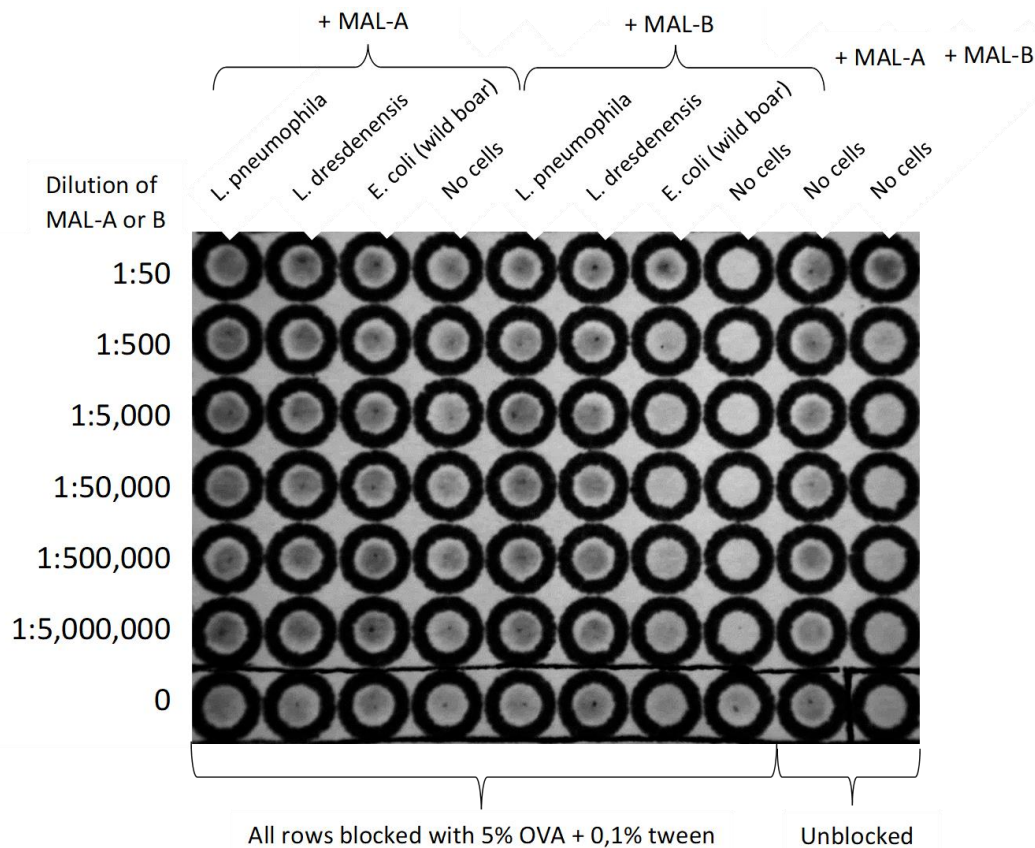


Figure A13: Paper-based ELISA for the test of mouse-anti-*Legionella* sera A and B (MAL-A & MAL-B) from two immunized mice. The patterned filter paper (cellulose paper 640 M) was first incubated with the bacterial suspensions of *L. pneumophila* Philadelphia, *L. dresdenensis* or an *E. coli* isolated from a wild boar. Unspecific binding was blocked with 5 % OVA + 0.1 % Tween and the antibody sera MAL-A and MAL-B were tested in dilutions ranging from 1:50-1:5,000,000 diluted in 1 x PBS. After washing, the second antibody goat-anti-mouse-HRP was added to each spot. After a second washing step the TMB working solution was added to each well and the signal was documented by a smart phone camera. The image was converted to black and white for a better detection of the signal differences. MAL-B showed a much lower non-specific background signal than MAL-A (columns 4 & 9) on the unblocked fiber (column 10) as well as on the blocked "no cells" control (column 8). At dilutions equal or greater than 1:500, MAL-B can already specifically discriminate between *Legionella* (columns 5 & 6) and *E. coli* (column 7), as no signal was detectable in the latter. A differentiation between *L. pneumophila* Philadelphia (column 5) and *L. dresdenensis* (column 6) was not visible to the naked eye and indicates that, as desired, the antibodies contained in the tested serum use a cross-species target for detection. The secondary antibody in the last row also showed a slightly non-specific signal, which would have to be subtracted if the intensity values were examined more closely. Based on these results, mouse-anti-*Legionella* serum B was selected for the further antibody development.

6.11. Bacterial viability test by staining with ChemChrome V6

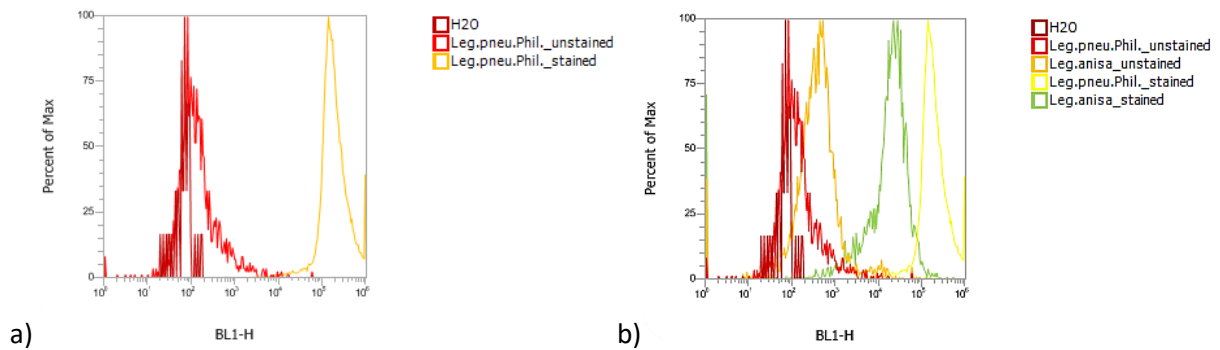


Figure A14: Fluorescence histograms of different *Legionella* species stained with ChemChrome V6. In this histogram plot, the horizontal axis corresponds to the height signal intensity of the blue channel (BL1) while the vertical axis represents the number of events (count) and shows the relative number and distribution of events. For comparison of several measurements the counts were normalized by the Attune software and displayed in a percentage scale from 0 to 100 %, where 100 % is the histogram peak value. a) The metabolic active stained *Legionella pneumophila* Philadelphia cells are showing a peak at 100,000 fluorescence units (yellow) and could be well distinguished from the unstained population showing a peak at 75 (bright red). As background controls ultrapure water (dark red) was taken. b) Also *L. anisa* could be successfully stained by ChemChrome V6 and distinguished from an unstained population. After comparing the two strains, it can also be observed that for the same inserted cell numbers, the fluorescence signal is greater for *L. pneumophila* Philadelphia (yellow) than *L. anisa* (green). The signal of the unstained cell population is higher when measuring *L. anisa* (orange) than *L. pneumophila* Philadelphia (bright red). However, the two stained strains can also be clearly distinguished well from each other based on their separate peak signals.

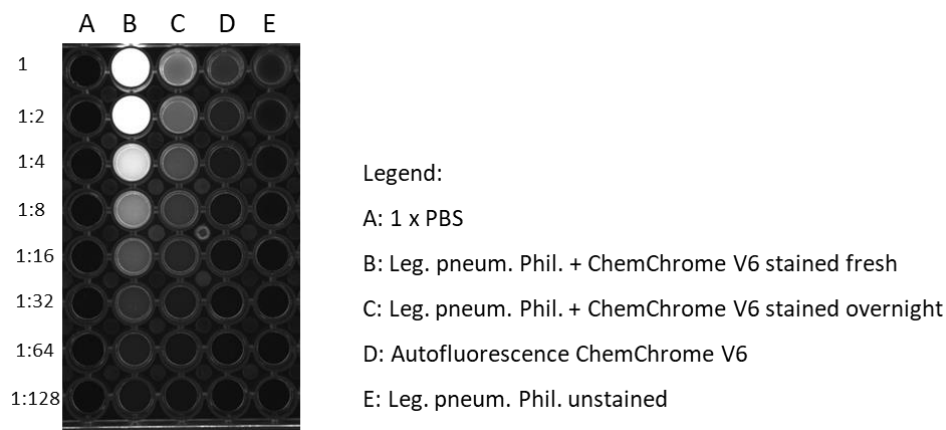


Figure A15: Dilution series of ChemChrome V6 for staining of metabolic active *L. pneumophila* Philadelphia cells. These results show that fresh staining (B) gives better results, as the signal from the overnight culture was less intense (C) and indicates that many cells were already no longer metabolically active. The fluorescence signal of both cultures decreases with increasing dilution of ChemChrome V6. The ChemChrome V6 also diluted freshly, shows a slightly background signal if it was tested undiluted. As controls pure 1 x PBS (A) and an unstained culture (E) at the same concentration as the stained culture were taken and showed no fluorescent signal. In the future, ChemChrome V6 can be used for the detection of *Legionella* even diluted, e.g., using a 1:4 dilution, and still provides good signals.

6.12. Octave script

```
function natascha1 (varargin)
  pkg load instrument-control
  pkg load signal
  pkg load statistic
  fprintf("Hier startete Natascha Messplatine v.1\n");
  system("gpio export 23 out");
  system("gpio -g write 23 0");
  global opts;
  init_opts();
  init_gpio;
  opts.adc = i2c("/dev/i2c-1"); # init I2C
  set_U_bias(1.66666);
  set_U(0);
  pause(5);
  if 0
    system("gpio -g write 23 1");
    W=[];
    for j=1:100
      W=[W; get_E1() get_E2() get_E3()];
      mW=mean(W,1);
      fprintf('E1_offset=%f E2_offset=%f E3_offset=%f \n', ...
        mW(1)+opts.E1_offset,mW(2)+opts.E2_offset,mW(3)+opts.E3_offset);
      fflush(stdout);
    end
    system("gpio -g write 23 0");
    fprintf("\nopts.E1_offset=%f; opts.E2_offset=%f; opts.E2_offset=%f; \n\n', ...
      mW(1)+opts.E1_offset,mW(2)+opts.E2_offset,mW(3)+opts.E3_offset);
    fflush(stdout);
    return;
  end
  opts.E1_offset=0.045645; opts.E2_offset=0.022917; opts.E2_offset=0.034054;
  if 0
    set_U(0);
    system("gpio -g write 23 1");
    pause(1);
    #system("gpio -g write 23 0");
    return;
  end
  opts.U_offset = 0.963;
```

```

if 0
    system("gpio -g write 23 1");
    U_max=45;
    du=U_max/5; U_l=[]; MZdR=[]; U=[];
    for u=[du:du:U_max U_max:-du:-U_max -U_max:du:0]
        if abs(u)<U_max/10 continue; end
        set_U(u); pause(1);
        u_l=get_E4();
        fprintf('%s %s\n',sprintf('%10f',u),sprintf('%10f',u_l));
        mZdR=-u_l/u*1e+6;
        U_l=[U_l u_l]; MZdR=[MZdR mZdR]; U=[U u];
    end
    coeffs=regress(U_l,[ones(size(U))' U'])
    dE4_Offset=coeffs(end-1)
    Z=1e+6*coeffs(end)
    fprintf('E4_offset=%f\n',dE4_Offset+opts.E4_offset);
    system("gpio -g write 23 0");
    #plot(U,U_l,');
    return;
end
opts.Z_l=-616.35; opts.E4_offset=-0.008317; # Jumper 4 ( 1k) Messbereich 1000µA
system("gpio -g write 23 1");
t_mess=173
dt=0.5; # das minimale Zeitintervall ist 0.2s
tic; t_0=toc; t=t_0; n=1;
out_string=sprintf('%10s %10s %10s %10s %10s %10s %10s %10s %10s %10s\n',t_in_s,'U_in_V','E1_in_V','E2_in_V','E3_in_V','I_in_muA','s01_in_muS','s12$
fname=['messung_' datestr(now(),'yyyymmdd_HHMMSS') '.log'];
fid=fopen(fname,'w');
    fprintf('%s',out_string);
    fprintf(fid,'%s',out_string);
fclose(fid);
while t<t_mess+dt
    U=45; t=toc; #U=t-dt;
    #U=25+35*sin(2*pi*t/50);
    set_U(U); t=toc; while (t-t_0)<(n*dt) pause(0.005); t=toc; end
    E1=get_E1();
    E2=get_E2();
    E3=get_E3();
    I=get_E4()/opts.Z_l*1e+6; # Strom in µA
    S01=I/E1;
    S12=I/(E2-E1);

```

```

    S23=I/(E3-E2);
    S34=I/(U-E3);
    out_string=sprintf('%s %s %s %s %s %s %s %s %s\n',sprintf('%10.2f',t- dt),sprintf('%10.3f',U),
    sprintf('%10.3f',E1),sprintf('%10.3f',E2),sprint$
    out_string=strrep(out_string,',','');
    fid=fopen(fname,'a');
    fprintf('%s',out_string);
    fclose(fid);
    n=n+1;
end
set_U(0);
system("gpio -g write 23 0");
return;
function y=get_U_bias0()
global opts;
i2c_addr(opts.adc, 0x48); # Set i2c slave address, see datasheet (Table 8)
opts.control_low =opts.sps128+opts.comp_after_2_conversion+opts.comp_pol_active_high;
opts.control_high=opts.flag_single+opts.FSR4_096+opts.singleshot+opts.P3;
i2c_write(opts.adc, uint8( [1 opts.control_high opts.control_low] ));
a=0; while a(1)<128 a=i2c_read(opts.adc, 1); end # wait until conversion is finished
i2c_write(opts.adc,uint8(0)); val=double(i2c_read(opts.adc,2)); y=val(1)*256+val(2); if y>(2^15-1) y=y-2^16;
end
y=y*4.096/(2^15-1)-opts.U_bias_offset; # Volt
function y=get_U_bias1()
global opts;
i2c_addr(opts.adc, 0x49); # Set i2c slave address, see datasheet (Table 8)
opts.control_low =opts.sps128+opts.comp_after_2_conversion+opts.comp_pol_active_high;
opts.control_high=opts.flag_single+opts.FSR4_096+opts.singleshot+opts.P3;
i2c_write(opts.adc, uint8( [1 opts.control_high opts.control_low] ));
a=0; while a(1)<128 a=i2c_read(opts.adc, 1); end # wait until conversion is finished
i2c_write(opts.adc,uint8(0)); val=double(i2c_read(opts.adc,2)); y=val(1)*256+val(2); if y>(2^15-1) y=y-2^16;
end
y=y*4.096/(2^15-1)-opts.U_bias_offset; # Volt
function y=get_E1()
global opts;
i2c_addr(opts.adc, 0x48);
opts.control_low =opts.sps128+opts.comp_after_2_conversion+opts.comp_pol_active_high;
opts.control_high=opts.flag_single+opts.FSR2_048+opts.singleshot+opts.P2_N3;
i2c_write(opts.adc, uint8( [1 opts.control_high opts.control_low] ));
a=0; while a(1)<128 a=i2c_read(opts.adc, 1); end # wait until conversion is finished
i2c_write(opts.adc,uint8(0)); val=double(i2c_read(opts.adc,2)); y=val(1)*256+val(2); if y>(2^15-1) y=y-2^16;
end
y=y*2.048/(2^15-1);
y=-y*200/3.3-opts.E1_offset; # Volt

```

```

function y=get_E2()
    global opts;
    i2c_addr(opts.adc, 0x48);
    opts.control_low =opts.sps128+opts.comp_after_2_conversion+opts.comp_pol_active_high;
    opts.control_high=opts.flag_single+opts.FSR2_048+opts.singleshot+opts.P1_N3;
    i2c_write(opts.adc, uint8( [1 opts.control_high opts.control_low] ) );
    a=0; while a(1)<128 a=i2c_read(opts.adc, 1); end
    i2c_write(opts.adc,uint8(0)); val=double(i2c_read(opts.adc,2)); y=val(1)*256+val(2); if y>(2^15-1) y=y-2^16;
end
    y=y*2.048/(2^15-1);
    y=-y*20/33-opts.E4_offset; # Volt
function set_U_bias(v)
    global opts;
    v= v/3.3*opts.maxpwm;
    v= round(v);
    system(["gpio pwm 23 " num2str(v,'%d')]);
function set_U(v)
    global opts;
    v=v-opts.U_offset;
    v= 20000 - v*200;
    v= round(v);
    system(["gpio pwm 26 " num2str(v,'%d')]);
function init_opts()
    global opts
    opts.flag_single=0b10000000;
    opts.P0_N1   =0b00000000;
    opts.P0_N3   =0b00010000;
    opts.P1_N3   =0b00100000;
    opts.P2_N3   =0b00110000;
    opts.P0      =0b01000000;
    opts.P1      =0b01010000;
    opts.P2      =0b01100000;
    opts.P3      =0b01110000;
    opts.FSR6_144 =0b00000000;
    opts.FSR4_096 =0b00000010;
    opts.FSR2_048 =0b00000100;
    opts.FSR1_024 =0b00000110;
    opts.FSR0_512 =0b00001000;
    opts.FSR0_256 =0b00001010;
    opts.continuous=0b00000000;
    opts.singleshot =0b00000001;
    opts.sps8      =0b00000000;

```

```
opts.sps16 =0b00100000;
opts.sps32 =0b01000000;
opts.sps64 =0b01100000;
opts.sps128 =0b10000000;
opts.sps256 =0b10100000;
opts.sps474 =0b11000000;
opts.sps860 =0b11100000;
opts.comp_mode_traditional =0b00000000;
opts.P1_N3 =0b00100000;
opts.P2_N3 =0b00110000;
opts.P0 =0b01000000;
opts.P1 =0b01010000;
opts.P2 =0b01100000;
opts.P3 =0b01110000;
opts.FSR6_144 =0b00000000;
opts.FSR4_096 =0b00000010;
opts.FSR2_048 =0b00000100;
opts.FSR1_024 =0b00000110;
opts.FSR0_512 =0b00001000;
opts.FSR0_256 =0b00001010;
opts.continuous =0b00000000;
opts.singleshot =0b00000001;
opts.sps8 =0b00000000;
opts.sps16 =0b00100000;
opts.sps32 =0b01000000;
opts.sps64 =0b01100000;
opts.sps128 =0b10000000;
opts.sps256 =0b10100000;
opts.sps474 =0b11000000;
opts.sps860 =0b11100000;
opts.comp_mode_traditional =0b00000000;
opts.comp_mode_window =0b00010000;
opts.comp_pol_active_low =0b00000000;
opts.comp_pol_active_high =0b00001000;
opts.comp_no_latch =0b00000000;
opts.comp_latch =0b00000100;
opts.comp_disable =0b00000011;
opts.comp_after_1_conversion=0b00000000;
opts.comp_after_2_conversion=0b00000001;
opts.comp_after_4_conversion=0b00000010;
opts.maxpwm =40000;
opts.U_R_offset = 0;
```

```

    opts.l_offset = 0;
    opts.U_C_offset = 0;
    opts.U_bias_offset = 0;
    opts.E1_offset = 0;
    opts.E2_offset = 0;
    opts.E3_offset = 0;
    opts.E4_offset = 0;
    opts.U_offset = 0;
function init_gpio
    global opts;
    gpio_initialized=0;
    if exist('/tmp/gpio_initialized')
if exist('/tmp/gpio_initialized')
        fid=fopen('/tmp/gpio_initialized'); x=strtrim(fgets(fid)); fclose(fid);
        if strcmp(x,'1'); gpio_initialized=1; end
    end
    if gpio_initialized==0
        system("gpio mode 23 pwm"); # gpio 23 entspricht U_bias
        system("gpio mode 26 pwm"); # gpio 26 entspricht U_soll
        system("gpio pwm-bal");
        system("gpio pwmc 8");
        system(["gpio pwmr " num2str(round(opts.maxpwm))]);
        system(["gpio pwm 23 " num2str(round(opts.maxpwm/2))]);
        system(["gpio pwm 26 " num2str(round(opts.maxpwm/2))]);
pwm20000=-10V
        fid=fopen('/tmp/gpio_initialized','w'); fprintf(fid,'1'); fclose(fid);
        gpio_initialized=1;
    end
end

```

7. Acknowledgement

Bei Prof. Carsten Beta und Dr. Robert Niedl möchte ich mich ganz herzlich für das spannende Thema, die wissenschaftliche Freiheit und die stetige Unterstützung und Ermutigung während meiner Doktorarbeit bedanken. Robert deine grenzenlose Motivation für biotechnologische Fragestellungen hat mich immer wieder angesteckt. Danke auch dafür, dass du immer an mich geglaubt hast. Lieben Dank Carsten, dass deine Tür für mich immer offenstand und du mir mit deiner fachlichen Expertise jederzeit weitergeholfen hast.

Auch bei Prof. Dieter Jahn und Prof. Frank Bier möchte ich mich für die Übernahme der Gutachten besonders bedanken.

Prof. Fred Lisdat möchte ich für die hilfreichen Ratschläge und die Unterstützung bei dem Verfassen der Publikation danken.

Klaus Hellmuth gilt mein Dank für die Durchführung der Schmelzkurven und Gero Göbel für die Bereitstellung der mikroskopischen Aufnahmen der Elektroden.

Mein Dank gilt zudem all meinen Kollegen/innen, mit denen ich in den letzten Jahren zusammengearbeitet habe. Danke für eure Unterstützung!

Dr. Alexander Anielski möchte ich für die elektronischen Messkreationen bedanken ohne die diese Arbeit nicht möglich gewesen wäre. Darüber hinaus danke ich dir für deine Hilfe und dein offenes Ohr zu jeder Zeit, sowie für kulinarische Pausen, wenn Fotosynthese wieder einmal nicht ausreichend war.

Bei Marius Hintsche möchte ich mich für die geteilte Hingabe zum ISO-Datum und diverse Ohrwürmer, die entweder „egal“ oder aus „Holz“ waren bedanken. Es hat mir immer viel Spaß gemacht mit dir im Labor zu arbeiten.

Meinen Kollegen/innen Nicole, Vitali, Natalia, Marina und Nina möchte ich ganz besonders für die schöne Arbeitsatmosphäre und die tolle Zusammenarbeit danken. Nicole dein offenes Ohr und kulinarischen Köstlichkeiten kamen oft zum rettenden Zeitpunkt. Nina du bist eine Inspiration und Stütze zugleich, ich bin sehr froh dich kennengelernt zu haben.

Besonderer Dank gilt auch meinen Mitstreitern an der Universität Potsdam, besonders Ted, Maike, Vera, Seti und Kirsten. Danke, dass ihr mich als „externer Sonderling“ in euren Kreis aufgenommen habt und mich immer mit offenen Armen empfangt, wenn ich nach Potsdam komme. Auch wenn das Ziel manchmal unerreichbar scheint, bin ich felsenfest davon überzeugt, dass ihr eure Arbeiten mit Bravour meistern werdet.

Das Beste kommt bekanntlich zum Schluss, meine unendliche Dankbarkeit möchte ich meiner Familie aussprechen. Ohne meine Eltern Gabi und Burckhard und meinen Partner Lukas hätte ich in dem abenteuerlichen Feld der Biotechnologie keinen Bestand gehabt. Danke, für eure immerwährende Liebe und Unterstützung, das Verständnis, wenn die Arbeitstage wieder einmal länger geworden sind und die zahlreichen Aufmunterungen, wenn es an meinem Forschungshimmel gewittert hat. Ich habe wirklich gelernt auch nach Dauerregen, scheint irgendwann wieder die Sonne. Ihr seid wirklich die beste Familie, die man sich nur vorstellen kann.

Declaration

I hereby declare that I have carried out this work and written this thesis by myself only with the help of the indicated means.

Natascha Heinsohn